

Detailing Aspects of the Reinforcement in Reinforced Concrete Structures

Retaining wall (case study)

By

Timothy Ovainete Saiki

in partial fulfilment of the requirements for the degree of

Master of Science
in Civil Engineering

at the Delft University of Technology,
to be defended publicly on Thursday July 28, 2016 at 10:00 AM.

Supervisor:	Prof. dr. ir. D.A. Hordijk	
Thesis committee:	Dr. ir. drs. C.R. Braam,	TU Delft
	Dr. ir. P.C.J. Hoogenboom,	TU Delft

An electronic version of this thesis is available at <http://repository.tudelft.nl/>.



Acknowledgement

I would like to express my gratitude to Prof.dr.ir. D.A. Hordijk for his invaluable contribution to this MSc thesis. The guidance he provided and the quality he demanded at all times were vital to this achievement. I would also like to express my gratitude to my direct supervisor, Dr.ir.drs. C.R. Braam for his patience, the knowledge he shared and other contributions made during the course of this MSc thesis. I also like to express deep gratitude to Dr. Ir. P.C.J. Hoogenboom for the guidance he provided and the support he provided towards the realization of this thesis.

Finally I would like to then my wife (Vovo) and daughters (Ofushi & Enworo) for the unconditional support they gave me over the past two year. I look forward to returning to you soon, never to leave again. Thank you a million times!!!

Timothy O. Saiki

Delft, July 2016

Summary

This thesis studies the impact of reinforcement detailing on the behaviour of a reinforced concrete structure. Using a retaining wall as a case-study, the performance of two commonly used alternative reinforcement layouts (of which one is wrong) are studied and compared. Reinforcement Layout 1 had the main reinforcement (from the wall) bent towards the heel in the base slab. For Reinforcement Layout 2, the reinforcement was bent towards the toe. This study focused on the reinforcement details used in the D-region, and on how it impacts the capacity, joint efficiency and failure mode of the structure.

First, a literature review is carried out which focused on the behaviour of corner joints from experimental works available in literature. Next, a strut and tie model of the D-region is made. From the strut and tie model, the opening moments acting on the structure subjects the re-entrant corner region to a concentration of tensile stresses, while a compressive stress field acts concurrently with transverse tension within the core of the joint. The internal forces within the D-region are evaluated, and the required steel areas computed. Afterwards, ATENA FEM software is used to model the structure, and to study the impact of the alternative reinforcement layouts on the capacity and behavior of the structure. Some aspects of the structural behavior studied include the stress and strain distribution in the concrete, crack width, crack pattern, steel stress and strain distribution etc.

The results obtained from the FEM analysis was sensitive to bond model defined in the material model. When perfect-bond was assumed in the FEM analysis, Reinforcement Layout 1 attained a joint efficiency of 72.4%, while Reinforcement Layout 2 achieved 88% joint efficiency. In his experimental works on similar details, Nilsson (1973) had obtained a joint efficiency of 60% for Reinforcement Layout 1, a range between 82% to 102% for Reinforcement Layout 2. The disparity between FEM result and experimental result for Reinforcement Layout 1 occurred because perfect-bond was assumed in the FEM model. With cracking playing prominent role in this structure, perfect bond assumption is not valid, and some slip is inevitable. To verify, a bond-slip relation is used to model the structure, resulting in 62% joint efficiency for Reinforcement Layout 1, and 82% joint efficiency for Reinforcement Layout 2. These values obtained with bond-slip model are much closer to experimental values than those obtained with perfect bond.

The reinforcement layout used also had significant impact on the joint behavior. In Reinforcement Layout 1, the reinforcement (tie) from the wall was not properly anchored in the nodal region in the slab. The compressive stress field (i.e. inclined strut) was observed to flow past the bent part of the reinforcement without much interaction. The force transfer between the inclined strut and the tie was not effective. Also, wide cracks occurred along the inclined strut from the action of transverse tension (caused by the opening moment). These cracks which further weakened the strut. This detail had a diagonal tension cracking failure mode. For Reinforcement Layout 2, a clearly defined nodal region exists. A CTT node formed allowed for effective force transfer (at the node) between the concrete and steel. Furthermore, the bent part of the reinforcement crossed the path of the inclined strut, and helped to control crack width. The reinforcement also provided confinement to the inclined strut which further increased its strength. This detail prevented diagonal tension cracking failure, hence the higher capacity it achieved. Failure was by crushing of concrete along the joint – slab interface, after formation of a wide vertical crack extending from the re-entrant corner downwards into the slab. Adding a diagonal bar, placed 45° around the re-entrant corner, helped to control this re-entrant corner crack, thus ensuring that over 100% joint efficiency is achieved. In conclusion, Reinforcement Layout 1 is a poor detail. Though common in practice, a node is not properly formed in this detail, thus force transfer capacity between concrete and steel is not effective. This detail should be avoided.

Contents

Acknowledgement	v
Summary	vi
Contents	viii
1 Introduction	1
1.1 Background	1
1.2 Aim of the study	1
1.3 Method of study	2
1.4 Outline of the report	2
2 Detailing of structures and Strut and Tie Model	4
2.1 Extent and behaviour of D-regions	4
2.2 Strut and tie model	5
2.3 Developing the strut and tie model	7
2.4 Dimensioning of strut and tie	9
2.4.1 Struts	10
2.4.2 Ties	12
2.4.3 Nodes	12
2.4.4 Dimensioning and design of struts, ties and nodes	15
2.5 Applications of strut and tie model	18
2.5.1 Corbels	18
2.5.2 Corner Joints	20
2.6 Detailing	27
2.6.1 Some basic rules	27
2.6.2 Bond and anchorage	29
2.6.3 Splicing of bars	31
3 Behaviour and detailing of corner joints	33
3.1 Detailing requirements for corner joints	33
3.2 Failure modes of monolithic concrete joints	34
3.3 Typical experimental programme	35
3.4 Behaviour of different corner joint details	37
3.4.1 Nilsson (1973)	37

3.4.2	Nabil, Hamdy and Abobeah (2014).....	49
3.4.3	Campana, Ruiz and Muttoni (2013)	50
3.4.4	Impact of reinforcement ratio on corner joint efficiency	50
3.4.5	Improving corner joint details with steel fibres.....	53
4	Finite Element Method	54
4.1	Overview of the FEM process	54
4.1.1	Pre-processing.....	55
4.1.2	Analysis (or solution).....	56
4.1.3	Post-processing	57
4.2	Behaviour of concrete, steel and their composite	58
4.2.1	Concrete	58
4.2.2	Reinforcement	60
4.2.3	Concrete-steel interaction	62
4.3	Constitutive model	63
4.3.1	Concrete material model (SBETA).....	64
4.3.2	Material stiffness matrix	69
4.4	Non-linear analysis.....	70
4.4.1	Solution procedure.....	70
4.4.2	Iteration schemes and convergence criterion	71
5.	Analytical design using strut-and-tie model	73
5.1	Strut and tie analysis of the joint	74
5.2	Reinforcement design	81
5.3	Background to detailing	82
6.	Finite Element Analysis of the D-region.....	85
6.1	FEM Layout	85
6.2	Study on depth of embedment and direction of bend	86
6.2.1	Variant 1 – No embedment depth provided.....	87
6.2.2	Study on variants with embedment depth provided.....	89
6.2.3	Study on direction of bend of reinforcement	93
6.2.4	Variant 6 – Improved detail with diagonal bar at re-entrant corner	96
6.2.5	Summary on preliminary study.....	98
6.3	Focus on thesis variants	101

6.3.1	Reinforcement Layout 1.....	102
6.3.2	Reinforcement Layout 2.....	112
6.4	Impact of bond model on FEM results.....	117
6.4.1	Comparison of perfect bond assumption with bond-slip model	118
6.4.2	Variants 2 – 6 with bond-slip model	121
6.4.3	Thesis variants (or layouts) with bond-slip model	125
6.5	Satisfactory details.....	129
6.5.1	Reinforcement Layout 2 + diagonal bar at re-entrant corner	129
6.5.2	Looped detail + diagonal bar at re-entrant corner	131
6.6	Summary to this section of study	131
7	Conclusions and recommendations.....	133
7.1	Conclusions	133
7.2	Recommendations	136
	References	138
	Appendix 1: Background to study case.....	141
	Appendix 2: Bond.....	145

1 Introduction

1.1 Background

Detailing of structural members and connections is a very important aspect of the design process. Though it is often viewed as preparing working drawing for a structure, it plays a crucial role in the performance on the final structure. It actually communicates the engineer's design to the contractor who oversees the construction on site. Where this communication is poor, the structure that is built may be different from what was assumed in design. Similarly, its behaviour and capacity might differ from what was estimated in design. Many structural failures that have occurred in history have been attributed to poor or wrong details. Calamitous incidents like the structural failure of Ronan point (in 1968), Hyatt Regency (in 1981) etc. could have been prevented if more attention had been paid to its structural detailing.

In reinforced concrete structures, detailing plays a vital role in how the structure behaves. Being a composite structure, the location of steel has significant influence on the stress distribution within the structure, and consequently on its behaviour. A poorly designed detail in reinforced concrete can result in localized stress concentrations within the structure, which could result in failure. Such premature failure of structures occurs even where the structural members were designed to meet code requirements. Often, these failures occur in connection regions or corners (where there is an abrupt change in section), or in regions subjected to concentrated loading (like supports etc.). These regions are referred to as disturbed regions (or D-region). Sometime however, poor detailing might not result in structural failures, but lead to a deterioration of the structure. Some typical deteriorations in reinforced concrete include formation of large cracks, spalling of concrete, corrosion of embedded steel etc. All these can be prevented or controlled with adequate detailing of the structure.

A key objective in structural design is to produce structures that have adequate capacity for the load they would be subjected to in their design life. How does the reinforcement detailing aid or prevent the achievement of this objective? In this report, a study is undertaken into the detailing aspects of reinforced concrete structures. The focus would be on the corner joints (or connections) between structural members in the D-regions. Some typical corner joints often seen in practice include beam-column, joints, wall-base joints in retaining walls and liquid retaining structures, wing-walls of abutments etc. The behaviour of these regions would be studied with the aim of understanding some key issues that would help a designer to achieve a satisfactory detail design.

1.2 Aim of the study

Since there are many types of structures available in practice, it would be impossible to cover all possible joint and detail types in a thesis work like this. For that reason, a specific case study would be utilized in this study. Figure 1.1 shows two variants of a retaining wall structural detail often encountered in practice. From a literature review, there appears to be a significant difference in the capacity of both details, despite the area of the reinforcement being similar in the connected members. Looking at the figure 1.1, the only difference between both is seen in how the wall-base joint is detailed. Why does such a discrepancy in capacity exist for these details which are very commonly used. Some specific aspects this study aims to answer are enumerated below:

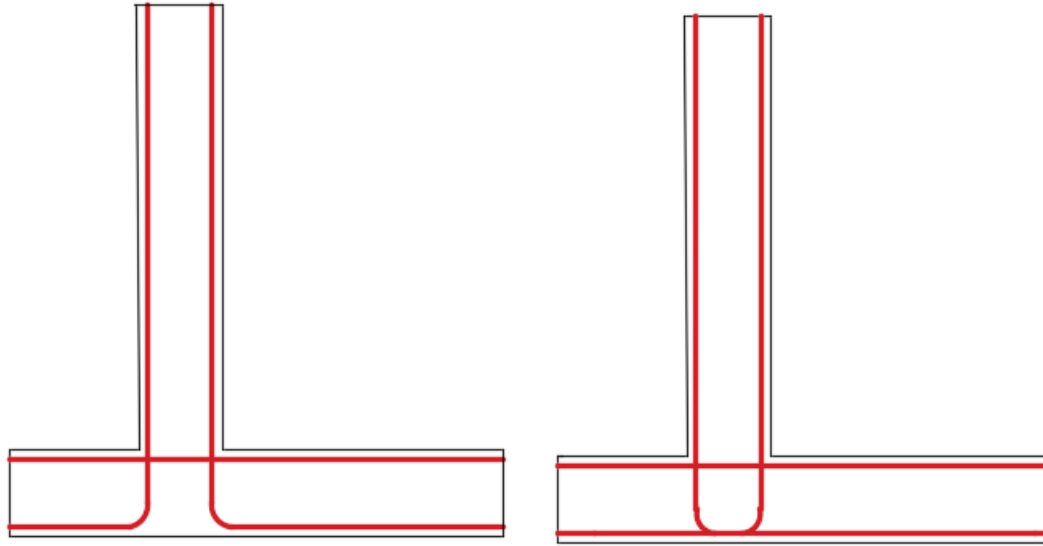


Figure 1.1 – Typical reinforcement layouts for retaining wall

- How efficient are the above joint layouts, and do they allow the structure to achieve its full capacity?
- Does the reinforcement layout affect the stress and strain distribution in the joint? How?
- Does it matter if the main tension reinforcement from the wall is bent towards the toe instead of towards the heel, and vice versa?
- How is failure likely to occur where these details are used?
- If these structural details are not 100% efficient, what improvement can be made to the structural detail?

While the retaining wall is used in this thesis work as a case study, the findings are applicable to other structures with similar reinforcement details, and subjected to similar loadings.

1.3 Method of study

The three approaches that would be used for this study includes:

- A literature review that focuses on the behaviour of corner joints.
- Strut and tie modeling of the case study section, with the intention of gaining insight in the structural behaviour of the joint.
- Finite element method (FEM) using ATENA finite element software

1.4 Outline of the report

With corner joints typically being D-regions, beam theory cannot be utilized for their design. Eurocode 2 (subsequently called EC2) recommends the use of strut and tie methods for designing and detailing them. This thesis starts with a literature review on strut and tie methodology. The concept of struts, ties and nodes, and how to dimension them are discussed in the next chapter. With strut and tie understood, its application to typical D-regions like corbels and corner joints is researched from literature.

Chapter 3 is an extensive literature study on the behaviour of corner joints based on experimental works available in literature conducted by several researchers including Nilsson (1973), Nabil, Hamdy and Abobeah (2014) etc. These experimental works give practical insight into the actual behaviour of carefully prepared specimen (with different detailing layouts). The work of Nilsson (1973) is particularly interesting as he provided actual pictures at failure for some of the specimen he experimented with. These pictures give even deeper insight into the behaviour, crack patterns, failure mode etc. on the joint specimens he tested.

Chapter 4 of the report introduces the subject of finite element method. The focus of is on understanding the material models used in the FEM software. For this work, the SBETA element in ATENA is used to model concrete, and the elastic-perfectly plastic bilinear material model for steel. Adequate information on these models and how they are implemented in the stiffness matrix is discussed in chapter 4.

In Chapter 5, a strut-and-tie design of the case study retaining wall is undertaken. The geometric dimensions and capacity of the struts, nodes and tie are determined in this part of the report. Based on the ties, reinforcement required is computed. The strut and tie analysis gives insight into the behaviour of the joint when loaded.

Further study on the retaining wall is presented in chapter 6 using FEM. Some aspects studied in this section include the influence of anchorage length, impact of the direction to which a bar is bent, and the role of diagonal bar at re-entrant corner. Specific areas of interest include the joint efficiency of the structural details, their influenced on stress and strain distribution within the joint, cracking behaviour, eventual failure mode etc. As both of the structural detail in figure 1.1 did not meet 100% joint efficiency required, some modifications were made to the details, after understanding the reason for their premature failure. Two alternative details that meet the design requirements were achieved, and are presented.

2 Detailing of structures and Strut and Tie Model

A key assumption from the beam theory is that “plane sections remain plane after bending, thus implying a linear distribution of strain across the section”. This assumption is the basis of many standard design methods for structural members’ Bernoulli (or B-regions). However, this assumption is not valid for disturbed or discontinuous (or D-regions) of the structure. Such regions can exist as geometric discontinuities (e.g. near openings, re-entrant corners, changes in cross section etc.) or statical discontinuities (e.g. near support reaction or concentrated loads). The use of the beam theory would be inappropriate for the design of these regions. Typical approaches that have been used in the past to design these regions are largely based on rules of thumb, past experience etc. Eurocode 2 (clause 6.5.1 and clause 9.9) however recommends that such regions are designed with strut and tie models. This chapter discusses the use of strut and tie models for designing D-regions, and how it could help in detailing of reinforced concrete structures.

2.1 Extent and behaviour of D-regions

Figure 2.1 shows a concentrated compressive load ‘P’ applied to a rectangular section. The effect (or stress) caused by the load is compared at different sections along the depth of the member. While significant localized stress is observed in the vicinity of the load, the stress distribution across the section becomes almost uniform at a certain distance from the point of load application. This principle (known as Saint Venant principle) is used to determine the extent of the D-region in a structure.

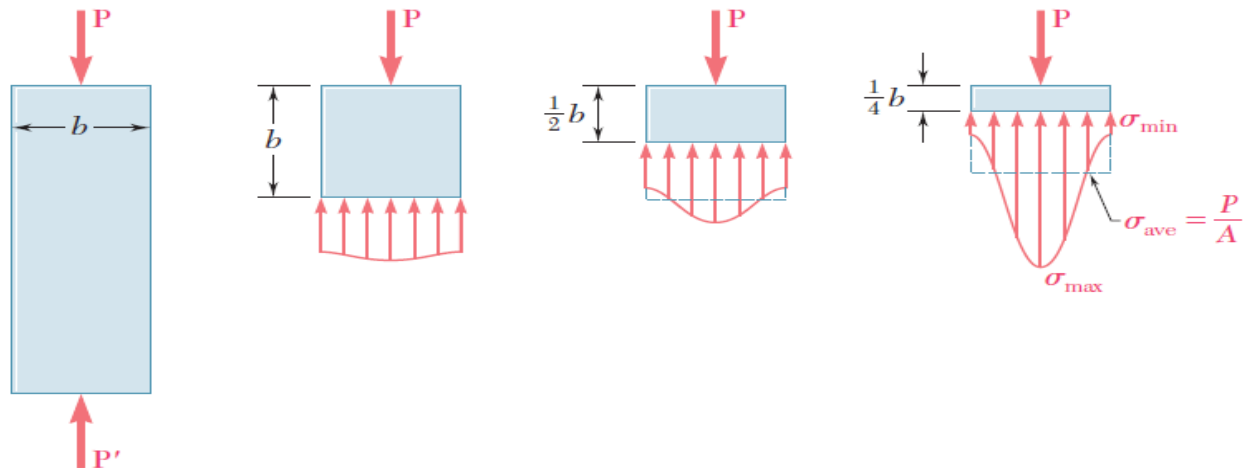


Figure 2.1 – Illustration of Saint Venant’s principle (Beer et al, 2011)

Based on this principle, the extent of D-regions is usually taken as one member depth or width (the larger of both) from the point of statical or geometric discontinuity. Tjhin and Kuchma (2002) illustrated this with a frame structure as shown in Figure 2.2.

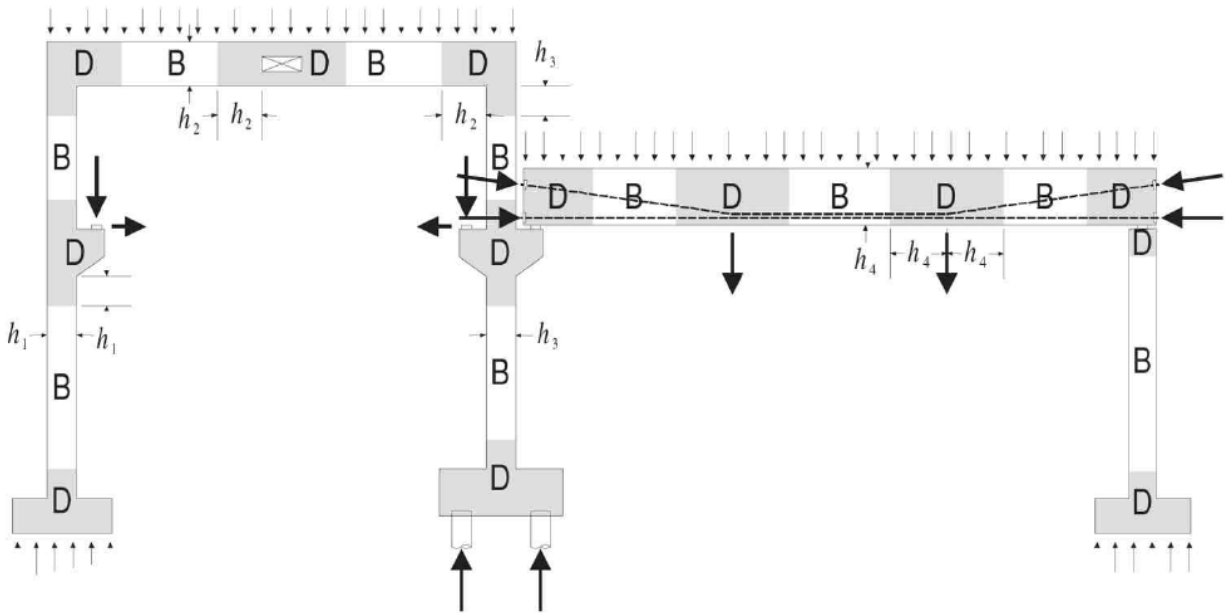


Figure 2.2 - Illustration of B and D regions in a structure (Tjhin and Kuchma, 2002)

The B-regions (where B is Bernoulli) represent those regions of the structure where the assumption of linear strain distribution is valid. The stresses and strains in these regions are quite regular so that they can be modeled mathematically quite easily, complying with equilibrium and compatibility conditions. The internal state of stress of B-regions can be easily obtained from the section forces (i.e. moments, axial forces and shear forces) from structural analysis. Using sectional properties like area, moment of inertia etc., the internal stresses can be easily computed from beam theory.

On the other hand, D-regions are regarded as disturbed, and the stress distribution as irregular; thus not easy to represent mathematically. Using sectional analysis for D-regions would give inaccurate results. Hsu and Mo (2010) note that it is difficult to apply compatibility conditions here. Thus stresses in D-regions are normally determined by equilibrium condition alone, while strain is not usually considered. The design actions used to compute forces in a D-region are its boundary stresses on account of external actions. In design, these regions are usually isolated as free bodies, and the boundary stresses are applied to them.

When the D-region is uncracked, the stress distribution may be computed with elastic theory and linear finite element method. However, once it is cracked, the stress field is disrupted, and a redistribution of internal forces occurs. Linear elastic analysis would no longer be realistic at this stage, and Strut and tie models become suitable. However, finite element analysis could still supplement the strut and tie method especially in knowing the stress state just before cracking. Also, where the nonlinear effects are realistically incorporated, the finite element could still prove useful even in the cracked stage

2.2 Strut and tie model

This is a technique in concrete mechanics that models the stress flow (or trajectory) from the loaded edges through the concrete section to the supports using an imaginary truss inside a concrete structure. The models used for in-plane stress conditions, comprises of fictitious concrete struts and steel ties (which carries compressive and tensile stress respectively), and nodal joints where they intersect. The method is based on

the lower bound (or static) theorem of Plasticity. An illustration of what lower bound (or static) solution means is shown in Figure 2.3.

condition	static solution	complete solution	kinematic solution
equilibrium	ok	ok	ok
yield condition	ok	ok	?
mechanism	?	ok	ok
result	lower bound $[Q_S] \leq [Q_R]$	collapse load $[Q_R]$	upper bound $[Q_K] \geq [Q_R]$
method	static method	—	mechanism method

Figure 2.3- An overview of solutions in plastic theory (Muttoni, Schwartz and Thurlimann, 1997)

Being a lower bound, a strut and tie model meets both equilibrium and the yield condition of the plastic theorem. It does not consider mechanism conditions (i.e. formation of plastic hinges). Thus, the solutions obtained is usually lower than the failure load, thus on the safe side. Thus an acceptable strut and tie model is one that:

- ✓ Is in equilibrium with the applied load case i.e. $\sum F_i = 0$ at all nodes where $n = 1, 2 \dots n$)
- ✓ The design (or factored) member forces in all nodes, struts and ties do not exceed their design strengths i.e. $F/A \leq f_{design}$

This method is based on the theory of plasticity, which requires ductile material. Since concrete however has limited ductility, a strut and tie model needs to be chosen in such a way that the deformation capacity is not exceeded at any point. This is achieved by attuning the strut and tie members of the model to the size and direction of internal forces obtainable from the elastic stress trajectory (Schlaich, Schafer and Jennewein, 1987). Oriented this way, a strut and tie models the real behaviour of the structure better, and minimizes redistribution of forces after cracking. To further improve ductility in the D-region, most codes recommend providing distributed reinforcement as part of the design. Typical requirements or convention for strut and tie includes:

- ✓ The struts and ties can support only uniaxial forces.
- ✓ Struts cannot overlap each other.
- ✓ Tensile strength of concrete is neglected.
- ✓ External forces are applied at nodal points. Distributed loads can be resolved into concentrated loads, and similarly applied at nodes.
- ✓ Adequate detailing anchorage is requisite for reinforcement (or ties),
- ✓ For ductility, yielding of a tie should occur before strut or nodal zone failure.

Figure 2.4 is a flowchart that illustrates the process of designing a D-region using strut and tie methodology.

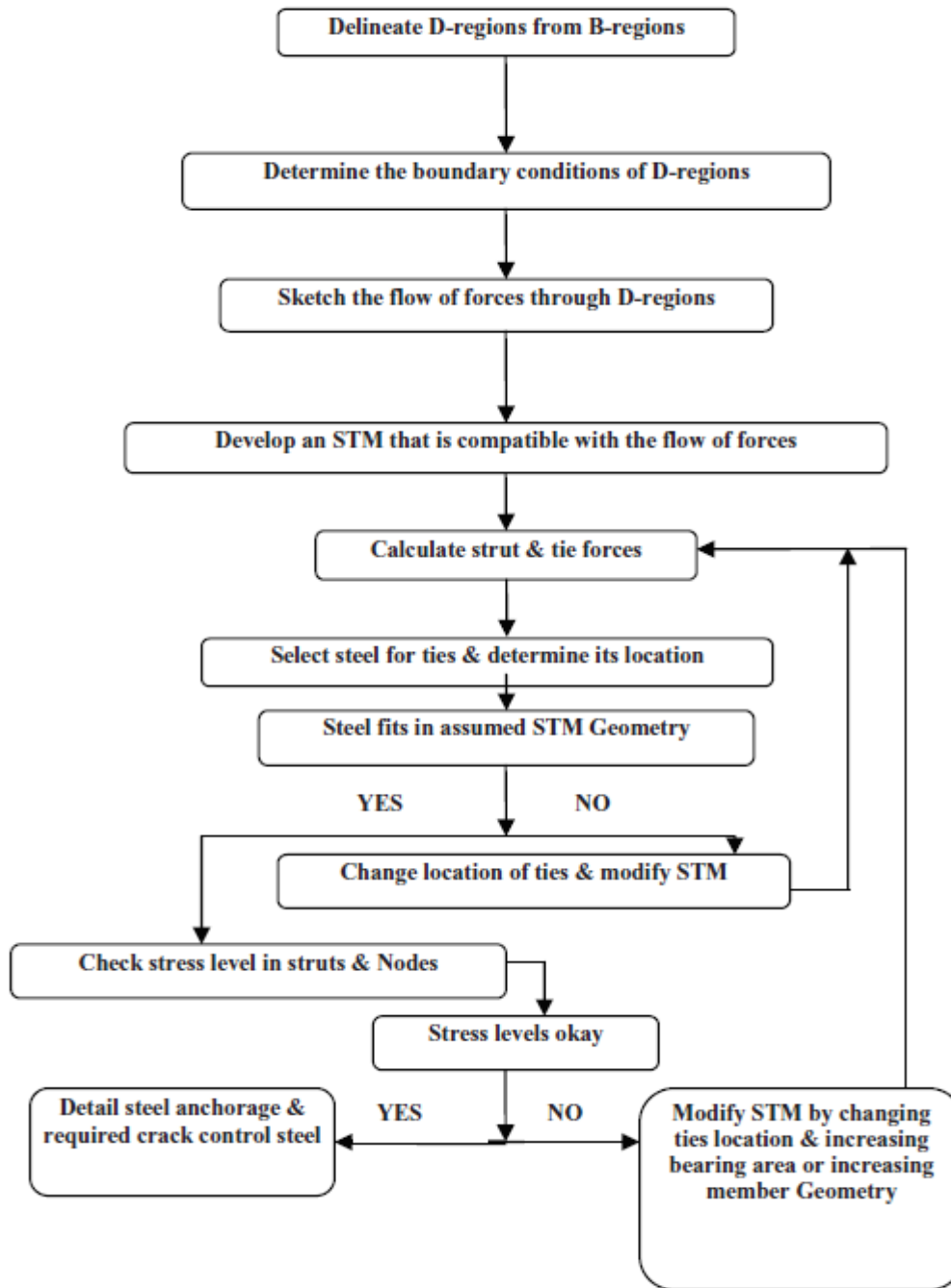


Figure 2.4 – An overview of the Strut and tie design process (Shah, Haq and Khan, 2011)

Background knowledge for the first two activities in Figure 2.4 has been discussed in sections 2.1 and 2.2. The next few sections discuss the remaining activities in the flowchart.

2.3 Developing the strut and tie model

After isolating a free body diagram of the D-region, and determining the design actions (i.e. stresses or effects due to moments, shear and axial forces at the border between the B- and D-regions), the next step in the strut and tie model is the selection of an internal truss to carry the resultant forces across the D-region to its supports or boundaries. Selecting that truss is the goal of the third and fourth steps of the flowchart

presented in Figure 2.4. This section discusses how to develop that truss. Three methods typically used to develop the truss are:

1. Load path method
2. Modeling from elastic stress trajectory, and
3. Standard or existing models

Load path method

The load path simulates the path (or line) through force is carried from the point of loading to the supports. The boundary stress diagrams are subdivided in a manner that they correspond to an equivalent stress resultant of same magnitude in the opposite side of the D-region (Schlaich and Schiifer, 1991). A load-path becomes obvious when the corresponding stresses are connected by streamlines. This is illustrated in figure 2.5. The curved streamlines are replaced with polygons, and further struts (C) and ties (T) may be added for transverse equilibrium. There are many examples in literature done with this method.

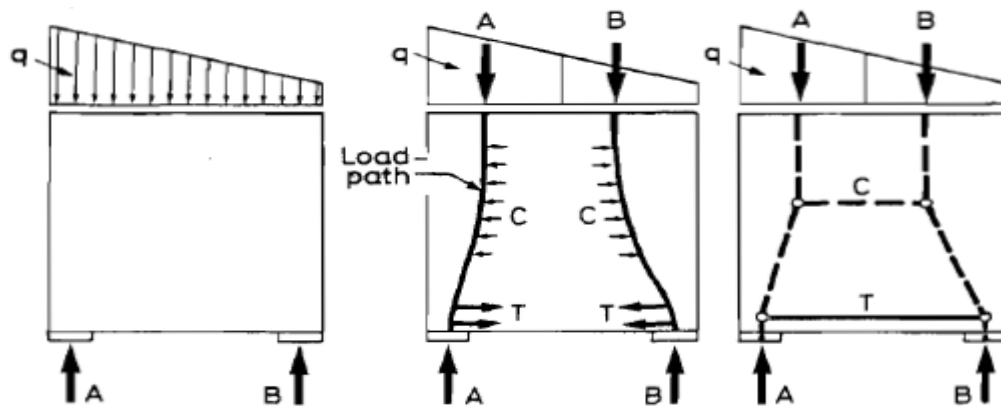


Figure 2.5 – Illustration of the load path method

Modeling from elastic stress trajectory

There are many software and finite element programs available that can model elastic stress in concrete sections. Using such a program, the strut direction is usually aligned with the average and main directions of the principal compressive stresses. Similarly, the direction of the ties corresponds with the direction of the principal tensile stresses from linear elastic analysis. This method can be used in conjunction with the load path method.

Standard or existing models

A review of literature suggests that some typical models appear very often in different ways and combinations. This is not surprising since only a limited number of D-region exist with significantly different stress pattern (FIB, 2010a). These models can be easily combined and/or adjusted to accommodate various situations. Thus typical existing models available in literature can provide practical information for developing models for D-regions. Figure 2.6 shows some examples of some common strut and tie models.

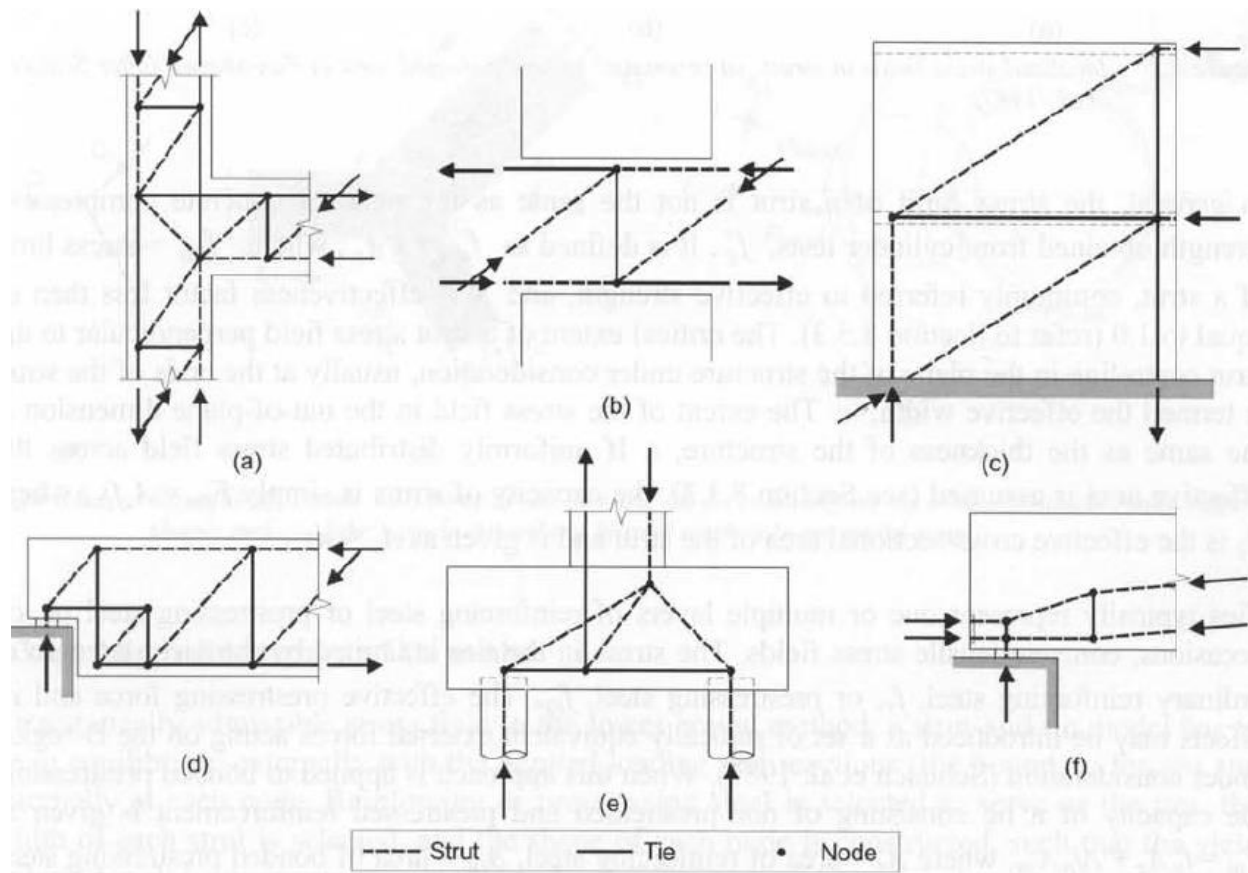


Figure 2.6 – Strut and tie models for typical D-regions (FIB, 2008)

While figure 2.6 shows some typical strut and tie models for some D-regions, there exist many alternative strut and tie models that could fit into the D-region. Thus there is no unique solution for any D-region. One reason for this non-uniqueness is the fact that the structural behaviour is influenced (to a large extent) by the chosen reinforcement layout. This fact provides the designer an opportunity to adapt the structure to meet the design requirement of any given case. Since no unique solution exists, designers aim for a sufficiently good and effective solution that is economical without compromising structural safety. However, where a choice is to be made among several alternative models, Eurocode 2 clause 5.6.4(5) suggests optimization by energy criteria.

2.4 Dimensioning of strut and tie

As shown in figure 2.7, a typical strut and tie model comprises of compression struts, tensile ties and nodal regions. In this section, each of these components would be discussed, and details would be given on how they are dimensioned, and how the strengths are determined for design purposes. A lot of literature is available on this topic, with authors using various standards including ACI 318 (from American Concrete Institute), AASHTO, CEB-FIP Model code, Eurocode, NCHRP etc. While most of the requirements are largely similar, there are nevertheless noticeable differences. For this thesis work, the guiding documents would be the Eurocode 2 and CEB-FIP requirements.

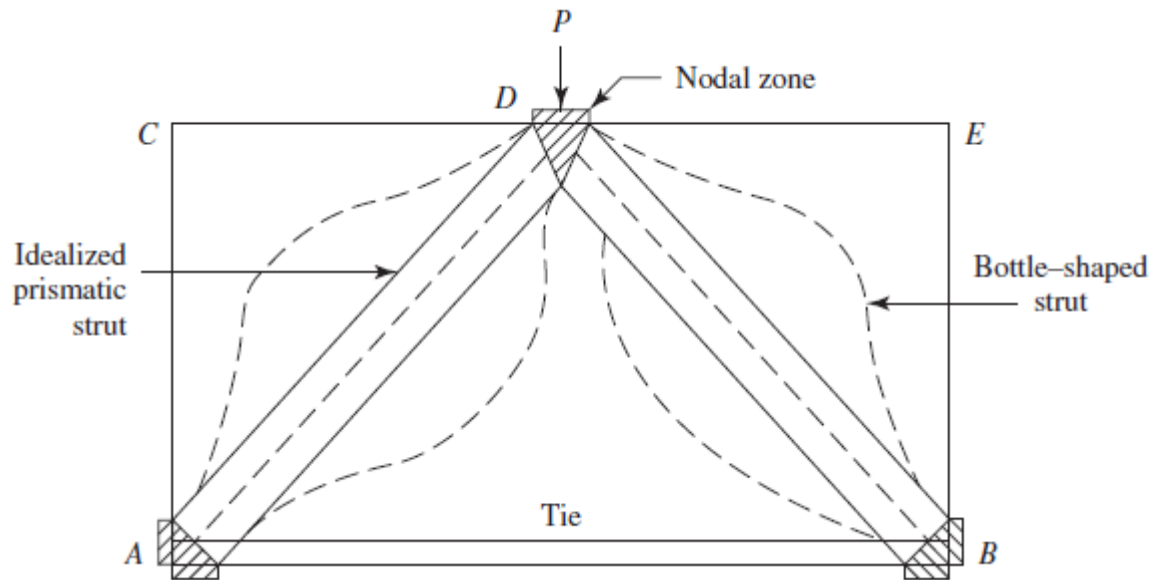


Figure 2.7 – Strut and tie model (for illustration)

2.4.1 Struts

This is an internal compressive member in a strut and tie model that represents the compressive stress field within the concrete section. The centerline of the strut is oriented along the principal compressive stress trajectory in the uncracked stage. The strut can be of unreinforced or reinforced concrete. From figure 2.7, the members AD and DB are the strut. The shape of struts could be prismatic, bottle-shaped or fan shaped. The prismatic strut (as in figure 2.7) is parallel between two nodes, and it is assumed that the bearing area does not change. The bottle-shaped strut is wider along the length (than at the ends) as stresses are allowed to spread in the section. The dashed lines in figure 2.7 demonstrate spreading of the stress along the strut length. In a bid to maintain equilibrium, this spreading of stress gives rise to transverse tensile stresses that could result in splitting cracks as illustrated in figure 2.8. After cracking, the strut may fail if transverse reinforcement is not provided. Where provided, transverse reinforcement would control longitudinal splitting cracks, and the failure mode would then be governed by crushing. The likelihood of transverse splitting makes the bottle shaped strut to be inherently weaker than a prismatic strut. For the fan-shaped strut, an array of struts at different angular orientation originates from, or meet at a single node.

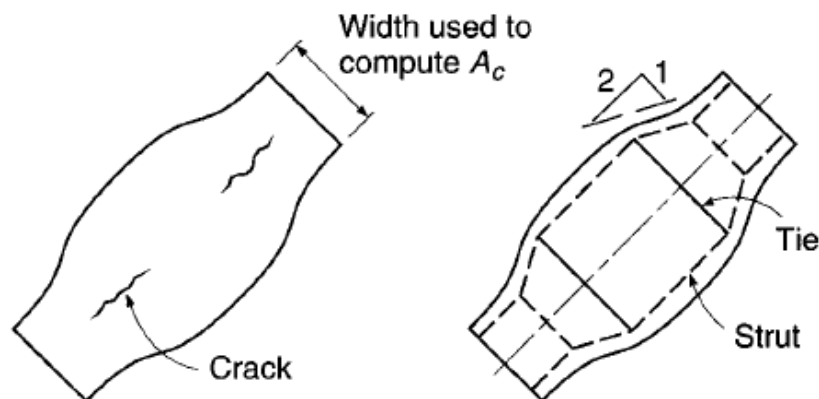


Figure 2.8 – Cracks in bottle-shaped strut from transverse tensile stress (Nilson, Darwin and Dolan, 2004)

EC2 gives guidance on estimating the transverse tensile forces in a bottle-shaped strut. There are two possibilities depending on whether the strut is partially disturbed (i.e. partial discontinuity in figure 2.9a) or fully disturbed (i.e. full discontinuity in figure 2.9b). Partial discontinuity occurs when the width of the strut is less than half of its height i.e. ($b \leq H/2$ in figure 2.9a). In this case, a B-region can occur between two D-regions in the strut. The transverse tensile force in the strut can be obtained from expression 6.58 of EC2 shown below:

$$T = \frac{1}{4} \cdot \frac{b - a}{b} \cdot F$$

For a fully disturbed strut, the entire section is a D-region, and can be obtained from expression 6.59 of EC2 given thus:

$$T = \frac{1}{4} \cdot \left(1 - 0.7 \frac{a}{h}\right) \cdot F$$

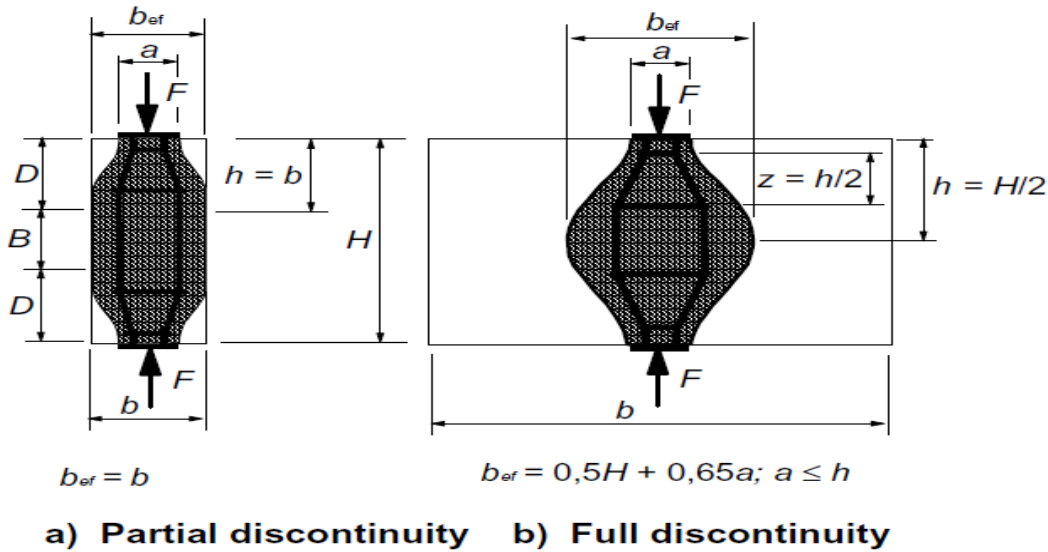


Figure 2.9 - Determination of transverse tensile forces in a bottle-shaped compression strut

The capacity of struts (F_{cu}) can be estimated with the expression:

$$F_{cu} = A_c \sigma_{Rd,max}$$

Where A_c is the effective cross sectional area of the strut and $\sigma_{Rd,max}$ is the effective design strength. This expression highlights two important characteristics of the strut for design i.e. the strength of the strut and its geometrical dimensions. The strength will be discussed in this section whereas the geometrical dimension are explained in 2.4.4.

The design strength of concrete struts is influenced by the multi-axial stress state and the presence of cracks and/or reinforcement. If the concrete is subjected to uniaxial compression, Eurocode 2 clause 6.5.2(1) allows the design strength of the concrete to be used.

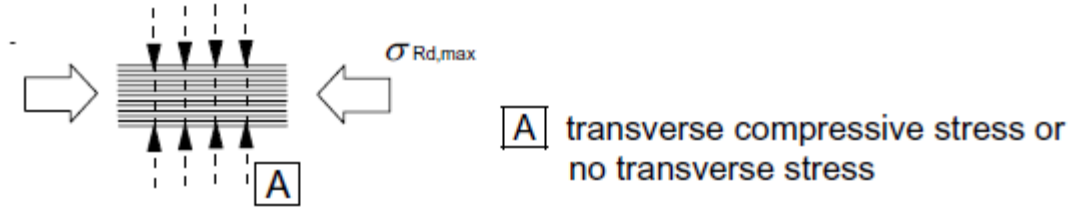


Figure 2.10 – Design strength of concrete strut (no transverse tension)

i. e. $\sigma_{Rd,max} = f_{cd}$

Where $f_{cd} = \alpha_{cc} f_{ck} / \gamma_c$

Where f_{ck} is the characteristic (5%) cylinder strength at 28 days, α_{cc} is a coefficient that takes load duration effect into account with a value between 0.8 and 1.0. A value of 0.85 is used in this work. γ_c is the material partial safety factor for concrete taken as 1.5 from table 2.1N of EC2. Eurocode allows for a higher design strength where multi-axial compression does exist as in figure 2.10. Bhatt, MacGinley and Choo (2014) note that this increase in design strength when biaxial compression exists could be up to 10%. Where axial compression of the strut is accompanied by transverse tension, a lower design strength is used expressed as:

$$\sigma_{Rd,max} = 0.6 [1 - f_{ck}/250] f_{cd}$$

2.4.2 Ties

These are tension member in the strut and tie model. The tie consists of the reinforcement (prestressed or non-prestressed), and a portion of concrete concentric around the diameter of the tie. The concrete portion defines the effective width of the tie. This concrete however does not contribute to the tensile strength of the tie. It nevertheless adds the stiffness by the tension stiffening effect, and thus helps to control deformations. The steel bars used as ties could be in one layer or smeared in several layers over the length of the tensile zone. The centroid and direction should however be the same as that of the tie in the model. When distributed in several layers across the tensile zone, better crack distribution would be achieved. The capacity (F_{tu}) of ties is expressed thus:

$$F_{tu} = f_{yd} A_s + \Delta f_p A_p$$

Where the design strength of steel $f_{yd} = f_{yk} / \gamma_s$ (with $\gamma_s = 1.15$ from table 2.1N of EC2). The tie could also be prestressed reinforcement (as is seen in the expression). However, only the increase in prestressing steel stress Δf_p is available to function as tie. A_s and A_p are cross sectional areas of reinforcing and prestressing steel respectively. The ties need to be properly anchored into the nodes so that the tensile strength of the tie can be fully developed, and to prevent premature tie failure. Section 2.6 of this report discusses the EC2 requirements on anchorage and other aspects of detailing.

2.4.3 Nodes

Nodes are the points where the forces in struts and ties intersect and balance within the strut-and-tie model. According to the model, forces converge, and they are transferred or redirected at that point. A node is essentially a defined volume of concrete, acted upon by different forces. Conceptually, MacGregor and Wight (2005) note that they are idealized as pinned joints where three or more forces meet, and are in equilibrium i.e.

$$\sum F_x = 0 \quad \sum F_y = 0 \quad \text{and} \quad \sum M = 0$$

The $\sum M = 0$ condition requires the line of action of all active forces to pass a common point.

Schlaich, Schafer and Jennewein (1987) described the concept of nodes as a “simplified idealization of reality”. The forces that meet at a node are in reality stress fields represented by struts, reinforcing bars which are anchored around the nodal region, and externally applied concentrated loads or support reactions. Where wide concrete stress fields meet each other, or where there is close spacing of reinforcement ties, the node is referred to as smeared. If the strut or tie represents a concentrated stress field, the node is singular. Figure 2.11 presents a good illustration of singular and smeared node from the work of Cunningham (2000). Singular nodes are where stress concentrations typically occur; they are critical, and often govern the dimensions of structural elements. They occur where there are concentrated external forces (like prestressing forces, support reactions, anchorage zone with a concentration of reinforcements, at bends in reinforcing bars etc.), and geometrical discontinuities like re-entrant corners, around openings etc.

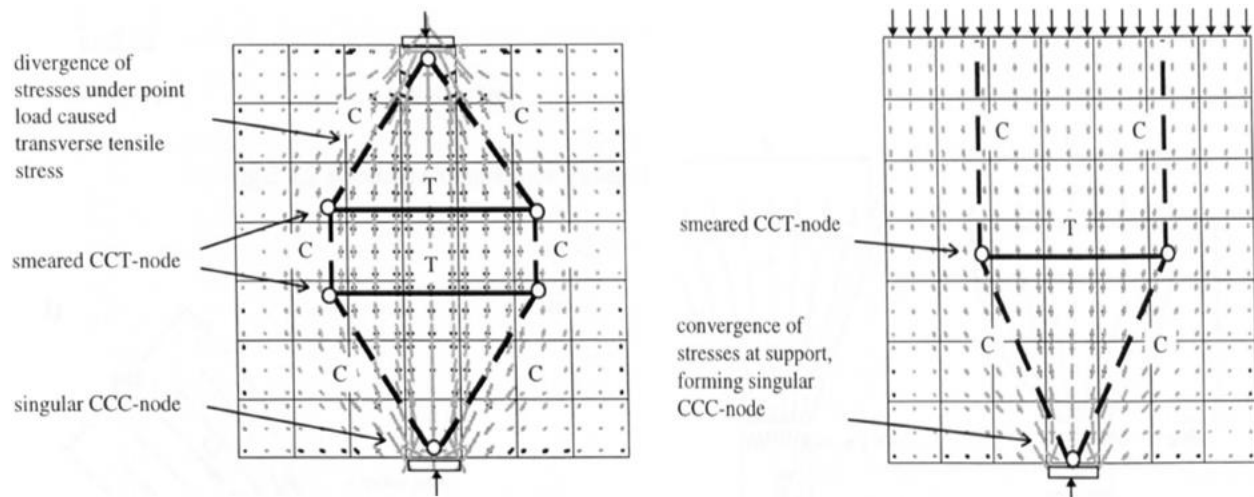


Figure 2.11 – Singular and smeared nodes (Cunningham, 2000)

Based on the combination of compressive (C) and tensile (T) forces acting on the nodal zone, nodes can be classified into four basic types as illustrated in figure 2.12.

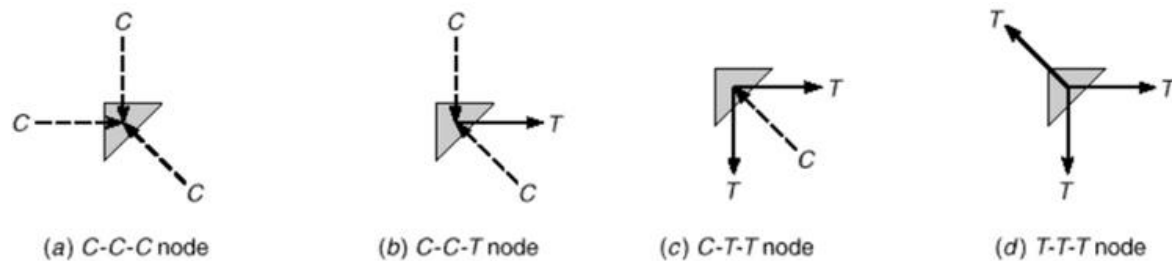


Figure 2.12 – Classification of nodes

Though figure 2.12 shows nodes subjected to different stress combinations, it should be noted that the forces in the node are ultimately balanced by compressive stresses. This is quite obvious in the case of the CCC node where three compressive forces act on the node. It is nevertheless true for the remaining cases where one or more tensile stresses act on the node. Ties are assumed to pass through the node in such a way that they exert a compressive stress on the far side of the node. This is illustrated in figure 2.13 where

adequately designed anchorages transfer the tie forces “from behind” in such a way that they exert compression on the nodes. Compressive stress transfer (from the ties) is achieved via anchor plates, bond forces and radial pressure. For stress transfer via bond, it is important that the full anchorage length of the reinforcement is achieved if it is to be effective.

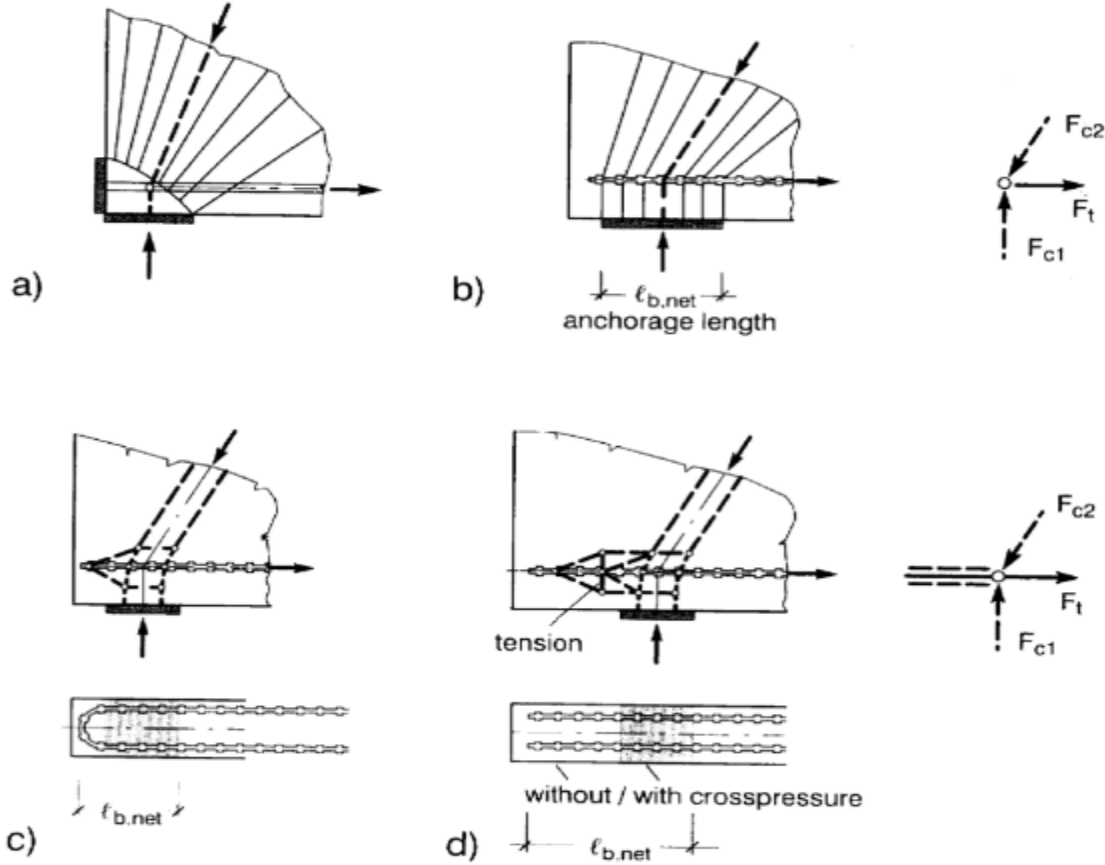


Figure 2.13 – Reinforcement anchorage in tension-compression nodes. (a) by anchorage plate behind node (b) by bond transfer within node (c) via bond and radial pressure, and (d) by bond “within and behind” node (FIB, 2010b)

The stress state of the nodes is essentially biaxial (for 2D) or triaxial (for 3D)¹. The multi-axial state of stress and the presence of cracks and/or reinforcements has influence on the effective material design strength of nodes. Section 6.5.4 of EC2 gives guidance for determining the maximum stress (σ_{Rdmax}) which can be applied at the edges of the node. The general expression is presented thus:

$$\sigma_{Rdmax} = k_i \cdot [1 - f_{ck}/250] \cdot f_{cd}$$

Where

- $k_1 = 1.0$ for CCC node
- $k_2 = 0.85$ for CCT node
- $k_3 = 0.75$ for CTT node, and

¹ Strut and tie model for 3D would be very complex. In practice, the 3D is separated into its constituent 2D region and modeled.

Where $f_{cd} = \alpha_{cc} f_{ck} / \gamma_c$ (with α_{cc} taken as 0.85 in this work and $\gamma_c = 1.5$)

From the above expression, it should be observed that the nodal strength is lower than the typical design value once there is tension. When a tensile tie is anchored in the nodal zone, there is likely to be incompatibility between tensile strains in the reinforcing steel and compressive strain of the node. This weakens the node, and is thus the reason for the reduced allowable stress (strength). A reasonably large angle is recommended between a strut and a tie that meet at a node. This is to minimize the strain incompatibilities that would occur when struts shorten, and ties lengthen in almost same direction. With decreasing angle, the tensile strain around the strut increases, resulting in lowering the effective strut strength. FIB (2008) cites Rogowsky and MacGregor (1983) as recommending an angle between 25 and 65 degrees for slender beams. EC2 6.5.4(5) allows up to 10% increase in design compressive stress if the angle between strut and tie is at least 55 degrees. That same clause gave other conditions where maximum allowable stress (σ_{Rdmax}) more than 1.0 can be used. Where triaxial compression is achieved, a value up to 3.0 can be used. The capacity of nodes can be expressed by the expression:

$$F_{node} = \sigma_{Rdmax} \cdot A_{node}$$

Where σ_{Rdmax} is determined as earlier discussed in this section, and A_{node} is the area of the face of the node acted upon by the strut or the tie. Ideally, this face should be perpendicular to the axis of the average principal stress in the node region/boundary. Stated another way, this nodal face should be taken perpendicular to that of the strut or tie acting on that face. This geometrical or dimensional aspect of strut and tie models is the focus of the next section of this report.

2.4.4 Dimensioning and design of struts, ties and nodes

Prior to verifying principal concrete stresses in the struts and nodes, it is imperative to:

- ✓ estimate the forces acting on the node,
- ✓ define the geometry (i.e. width and thickness) of the node, and
- ✓ define a representative concrete strength for the node (treated in 2.4.3).

Forces acting on the nodes are typically from struts, ties, support reactions and concentrated loads. Forces acting on the face of each node can be easily computed by treating each node like a pinned joint, and ensuring equilibrium in the structural system. Where more than three forces act on a node, or where two or more struts meet at the same face, the problem can be simplified by resolving them in such a way that only three forces remain. All forces acting on the node can easily be obtained using the method of joint resolution (from structural analysis), ensuring horizontal and vertical force equilibrium.

2.4.4.1 Dimensioning strut and tie components

The nodes, struts and ties of the idealized truss in a strut-and-tie model usually have theoretical dimensions. These dimensions are its width and thickness. The thickness is often taken as equal to the member thickness. The effective width of a strut and the nodal zone are often the unknowns in strut and tie design. They are determined based on the forces acting on the node, and the dimensions of the adjoining element. The product of the effective width and thickness is called the bearing area. A useful concept in dimensioning struts and nodes is that of “hydrostatic nodes”.

A nodal zone is “hydrostatic” if the stress on each face of the node is the same. The nodes are dimensioned in such a way that the ratio of their width is proportional to the compressive stress acting on that face. As

an example, the relationship between the nodal width (w_1, w_2 and w_3) and the corresponding compressive forces on the node (C_1, C_2 and C_3) for the node in figure 2.14 is expressed as:

$$\frac{C_1}{w_1} = \frac{C_2}{w_2} = \frac{C_3}{w_3}$$

The use of a hydrostatic node provides a relatively simple means of dimensioning nodes. Often, one side of the node is in contact with an external load or reaction, with the dimension determined by bearing plate, column base etc. In such cases, the dimensions of the other sides are computed with respect to this, with the goal of maintaining constant stress on each face. While figure 2.14 shows a CCC node, the concept of hydrostatic node also applies to nodes with tension in one or more faces. Geometry for tensile ties can be computed assuming an imaginary bearing plate at the end of tie which exerts pressure on the node. This concept provides a simple and useful approach to dimension nodes.

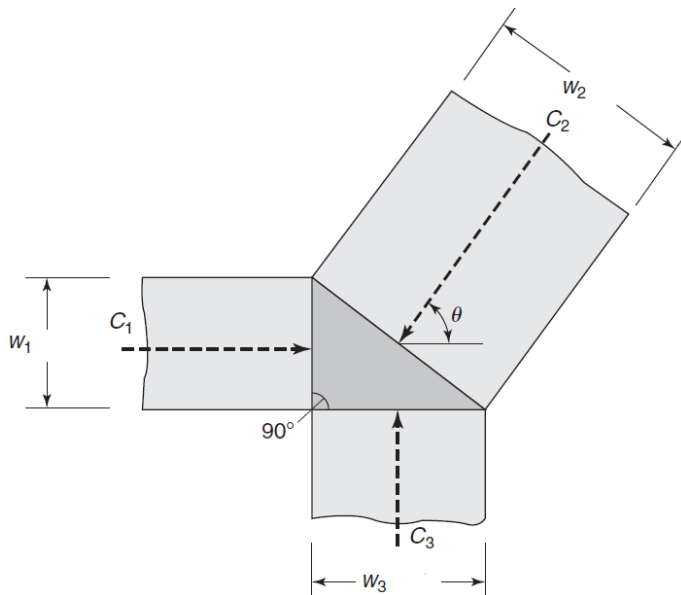


Figure 2.14 – Dimensioning of hydrostatic node

Sometimes however, the length obtainable using a hydrostatic is inadequate to allow for proper anchorage of the tie. An alternative approach available in literature is referred to as the “extended nodal zone”. This is not discussed further as it is not used in this thesis work.

2.4.4.2 Verification in strut and tie model

With the strength and dimensions of the nodes, strut and ties determined, the next step in strut and tie design approach is verification. The verification concerns two important aspects, namely:

- ✓ Verification of compressive stress in struts and nodes,
- ✓ Check for the safe anchorage of ties

Compressive stress check in nodes and struts

This check is to assure that the average compressive stresses from loading do not exceed the maximum permissible stress (σ_{Rdmax}) of the concrete strut or nodal region.

Where the bearing area is too small, a high compressive stress may be the result, and the width of the strut insufficient to resist it. Where this happens, it can be resolved by increasing the bearing surface, thus leading to reduced stresses in the struts.

Check for the safe anchorage of ties

If the stress levels in the strut and node are satisfactory, the ties would next be designed/detailed. Ties are important to control cracking in the member. Tie design includes determining the location and magnitude of tensile forces in the section, selecting the area of steel, ensuring proper anchorage of the reinforcement, checking of mandrel diameter (where reinforcement is bent) and ensuring the reinforcement provided fits within the width. FIB (2010a) recommends distributing the reinforcement over the width of tensile zone, as it would lead to better crack control performance. This distribution however should conform to bar spacing requirements from relevant standards or codes.

2.5 Applications of strut and tie model

Typical examples of D-regions for which strut and tie modeling is used include deep beams, dapped ends, regions around supports or concentrated loads, corbels, openings in structural elements, beam-column joints, wall-base joints etc. The stress distribution in these regions is rather complex (compared to adjoining B-regions), and initiation of structural failures is more prevalent from these regions. In this section, a brief overview of some of these D-regions is discussed demonstrating the use of strut and tie modeling. The influence of detailing on the performance of these regions is discussed briefly. The impact of detailing on the performance of corner joints is discussed in more details in the next chapter.

2.5.1 Corbels

A corbel is a short element that projects out of a wall or column to support a load. It is often used in precast concrete design to support precast beam at the column. It is usually cast monolithically as part of the column or wall. They are designed to provide vertical reaction (or resistance) to concentrated shear loads from beams (see F_{sd} in figure 2.16).

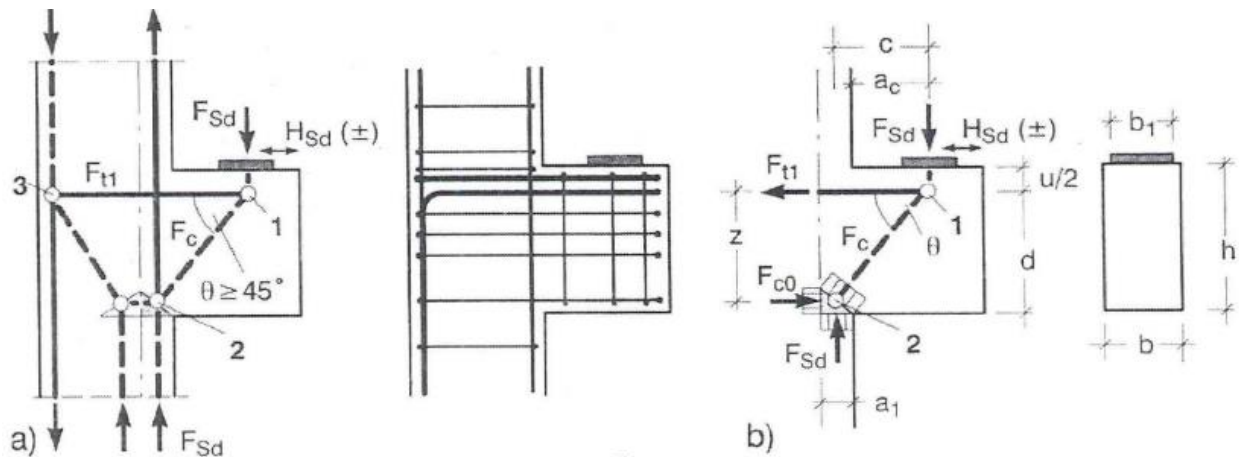


Figure 2.16 – Strut and tie model for a typical corbel (FIB, 2010a)

Structurally, the corbel appears to transmit an opening moment to the rigidly connected column above, and a closing moment to the part of the column below it. The shear span to depth ratio (a_c/d) is usually less than 1.0, and the entire corbel and parts of the columns are thus D-regions. Figure 2.16 show strut and tie modeling of the corbel, with the dashed line representing struts and the bold line representing ties. As seen,

Figure 2.16 shows the main reinforcement aligned to ties from the strut and tie model. In addition, stirrups are used within the D-region (above and below the corbel reinforcement). A good detail noticeable from the corbel is the anchorage of the tie at node 1. The reinforcement extended beyond the node and was made into a horizontal loop just near the front face of the corbel. This ensures proper anchorage of the tie, with the steel strength fully developed on reaching the nodal region. Alternative good approaches could include the use of a bearing plate, steel angle and even large headed studs. Any of these is required for the tie to develop its full yield strength when it is at the node. The use of a horizontal hook would add some confinement to the concrete, and thus improve the behaviour. However, using vertical hook for a corbel is poor detailing practice and could lead to shearing off the concrete at the corbel face. Other possible failure modes that can be attributed to poor detailing include anchorage failure, premature yielding of the tie, failure of the compression strut by crushing etc. Figure 2.17 shows some detailing aspects of a double corbel.

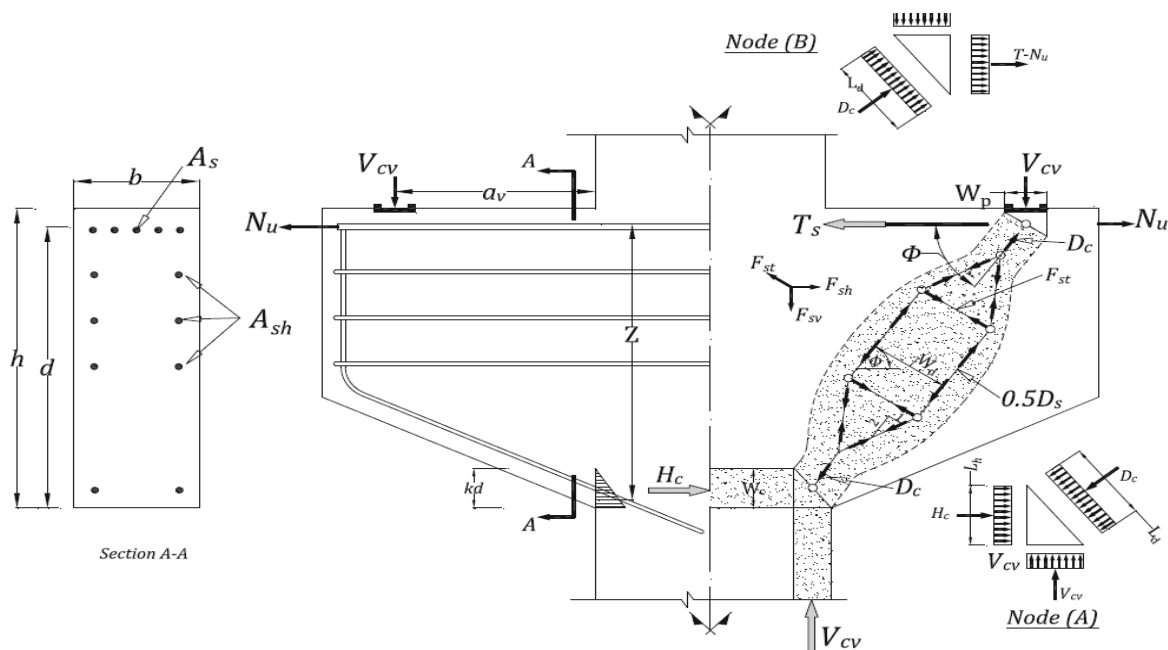


Figure 2.17 – Design and detailing for a corbel (Kassem, 2014)

Figure 2.17 show the strut and tie model utilized for this double corbel on the right, and the structural details on the left of the double sided corbel. A bottle-shape strut is used as the inclined compression member. For verification, the principal compressive stresses caused by the applied load is compared with the maximum stress allowable for the struts and nodes. With the stresses satisfactory, the ties are designed along with the anchorage to meet code requirement. This illustrates how strut and tie models are used for corbel design and detailing.

19

safety factor of 1.125 if designed by strut and tie. Several other studies that compared the result of strut-and-tie models with experimental results gave similar results (though with some scatter). The strut and tie approach in most cases predicted slightly lower strength than the outcomes from the experiments. This validates strut and tie methodology as a useful design tool, and verifies that it predicts safe lower-bound solutions.

2.5.2 Corner Joints

Strut and tie methodology is also a useful tool for the design and detailing of corner joints. Figure 2.18 shows example of corner joints that are common in practice. They are typically found as interior or exterior beam-column joint, wall-base connections, wing walls, abutments etc. The internal stress distributions in these sections are disturbed, and thus the conventional equations for beams, columns or walls are likely to predict inaccurate internal stress distributions. In this section, the application of strut and tie methodology to these sections would be illustrated. The stress state in these joints, the use of strut and tie, and typical detailing practice for these joints are presented. The next chapter of this report however focuses on the detailing aspect of some of these joints, and their behaviour when subjected to an opening moment.

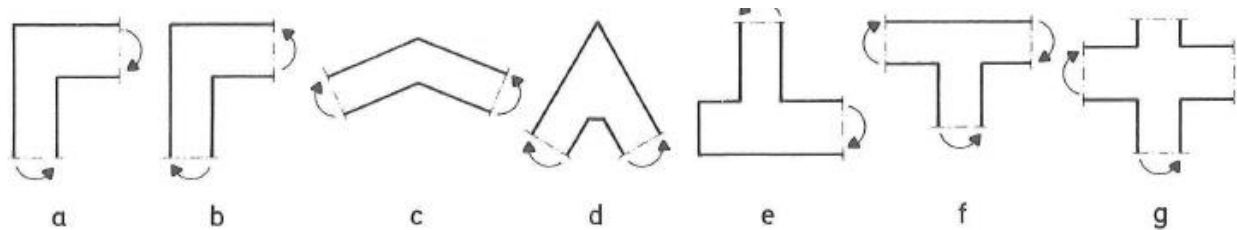


Figure 2.18 – Corner joints type (a) 90° corner subjected to closing moment (b) 90° corner subjected to opening moment (c) obtuse corner subjected to opening moment (d) acute corner subjected to closing moment (e) Retaining wall stem-base joint (f) T-joint and (g) X-joint (Nilsson, 1973)

Being the juncture where different structural elements meet, the stress distribution in corner joints is rather turbulent when compared with adjacent members it is connecting. An example is a beam-column joint where a beam frames into a column. At that juncture, the chord forces (compressive or tensile) in the horizontal beam deviate into the column which is vertical. This deviation by the chord generates radial principal stresses as illustrated in figure 2.19a for a frame corner subjected to pure bending. Depending on the type of bending moment, these radial stresses could be tensile (for opening moment) or compressive (for closing bending moment). Figure 2.19b shows a typical stress distribution for opening bending moment. The scenario is different if the moment is closing.

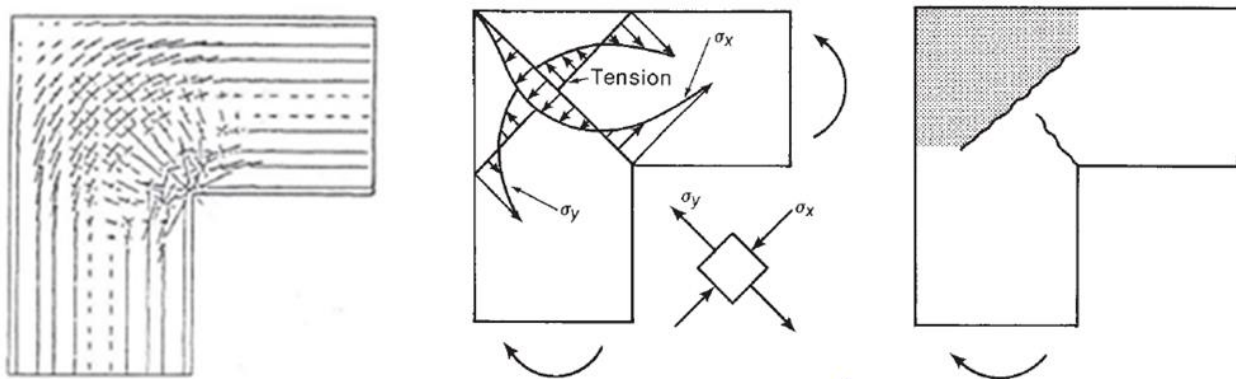


Figure 2.19 – (a) Principal stresses in frame corner subjected to opening moments (b) Elastic stress distribution along corner diagonal (σ_x) and normal to corner diagonal (σ_y) (c) Cracks MacGregor and Wight (2005)

The theory of elasticity is valid for computing the stress distribution in the section prior to the occurrence of cracks. After cracking however, it ceases to be valid. At working stress (after cracking) up to ultimate failure, the joint can be treated like a composite structure made up of concrete and reinforcing steel. This makes it more complicated than the elastic stage which basically treated the section like a homogenous body. Despite being only valid before cracking, the elastic stress distribution nevertheless gives an idea on the behaviour of the structure, and provides guidance on optimal arrangement of reinforcement. After cracking, strut-and-tie methodology becomes a good tool to study the behaviour of the cracked corner joint. The subsequent part of this section illustrates the use of the strut and tie methodology for some commonly used corner joints.

2.5.2.1 Beam-column joints subjected to opening moments

Opening bending moments puts the inner corner in tension, and the outer corner in compression. This type of loading is seen in problems like the corner joint of L-shaped retaining walls, abutments of bridges, outer corner of a liquid retaining structure etc. Studying the principal stresses along the diagonal (figure 2.19b) shows elevated tensile stresses around the re-entrant corner and additional tensile stresses in the middle (core) of the joint. If ideal elastic material behaviour is assumed, the stress at the re-entrant corner (where the principal stress trajectories bend sharply) would be almost infinite. However, being inelastic, the concrete deals with the high localized stress by cracking around the re-entrant corner. Also, the tensile radial stress (σ_y in figure 2.19b) could lead to transverse cracks inside the corner joint as seen in figure 2.19c. Proper detailing of the joint is required to control the cracks, and prevent premature failure of the joint.

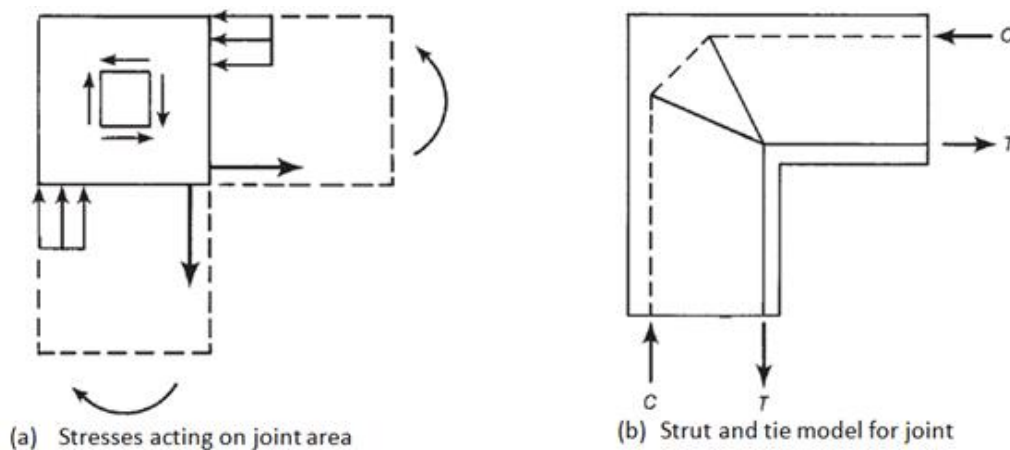


Figure 2.20 – Developing strut and tie model for an opening moment (MacGregor and Wight, 2005)

Strut-and-tie methodology provides a useful tool to model this corner joints. As stated in section 2.3, a suitable strut-and-tie model for this problem would align the struts and ties of the idealized truss parallel to the direction of the principal stresses obtained from linear elastic analysis. An illustration of this is presented in figure 2.20. The stress field in the corner joint from figure 2.19a is represented by a free body diagram in figure 2.20a, with compressive stresses at the outer corner and tensile stress at inner corner. The resultant of these stresses is transferred through the joint using an idealized truss. An example of such truss is shown

in figure 2.20b, where the dashed line represent struts, and the bold lines represent ties. Depending on the engineer, truss models of varying complexity can be assumed. Three possible truss models are presented in figure 2.21, with the first variant relying on a single deviation of the compressive. The detail in figure 2.21b achieves double deviation of the compressive strut by using external anchor plates. Multiple deviation of the compression strut is possible depending on the reinforcement layout in the corner joint as is illustrated in figure 2.21c. Whichever model is used, it should be ensured that the actual reinforcement layout conforms to the assumed model, as the positioning of reinforcement within the corner joint has profound influence on its performance.

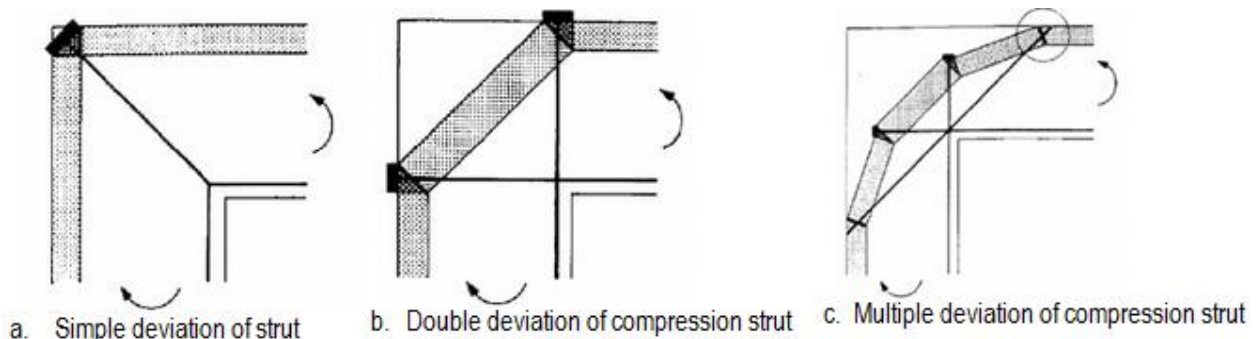


Figure 2.21 – Strut and tie variants for a corner joint (Muttoni, Schwartz and Thurlimann, 1997)

With the strut and tie model, it is easy to visualize the flow of forces in the structure, and thus properly locate the reinforcement. As earlier stated, the reinforcement should be aligned to the direction of the ties from strut and tie, and should be adequately anchored so that the full strength is developed in the node. Typical reinforcement layouts utilize steel in form of loops, hairpins, straight bars, stirrups (straight and diagonal), diagonal bars etc. in various combinations. Figure 2.22 shows some typical detailing layouts for corners subjected to opening moments.

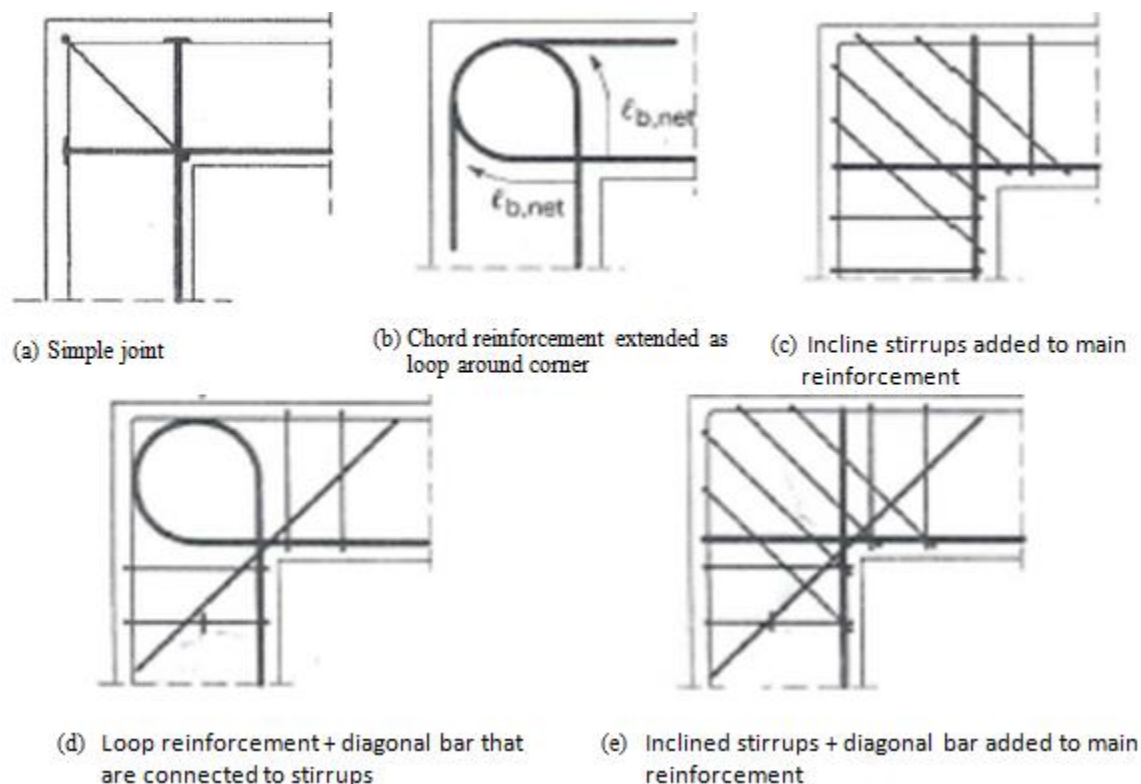


Figure 2.22 – Alternative reinforcement layouts for corner joint

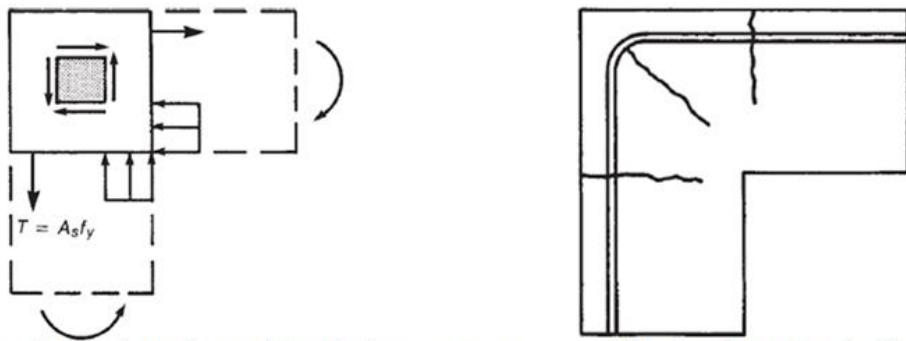
The first is a simple joint in which the tension reinforcement is anchored within the compression chord depth (near the outer face). It is not very effective in deviating the compression chord since it does not enclose it. It is a design that can only resist small opening moment. The behaviour is improved if the tensile chord is extended in the form of a loop around the corner as in figure 2.22b, or when inclined stirrups are used as in figure 2.22c. These layouts reflect better that path of the internal forces in the joint. A drawback of both of these alternatives is seen in the re-entrant corner where the reinforcements diverge from the principal stress in that region by about 45° . Cracking could still occur at that point, causing a reduction in the efficiency of such joint layouts. Further improvement can be achieved by using a diagonal bar inclined around the re-entrant corner. FIB (2010a) recommends the use of inclined bars for all types of re-entrant corners such as those on dapped ends, openings, corbels etc. The use of inclined bars limits the crack growth at re-entrant corners, and consequently slows down crack propagation in the joint. Some detailers use haunch at the re-entrant corner to further reduce the stress concentration.

It is important to balance the requirement from strut and tie with practicability during construction. An instance is the inclined stirrups in figures 2.22c and 2.22e which could be difficult to position (in practice), and could congest the inner corner (when positioned). Such considerations should be put in mind while designing details. The next chapter of this report studies corner joints more in-depth. More information on the behaviour of different details, and its efficiency would be discussed there.

2.5.2.2 Beam-column joints subjected to closing moments

Under gravity loads, the knee (or corner joint) is typically subjected to closing moments. The elastic stress distribution in this loading scenario is opposite the case of opening moments. The radial stresses are now compressive unlike the opening case that was tensile. A schematic showing the action and corresponding

effect is presented in figure 2.23. The flexural action generated by the applied moment acts against an idealized free body (represented by the square corner in figure 2.23a). The free body is thus subjected to uniform shear. The top part is now in tension, while the inner portion around the re-entrant corner are in compression. As was shown in figure 2.19b (for opening moment), almost infinitely large stresses would occur at the re-entrant corner. The stress concentration is however compressive, and the consequent local strains at that points would be absorbed by the plastic behaviour of the concrete. This is unlike the case of an opening moment where the concrete cracked under the stress (which was tensile).



(a) Corner joint subjected to closing moment (b) Crack pattern in the joint

Figure 2.23 –joint subjected to closing moment (MacGregor and Wight, 2005)

Figure 2.23b shows the crack pattern for a corner joint loaded with closing moments. At the edges of the corner, there are cracks mainly from the concentrated shear at the joint. These crack are propagating from outside-in, thus the need for main reinforcement perpendicular. There is also a major crack along the diagonal on the corner originating from around the bent part of the bar, and propagating towards the re-entrant corner. Figure 2.24a illustrates the cause of this diagonal crack. The four forces acting (two tension and compression) introduce shear stresses τ in the disturbed region (see the core area in figure 2.24a). The concrete cracks in a direction perpendicular to the principal stress (σ_1) caused by the shear stresses hence the diagonal crack. Detailing of such joint plays a critical role in controlling such cracks, and in achieving a high joint efficiency.

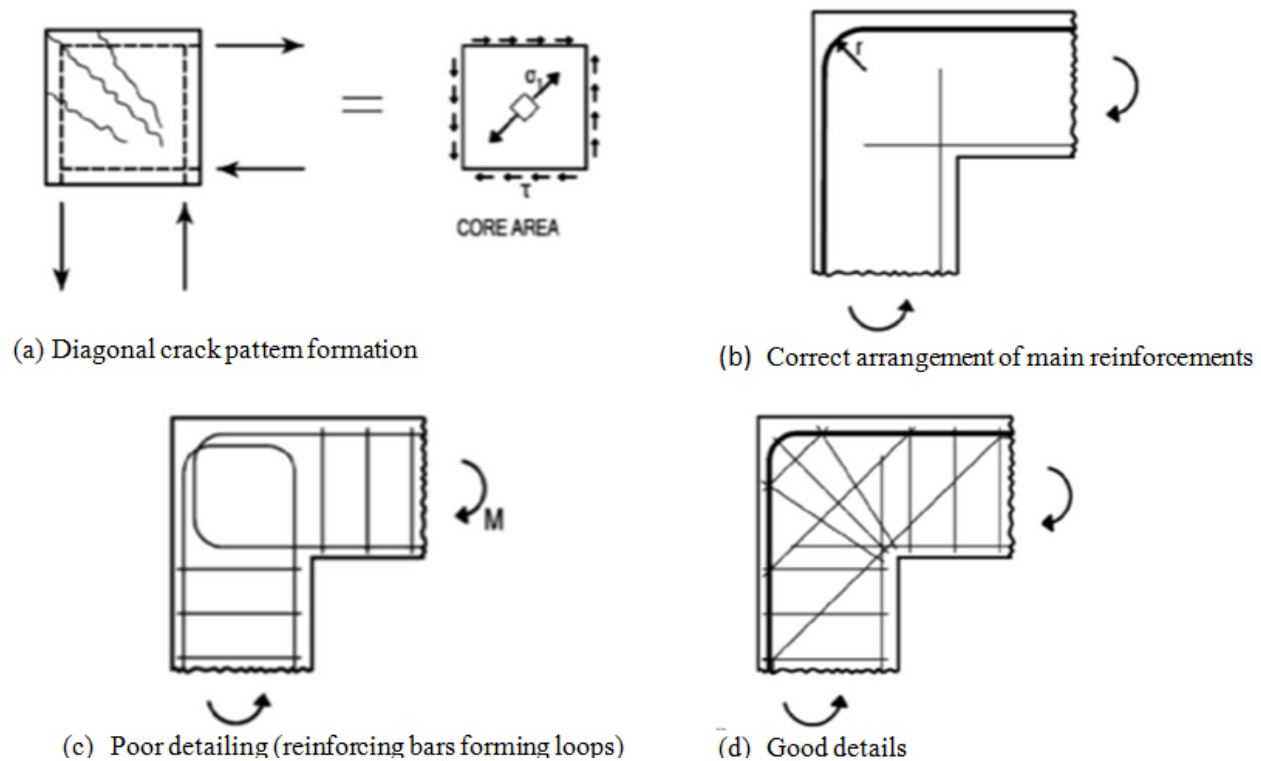


Figure 2.24 – Detailing aspect of the corner joint with closing moment (Hsu and Mo, 2010)

Figure 2.24b shows a good way of laying out the primary reinforcement. The outer bars used as tension reinforcement are continuous and have sufficient anchorage. A key concern however is the likelihood of strut failure due to high bearing stresses within the bend. The corner radius of the main tension reinforcement should be such that it meets eurocode requirements on mandrel diameter, as it has significant influence on local crushing of concrete underneath it, as well as on the failure of the diagonal strut. In the details of figure 2.24b, compression reinforcement is used. The compression reinforcement was extended deep into the joint for at least a length that meets anchorage requirement.

Figure 2.24c shows a detail in which the reinforcing bars form loops at the end of the beam and column. This detail is attractive as the separation of beam reinforcement from that of the column makes construction easier. However, the joint efficiency of this detail could be as low as 34% (Hsu and Mo, 2010). An ideal solution for this joint is shown in figure 2.24d where the tension reinforcement is made continuous. Diagonal bars are placed parallel to the principal stress (σ_1 in figure 2.24a) to control the diagonal cracks. Inclined stirrups are also used, which extend from the re-entrant corner outwards. Also, normal stirrups are used. At first glance, the inclined stirrups seem unnecessary, however, they help in two ways: concrete around the re-entrant corner is subjected to compressive stress concentration. These inclined stirrup would provide confinement for concrete in that area thus improving its compressive strength. Secondly, the concrete just below the curved part of the main reinforcement is subjected to a severe bearing pressure. These inclined stirrups around the corner help to prevent premature failure.

2.5.2.3 T-joints

T-joints are typically found in the base of retaining walls, beam to column connection, pile caps etc. They could be subjected to opening moments; for instance a retaining wall that is subjected to a moment from the retained earth's active pressure; a multi-celled liquid retaining tank filled on one side exerts moments;

or a beam-column joint that typically transfers moments from the beam ends into the column. The load could appear to be opening one side of the T-joint, while simultaneously closing the other. The Strut-and-tie methodology is a good tool for such problems. Figure 2.25 shows three different ways the T-joint of a corner joint (e.g. beam to outer column) is loaded and simple strut and tie models used to represent them:

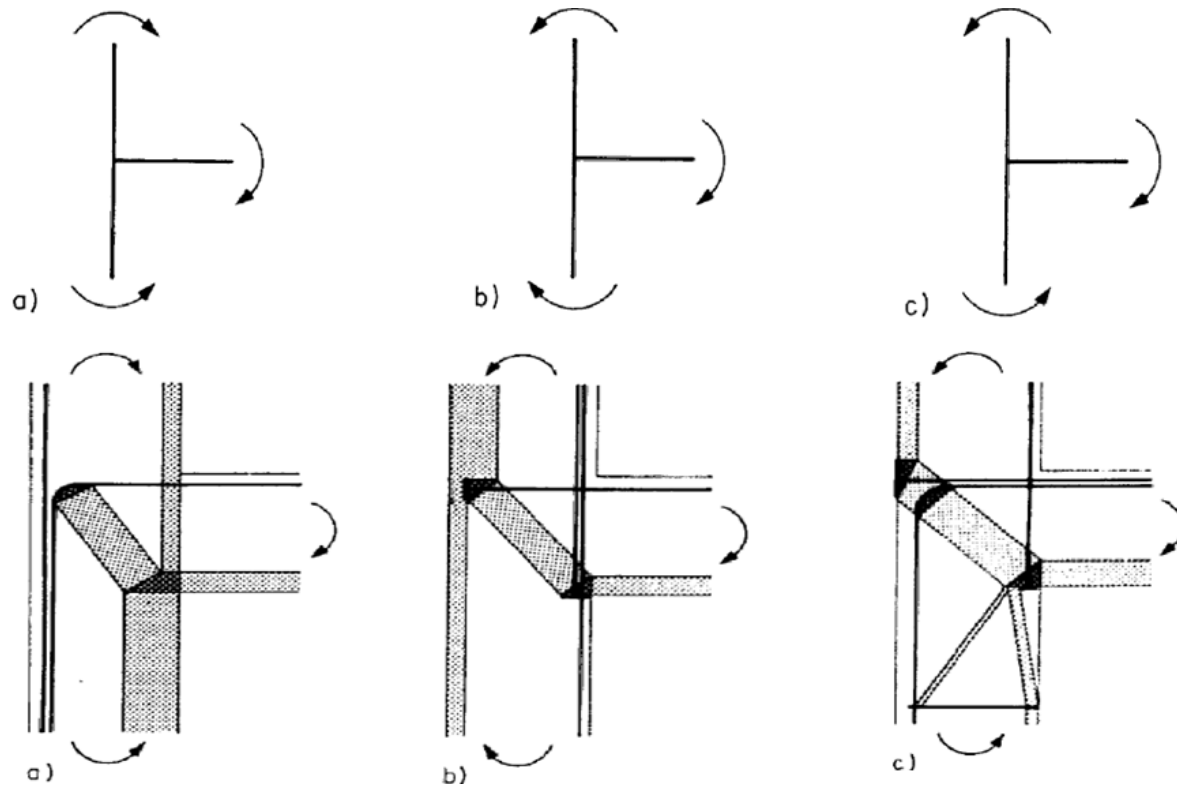


Figure 2.25 – Strut and tie models for some T-joints (Muttoni, Schwartz and Thurlimann, 1997)

Like the other corner joints discussed earlier in this section, the detailing of T-joints is likewise very important. Some typical details are shown in figure 2.26. Though commonly used, the detail layout in figure 2.26a is actually unsatisfactory. The reinforcement from the wall (or vertical member) does not have much interaction with horizontally placed reinforcement in the slab. Thus, diagonal cracking is able to propagate between them, and often results in premature failure. In the detail of figure 2.26b where the reinforcement is made as a hook, the hook made by the reinforcing bar acts in a way to resist (or control) opening of the inclined crack, and it plays a role in anchoring the diagonal strut in the node. The performance of joints, and their failure modes is discussed extensively in the next chapter of this work.

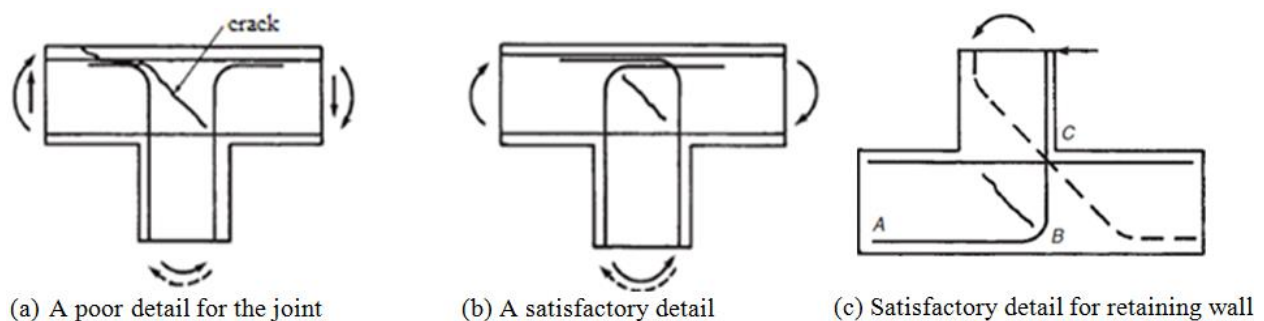


Figure 2.26 – Details for T-joints and retaining wall (Macgregor and Wight, 2005)

There are many literature available on these D-region and on others types not discussed in this report. Examples include X-joints (as found in interior beam-column joint), deep beams, dapped end, ledge girders, pile caps etc. These design of these D-regions follow similar principles as has been discussed in this literature review. With detailing playing a decisive role in the behaviour of D-regions, the next section of this report consider general detailing rules in EC2.

2.6 Detailing

Detailing is often regarded as the process of preparing drawings that show the size and location of reinforcing steel in a concrete structure. It communicates the engineer's design to contractor's supervisors on site who oversee the actual execution. A good detail would make sure that the reinforcing bar and concrete interacts efficiently, and perform satisfactorily to all range of loads it is subjected to in its design life. In this section, a rather short review of some detailing rules are reviewed. Some reasons why reinforcing bars are used in concrete include:

- To carry tensile forces
- To control cracks from flexural and tensile load, as well as imposed deformations.
- To impart strength and ductility to the structure
- For providing confinement to concrete in compression
- To contribute to compressive strength, when concrete alone is incapable of resisting the internal pressures.
- To protect against spalling
- As temporary support for other reinforcing bar during construction, etc.

Concrete structures should be detailed to satisfy safety, durability and serviceability requirements. For D-regions, EC2 section 9.9 clause-1 recommends designing D-regions with strut-and-tie models, and detailing them according to the rules in Section 8. Some of those rules set forth in section 8 of EC2 are summarized in this section.

2.6.1 Some basic rules

Concrete cover of reinforcement

This is usually governed by requirements for durability (mainly the environmental exposure condition) and fire resistance. The requirement for bond and anchorage is also taken into account in design codes. The cover provided should be such that it allows for safe transmission of bond forces (which is a key component of anchorage design). The cover in the region of bar curvature (for bent bars, hooks and loops) also plays a role in preventing bursting. EC2 and other design codes provide guidance on this subject.

Spacing between bars

When multiple bars are used in one layer, or bars are arranged in several layers, they should be detailed in such a way that the reinforcing bars can be fully encompassed by concrete, and the available area adequate for the transfer of forces from steel to concrete. This is only possible if a minimum spacing is provided in which concrete can be poured and compacted for development of bond. Consequently, EC2 requires a clear distance between bars which should not be less than the minimum bar diameter, 20 mm, or maximum aggregate size plus 5 mm. Reinforcing bars can however be in contact along the lap length, and when wire mesh (with twin bars) are used. In summary, minimum bar spacing should be adhered to facilitate the development of adequate bond.

Allowable mandrel diameter

Design codes typically give guidance on minimum diameter to which a bar can be bent to prevent bending cracks in the reinforcement or failure of concrete enclosed in the bends. Table 8.1N of EC2 recommend a minimum mandrel diameter of 4ϕ for 16 mm bars and below, and at least 7ϕ for the bar diameter for bar diameters larger than 16 mm . This mandrel diameter restriction would be useful for our details especially hooks, bends and loops.

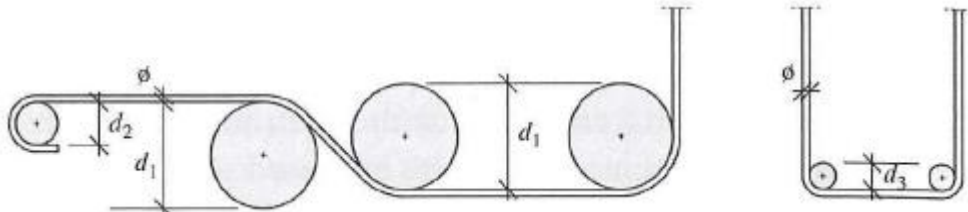


Figure 2.27 – Mandrel diameter defined by fib model code 2010

The FIB model code 2010 recommends even larger minimum mandrel diameters. Figure 2.27 shows the model code depiction of minimum mandrel diameters where d_1 represents bends with a recommended minimum diameter of 15ϕ . An example of such bend was shown in figure 2.24b where a tension tie was used to transmit tension force (from a closing moment) from the beam to the column. A mandrel diameter d_2 (for hooks and loops) of 6ϕ is allowed for bar sizes smaller than 20 mm , and up to 10ϕ for larger rebars. The code allows mandrel diameter d_3 of 4ϕ only for stirrups with bar size smaller than 16 mm . A reduced mandrel diameter is allowed where transverse reinforcement is provided.

Minimum and maximum areas of reinforcement

For small loads acting on a reinforced concrete member, the entire concrete section contributes to strength. A point however comes when the concrete cracks due to tension, and the tensile force is transferred to steel. Where the steel provided is insufficient, the sudden brittle failure could occur. Codes define a minimum reinforcement provision to prevent sudden failure by ensuring the section's resisting moment exceeds the cracking moment. Section 7.3.2 of EC2 expression for minimum reinforcement area ($A_{s,min}$) that should be provided within the tension zone is thus:

$$A_{s,min} = k_c k f_{ct,eff} A_{ct} / f_{yk}$$

Where k_c is a stress distribution coefficient, k is to accommodate for nonlinear stress distribution, $f_{ct,eff}$ is the tensile strength of the concrete at time of cracking, and A_{ct} is the area of concrete in tension prior to the initiation of the first crack. With this minimum reinforcement provided, thermal and shrinkage cracks (that arise on account of restrained deformations) would be better controlled. Rather than resulting in one or a few wide cracks in case reinforcements yield, greater number of distributed cracks with lesser crack width would occur. Such small crack may not impair the serviceability and durability of the structure, and may even benefit from self-healing. Thus this provision is made to prevent brittle failure and wide cracks, as well as to resist forces from imposed deformation (which is related to serviceability limit state design).

Congesting the section with reinforcement could make it difficult to attain good compaction of concrete around the reinforcement. Consequently, a maximum reinforcement ratio is defined expressed as:

$$\frac{100A_s}{A_c} \leq 4\%$$

Where A_s is steel area and A_c is area of concrete.

2.6.2 Bond and anchorage

Anchorage is simply the embedment of steel reinforcement in concrete to carry load (by bond) between the concrete and steel. It can be achieved relying on bond only (for straight bars), or by a combination of bond together with additional resistance provided by:

- Hook, bend and loops
- Welded transverse bar
- Head attached or welded to the end of the bar

Hooks, bends and loops are effective for only bars in tension, and do not contribute to compression anchorage. FIB (2010b) even recommends that they should be avoided in compressed bars as they increase eccentricity of the bar, thus could negatively affect stability. The bearing of the end of a longitudinal bar on concrete however contributes to anchorage for bars in compression, but not for those in tension.

Longitudinal (or straight) bars anchorage is designed by providing adequate anchorage length. The length can however be reduced where bends, hook or loops are provided. For bends and hook however, it should be provided with a straight length (which is at least five times the bar diameter) beyond the curved part as shown in figure 2.28a and b. Note that the curvature of the bars should always conform with the minimum mandrel diameter discussed in the previous section (and section 8.3 of EC2). When anchorage is provided by a welded transverse bar (as in figure 2.28d), the anchorage length can be similarly reduced.

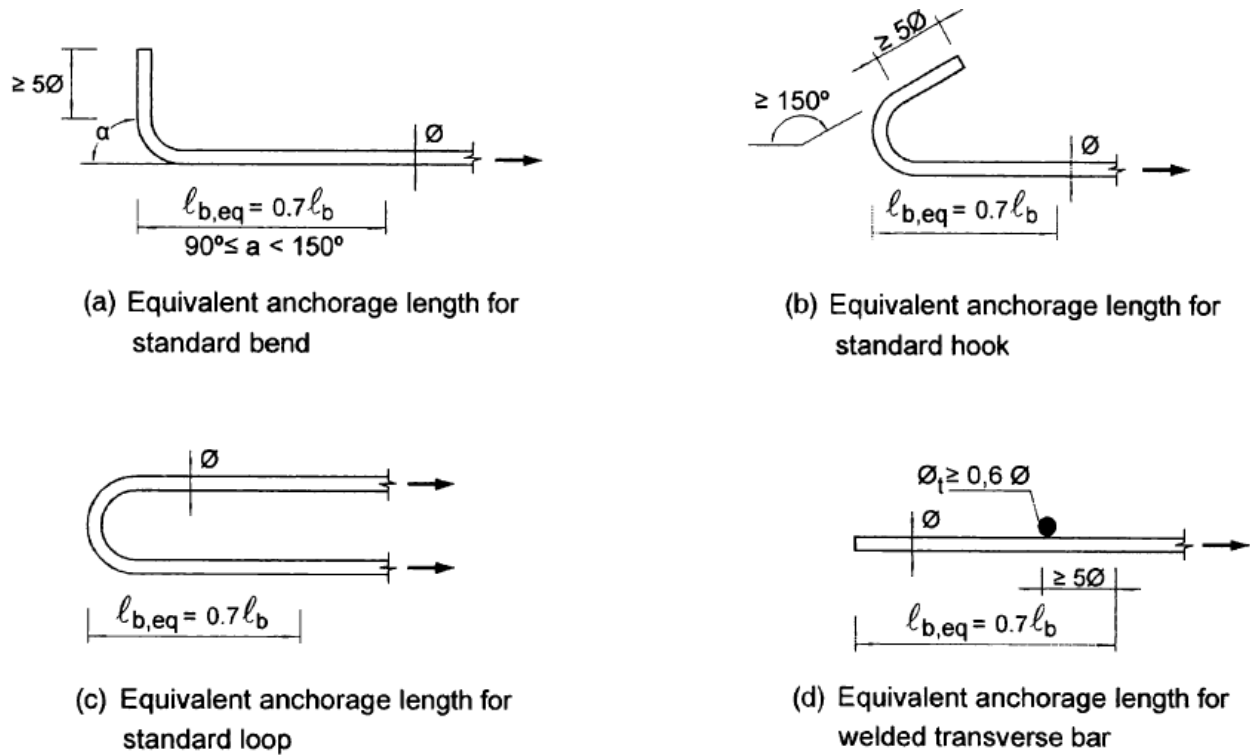


Figure 2.28 - Anchorage methods other than straight bars (Calavera, 2012)

Bond and anchorage length

Bond would be discussed briefly as it is a vital consideration in anchorage design. Experimentally, bond stress can be determined from a pull-out test. For design purposes however, section 8.4.2 of EC2 provides an expression for estimating ultimate bond stress (f_{bd}) which is thus:

$$f_{bd} = 2.25 \cdot \eta_1 \cdot \eta_2 \cdot f_{ctd}$$

Where the coefficient η_1 takes into account the quality of the bond, and η_2 related to diameter of bar used. Figure 2.29a shows a beam in bending with compression in the concrete at the top and tension in steel at the bottom. For this system of internal forces to exist in equilibrium, there must be a bond (or force transfer) between both materials. Where there is no bond, or it is inadequate, the steel would pull out causing the beam to fail. The anchorage of the reinforcing bar thus depend on the bond strength of the concrete, the contact area, and whether the steel is place where good bond conditions exist in the concrete.

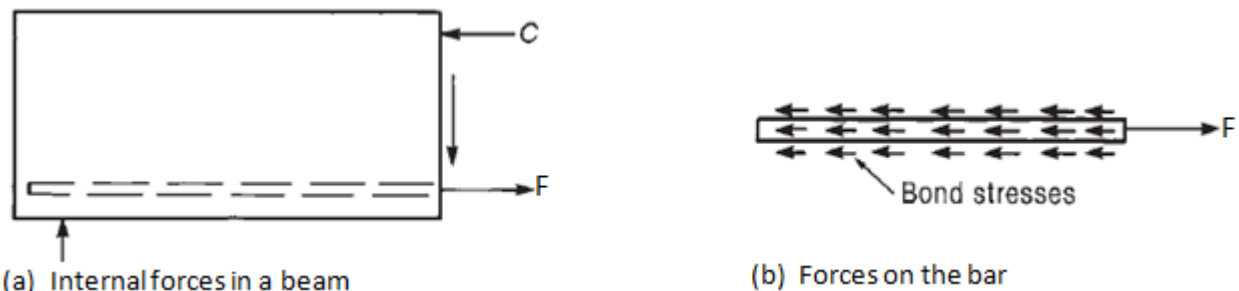


Figure 2.29 – Relating bond with required anchorage length

For equilibrium in the beam, the tensile pull-out force (F) must be balanced by the bond force. The pull-out force is the product of tensile steel stress and its cross sectional area, while the bond force is the product of bond stress and the contact area between concrete and steel within the anchorage length. Mathematically, this is expressed as:

$$\frac{\pi \phi^2}{4} \cdot \sigma_{sd} = l_{b,rqd} \pi \phi \cdot f_{bd}$$

Where ϕ is bar diameter, σ_{sd} is the design stress in the bar, $l_{b,rqd}$ is the basic anchorage length to prevent pull-out, and f_{bd} is an assumed constant bond stress acting over the full bar perimeter, and uniformly along its length. Ultimate bond stress (f_{bd}) can be determined using guidance provided in section 8.4.2 of EC2, while the design stress in the bar (σ_{sd}) is often taken as the design yield strength (f_{yd}) of the reinforcement (equal to $f_{yk}/1.15$). Thus, the basic required anchorage length ($l_{b,rqd}$) is expressed as:

$$l_{b,rqd} = \frac{\phi \sigma_{sd}}{4 f_{bd}} \quad \text{or} \quad l_{b,rqd} = \frac{\phi f_{yk}}{4.6 f_{bd}}$$

Any of the above expressions can be used to compute the basic anchorage length for straight bars. For bent bars, the measure for design length should be along the center line of the bar. There could however be beneficial effects from bar shape (i.e. for bent, hooked or looped anchorage), confinement by transverse reinforcements, pressure acting transversely to the splitting plane, welded transverse bars etc. Thus, EC2 make provision to reducing the basic anchorage length by introducing some coefficient. The design anchorage length from equation 8.4 of EC2 is thus expressed thus:

$$l_{bd} \geq \alpha_1 \cdot \alpha_2 \cdot \alpha_3 \cdot \alpha_4 \cdot \alpha_5 \cdot l_{b,rqd} \geq l_{b,min}$$

Where $\alpha_1, \alpha_2, \alpha_3, \alpha_4$, and α_5 are defined in Table 8.2 of EC2 and $l_{b,rqd}$ is the basic anchorage length. $l_{b,min}$ is also defined in equation 8.6 and 8.7 of EC2. α_1 accounts for shape with reduction possible for bent bars and none for straight bar. α_2 accounts for concrete cover with potential reduction of design anchorage length for large cover. α_3 which accounts for transverse cracking is discussed in next paragraph. α_4 accounts for possible benefits from welded transverse bar along the design anchorage length.

As spalling and longitudinal cracking are key concerns in anchorage design, transverse reinforcement should be provided where needed. Transverse reinforcement has the benefit of providing confinement. The transverse reinforcement could be stirrups or ties perpendicular to the bar, and enclosing the tension reinforcement and compression zone. It is important that they enclose the tension reinforcement as transverse reinforcement placed inside the anchoring bar is usually ineffective leading to $\alpha_3 = 1.0$, thus no benefit in terms of reduced anchorage length (Hendy and Smith, 2007). However, when placed outside i.e. between the anchoring bar and the concrete surface, α_3 could reduce to a minimum of 0.7. α_5 accounts for benefit gains where there is pressure acting transversely to the plane of splitting. This also provides compression to the concrete, and thus its beneficial effect can be considered leading to further reduction in required anchorage length.

2.6.3 Splicing of bars

Splicing (or lapping) of bars is often required to transfer forces from one bar to another. Splicing is achieved by lapping of joints, welding or mechanical devices (like couplers). EC2 requires that the detailing of laps

is such that it assures force transfer from a bar to the next, without causing spalling of concrete near the joint, nor should it lead to large cracks. Laps should not be placed where high stresses occur, and they should be staggered (not concentrated around a point). Expression for the required lap length is:

$$l_0 \geq l_{b,req} \cdot \alpha_1 \cdot \alpha_2 \cdot \alpha_3 \cdot \alpha_4 \cdot \alpha_5 \cdot \alpha_6$$

Where $\alpha_1, \alpha_2, \alpha_3, \alpha_4$ and α_5 are about same to those for anchorage length defined in the last section, and α_6 is a coefficient that takes into account the percentage of lapped bars relative to the total cross sectional area. For bars in tension, provision of transverse reinforcement around the lap zone is recommended to keep splitting forces under control and to restrict potential longitudinal cracks. For bars in compression, transverse reinforcement is also required where spliced. FIB (2010b) notes that lap of compressed bar typically fail by spalling of concrete cover around the splice ends. This happens because of high pressure at those end sections. To cater for this splitting forces, stirrup is placed before the beginning of the lap, and within 4ϕ of the lap length's end. Further information can be found in Eurocode when welded lap or mechanical device is used.

3. Behaviour and detailing of corner joints

This chapter of the report presents literature review into the impact of detailing on the performance of corner joints. General rules in codes pertaining to detailing was discussed briefly in the last chapter. However, those were just ‘rules’, and do not answer questions like “what is the best way to detail a corner?”, “how efficient is a proposed detail” etc. These questions constitute the essence of this chapter.

This section focuses mainly on available experimental works carried out on corner joints. Most of the experimental data and photographs in this chapter are from the work of Nilsson (1973). That author (I.H.E. Nilsson) undertook extensive experimental work on various joints (90° corners, obtuse and acute angled corners, T-joints, X-joint and retaining walls). With 78 different joints loaded to failure, the work provided insight into how corner joints with different reinforcement layouts, behave when subjected to opening moments. Other experimental works by Nabil, Hamdy and Abobeah (2014), Campana, Ruiz and Muttoni (2013) and Abdul-Wahab and Al-Roubai (1998) were also consulted.

The layout of this chapter is thus: the design criteria for corner joints is discussed first in next section. The reasons for failure of corner joints are then discussed in section 3.2. A typical experimental setup is discussed in section 3.3. Despite being researched by different individuals, and at different times, the experimental set-up, parameters measured etc. are comparable. In section 3.4, the behaviour of corner joints is discussed, giving insights into the behaviour and efficiencies of structural details, the failure mode that dominates, crack patterns etc.

3.1 Detailing requirements for corner joints

Corner joints are critical parts of the structure where elements intersect and force is transferred. From Park and Paulay (1975) and Nilsson (1973), the fundamental criterion a satisfactory corner joint should comply with are strength, ductility, crack control and ease of fabrication. These are discussed thus:

Strength: The joint should possess a moment capacity that is at least equal to that of adjoining members. The joint should not be the weak spot of the structure i.e. it should not prevent adjacent members from developing their full strength. A desirable scenario would occur where an adjacent beam (for instance) fails after reaching full capacity, with the joint still intact. This requirement should be taken into consideration when designing the reinforcement layout. ‘Joint efficiency’ is a term used in literature to express the ratio of the failure moment of the joint compared to that of adjacent members framing into it. This concept forms the basis of comparison of different structural details in this work.

Ductility: With a joint efficiency of greater than 100%, the joint would not govern, and plastic hinge formation would occur in one of the connected members. However, where this required efficiency is not met, brittle failure of the joint should be avoided. The joint should be capable of redistributing internal forces to adjacent members thus preventing brittle failure. For a statically indeterminate structure that is ductile, a redistribution of internal forces would occur, with adjacent members then carrying more load. Thus ductility is valuable in this case. However, for statically determinate structures like retaining walls and bridge abutments, there is no redistribution of moment. Strength (or moment capacity) remains the critical issue for such structures.

Ductility in reinforced concrete includes issues like compression reinforcement (to confine concrete), reinforcement layout (lapping or splicing), limiting stresses in concrete and steel, anchorage and bond, provision of transverse steel etc. These are all aspects influenced by detailing.

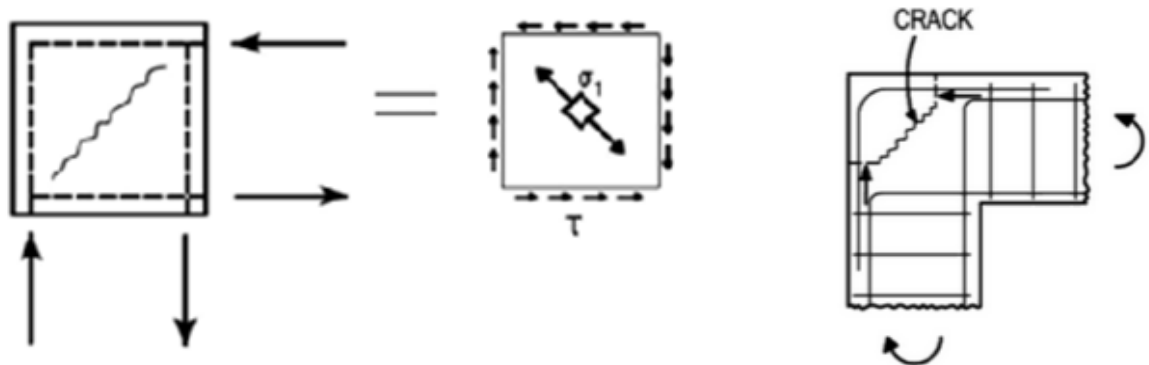
Crack width control: In section 2.5 of this report, cracking in corner joints were shown arising from stress concentration at a re-entrant corner and transverse tension stresses within the joint. A good detail should be able to control those cracks to an acceptable limit. Excessive crack widths fail the serviceability criterion, and could have impact on the capacity. Cracks reduce the effective concrete compressive strength, and could promote moisture ingress which would result in rebar corrosion. An objective of detailing is controlling the initiation and propagation of these cracks.

Ease of fabrication: A good detail should be easy to fabricate, and should not negatively affect the ease of placing and compacting concrete. Easy-to-make and friendly-for-construction layout of reinforcing bars that meets requirement should be the goal of detailing.

3.2 Failure modes of monolithic concrete joints

In order to assess the behaviour of corner joints, it would be necessary to understand the typical modes in which their failure do occur. The amount of reinforcement, and how it is laid out influences the failure mechanisms that could develop in a joint. CEB (1996) and Nilsson (1973) presents several modes discussed in this section.

Diagonal tension cracking failure: occurs in the core of corner joints due to the presence of quite large shear forces acting concurrently with the applied opening moments. This mode of failure is illustrated in figure 3.1a.



a). Model depicting crack pattern

b). A poor layout with diagonal crack

Figure 3.1 – Diagonal tensile failure illustration (Hsu and Mo, 2010)

The flexural action generated by the applied moment acts against an idealized free body (represented by the square corner in figure 3.1a) subjected to uniform shear. This combined action of shear and flexural stresses results in the tensile principal stress σ_1 inclined at an angle in figure 3.1a. Diagonal tensile cracking occurs in a direction perpendicular to σ_1 once the transverse tensile stresses exceed the concrete tensile strength. A diagonal crack is still seen in figure 3.1b despite many reinforcement being located in the vicinity. The crack occurred because of the way the reinforcement was laid out. Ideally, reinforcement representing tensile ties should be oriented in the direction of the principal stress (σ_1) if they are to be effective in controlling the crack.

Diagonal tensile cracking failure is a rather brittle failure, and could lead to premature failure of the structure. As would be seen in the corner joints discussed in section 3.4, most joints that fail in diagonal tension cracking tend to have rather low joint efficiencies. Diagonal tension cracks should be taken into consideration when detailing any joint type subjected to opening moment.

Splitting crack failure: This failure mode occurs where the reinforcement interacts with concrete in such a way that substantial tensile stress occur perpendicular to the direction of the reinforcing bar. This could result in splitting of the concrete, resulting in a rather brittle failure. This failure mode is more associated with closing moments, thus not discussed further.

Anchorage failure: occurs from failure to properly anchor reinforcement (or ties) in nodal zone, resulting in insufficient interaction between the concrete and steel. When the anchorage length is smaller than required, the bar could actually be pulled out leading to a rather brittle type of failure. Spalling of the concrete around (i.e. just outside) bent reinforcing bar, and local crushing of the concrete under the bent bar lead loss of bond strength, and could thus lead to anchorage failure. Alternating loads acting on the joint could also cause gradual reduction of bond strength and reduction of effective anchorage length. In these and several other ways not mentioned, anchorage failure could occur leading to sudden failure of the structure.

Avoiding anchorage failure is thus a critical part of designing details. EC2, FIB model code 2010 and many other standards and codes provides guidance/rules on anchorage design.

Yielding of reinforcement: This failure mode is caused by yielding of the reinforcement within the corner joint. Apart from large deformations that result, secondary cracks could also occur prior to failure. It is an undesirable failure mode if yielding occurs in the corner joint, with the adjoining member still intact.

Crushing failure of concrete: Concrete crushing could occur along the compressed diagonal concrete strut. For bottle-shaped struts, transverse tensile stresses occur that results in cracking and reduced compressive strength. Crushing caused this way can be prevented or delayed if joint confining steel is provided. Another location where crushing could occur is around bent reinforcements, especially if the radius of curvature used is small. Complying with the code requirement for minimum mandrel diameter could prevent this from happening.

Fracture of reinforcement around bend: This mode of failure can occur if very small radius of curvature is used in the bent portion of reinforcing steel during construction. If bent sharply, reinforcements could have cracks and reduced deformation capacity, and thus more susceptible to failure. Complying with minimum mandrel diameters in codes could prevent this failure type.

3.3 Typical experimental programme

To aid a study of the behaviour of corner details, an experimental programme is first designed. This process usually includes decision on the number and type of specimen to be used, materials strength and properties, setup of the tests, parameters to be measured, and how they would be measured. Finite Element method (which will be used in my own work) is essentially a computer simulation of such experiment. The key components of the experimental programme is discussed thus:

Specimen: The specimen required depends on the objective of the study. The most common corner specimens studied in literature include 90° corners, obtuse angled corners (usually between 120° to 135°), and acute angled corner (usually 60°). Important attribute to be decided include the specimen dimensions (length, width and thickness), reinforcement layout (including main reinforcement, stirrups etc.). An important (though seemingly minor) aspect is the way specimen are identified with number and grouped. This specimen numbering and grouping is made in such a way to reflect the objective to be studies, and the order/batch in which they would be tested.

Materials: Knowledge of the properties of materials used is crucial to the study. As an example, stress in concrete may not be readily known in an experiment. However, it may be possible to measure the compressive strain. Using the constitutive relation $\sigma_c = E_c \cdot \epsilon_c$, it can be computed where the material properties are known. Such information can give idea of when yielding occurs, how internal stress redistribution takes place etc. Important material properties in such tests include the elastic modulus, material strength (tensile and compressive for concrete and steel) etc.

Test setup: Examples of experimental setup for investigation into corner joints is illustrated in figure 3.2. Two ends of the specimen are placed on a support, with at least one being a roller. Several measuring instruments are placed at specific parts of the specimen, and static load is applied in incremental steps till failure occurs. A calibrated hydraulic jack is usually used for applying load to the specimen. After each load step, a time interval is usually allowed before the next load step to ensure that crack propagation had stopped, and that conditions within the specimen could be regarded as stationary. Where possible, the test could be performed using a deformation controlled approach. This provides more information than load controlled experiment, especially on the phase after the peak load.

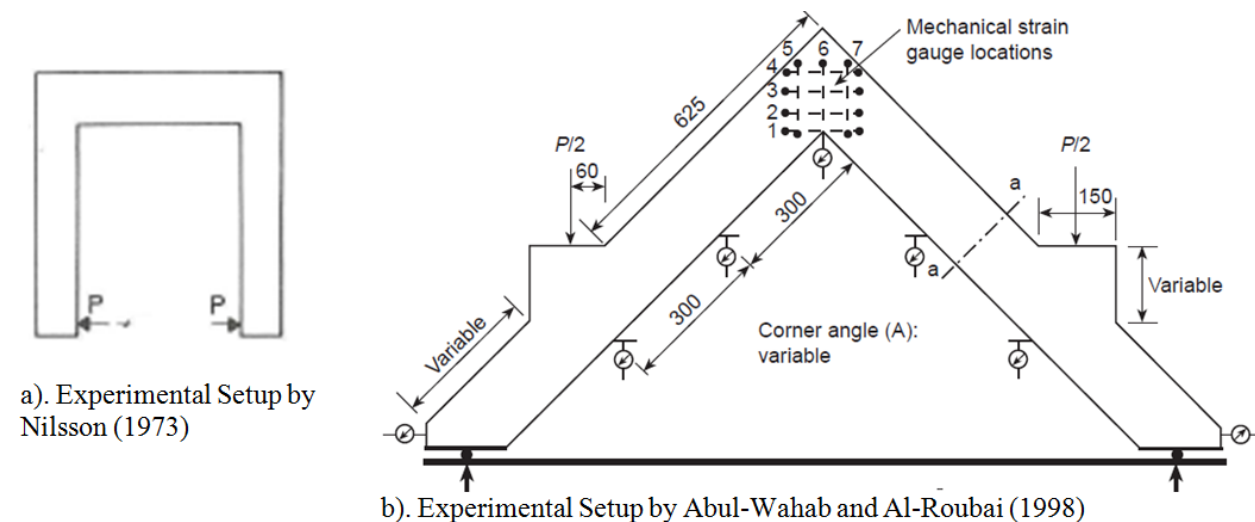


Figure 3.2 – Example of experimental setup for corner joint investigation

Measurement and data collection: In addition to the applied load which is recorded at each load step, several other data is collected for study during the experiment. The most common ones are discussed below:

Reinforcement strains: Strain gauges placed upon bars at specific points of the structure measure its strain. Reinforcement strain data could be used to compute the stress where it is located, and this would give idea

whether the reinforcement yielded or not before failure. Reinforcement strain could also give an indication on the effectiveness of the anchorage.

Concrete strains: Strain gauge mounted on the concrete surface are also used to monitor concrete strain. In his publication, Nilsson (1973) used concrete strain data to verify Bernoulli's linear strain assumption.

Deflection and corner deformations: Deflection at the level of load (and at other points) is usually measured with dial gauges, displacement transducer etc. Also, inclinometers are used to measure relative rotation.

Crack width measurement: Photogrammetric measurements are usually made after each load step to trace crack development, and measure the crack width during experiment. Several of such photographs would be examined in the next section of this chapter of the report..

3.4 Behaviour of different corner joint details

Many recommendation have been made in literature on how corner joints should be detailed. But how do we know which is more efficient? How does a chosen reinforcement detail affect the behaviour and capacity of the structure? This section of the report discusses these questions based on some experimental work that has been done. The work of Nilsson (1973) would be discussed mainly, and extra perspectives added from other literature.

3.4.1 Nilsson (1973)

I.H.E. Nilsson's work is important mainly because it covered a wide range of corner types, but also because he provided photographs (from his experiments) that vividly illustrate the joint behaviour at failure. Some aspects of his research work is discussed in the next four sub-sections. All pictures in this section are taken from this author work's (except otherwise cited).

3.4.1.1 90° angled corners

Several reinforcement layouts were cast into the 90° angled specimen and loaded to failure. The behaviour of specimens with these layout and their respective joint efficiencies is discussed here.

The traditional reinforcement layout: Figure 3.3a shows illustrates this layout, and a picture of it is shown in figure 3.3b. When loaded with opening moments, the inner (re-entrant) corner cracks at very low stress due to tensile stress concentration at that point. With further loading, another crack initiates around the bent part of the main reinforcement. This crack grows propagating inwards till the outer part of the corner becomes detached. Photograph of this crack pattern is shown in figure 3.3c.

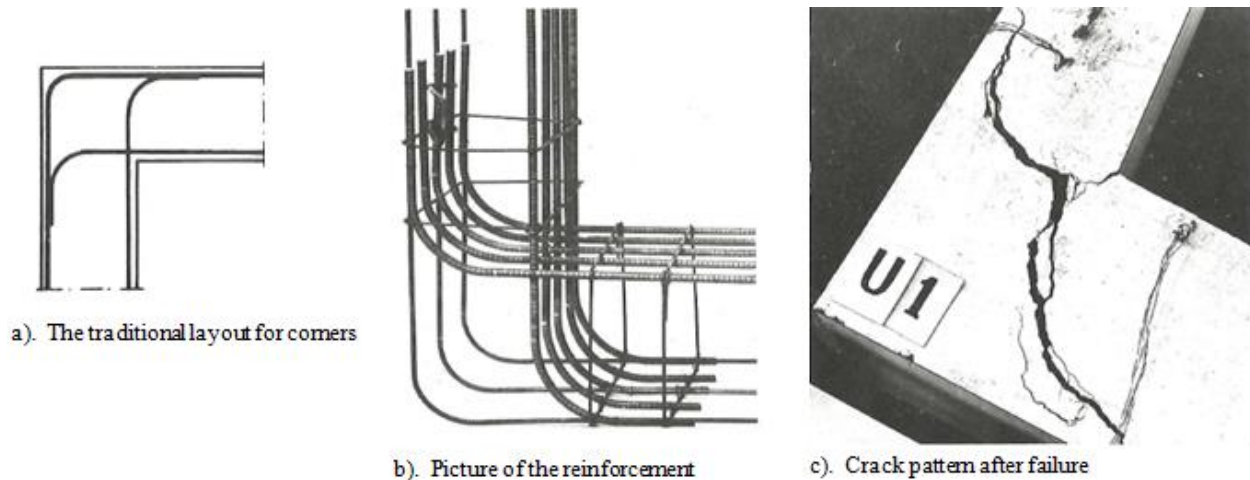


Figure 3.3 – The tradition reinforcement layout (Nilsson, 1973)

While this corner joint failed with large deflections measured, there were no signs of damage on the adjacent connected members as failure occurred at a moment around one-third of the calculated moment (32% joint efficiency). Furthermore, from reinforcement strain measurement, the computed steel stress was below 50% of its yield stress, thus not yet yielded. Failure occurred because the concrete could not carry the principal tensile stress (σ_1 in figure 3.1), and there were no reinforcement to carry it. This is a diagonal tension cracking failure. Overdesigning the main reinforcement or compression reinforcement would not prevent it either as they are not located where the crack would initiate. Thus there is need for improvement.

Hairpin reinforcement layout: This reinforcement layout is illustrated in figure 3.4a, with a photograph in figure 3.4b. In the traditional reinforcement layout earlier discussed, notice that the crack leading to diagonal tension failure initiated around the bent reinforcement. The hairpin layout improves this detail by removing that bend.

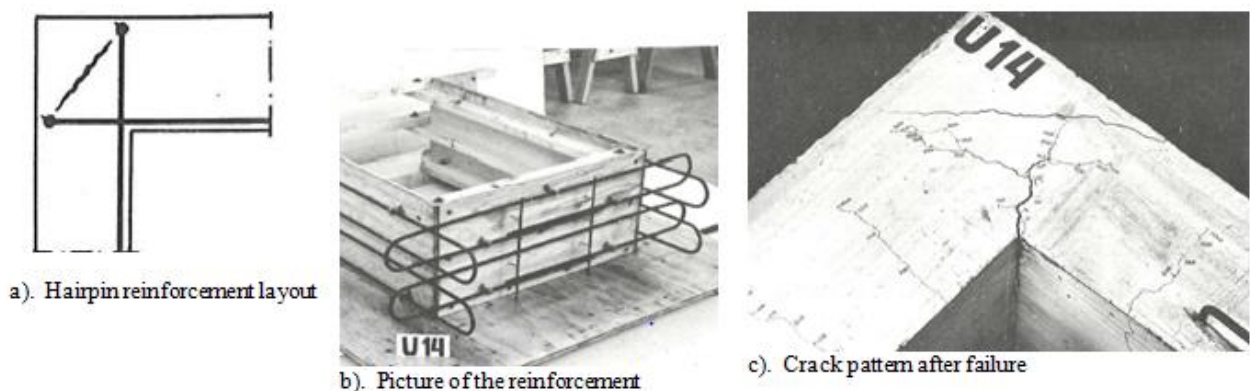


Figure 3.4 – The hairpin reinforcement layout (Nilsson, 1973)

Like the result of the traditional layout, this one also fails due to diagonal tension cracking as shown in figure 3.4c. However, it needed larger applied loads to failures, thus giving a higher joint efficiency of 68%. Diagonal cracking was forced to the corner of the hairpin (in comparison with the traditional layout) thus resulting in the larger capacity of this joint.

Reinforcement with loops: Figures 3.5a and b illustrates the looped reinforcement layout. When the applied load was still low, a corner crack occurred at inner (re-entrant) corner. Upon further loading, this crack divided and propagated along the loop. The concrete portion outside the loop was detached as seen in figure 3.5c. Compared with the earlier two reinforcement details earlier discussed, this gave a higher joint efficiency of 77%.

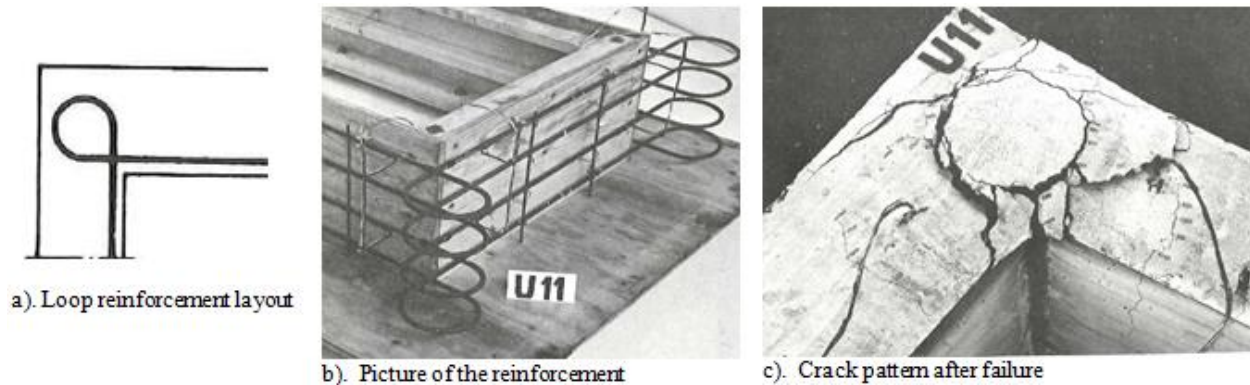


Figure 3.5 – The loop reinforcement layout (Nilsson, 1973)

The higher strength is on account of how the loop works. As the corner opening moment increases, the loop tends to tighten, thus restraining the concrete within it. This way, diagonal tension within the loop is prevented thus the improvement in moment capacity.

At the time of failure, the reinforcement at the corner section in this case had reached yield. But why did it yield without attaining 100% joint efficiency? Nilsson (1973) gives the reason as being on account of a “reduced lever arm to the compression zone resultant in the corner”. Thus, there is a potential of increasing the joint capacity if the loop can be taken out nearer to the corner. Two variants of looped details are shown in figure 3.6. The first with the loop rather far from the outer corner fails due to diagonal tension with the outer corner being pushed off. The second improves the detail by pushing the loop towards the outer corner as much as possible, and further filling the corner with a bent bar. With this improvement, a joint efficiency of 87% was achieved by Nilsson (1973).

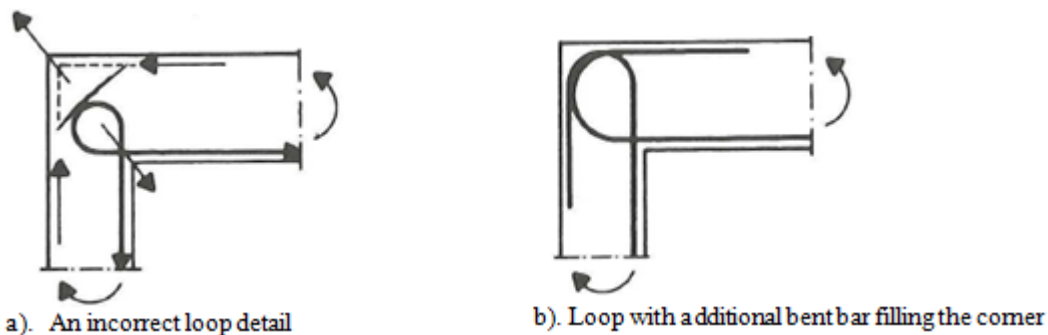
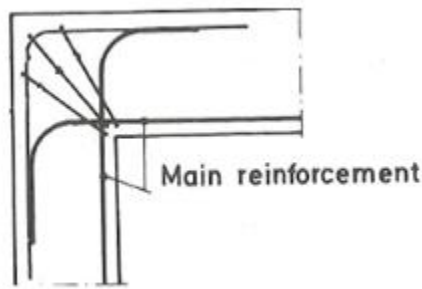
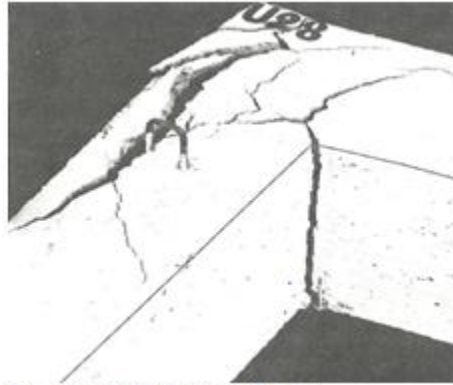


Figure 3.6 – Improving the loop reinforcement layout

Corner detail with stirrups: Having seen how diagonal tension cracking affects joint capacity, it is desirable to either prevent it or control it. A logical solution would be using inclined stirrups in a direction of the principal tensile stress (i.e. perpendicular to the crack direction) as illustrated in figure 3.7a. The crack pattern at failure is shown in figure 3.7b.



a). Tradition layout with stirrups

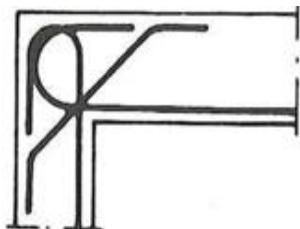


b). Crack pattern after failure

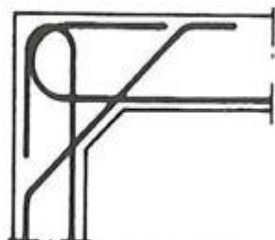
Figure 3.7 – Corner joint with stirrups (Nilsson, 1973)

This layout gave a joint efficiency of 79% thus significantly increasing capacity when compared to the case without stirrups in figure 3.3a. The use of stirrups obviously strengthens and improves performance of the corner joint. At failure, though neither the main reinforcement nor the diagonal stirrups yielded, diagonal cracks still occurred, in addition to the cracks at re-entrant corner.

Improved loop with diagonal bar at re-entrant corner: The looped detail in figure 3.6b prevented diagonal crack but still did not achieve 100% joint efficiency. In this new detail, that detail is further improved by adding a diagonal around the inner corner to control the cracks that normally initiate at the re-entrant corner, thus preventing separation of the inner corner. This detail is illustrated in figure 3.8a. A haunch is introduced in figure 3.8b. Both sections were loaded till failure.



a) Modified corner with diagonal (no haunch)



b) Modified corner with diagonal (haunch present)



c). Crack pattern for corner without haunch

Figure 3.8 - Improved loop with diagonal bar at re-entrant corner (Nilsson, 1973)

Figure 3.8c shows the crack pattern just prior to failure. Notice how the corner joint remain intact while the adjacent member is almost fully cracked. At failure, yielding of the reinforcement occurred in the members outside the corner joint. Thus, both for haunched and un-haunched joints, the corner joint were stronger

than the connected members. Nilsson (1973) reported joint efficiencies between 114% to 123%, depending on the ratio of diagonal bar area to the main reinforcement area. The higher joint efficiencies were attained when the area of the diagonal bar area is about half that of the main reinforcement. The slightly lower joint efficiencies were obtained as the ratio of inclined bar area to main reinforcement area increased.

In comparison with the earlier discussed details, both of these details in figures 3.8a and b also gave much lower crack widths at the re-entrant corner. This is on account of the stiffening effect on the corner by the inclined bar. The haunch corner gave the lowest crack width, but the moment capacity and joint efficiencies were about the same. Thus the only benefit of the haunch over the corner without haunch is the lower crack widths. With increasing haunch size, the corner crack width decreased and vice versa. In practice, the joint without haunch may be preferable since a haunch actually complicates shuttering requirement during construction.

3.4.1.2 Obtuse and acute angled corners

Many corner joints occur that are not at 90°, and are similarly subject to stress disturbance; this section of the report discusses its behaviour and detailing based on the outcome of Nilsson (1973) experiments.

Obtuse angled corner: despite the connected element at the corner being at a different corner angle, the elastic stress distribution is strikingly similar to that of a right-angled corner as shown in figure 3.9 for a section subjected to opening corner. As before, tensile stress concentration (σ_x) occurs at the inner re-entrant corner, and transverse tensile stresses (σ_y) within the joint.

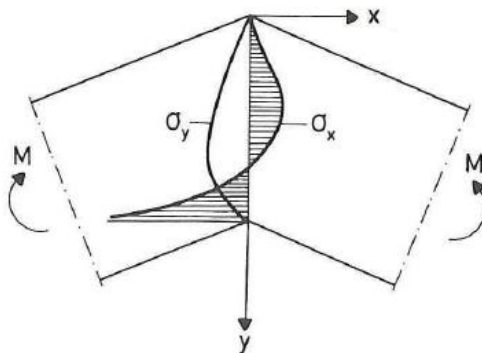


Figure 3.9 – Elastic stress distribution for an obtuse-shaped corner (Nilsson, 1973)

Nilsson (1973) performed tests on several obtuse-shaped corner specimen some of which the reinforcement detail and crack pattern are presented in figure 3.10. The joint efficiencies, crack initiation and propagation patterns etc. are comparable with the 90° corner case. For the traditional reinforcement layout (figure 3.10a), diagonal tension cracking failure occurred with the crack following the outline of the bent reinforcement (figure 3.10b), and the outer compressive portion being pushed off. Failure occurred because the tensile stresses inside the joint (σ_y) exceeded that of the concrete, and was not resisted by steel. The main reinforcements were below the yield stress and failure was sudden, with only a 49% joint efficiency attained for this layout. Even if compression reinforcement were provided, this failure would still have occurred.

A much higher joint efficiency of 88% was achieved with the improved loop detail in figure 3.10c. This improvement is on account of the loop which tightens as the corner opens, thus compressing the concrete within the loop and restraining the splitting tensile forces. The bent bar on the outer part of the loop takes the loop to the corner so as to maximize lever arm, and thus moment capacity. As with the 90° corner case,

the reinforcement yielded at the corner at failure. But why did it fail before reaching 100% joint efficiency? Failure occurred on account of the wide crack at the re-entrant corner. This crack propagated inwards, and divided along the looped reinforcement, and grew till failure occurred. If this re-entrant corner crack can be controlled, even higher efficiencies would be achieved. The next detail in figure 3.10e achieves just that.

In figure 3.10e, the diagonal bar passing along the re-entrant corner stiffens it, thus controlling the crack propagation. This way, wide cracks occurred in the connected beam while the corner joint was still intact at failure. Depending on the ratio of the inclined bar to the main reinforcement, joint efficiencies in excess of 120% were achieved for some specimen. In a particular sample where the ratio of the inclined bar was too small, the inclined bar yielded before failure, and the corner failed with 88% joint efficiency (just as the case without diagonal bar). Nilsson (1973) established an approximate ratio of 50% if the inclined reinforcement is to fail about the same time bending failure occurs outside.

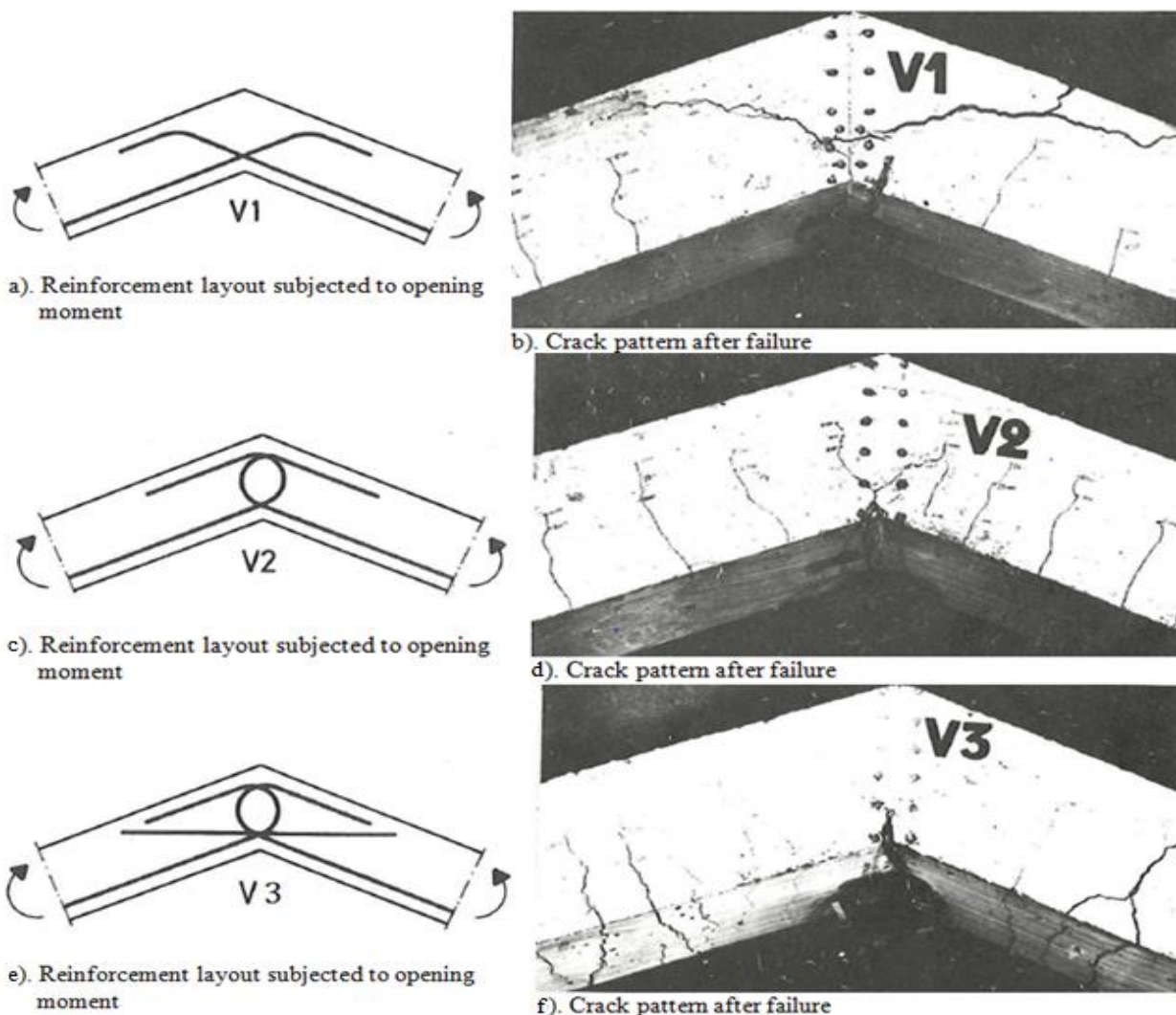
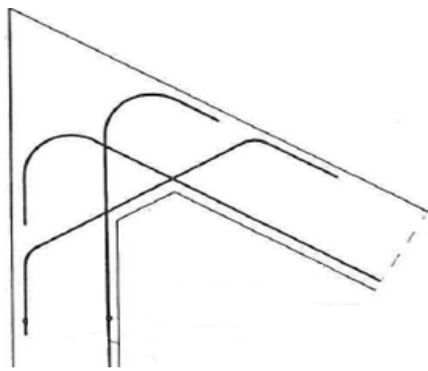


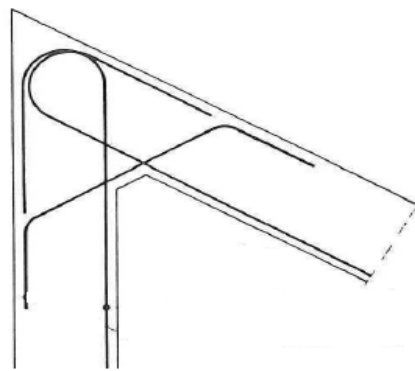
Figure 3.10 – Reinforcement detail for obtuse corner joints and their crack patterns (Nilsson, 1973)

Acute angled corner: also exhibit similar behaviour like the obtuse and 90° corners. As expected, the acute angled detail in figure 3.11a failed by diagonal tension cracking with an efficiency of 51% despite

providing a diagonal bar and a haunch, while the improved loop in figure 3.11b with diagonal bar achieved 102%.



a). Traditional acute angle with diagonal bar



b). Traditional acute angle with diagonal bar

Figure 3.11 – Acute angled details

3.4.1.3 Cantilever retaining wall

Retaining walls are important civil engineering structures used to resist combined earth and hydrostatic loading. Cantilever retaining walls often have the shape of an inverted T, with a thin vertical wall framing into the base slab. The joint between the stem and the base slab is similar to a corner joint subjected to opening moment. The conventional design approach treats the wall, the base slab projecting toward the toe, and the base slab projecting towards the wall as separate cantilever, and designs them based on beam theory. While beam theory is satisfactory outside the corner joint, it does not suffice in the D-region. Detailing of these region is usually done based on past experience, or guidelines available in several detailing manuals. The behaviour of some retaining wall corner details on which Nilsson (1973) performed experiments on is discussed in this section.

Corner detail with main bar bent towards the heel: This structural detail is illustrated in figure 3.12a with crack pattern at failure shown in figure 3.12b. This detail had only 60% joint efficiency with brittle failure occurring due diagonal tension cracking of the corner joint. After the first crack occurred, further increase in load caused the crack to propagate along the bent bar till failure. From the knowledge of strut and tie model, it is obvious that the diagonal compressive strut (i.e. compression field) and the tie (i.e. the main reinforcement) were not properly anchored in the node, because of the orientation of the reinforcing bar. In fact, it could be that the reinforcing bar (tie) did not pass through the node as is required from strut and tie methodology.

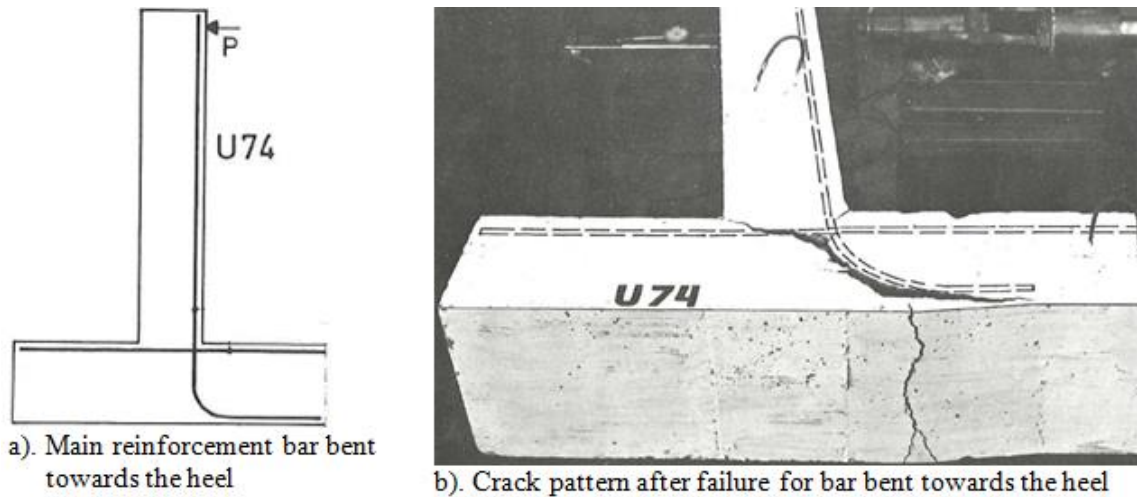


Figure 3.12 - Corner detail with main bar bent towards the heel (Nilsson, 1973)

Retaining wall with hairpin reinforcement: In the detail just discussed bent towards the heel (figure 3.12a), it was noted that the tie did not pass through the node. In a hairpin reinforcement layout (figure 3.13a), the tie is now taken into the node and there is proper anchorage. The joint efficiency now improves to 71%, but still fails by diagonal tension cracking with the toe pushed off. Though better anchored in the node, the hairpin reinforcement did not prevent or control the transverse cracks that formed within the core of the joint. A better solution is still required.

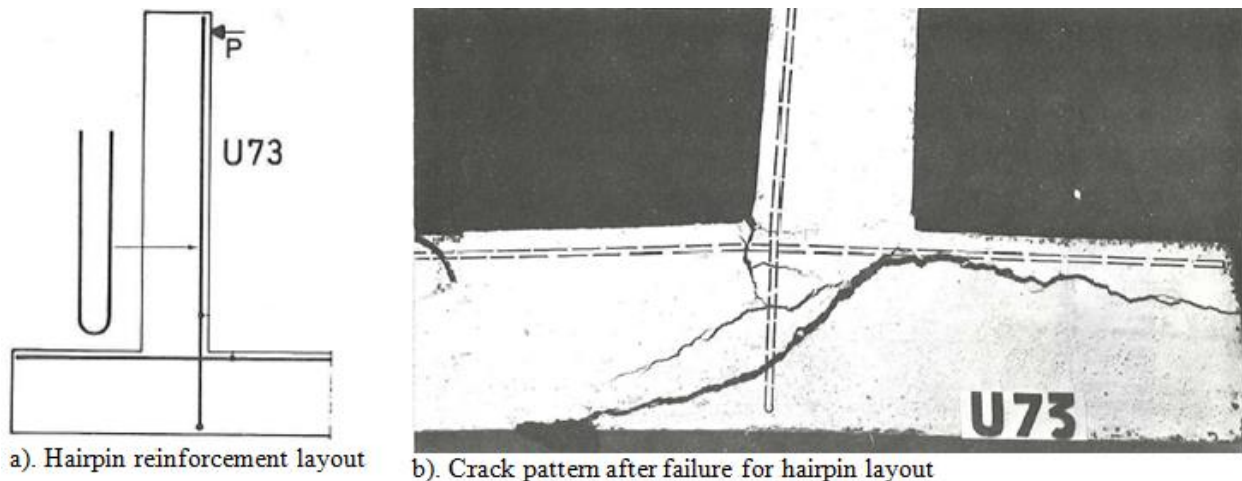


Figure 3.13 – Retaining wall corner detail with hairpin reinforcement (Nilsson, 1973)

Corner detail with main bar bent towards the toe: A good solution to preventing diagonal tension crack can be obtained by bending the main reinforcement from the wall into the toe of the base slab. With the bent part of the bar crossing the parts of the joint where diagonal tensile stress occur from opening moment, higher moment capacities should be expected. Also, the diagonal compression strut in the joint would now be better anchored by the bent part of the reinforcing bar. The joint efficiency with this layout would depend much on the adequacy of anchorage, which in turn depends on the length of the toe.

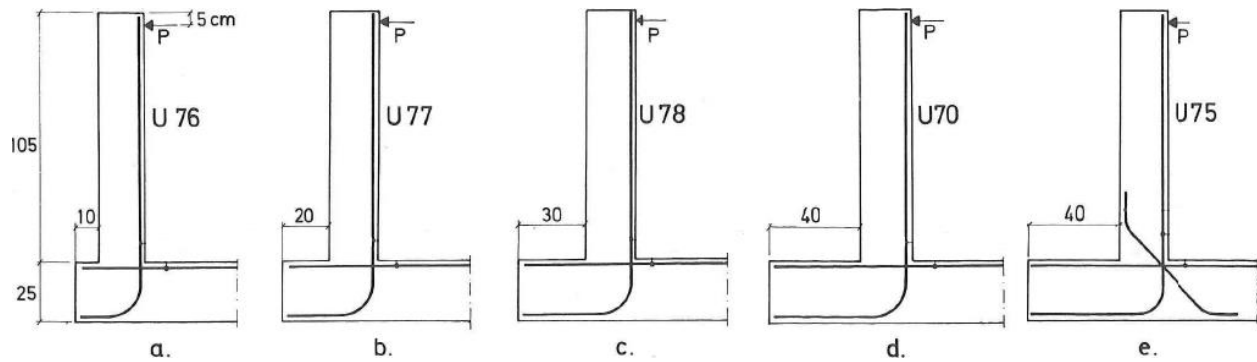


Figure 3.14 – Dimensions of cantilever retaining wall variants (Nilsson, 1973)

For anchorage by bond, sufficient anchorage length is required to prevent failure. Where anchorage length is inadequate, bond failure would occur as the stress transfer capacity erodes. For retaining walls, the length of the toe would determine the length available for anchorage. Figure 3.14 shows five variant specimens of this reinforcement layout which differ only in the length of the toe (for the first four), and the addition of inclined reinforcement (for the fifth detail). The specimen were loaded to failure and the behaviour studied.

The joint efficiency for the first three walls were 94%, 99% and 94% respectively. This improved efficiency occurred because diagonal tensile cracking was prevented by the bent reinforcement. Bond failure occurred in the joints due to a lack of adequate anchorage length at the upper face of the base slab. This failure type is shown in figure 3.15 for the first two details in figure 3.14. Accompanying this failure are wide corner cracks much larger than the crack widths caused by bending in the adjacent connected members.

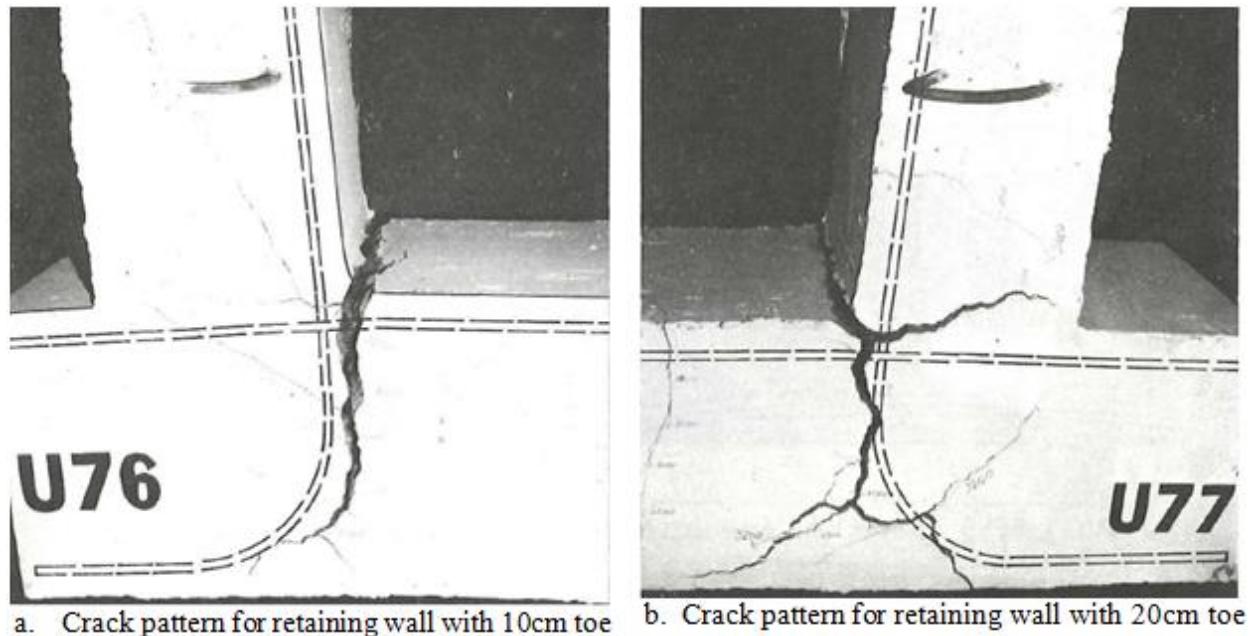


Figure 3.15 – Bond failure in joint due to insufficient anchorage length in upper face (Nilsson, 1973)

The fourth variant with 40cm toe length had sufficient anchorage length, and thus reached 101% joint efficiency, with the steel at the corner section yielded. It still had wide corner cracks at working load. Figure 3.16a shows this variant with a 0.55mm crack width at working load.

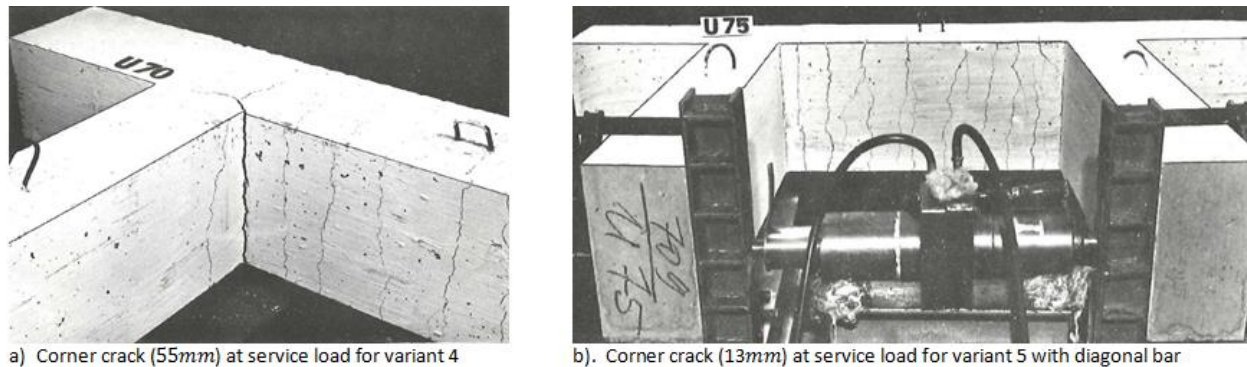


Figure 3.16 – Crack width comparison (effect of diagonal bar) (Nilsson, 1973)

To reduce these cracks, a diagonal bar was added to the re-entrant corner (see figure 3.14e) and loaded to failure. The addition of the diagonal bar caused a reduction in corner crack width from 0.55mm (at a working load corresponding to 55% of the calculated capacity), to a crack width of 0.13mm. As with previously discussed cases, the diagonal bar caused the improvement of crack width reduction at the corner, and increased joint efficiency of 119%.

Solution for short toes: The importance of adequate anchorage length has been discussed. However instances could occur where the space is insufficient to allow for adequate length of toe. Nilsson (1973) experimented on several specimens detailed with a combination of the improved loop and a diagonal bar at the re-entrant. Joint efficiencies between 113% and 117% was achieved for different specimens. Two among the details he proposed are presented in figure 3.17.

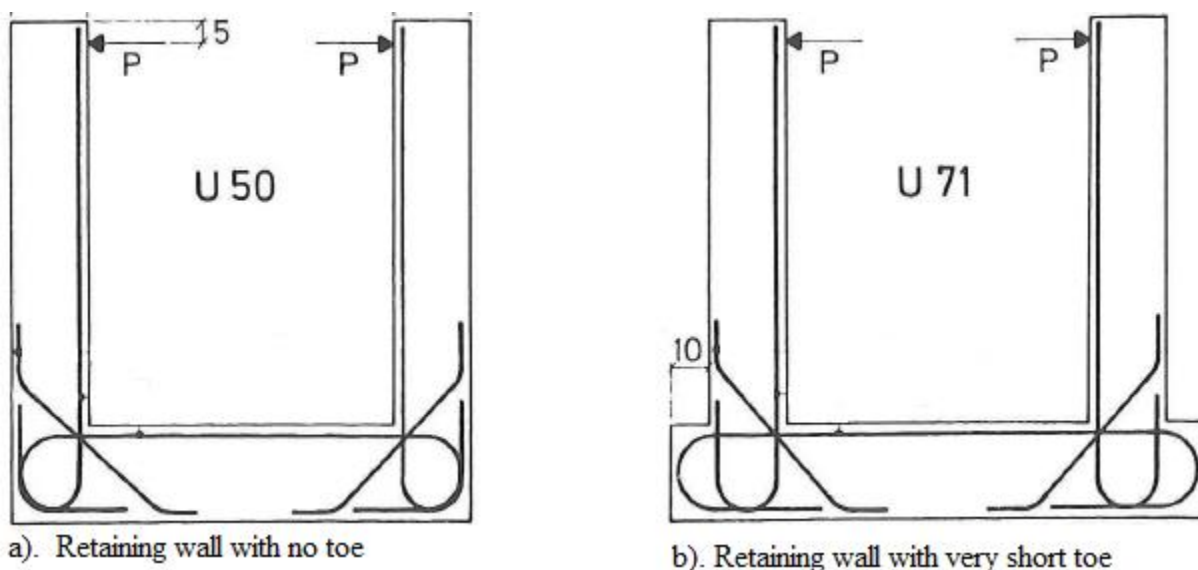


Figure 3.17 – Reinforcement layout for retaining walls with short toe (Nilsson, 1973)

3.4.1.4 T-Joints

The retaining wall discussed in the last section is actually a T-joint. T-joints are common in buildings and other structures. A distinction is made between two types of T-sections; the first type connects elements with small width e.g. beam to column connections in buildings. The use of stirrups is a common feature of this type of T-joint as seen in figure 3.18a. The truss analogy can be used to study how internal forces are distributed in the section with the stirrups as the tie and concrete being the strut. Figure 3.18b and c shows two ways of distributing forces in the section, and a crack pattern shown in figure 3.18d. This type of T-joint is however not the focus of this work however.

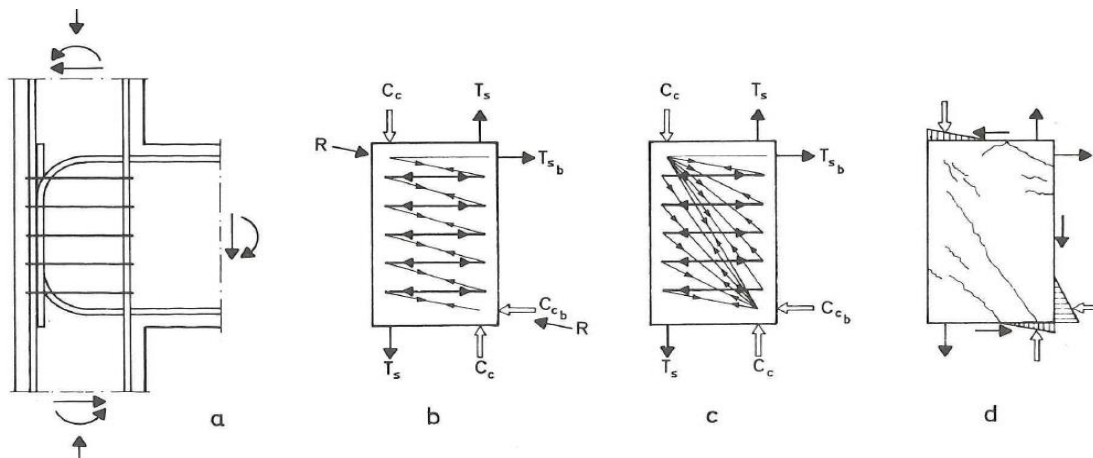


Figure 3.18 – Beam-column T-joint connecting members with small width (Nilsson, 1973)

The other type of T-joint (which would be discussed subsequently) connects members with large longitudinal dimensions e.g. a joint between wall and slabs. Stirrups are typically not used in these as it would be uneconomical, and they could pose problems in construction. This type of corner joint behaves in a similar manner to the various joint types that have earlier been discussed in this chapter. Brief discussion on joint efficiency and crack pattern is undertaken in this section.

The conventional reinforcement layout: This detail illustrated in figure 3.19a is quite common in practice and literature, despite the tie not being properly anchored in the node. From Nilsson's (1973) work, the joint efficiency could be as low as 40%. Cracking first occurred at the re-entrant corner, followed by a diagonal tension cracking as shown in figure 3.19b. This brittle failure mode should be avoided.

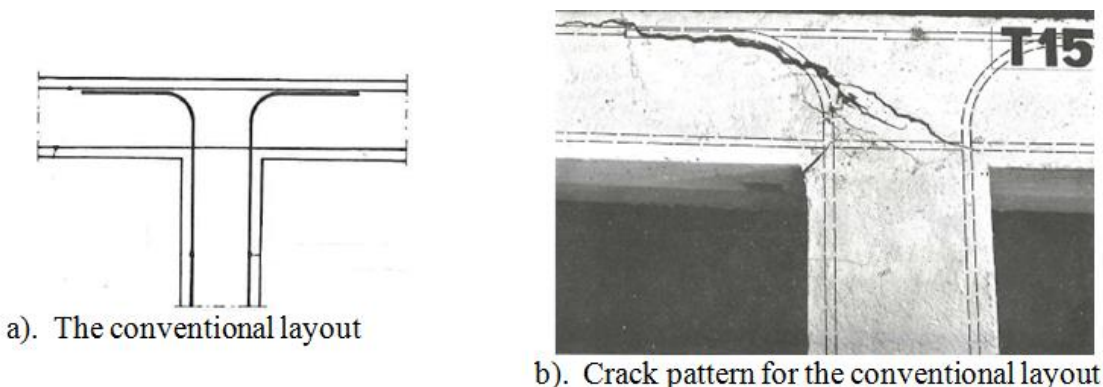


Figure 3.19 – The conventional reinforcement detail for T-joints (Nilsson, 1973)

Hairpin reinforcement layout: To properly anchor the tie in the node, the reinforcement are laid out like hairpin as seen in figure 3.20a. Despite the better anchorage, only a joint efficiency of 58% was achieved as diagonal cracking caused premature failure of the joint. As earlier stated, the compression reinforcement near the outer corner does not help as the transverse tensile stresses that cause this cracking are inwards. The crack pattern is shown in figure 3.20b.

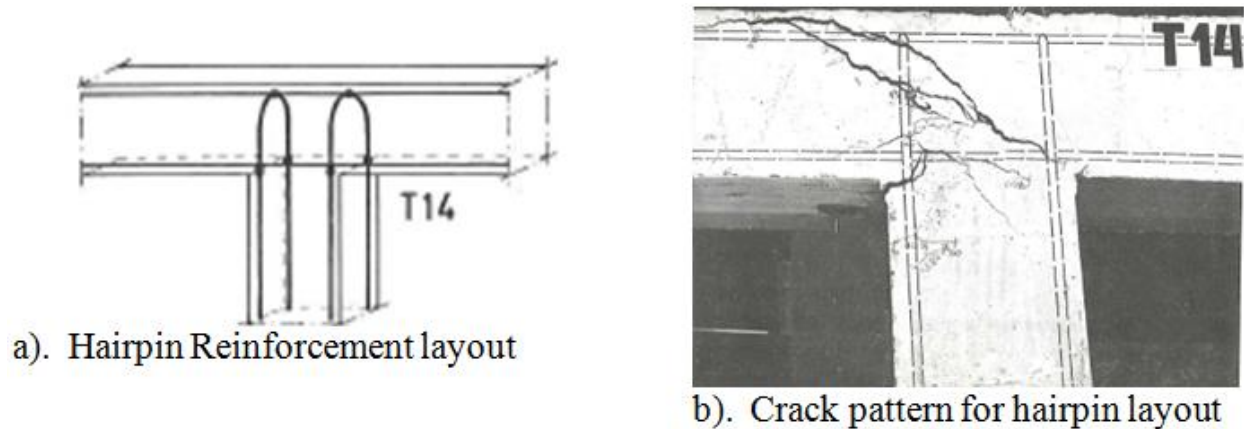


Figure 3.20 – Hairpin reinforcement layout for T-joints (Nilsson, 1973)

Hairpin layout turned around 90°: In figure 3.21a and b, the hairpin is now rotated about 90° in such a way that it would control transverse tensile cracking. The reinforcement is now in the direction of the diagonal tensile i.e. perpendicular to the crack direction. This detail attained an improved joint efficiency of 79%.

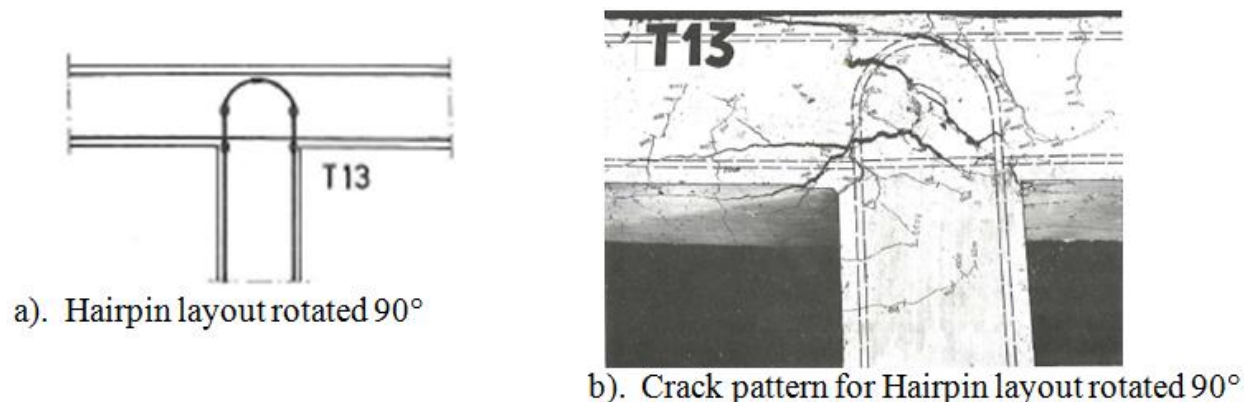


Figure 3.21 – Hairpin reinforcement layout for T-joints (Nilsson, 1973)

A satisfactory detail: With diagonal tension cracking prevented by rotating the hairpin, a more satisfactory detail can be obtained by designing proper anchorage for that layout. This is achieved by separating the tension and compression components of the hairpin, and providing sufficient anchorage length for both. Thus, we now have two bars instead of just one as shown in figure 3.22a.

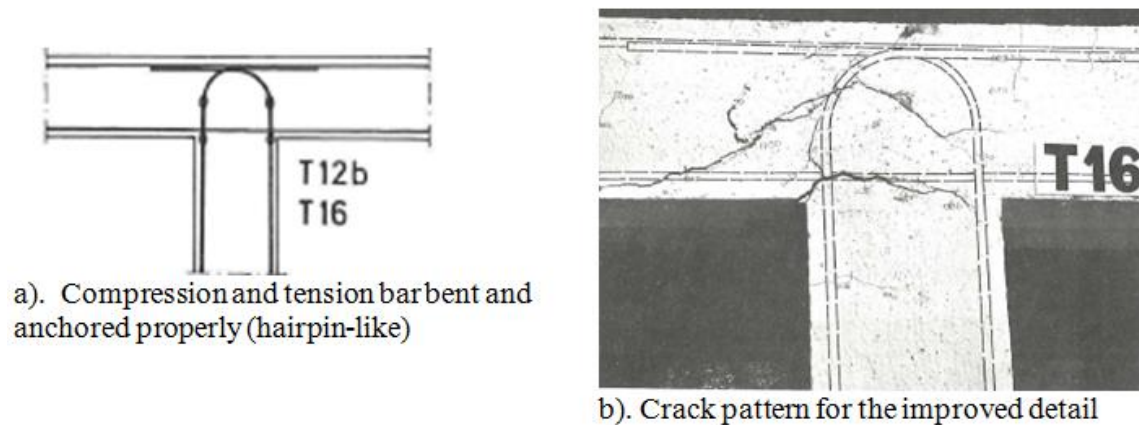


Figure 3.22 – A satisfactory detail for T-joints (Nilsson, 1973)

This reinforcement layout prevented diagonal tension cracking and anchorage failure simultaneously, thus resulting in a joint efficiency between 104% and 110%. Failure for this detail occurred due to reinforcement yielding in the leg (close to the slab). This detail thus met our objective of strength, ductility, crack and ease of construction.

In concluding this section of the report, it should be noted that Nilsson (1973) regarded the use of stirrups in corner joints as difficult to construct on site. It could also lead to congestion of the joint which may result in difficulties during pouring and compacting of concrete. Unlike Nilsson however, several other researchers recommend the use of stirrups within the corner joint to control diagonal tension crack failure. A brief summary of some additional research publications would be presented next. Since extensive review of corner joint behaviour has been discussed already based on Nilsson, only additional information would be highlighted in the review of their papers.

3.4.2 Nabil, Hamdy and Abobeah (2014)

Nabil, Hamdy and Abobeah (2014) performed an experimental study on eleven corner joints subjected to opening moments to study the joint efficiencies, crack and deformation pattern, effect of stirrups, joint size, comparison with closing joints etc. The behaviour and crack pattern are comparable to that from Nilsson's work thus with diagonal tension playing a governing role in many of the specimen. In this section, some few points from that report is discussed.

The use of looped reinforcement arrangement of the main tension reinforcement properly done gave the best result. Adding a diagonal bar at the re-entrant corner improved the result even further for looped details. However, the use of diagonal bar does not help significantly for details susceptible to diagonal tension cracking. However, where stirrups were used for such details, and placed in a fan-shaped arrangement (i.e. smearing outwards from the inner corner to the outer, thus crossing the crack trajectory) improvement were made and the joint thus reached full capacity. This is however contrary to the result Nilsson (1973) obtained with stirrups, as the stirrups gave marginal benefit in that case, without reaching 100% efficiency. More experiments from other authors could clarify this discrepancy.

On the impact of increasing joint size for a corner joint susceptible to failure by diagonal tension failure, three sample of different size with comparable reinforcement ratio (for the tradition layout in figure 3.3a). The specimen sizes were $150 \times 250 \text{ mm}^2$, $150 \times 350 \text{ mm}^2$ and $150 \times 450 \text{ mm}^2$. Thus, with each increase in specimen thickness, the lever arm increased. As expected, the failure load increased with

increasing specimen thickness, thus the section could carry more. However, the joint efficiency reduced with increasing thickness, as the sections still failed by diagonal tension. Diagonal tension failure depends on the tensile strength of the concrete (where stirrups or crossing reinforcement is not provided), and thus increasing section thickness only increases the length of the crack path, but not concrete tensile strength.

A comparison was also made of the corner joint efficiency when subjected to opening moment versus closing moment. About 33% higher efficiencies were obtained for closing moments when compared with opening moments. Generally, opening moment seems a more severe load for corner joints than closing moments.

3.4.3 Campana, Ruiz and Muttoni (2013)

The above-named authors performed experiment on sixteen corner specimen (most of which were of 125° angle). The result were also comparable to those obtained by Nilsson (1973), thus only few interesting aspects of this work would be discussed here

On the comparison of the layout of the main flexural reinforcement, the looped detail gave best result though below 100% efficiency. It was improved by the addition of diagonal bar at the re-entrant corner. The use of stirrups in the corner joints also increased the capacity of the traditional layout (which is susceptible to diagonal tension failure) with over 100% efficiency achieved. Though Nilsson's (1973) study differed on this issue of diagonal reinforcement, the effectiveness of stirrups is however been confirmed by Campana, Ruiz and Muttoni (2013) and Nabil, Hamdy and Abobeah (2014). In addition, other authors like Park and Paulay (1975), Lao and Hsu (2010) etc. It is also one of the two recommended details for opening corner in EC2 Annex J.2.3. In all these cases, the use of stirrup is combined with a diagonal bar at the re-entrant corner. In his work, Nilsson only used inclined stirrups without the diagonal bar at the re-entrant corner. Much higher joint efficiency could have been achieved otherwise.

3.4.4 Impact of reinforcement ratio on corner joint efficiency

With diagonal tension being a key reason for the premature failure of many joint types, this section take a closer look at it. Figure 3.23a shows a corner joint with external acting forces illustrated. For equilibrium, the resultant of the tensile forces should be equal to the resultant of the compressive forces i.e. $\sqrt{2}F_c = \sqrt{2}F_s$. Just prior to cracking, the elastic stress (σ_y) distribution along the eventual crack surface is as illustrated in figure 3.23b. The length of the tensile stress distribution on that crack surface corresponds to the theoretical length of diagonal crack denoted as l_{dc} . The shape of the tensile stress distribution approximates to that of a parabola.

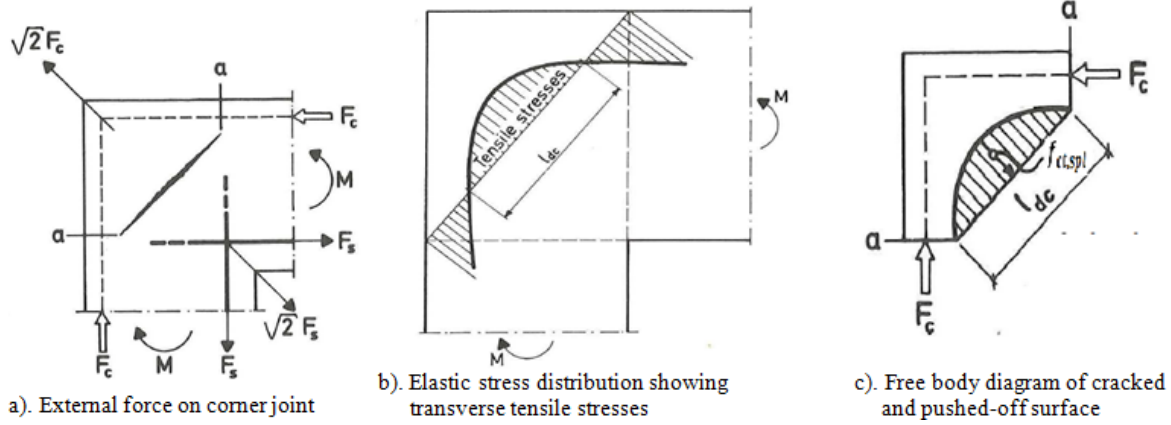


Figure 3.23 – Derivation of expression for diagonal cracking moment (Nilsson, 1973)

At failure, the outer part of the corner joint would be pushed off from the corner as shown in figure 3.23c. The tensile splitting stress acting on the cracked surface should follow from the external force. Using the equation of a parabola, the tensile stress distribution on the cracked plane is related to the external tension force by the expression:

$$\sqrt{2}F_s = \frac{2}{3} \cdot f_{ct,spl} \cdot b \cdot l_{dc}$$

Thus $F_s = \frac{\sqrt{2}}{3} \cdot f_{ct,spl} \cdot b \cdot l_{dc}$

Where $f_{ct,spl}$ is the tensile splitting strength of concrete and 'b' the thickness of the section. With the bending moment being the product of steel force and lever arm i.e. $F_s \cdot z$, and assuming the lever arm is $0.8d$ (with 'd' being the effective depth), the diagonal cracking moment M_{dc} can be expressed as:

$$M_{dc} = \frac{\sqrt{2}}{3} \cdot f_{ct,spl} \cdot b \cdot l_{dc} \cdot 0.8d = 0.38f_{ct,spl} \cdot b \cdot l_{dc} \cdot d$$

The expression shows that diagonal moment cracking capacity of the joint depends on the tensile splitting strength of the concrete. This accounts for why diagonal tensile cracking failure mode is brittle. To promote plastic behaviour in the corner joint, it is desirable that the tension reinforcement yields before diagonal cracking occurs. Thus, $F_s \geq A_s \cdot f_y$

Substituting the earlier derived equation for F_s into the above equation would result in:

$$A_s \cdot f_y \leq \frac{\sqrt{2}}{3} \cdot f_{ct,spl} \cdot b \cdot l_{dc}$$

With the area of steel $A_s = \omega \cdot b \cdot d$ where ω is the flexural reinforcement ratio. With this information, the reinforcement ratio could be related to the tensile splitting strength with the expression:

$$\omega \leq \frac{\sqrt{2}}{3} \cdot \frac{f_{ct,spl}}{f_y} \cdot \frac{l_{dc}}{d}$$

Depending on the concrete and steel properties used in the experiments, Nilsson (1973) calculated a maximum reinforcement ratio of 0.3% in his work. This means that brittle failure would not occur for the

specimen (used for that work) if the main reinforcement ratio was less than or equal to $0.3\%^2$. The steel would yield and the joint would be ductile. However, using such a low reinforcement ratio would only work for rather small forces. For the load types typically encountered in practice, such a low reinforcement ratio would yield resulting in large cracks and deformations, and subsequent failure. The reinforcement ratio for most structures in practice ranges from 0.5% to 2%.

The expression however makes a lot of sense, in view of the fact that diagonal tensile stresses occurs mainly due to large shear forces in the corner joint as was illustrated in figure 3.1a. As the force in the reinforcement increases, the shearing stresses with the joint also increases, thus resulting in higher splitting tensile stresses. For this reason, Park and Paulay (1975), Kaliluthin, Kothandaraman and Suhail-Ahamed (2014) etc. recommend increasing shear (transverse) reinforcement for medium to highly reinforced sections. In addition to the surrounding concrete, it would provide confinement to the concrete. Though the concrete could still crack, the concrete within the cracks would still contribute to performance of the joint via tension stiffening effect, hence reduce deformation in the section.

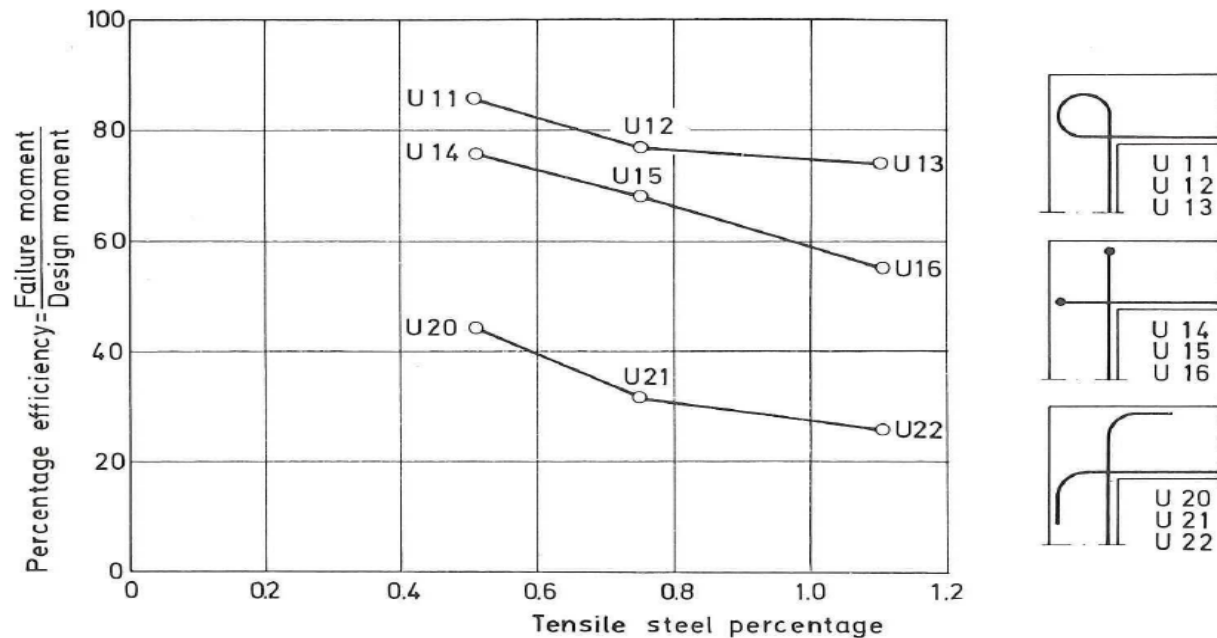


Figure 3.24 – Effect of reinforcement ratio on joint efficiency (Nilsson, 1973)

As a summary to this section, an increasing reinforcement ratio causes increased flexural strength, but reduced joint efficiency. The impact of the reinforcement ratio is illustrated in figure 3.24 from the work of Nilsson (1973). As seen in the illustration, for the same detail type, joint efficiencies reduced with increasing reinforcement ratio. This could be improved with transverse reinforcement. As earlier discussed, looping the tensile reinforcement in the corner joint could also be effective in reducing susceptibility to diagonal cracking. With increasing tension force in the reinforcement, the loop tightens the concrete in the

² This value depends on the properties of concrete and steel used, and to some extent on the geometry. Using the geometry of Nilsson, but for C30/37 concrete, and B500 steel, an even lower maximum reinforcement ratio of 0.24% for plastic behaviour in the joint is found.

core of the corner putting it in compression. This is also an efficient means if the designer wants to avoid the use of stirrups.

3.4.5 Improving corner joint details with steel fibres

In concluding this chapter, improvement (in terms of strength and behaviour) of a corner joint subjected to an opening moment using steel fibres was studied by Abdul-wahab and Al-Roubai (1998). Twenty-three corner specimen with varying amount of steel fibres (maximum was 2% by volume). Only two reinforcement details were used i.e. the looped layout (without diagonal at re-entrant corner) and looped layout (with diagonal at re-entrant corner). The corner angles were also varied from 60° to 150°. Some impact of steel fibres on the corner joints' performance is discussed next.

Addition of steel fibres had noticeable impact on the failure mode. Without the fibres, diagonal tension failure governed in the samples. Diagonal tension failure also governed for all corner specimens with 0.5% fibre content, and most of the 1.0% fibre content. However, for samples with 1.5% and 2.0% steel fibres in the joint, the failure mode became yielding of reinforcement at the adjoining member's away from the joint.

The addition of fibres also influenced the joint efficiency positively. For instance, a 90° corner specimen without steel fibres (and without diagonal bar at the re-entrant corner) achieved only 47% efficiency. This improved to 99.3% when a diagonal bar was added to the inner corner (without steel fibres yet). When steel fibres were added, 103.6%, 107.7% and 135.6% joint efficiencies were reported for 0.5%, 1.0% and 1.5% steel fibres by volume. Based on their tests on several samples, Abdul-Wahab and Al-Roubai (1998) predict up to 73% improvement in joint efficiency using steel fibres in the range of 1 – 2%.

Steel fibres also had significant impact on crack behaviour and the cracking moment. The initial cracking moment increased both with fibre content, and the fibre aspect ratio (l/d). Also, the crack width reduced with increasing fibre content, and cracks were distributed even into the adjoining member away from the joint. The gradual addition of fibres caused a gradual reduction in diagonal tension cracks, with increasing flexural cracks occurring along the adjacent members.

From Abdul-wahab and Al-Roubai (1998), the benefit of using steel fibres in corner joints is quite obvious. It improves both pre-crack strength, and post-crack behaviour. If used in lightly reinforced corner joints, improved structural behaviour would be achieved in terms of higher joint efficiency, better crack control, ductility (post-crack behaviour) etc.

4 Finite Element Method

The finite element method (FEM) is a numerical technique used for solving field problems. Field problems usually entail the determination of one or more dependent variables spatially, e.g. stress distribution in a corbel, heat distribution in a non-homogenous body etc. Mathematically, such problems are usually described by differential or integral equations. Sometimes however, analytical solutions to these equations could be time-consuming or cannot be obtained, and we revert to approximate solutions from numerical analysis. FEM is one of such numerical techniques. It is thus applicable for section complex geometries (like our D-regions) where our analytical approach from mechanics could not be depended upon. In this thesis work, it is used alongside the strut-and-tie model to study the impact of detailing in the performance of D-regions. Numerical methods give approximate solutions (not exact), and thus need to be validated with experiments or analytical results before being adapted for use.

The main idea in FEM is that the structure can be discretized into a number of finite elements connected at their nodes and along the inter-element boundaries. This process of discretization is known as meshing, and should be done in such a way that there is no gap or overlap between elements. The elements usually have physical properties like thickness, Poisson ratio, elastic modulus etc., and a specific shape which could be triangular, quadrilateral, tetrahedral etc. Nodes are usually on the boundaries of the element, and connect an element to adjacent finite elements, and are where the degree of freedom is defined. The desired field variable is usually calculated in the nodes, and the result is approximated (by interpolation techniques) to get values at non nodal points. This way, the distribution of the field quantity is approximated element-by-element over the entire structure.

The finite element approach is well suited to computer application, thus resulting in many FEM software including ATENA, DIANA, ANSYS, ABAQUS etc. In this report, some knowledge required to use available FEM software for this work would be discussed. The main topics discussed here are material models and the approaches used for nonlinear modeling. An overview of the FEM process would be discussed first in the next section.

4.1 Overview of the FEM process

Before undertaking an analysis using FEM, the physical system to be modeled needs to be known and properly understood. The problem often starts with a real problem e.g. a high-rise building subjected to strong winds, a retaining wall resisting lateral loads from active earth pressure etc. These problems are then idealized using mathematical models which can be used to predict some aspects of the behaviour of the system. A preliminary solution to the problem can be obtained using the mathematical model. This would provide an initial result for comparison with the output from FEM. A flowchart showing the steps involved in a FEM project is illustrated in figure 4.1.

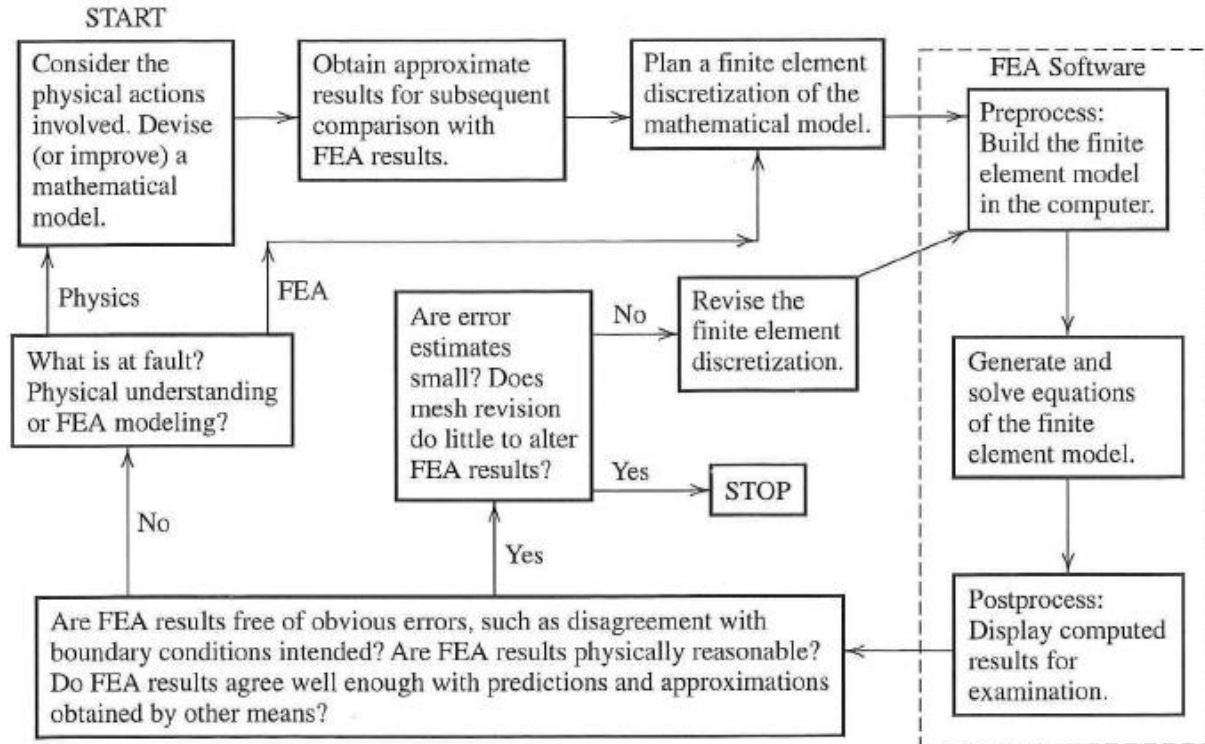


Figure 4.1 – Steps involved in a finite element analysis project (Cook et al, 2002)

From figure 4.1, three activities are undertaken in the FEM software namely Pre-processing, Analysis (or solution), and Post-processing . These phases would be briefly discussed next.

4.1.1 Pre-processing

The main essence of pre-processing is the geometry definition, discretization (or meshing) to finite elements, selection of element type and assigning them material properties, and applying boundary conditions from loads and supports. The concept of pre-processing would be explained using the example of a simply supported beam subjected to uniform loading. The displacement at mid-span is expressed as:

$$w = \frac{5}{384} \cdot \frac{q \cdot L^4}{E \cdot I}$$

Where w is unknown displacement (translation or rotation) to be solved, the various inputs required for FEM to compute this unknown are:

$\frac{5}{384}$ represents support (or boundary condition)

q represents load which could be concentrated force in the nodes, edge (or line) loads and body forces.

L^4 represents geometry of the model being studied.

E represents material properties like elastic modulus, Poisson ratio, nonlinear material effects etc.

I represents sectional properties of the structure.

From the above illustration, it is obvious that pre-processing phase is actually the model definition phase in FEM. It is a critical phase as any computed FEM solution would be of no value if they correspond to the wrong problem. In pre-processing, the right problem is defined.

4.1.2 Analysis (or solution)

This is the phase in FEM where the model created in pre-processing is numerically evaluated. The FEM software collects the governing algebraic equations into a matrix format, and computes for the unknown quantity. The spatial distribution of a quantity in FEM is done using a generalized coordinate system known as degree of freedom. These degrees of freedom (translational and rotational) are arranged in a column vector termed ‘nodal displacement’ $[u]$. Corresponding to each degree of freedom is a conjugate forcing term $[f]$ also arranged in a column vector. These are related by the expression:

$$[f] = [K][u]$$

This expression underpins the operations that take place in the ‘black box’ during FEM analysis. Key to the computation is the stiffness matrix $[K]$. The mathematics behind obtaining the finite element computations is not the object of this study (plenty of information available in many textbooks on FEM). However, an illustrative summary of the operations that take place here is presented in figure 4.2.

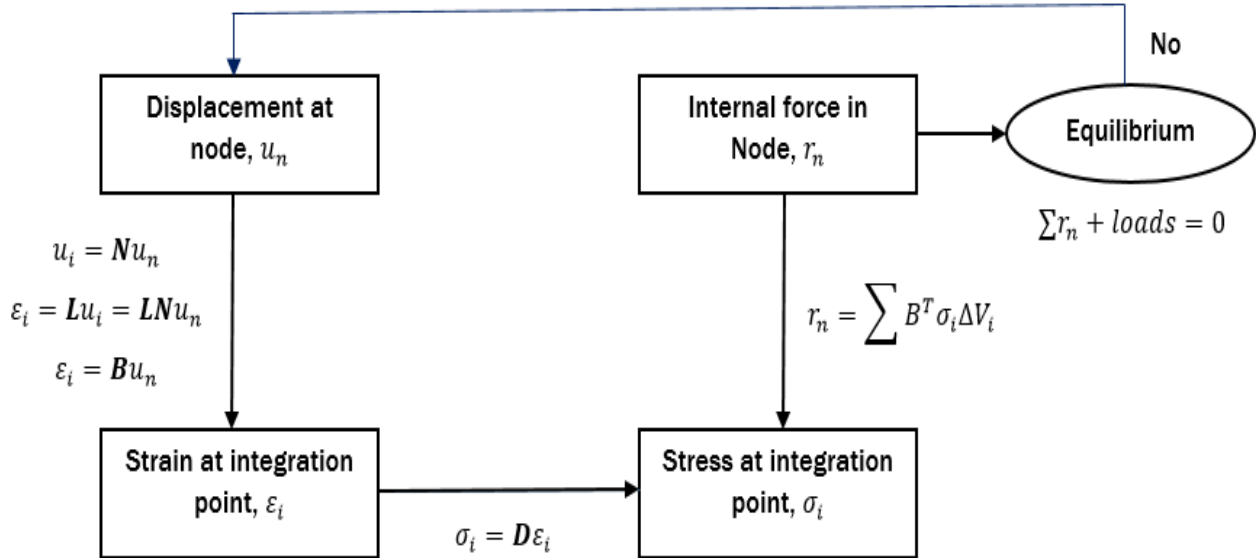


Figure 4.2 – Solution procedure in finite element analysis

Figure 4.2 is a displacement based formulation of FEM. It shows a prescribed displacement at a node, u_n interpolated to an integration point displacement, u_i . This is then differentiated to get the strains, ε_i at the integration point. This strain, ε_i is related to the stress, σ_i by the material model used. The stresses, σ_i integrated over a volume, ΔV_i is used to compute internal forces, r_n in the node. These internal forces must be in equilibrium with the applied loads. Thus we see the displacements and/or rotations related to the strains by the kinematic equations. The strains are then related to the stress by the constitutive equations, while the internal forces generated by the stresses are evaluated from equilibrium equations. From these three equations, the stiffness matrix that describe the behaviour of the element can be obtained. An illustration of these equations is shown in figure 4.3 for a plane stress with three degrees of freedom. Since the structure has been discretized in the pre-processing phase, several element stiffness matrices would be obtained with one for each element. The contribution for one element can be expressed as $K_e = \sum B^T DB \Delta V_i$. The FEM software combines all these element stiffness matrices into a global stiffness matrix for the structure. With the global stiffness matrix, the field quantities at the different nodes can be determined.

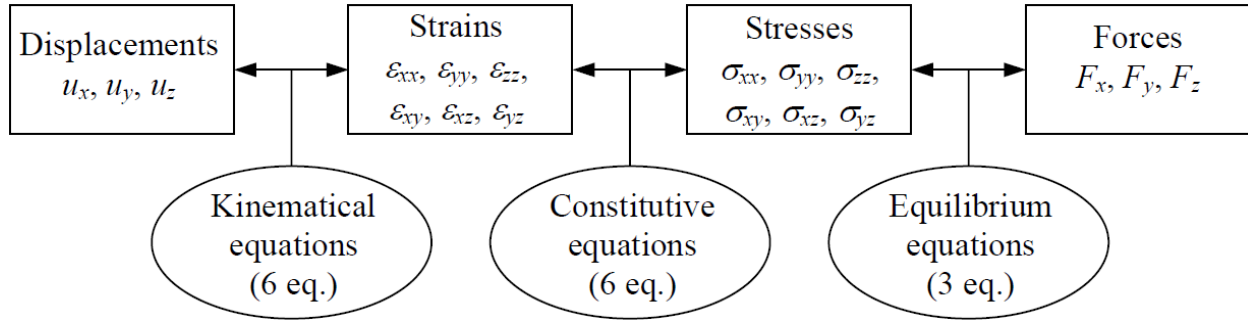


Figure 4.3 Relations between basic quantities in structural mechanics

Substantially more computational resources is required if any of the equations in figure 4.3 is non-linear. In this connection, we could have:

- Geometric nonlinearity – where either the kinematic equation or the equilibrium equation is nonlinear. Examples of geometric nonlinearity occurs when deformation is large enough that the equilibrium equations is determined based on the deformed structural geometry. Another case occurs if the load may change direction or magnitude with time, and is thus non-conservative.
- Physical (or materials) nonlinearity – occurs where material model is nonlinear. Most engineering materials exhibit nonlinear behaviour at high stress. Example of nonlinear behaviour in concrete include cracking, crushing, softening etc. Steel on the other hand exhibits plastic behaviour after yielding, strain hardening etc.

Since material nonlinearity play a crucial role in this work, a key goal in this chapter of the report is to discuss material behaviour, and how they are implemented in a typical finite element software.

4.1.3 Post-processing

Substantial volume of raw data is made available in the solution (or analysis) phase, which may be difficult or cumbersome to interpret. FEM software usually manipulate these data into more user-friendly formats like showing the deflected shape, stress plots, contours, animations etc. This is post-processing phase from the software. For the analyst however, it would be ill-advised to entirely rely on the solutions in the post-processor without some sort of check or verification. Some actions that the analyst should do as part of post-processing includes:

- Check for equilibrium e.g. at restrained nodes (i.e. supports), the reaction forces should closely balance the applied load. Where they don't closely balance, the validity of the solution is in doubt.
- Comparison with hand calculations or analytical solutions
- Visual examination (both qualitative and quantitative)
- Inspecting log files for warning or errors etc.

Once the above are checks are considered as satisfactory, the quantities of interest may be examined. FEM software provide numerical and graphical data that can be used for study.

Relying entirely on graphical plots for post-processing is not advised especially when studying the stresses and the strains. From figure 4.2, it can be seen that force and displacement are evaluated at nodes, while stresses and strains are evaluated at integration points. Thus, the stresses and strains are more accurate in

integration points, than in the nodes. In generating contour plots in most FEM software, the stresses and strain at the integration points are extrapolated to the nodal locations. Since a node is typically shared by more than one element, the extrapolated stress and strain data is usually averaged in order to have a smooth contour plot. This nodal averaging affects the accuracy of stress and strain data at nodes. For this reason, it might be more reliable to use stress and strain data from integration points. For force and displacement however, nodal point data are accurate as force and displacement are evaluated in the node. All these should be taken into consideration during post-processing.

4.2 Behaviour of concrete, steel and their composite

Reinforced concrete is a composite material that consists of concrete and steel part, each with different mechanical behavior. While separate material models are utilized in FEM to represent concrete and steel, these models are combined using other models to describe the behaviour of reinforced concrete. Reinforced concrete is an inherently nonlinear material. Many FEM software incorporate this material's nonlinearity in its material model in order to achieve structural behaviour close to reality. The response of a typical reinforced concrete element is shown in figure 4.4.

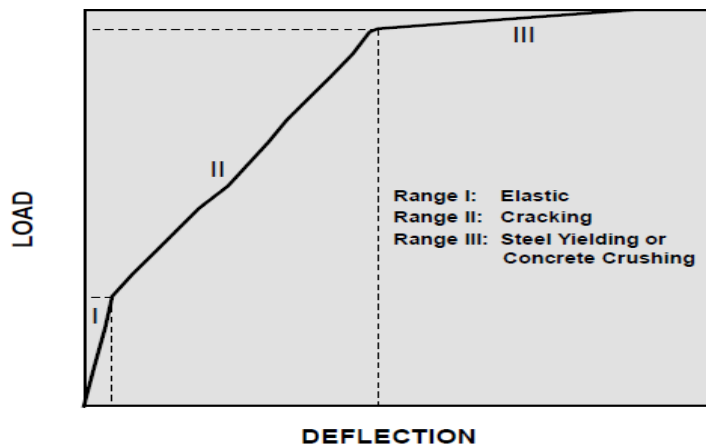


Figure 4.4 – Load-displacement behaviour of a reinforced concrete element

From figure 4.4, the behaviour of the reinforced concrete structure is divided into three ranges i.e. an initial uncracked linear-elastic stage, a less stiff range with crack propagation, and a plastic phase dominated by yielding of reinforcing steel and/or crushing of concrete. This behaviour is attributable to the nonlinear behaviour of the constituent materials. Nonlinearity in the behaviour of concrete is caused mainly by cracking of concrete in tension, crushing of concrete, biaxial or triaxial confinement of concrete. For steel, the effect of steel yielding, strain hardening, rupture etc. contribute to its nonlinear behaviour. For the composite material, additional nonlinear behavior is caused by tension stiffening, bond etc. In this section of the report, the focus would be on understanding key themes in the behaviour of concrete, steel and their composite action when combined. Afterwards, the discussion would focus on how these materials are implemented in the FEM software utilized for this thesis work (i.e. ATENA).

4.2.1 Concrete

Hardened concrete is a three phase material consisting of aggregate, mortar and the interfacial transition zone between them. Even prior to any load application on the concrete, a lot of micro-cracks already exist in the concrete especially at the interfacial zone between the mortar and aggregates. These micro-cracks greatly influence the mechanical behaviour of concrete, and their propagation during loading contributes

to nonlinear behaviour from low stress levels. The response of the concrete (studied by stress-strain relation) is not just nonlinear, but is also different in tension and compression. This section discusses the behaviour in compression and tension.

4.2.1.1 Concrete in compression

For concrete subjected to uniaxial compression, the stress-strain behaviour of plain concrete is illustrated in figure 4.5 divided in five zones. The response is initially nearly linear elastic (zone A) up to approximately 30% of the compressive strength. At this stage, there may be some growth in the micro-cracks already inherent in the material (from shrinkage and thermal cracks) and within the transition zone. Loading further to stress levels between 30% to 50% of peak stress (i.e. zone B) leads to gradual softening due to reduced material stiffness. This reduction in stiffness results from an increase in crack initiation and growth. The crack growth is however stable. Between 50% and 75% of peak compressive stress, further reduction in material stiffness is observed. Also, unstable cracks may be formed which grow when subjected to constant load. When beyond 75% of peak stress, the concrete response is increased strain even under constant load (zone D). This increased strain is due to spontaneous growth of cracks already formed, and agglomeration of micro-cracks into a continuous pattern. Beyond the peak stress, the stress-strain behaviour shows strain softening of the concrete until final failure by crushing. Figure 4.5 also shows the behaviour for cyclic loading. This would not be discussed in this text.

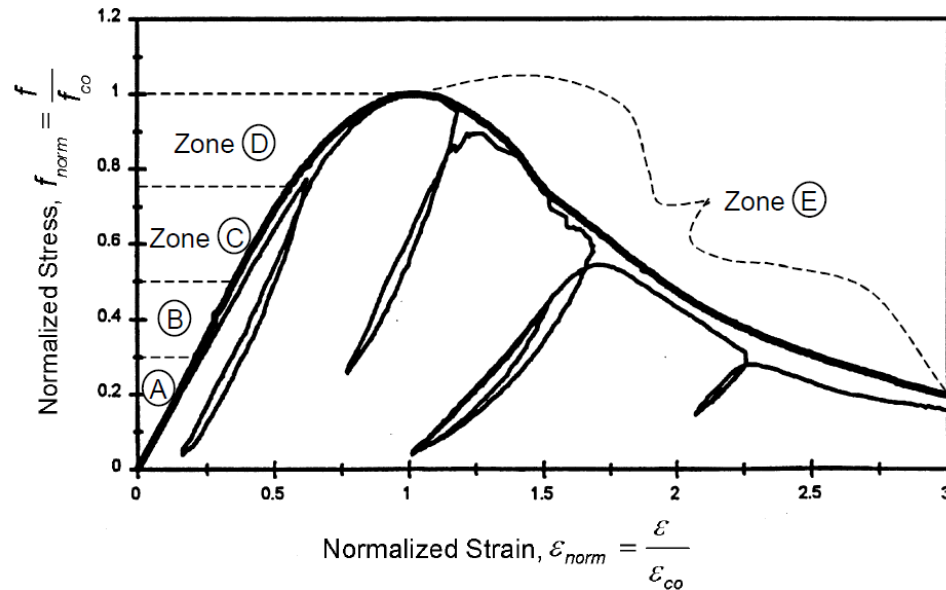


Figure 4.5 –Stress-strain curve for concrete in uniaxial compression (Bahn and Hsu, 1998)

For model development, this behaviour is often simplified to three phase i.e. an initial linear elastic behaviour at low stress level, an increasingly nonlinear material response up to peak stress accompanied by cracking and reduced material stiffness, and a post peak behaviour. A similar stress-strain behaviour is incorporated in the constitutive models for concrete available in most FEM software.

When subjected to multiaxial compression, higher compressive stresses with larger deformations can be carried by the concrete. FIB (2008) suggest that up to 25% increase in concrete strength can be achieved for concrete under biaxial compression, in addition to increased concrete ductility. Even higher values of

increased strength would be achieved for concrete in triaxial compression. This behaviour is taken into consideration for models used for concrete in some FEM software.

4.2.1.2 Concrete in tension

The behaviour of concrete in tension is also a vital aspect of the constitutive model for concrete. This may govern the response of a structural element that is inadequately reinforced. Also, concrete tensile strength is what determines when reinforcing steel is activated. A typical stress-strain curve for concrete subjected to uniaxial tension is shown in figure 4.6. Experiments to produce such data are usually displacement controlled as brittle failure would occur for load controlled test, thus resulting in only data up to the peak. Concrete exhibits a linear-elastic response till the tensile strength is reached, at which point some stable cracks initiate. If more strain is imposed on the concrete (in excess of that corresponding to the peak stress), a rapid loss of load capacity occurs. Also, the cracks earlier formed develop into a system of continuous cracks. Compared to its compressive strength, concrete has rather low tensile strength.

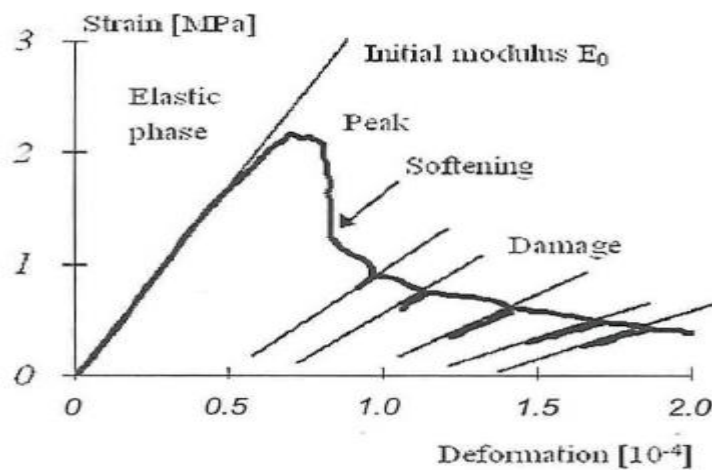


Figure 4.6 –Stress-strain curve for concrete in uniaxial tension (Torrenti et al, 2010)

Key aspects of concrete tensile behaviour required in constitutive models typically covers crack initiation, opening and propagation, and a realistic estimate of structural stiffness. After cracking, plain concrete is still able to resist some residual tensile stress across the crack where the crack width is small (FIB, 2008). These stresses (referred to as cohesive or bridging stresses) are small, and are thus usually ignored in traditional design. These bridging stresses decrease as crack width increases. This phenomenon is referred to as tension softening, and is modeled based on fracture energy in many FEM software.

4.2.2 Reinforcement

Steel bars used as reinforcement in reinforced concrete typically carry load along the bar axis, thus are generally assumed as one dimensional line elements. While it is relatively stiff and strong along the bar axis, it is assumed to have negligible shear stiffness and flexural rigidity. Thus, reinforced concrete is designed to exploit its strength along the bar axis. The stress-strain behaviour of steel is well established in literature, and is illustrated in figure 4.7.

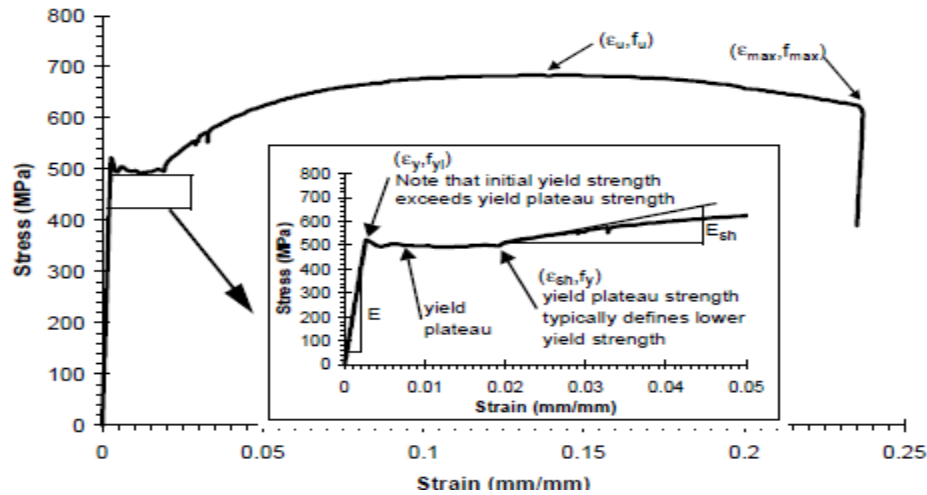


Figure 4.7 – Typical stress-strain behaviour for a reinforcing steel (Naito (1999) cited by Lowes (1999))

From figure 4.7, an initial linear elastic part is observed below material yield stress. For a strain in excess of that corresponding to the yield stress, a slight drop below initial yield stress is observed. This lower yield strength is maintained while strain increases to a point. Afterwards, strain hardening behaviour is observed with more load carried by the steel up to peak strength termed ‘ultimate strength’. More loading causes necking in the steel, and the capacity is reduced. At maximum strain, the reinforcement fractures and final failure occurs.

Simplified material models for reinforcing steel are used in FEM software mimic the behaviour described above. In ATENA, two models (i.e. a bilinear and multi-linear models) are available that are based on the above behaviour. The bilinear assumes an elastic-perfectly plastic behaviour. The multi-linear model allows the user to model the elastic stage, yield plateau, strain hardening stage and eventual fracture. Both of these models are illustrated in figure 4.8.

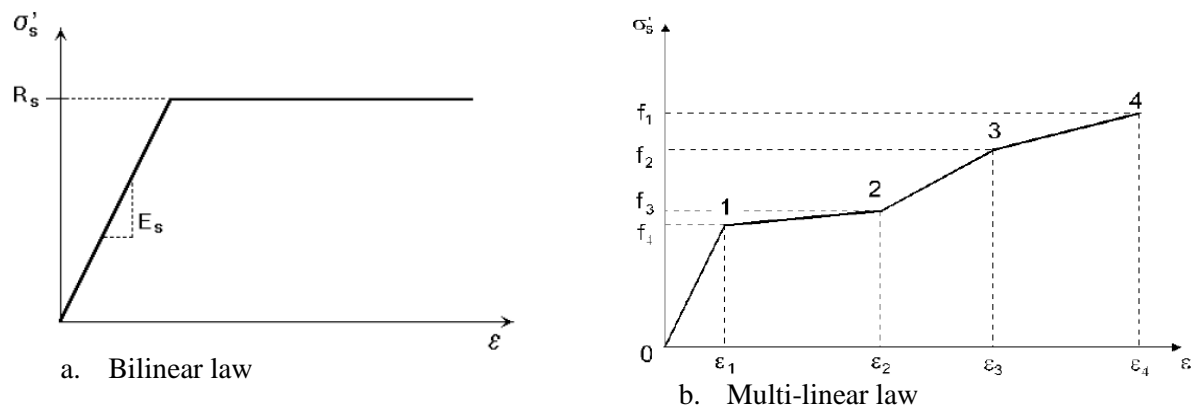


Figure 4.8 – Models utilized for reinforcement in ATENA

In FEM software, reinforcement typically adds stiffness to the location it is placed. They are generally treated as either discrete or smeared. Discrete reinforcement models each layer of reinforcement explicitly using axial members (usually truss elements) placed in the mesh. Smeared reinforcement on the hand, incorporates the average stress-strain relation of the composite (i.e. steel and concrete) into the stiffness matrix.

4.2.3 Concrete-steel interaction

In reinforced concrete, the two different materials (concrete and steel) interact together to act as a composite material. This composite action requires mechanisms for force transfer between concrete and steel. In this section, two aspects of that interaction and force transfer are discussed i.e. bond and tension stiffening.

Bond

Bond refers to the resistance against slip when pulling a reinforcing bar through concrete. This resistance is caused by mechanisms like adhesion between concrete and steel (for low bond stresses), friction, bearing of reinforcement ribs against concrete etc. The bond-slip relation is influenced by factors like bar surface texture (or roughness), concrete strength, concrete cover, orientation during casting etc. By ensuring force transfer between reinforcing bar and the surrounding concrete, bond makes them work together thus ensuring bearing capacity of the composite material.

As ribbed bars are more used in practice, this would be further discussed. Initial bond is by adhesion for low bond stress levels. Afterwards, force transfer between concrete and steel is governed by the ribs bearing against the concrete leading to higher bond stresses. This leads to formation of cone shaped cracks around the crest of the ribs. The bearing force (which are inclined to the bar axis) can be resolved into forces parallel to bar axis and perpendicular to it. The parallel component is balanced by the bond force, while circumferential tensile stresses are caused by the transverse (or radial) component. The radial force component can result in splitting bond failure (figure 4.9a) where radial crack propagate through to the cover. Pull-out failure (figure 4.9b) could occur due to the parallel force component. In this case, the concrete keys within the ribs shear off, and a sliding plane around the bar is formed.

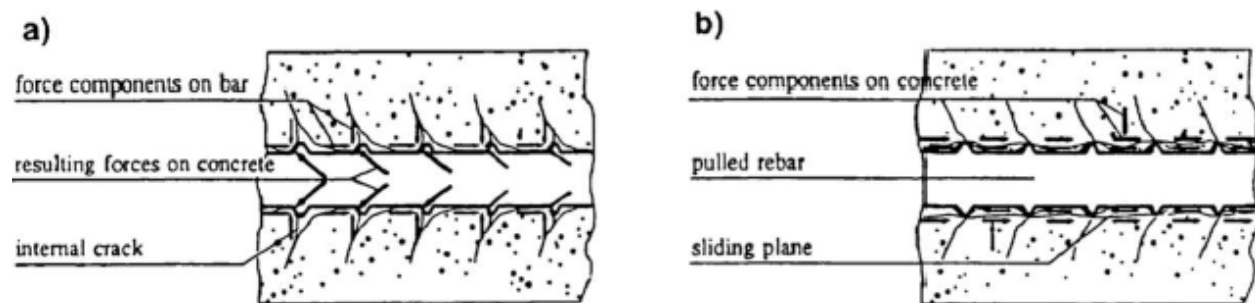


Figure 4.9 – Deformations around the reinforcing bar (Den Uijl and Bigaj (1999) cited by FIB, 2009)

For linear elastic analysis, the assumption of perfect bond suffices i.e. same displacement for concrete and steel at the location). Perfect bond also suffices for parts of the structure in compression, and for uncracked parts of the structure in tension. In cracked sections however, tensile force in the crack are transferred by the steel reinforcement, thus making the displacement of concrete and steel different along the transfer length, hence a slip. Several bond models are available in literature, and are incorporated in FEM software. These models typically define a relationship between bond stress (τ_b) and relative slip between steel and concrete. ATENA makes provision for three bond-slip models i.e. CEB-FIB model according to model code 1990, slip model by Bigaj, and a user defined model. Parameters required to use the first two models include concrete compressive strength, reinforcement type (smooth or ribbed) and diameter.

Tension stiffening

In a cracked section, the tensile forces are carried only by the steel while the concrete is assumed to have no stiffness there. For this reason, the stiffness of concrete in the vicinity of the crack is set to zero (as in the case of plain concrete). The tensile forces are transmitted by bond to the surrounding concrete over a transfer length. However, between the cracks, the concrete contributes to the stiffness of the element in a mechanism known as “tension stiffening”. Tension stiffening accounts for the difference between the response of a bare bar and an embedded reinforcing bar. From figure 4.10a, it can be seen that the embedded bar sustains a higher tensile force when compared to the bare bar for a defined strain. This increased capacity is due to contribution of concrete between the cracks. Figure 4.10b illustrates the contribution of concrete in more detail, with the concrete contribution reducing till the fully developed cracked stage, at which point it is assumed to have a constant value (stage c of figure 4.10b). That constant value for tension stiffening, $\Delta\epsilon_{ts}$ is represented by the difference in strain of the member, ϵ_{fdc} (at full developed crack stage) and the strain of the reinforcement, ϵ_s :

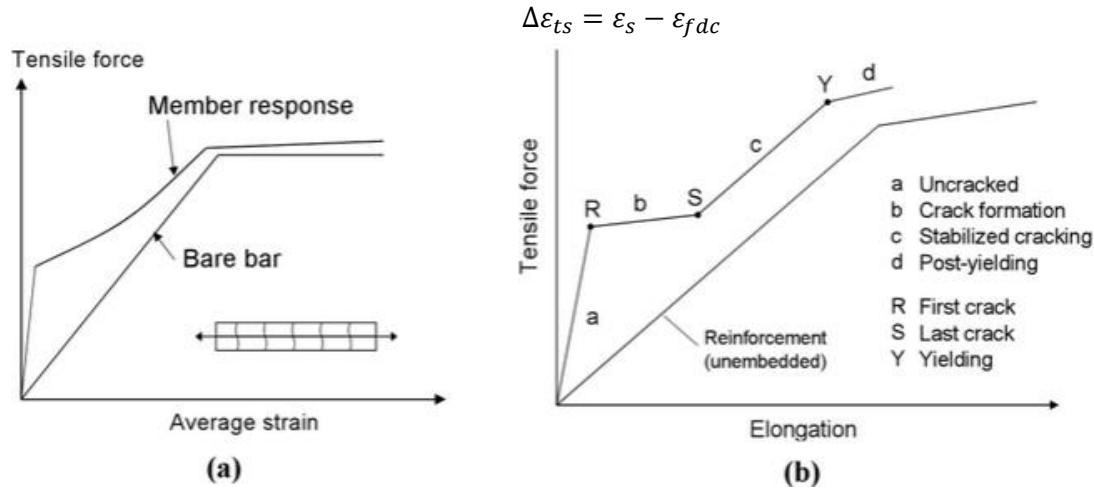


Figure 4.10 – Illustration of tension stiffening

Some ways of modeling tension stiffening include modifying the stiffness of the reinforcing bar, or alternatively, modifying the concrete stiffness (after the generation of crack) to carry tension force (FIB, 2008). The SBETA material model in ATENA (utilized for this work) takes tension stiffening into account, with its magnitude calculated directly from the strain in the reinforcement direction (Červenka, Jendele and Červenka, 2016).

4.3 Constitutive model

I would discuss the constitutive model utilized for this thesis work. The SBETA material in ATENA is used to model concrete, while a bilinear law model for reinforcing steel (specifically elastic-perfectly plastic stress-strain behaviour). In this report, I would present information on the SBETA concrete material model, and discuss the nonlinear behaviour is effected in the stiffness matrix (in uncracked and cracked stage) are obtained.

In ATENA SBETA model, material properties and cracks are modeled using a smeared approach. Assuming 2D plane stress condition, the constitutive model is described by the expression:

$$\boldsymbol{\sigma} = \mathbf{D}\boldsymbol{\epsilon} \quad \text{with} \quad \boldsymbol{\sigma} = [\sigma_x \quad \sigma_y \quad \tau_{xy}]^T \quad \text{and} \quad \boldsymbol{\epsilon} = [\epsilon_x \quad \epsilon_y \quad \gamma_{xy}]^T$$

Where σ , D and ε are the stress vector, material stiffness matrix and strain vector respectively of an element. This assumption is valid for uncracked concrete, which can be treated as isotropic material (with the steel properties transformed into an equivalent concrete section). Perfect bond is assumed to exist between the concrete and steel, thus common strain for all materials at a point. In modeling reinforced concrete (a composite material), the stress vector, σ and composite secant stiffness matrix of the material, D are decomposed into its concrete and steel component as:

$$\sigma = \sigma_c + \sum_{i=1}^n \sigma_{si} \quad \text{and} \quad D = D_c + \sum_{i=1}^n D_{si}$$

With the subscript 'c' denoting concrete, and 'si' denoting the reinforcing steel (where 'i' represent the number of bars). For the steel, it is the cumulative stress and stiffness (from each reinforcing bar) that is taken into account, hence the summation sign in the expression. The stress vector σ_c acts on concrete area, and the steel stress σ_{si} related to the steel area, A_{si} (for all steel provided). The stress and strain vectors are illustrated in figure 4.11 below.

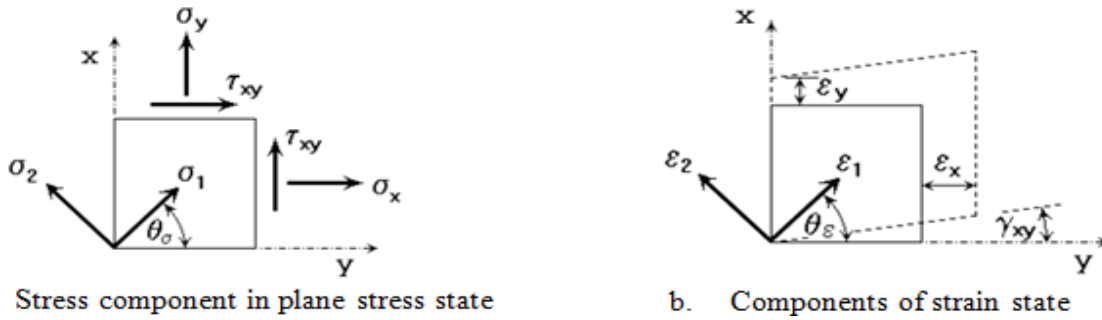


Figure 4.11 – Illustration of stress and strain vectors

The orientation of the principal axes of the stress and strain vectors in figure 4.11a and b are determined using the expressions:

$$\tan(2\theta_\sigma) = \frac{2\tau_{xy}}{\sigma_x - \sigma_y} \quad \text{and} \quad \tan(2\theta_\varepsilon) = \frac{\gamma_{xy}}{\varepsilon_x - \varepsilon_y}$$

Where θ_σ is the orientation of the first principal stress, and θ_ε is for the first principal strain. For isotropic material (like uncracked concrete), the orientations of the stress and strain are similar. For anisotropic material (like cracked concrete), their orientations could differ. In the remaining part of this section, the focus would be on the concrete material model (SBETA) and the constitutive relationship formulation.

4.3.1 Concrete material model (SBETA)

The SBETA material model used in the study incorporates the following features (Červenka, Jendele and Červenka, 2016):

- Non-linear behaviour in compression (includes softening and hardening)
- Biaxial strength failure criterion
- Compressive strength reduction after cracking
- Concrete fracture in tension based on fracture mechanics
- Allows for tension stiffening effect
- Provide two crack models: fixed and rotated crack models

- Shear stiffness reduction after cracking

In the SBETA material model, the stress-strain behaviour is defined by parameters referred to as the ‘effective stress’, σ_c^{ef} and equivalent uniaxial strain, ε^{eq} . In most cases, the effective stress is a principal stress. The equivalent uniaxial strain simulates the strain that would be produced in uniaxial test (in the direction of the stress causing the strain). The equivalent uniaxial strain is computed from the expression $\varepsilon^{eq} = \sigma_{ci} / E_{ci}$. Thus, the strain in any direction ‘i’ is computed from the stress, σ_{ci} and material modulus, E_{ci} associated with that direction. With this approach, the effect of Poisson ratio is ignored, and the nonlinearity in the material (from cracking, softening etc.) is associated with the governing stress, σ_{ci} . An illustration of the uniaxial stress-strain law is presented in figure 4.12.

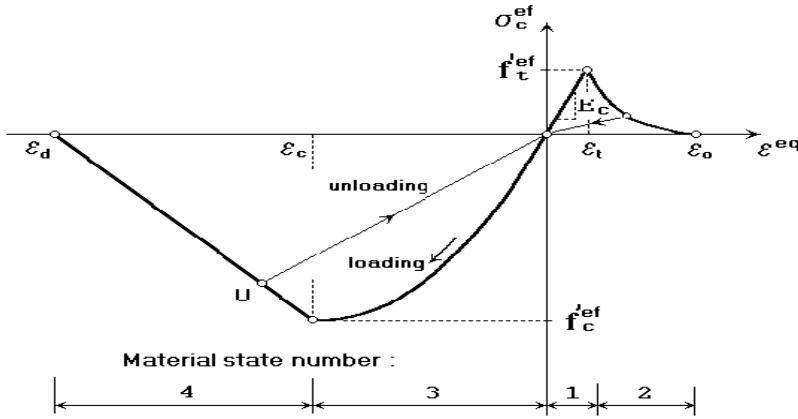


Figure 4.12 –Uniaxial stress strain law for concrete (Červenka, Jendele and Červenka, 2016)

The peak effective compressive stress, f_c^{ef} and peak tensile stress f_t^{ef} are computed from the stress-strain relation for concrete subjected to biaxial loading illustrated in figure 4.13. Thus, the SBETA element adopts an equivalent uniaxial stress-strain relation, with the peak stresses reflecting biaxial stress failure criterion. This uniaxial stress-strain law in figure 4.12 is used to compute the secant modulus (for material stiffness matrix) using the expression below:

$$E_c^s = \sigma_c / \varepsilon^{eq}$$

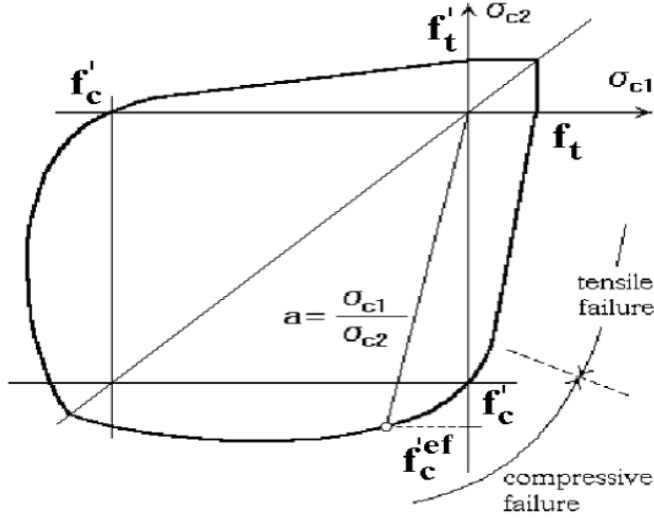


Figure 4.13 – Biaxial failure criterion for concrete

Figure 4.13 shows the biaxial failure criterion for used for the SBETA material model where σ_{c1} and σ_{c2} are principal compressive stresses in the concrete. $f'_c{}^{ef}$ is the effective concrete compressive strength, and f'_c is the uniaxial cylinder strength. Notice the increase in concrete strength (beyond cylinder strength) in the compression-compression due to biaxial compression. In the tension-tension state however, effective tensile strength is equal to the uniaxial tensile strength. In tension-compression state, both tensile and compressive strengths are lower, and ATENA make provision for this by the use of reduction factors. With the material tensile and compressive strengths (or limits) defined by the bi-axial criterion, the behaviour of the material pre-peak strength and post-peak strength would be discussed next.

Concrete in tension pre- and post-peak behaviour

Prior to cracking, concrete element in tension is assumed to behave in a linear elastic manner with the slope governed by the initial elastic modulus of the uncracked concrete, E_c . With $f'_t{}^{ef}$ being the effective tensile strength from the biaxial failure criterion, the pre-peak behaviour of concrete is expressed by the function:

$$\sigma_c{}^{ef} = E_c \cdot \varepsilon^{eq} \leq f'_t{}^{ef}$$

After cracking (i.e. post peak), two approaches are used to allow for cracking behaviour in the concrete. The first, which is based on fracture energy, G_f and a crack opening law is very useful in modeling crack propagation in the concrete. The second approaches utilizes a stress-strain relation for the concrete, and is not suitable for crack propagation prediction. The five alternative models available in SBETA element are shown in figure 4.14. The first three are based on the first approach that used fracture energy, and typically shows relation between the tensile stress and crack width. The last two are based on stress-strain relations. The exponential crack opening model would be used in this thesis work. The exponential crack opening law was derived by Hordijk (1991) as cited by Červenka, Jendele and Červenka (2016).

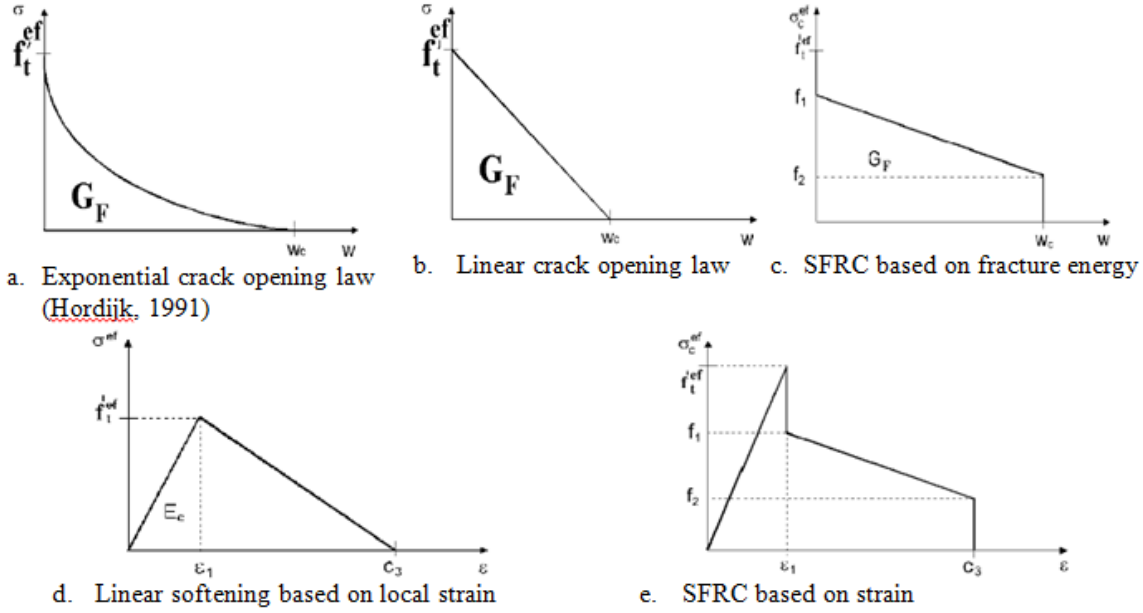


Figure 4.14 – Post-peak behaviour of concrete in tension

Compression behaviour pre- and post-peak

For the SBETA element, the behaviour of the concrete before the peak strength is computed using the expression below (the parameters in the equations are explained in figure 4.15):

$$\sigma_c^{ef} = f_c'^{ef} \cdot \frac{kx - x^2}{1 + (k-2)x} \quad \text{where } x = \frac{\varepsilon}{\varepsilon_c} \quad \text{and } k = \frac{E_0}{E_c}$$

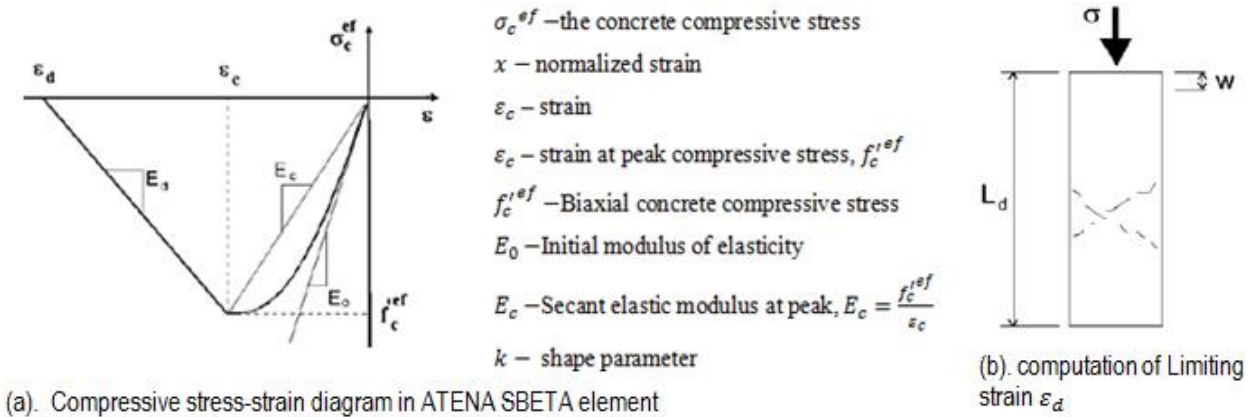


Figure 4.15 – compressive stress strain diagram to illustrate pre-peak and post-peak behaviour

The above expression (similar to equation 3.14 of EC2) is versatile as it enables a wide range of curves (even linear) to be plotted, thus making it applicable for both normal and high strength concrete. The parameter ' k ' which relates the initial elastic modulus to the secant elastic modulus may have a value equal to or greater than 1. It would have a value of 1 for uncracked and undamaged concrete, and a value greater than 1 once there is a damage (or deterioration) in the concrete as in the case of cracked concrete. This makes it possible to include a distributed damage behaviour in the model before peak, instead of a localized damage after peak.

For its post-peak behaviour, a linearly descending softening law is used for concrete in compression. From figure 4.15a, the post-peak softening slope is defined by two points: a point corresponding to the peak stress, f_c^{ref} and strain, ε_c , and second point corresponding to zero stress and a limit compressive strain, ε_d . The limit compressive strain, ε_d is computed from the expression below:

$$\varepsilon_d = \varepsilon_c + w_d / L'_d$$

Where w_d is the plastic displacement and L'_d is the band size as illustrated in figure 4.15b. Based on the experiments of Van Mier (1986) (cited by Červenka, Jendele and Červenka, 2016), the default plastic displacement, w_d recommended in the ATENA SBETA element is $w_d = 0.5mm$. The above expression is based on a fictitious compression plane model, which assumes that compression failure is localized in a fictitious plane. The band size, L'_d is used in an ATENA SBETA element to model this compression failure plane. Note that it is sensitive to element size used and element orientation.

Crack model

Cracking is initiated in concrete when the principal tensile stress, σ_1 exceeds the material tensile strength. The orientation of the crack is usually in a direction perpendicular to the tensile stress. The formation of a crack is one of the most important mechanisms that causes non-linearity in concrete. Two approaches used for modeling cracks in FEM software are the discrete crack approach, and the smeared crack approach. In the discrete crack concept, the cracking is lumped into a line or a plane (often done using interface elements), and formation of gaps between elements is allowed. In the smeared approach, cracking can occur anywhere in the mesh, and in any direction. The SBETA element uses the smeared approach in modeling cracks.

In smeared cracking, the effect of cracks is often spread over the area that belongs to an integration point. Three parameters needed for smeared cracking include the material tensile strength f_t^{ref} , the fracture energy G_f , and the shape of the softening diagram (defined by one of the five post-peak behaviour in figure 4.14). Two models of smeared cracks used in ATENA are the fixed crack model and the rotating crack model. Both of these are illustrated in figure 4.16.

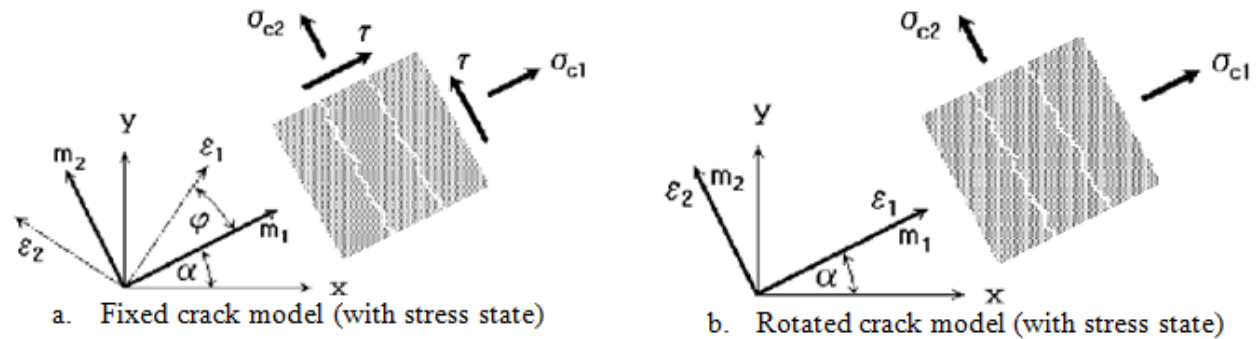


Figure 4.16 – Fixed and rotated crack model illustration (Červenka, Jendele and Červenka, 2016)

In the fixed model, the crack orientation is determined by the direction of the principal stresses at the moment cracking was initiated. For subsequent loading after first cracking, this direction remains fixed. In figure 4.16a, the crack axis is defined by the plane m_1 (the weak material axis) and m_2 (parallel to the crack). In uncracked concrete, the principal stress and strain coincide with this axis since isotropy is assumed for uncracked concrete. After cracking however, the principal strain axes ε_1 and ε_2 may not

coincide with the axes of orthotropy, m_1 and m_2 . Fixing the crack to the $m_1 - m_2$ coordinate axes causes occurrence of shear stresses on the crack face. Note that σ_{c1} and σ_{c2} in figure 4.16a are not principal stresses, but rather stress components normal and parallel to the crack plane respectively, and occur alongside the shear stress. These shear stresses occur because the directions of the principal strains axes ε_1 and ε_2 does not coincide with the axes of orthotropy which defines the crack.

In a rotated crack model, the axis of orthotropy (m_1 and m_2) are not constant, but allowed to rotate coaxially. This way, the direction of the principal stresses would always coincide with that of the principal strain. As a result, there no shear stress or strain would occur on the crack plane as illustrated in figure 4.16b.

4.3.2 Material stiffness matrix

The constitutive behaviour of reinforced concrete is described by the stress-strain relation expressed by:

$$\sigma = D\varepsilon$$

For steel: Starting with the steel, the material stiffness matrix of each steel member along the steel longitudinal direction is formulated thus:

$$\bar{D}_{si} = \begin{bmatrix} \rho_1 \bar{E}_{si} & 0 & 0 \\ 0 & 0 & 0 \\ 0 & 0 & 0 \end{bmatrix}$$

Where \bar{D}_{si} is the stiffness in the local (or bar) coordinate, and the effective secant modulus \bar{E}_{si} is evaluated from $\bar{E}_{si} = f_{si}/\varepsilon_{si}$, where f_{si} and ε_{si} can be determined from the stress-strain used for the reinforcing steel. From the matrix, only component along the axial direction (i.e. longitudinal or x-axis) has a value with the remaining terms being zero. The reinforcing bar is assumed to have negligible shear and flexural rigidity hence the reason for the many zeros in the matrix. With the stiffness determined along the steel bar coordinate, it would be transformed to the global coordinate according to the expression below:

$$D_{si} = T_{si}^T \bar{D}_{si} T_{si}$$

where $T = \begin{bmatrix} \cos^2 \alpha_i & \sin^2 \alpha_i & \cos \alpha_i \sin \alpha_i \\ \sin^2 \alpha_i & \cos^2 \alpha_i & -\cos \alpha_i \sin \alpha_i \\ -2 \cos \alpha_i \sin \alpha_i & 2 \cos \alpha_i \sin \alpha_i & (\cos^2 \alpha_i - \sin^2 \alpha_i) \end{bmatrix}$

For concrete: The stiffness matrix depends on the state of the concrete, whether uncracked or cracked. Uncracked concrete can be treated like an isotropic material, with the stiffness in the global coordinate axes expressed thus:

$$D_c = \frac{E_c}{1 - \nu^2} \begin{bmatrix} 1 & \nu & 0 \\ \nu & 1 & 0 \\ 0 & 0 & \frac{1 - \nu}{2} \end{bmatrix}$$

Where E_c is the initial concrete elastic modulus and ν is the Poisson ratio.

For cracked concrete, the assumption of isotropic material is no longer valid, and the concrete is treated as orthotropic. The axes of orthotropy is aligned with $m_1 - m_2$ axes (earlier defined for the fixed crack model

in figure 4.16), now becomes our local coordinate system. The material stiffness matrix for cracked concrete in this axes, $\bar{\mathbf{D}}_c$ is expressed thus:

$$\bar{\mathbf{D}}_c = \begin{bmatrix} \bar{E}_{c1} & 0 & 0 \\ 0 & \bar{E}_{c2} & 0 \\ 0 & 0 & \bar{G}_c \end{bmatrix}$$

Where \bar{G}_c is the secant shear modulus for concrete, and \bar{E}_{c1} and \bar{E}_{c2} are effective secant modulus in the m_1 and m_2 plane respectively (which correspond to principal tensile and compressive directions). Poisson ratio is ignored in the off diagonal terms of the matrix, hence the reason why they are set to zero in the matrix. Clause 3.1.3(4) of EC2 allow that Poisson ration for cracked concrete be taken as zero. Expressions for the effective secant moduli are thus:

$$\bar{E}_{c1} = \frac{f_{c1}}{\varepsilon_1}; \quad \bar{E}_{c2} = \frac{f_{c2}}{\varepsilon_2}; \quad \text{and} \quad \bar{G}_c = \frac{\bar{E}_{c1} \cdot \bar{E}_{c2}}{\bar{E}_{c1} + \bar{E}_{c2}} \quad (FIB, 2008)$$

f_{c1} represents the principal tensile stress (post-cracking) in the concrete. Non-linear effects like tension stiffening, tension softening etc. can be taken into account in models for calculating f_{c1} . Similarly, f_{c2} which represents the principal compressive stress, can be modeled to include nonlinear effects like compression softening, impact of confinement etc. The principal compressive strains ε_1 and ε_2 are determined from stress-strain relationship used. The global stiffness matrix is determined by transforming from the local axes back to the global reference axes. The material stiffness matrix can thus defined by:

$$\mathbf{D}_c = \mathbf{T}^T \bar{\mathbf{D}}_c \mathbf{T}$$

The contributions of concrete and all reinforcing steel bar are combined to determine the composite stiffness matrix for reinforced concrete. This is expressed thus:

$$\mathbf{D} = \mathbf{D}_c + \sum_{i=1}^n \mathbf{D}_{si}$$

The stiffness matrix is thus incorporated in the constitutive equation $\boldsymbol{\sigma} = \mathbf{D}\boldsymbol{\varepsilon}$ for use in FEM.

4.4 Non-linear analysis

In nonlinear FEM, the relationship between force and displacement is nonlinear due to physical non-linearity in the material, and/or geometrical linearity (already discussed in section 4.1.2). For such problems, the loading history becomes very important in FEM modeling, as the displacement in these case often depend on deformations state from earlier loading history. All these nonlinearity are typically reflected in the stiffness matrix as discussed in the last. For this reason, solution for nonlinear FEM cannot be computed right away (as in the linear case). Rather, the problem is made discrete, not only in space (with finite elements), but also in time with load increments. This section of the report summarizes approach to solving nonlinear FEM problems, iterative schemes typically used in software and convergence criterion (or norms). These aspects briefly discussed here are included in the solution procedure used in ATENA.

4.4.1 Solution procedure

With loading history being important, the use of incremental load steps is available in FEM software. With incremental procedures, the material behaviour would reflect better as the material stiffness is continuously modified with each load steps. Where a purely incremental approach is adopted, the results could drift from

the equilibrium path as illustrated in figure 4.17a (where ' k ' is the stiffness). Thus, some measure needs to be taken to eliminate or reduce the drift. This measure is achieved by using iteration techniques which eliminates (or reduces) the drift by ensuring equilibrium between external and internal loads. A pure iterative procedure also has its shortcomings. Best results is obtained by combining both approaches into an incremental-iterative procedure.

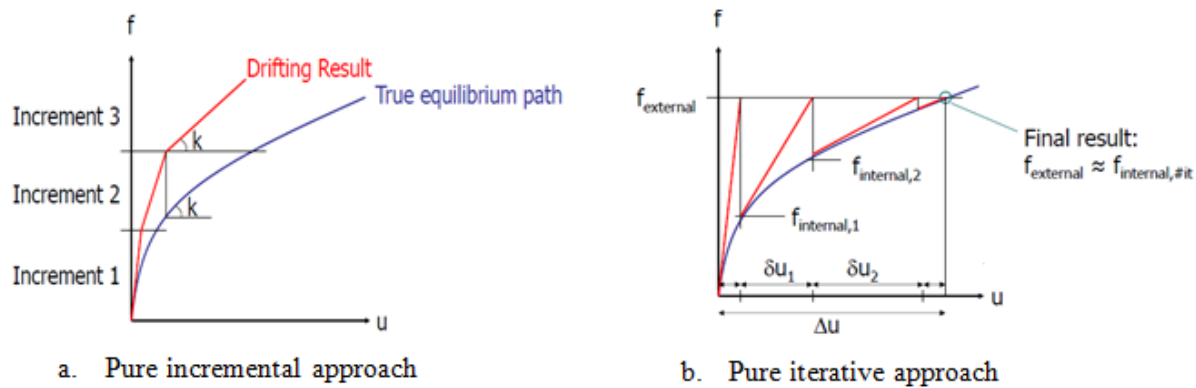


Figure 4.17 – Solution approaches for nonlinear FEM

In the incremental-iterative approach, loads are incrementally applied, and iteration schemes are used to achieve equilibrium (internal and external forces) at the end of the increment. The use of load increment is predictive, while the iterative computations (within each increment) is corrective and helps to eliminate or reduce drifting error.

Three popular ways of effecting load increments in FEM include force control, displacement control, and the arc-length method. In force control, external force is applied to nodes or elements in steps and the resulting displacement is monitored. For displacement control, prescribed displacements are applied to the nodes in incremental steps, and the resulting reaction force monitored. Displacement control is preferable as it more stable than force control, and predicts post peak behaviour like softening, snap-through effect etc. which would not be achieved with force control. Arc-length control utilizes automatic force increments initially followed by subsequent decrements to predict behaviour of the structure beyond the peak.

4.4.2 Iteration schemes and convergence criterion

Several algorithms are incorporated in FEM software to define the actual equilibrium paths. In incremental-iterative approach, these algorithms play a corrective role by ensuring equilibrium between external and internal forces. The most popular algorithms in use are the Newton-Raphson method and the modified Newton-Raphson approach. Are illustrated in figure 4.18.

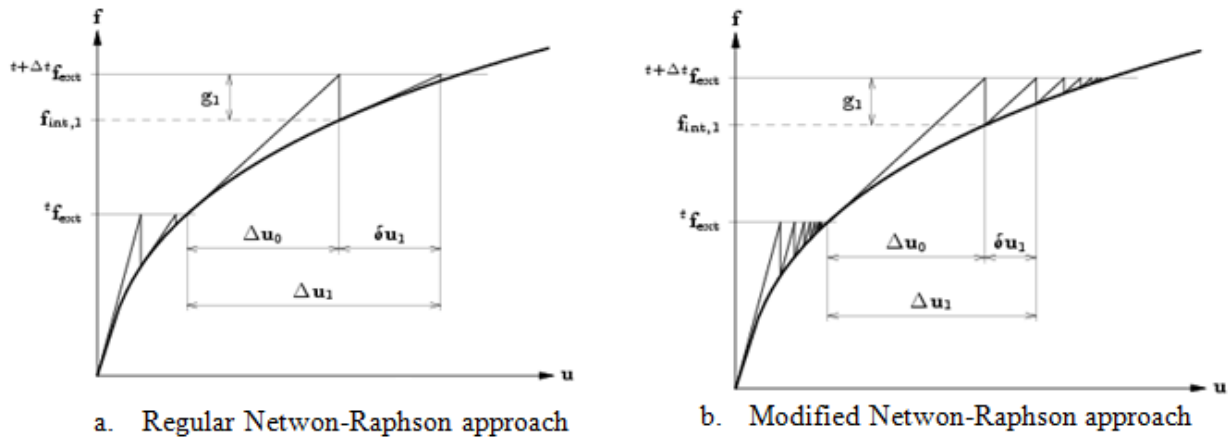


Figure 4.18 – Some iteration methods used for FEM

In the regular Newton-Raphson approach, the stiffness is updated in every iteration, thus the prediction at any time in the analysis is based on the last known state. Thus, the stiffness is not constant, and iteration stops when the solution converges to a value within the set tolerance. With this approach, fewer iterations are required for convergence to the final solution. For the Modified Newton-Raphson approach, the stiffness is only evaluated at the start of the load increment, and remains constant for further iterations within that increment. While this approach requires more iterations for convergence to be achieved, each iteration is faster and could require less computational resources.

The convergence criterion is also an important aspect of nonlinear FEM as equilibrium is sought between the internal and external forces for a displacement vector. The set convergence norm determines what solution is satisfactory, and when iteration should stop. Where the convergence criteria is loose, the solutions obtained are likely to be inaccurate. On the other hand, when the convergence criteria is too stringent, excessive time and effort may be spent in a bid to achieve unnecessary accuracy. Some of the convergence norms used in FEM software include force norm, displacement norm and energy norm. With force norm, the force imbalance between internal and external forces is only a small fraction of applied force. This convergence norm is very useful for load sensitive systems e.g. where stress relaxation occurs. For displacement based convergence, iteration stops when the displacement increment is only a small proportion of the initial displacement increment. This convergence norm is useful in a displacement sensitive scenario like creep. The energy norm criteria combines force and displacement. Iteration stops when the current update of energy becomes a small fraction of the initial energy in the system.

Conclusion: The finite element method would be used to study the role detailing plays in the performance of structures. This chapter has provided some background knowledge to understanding how it works.

5. Analytical design using strut-and-tie model

To investigate the significance of structural details in a structure, a retaining wall would be used as a case study. The case study retaining wall is designed to support a backfill height of 4.5m . Estimation of loads, initial sizing of the structure and stability checks were performed and reported in Appendix 1. A schematic of the retaining wall is illustrated in figure 5.1.

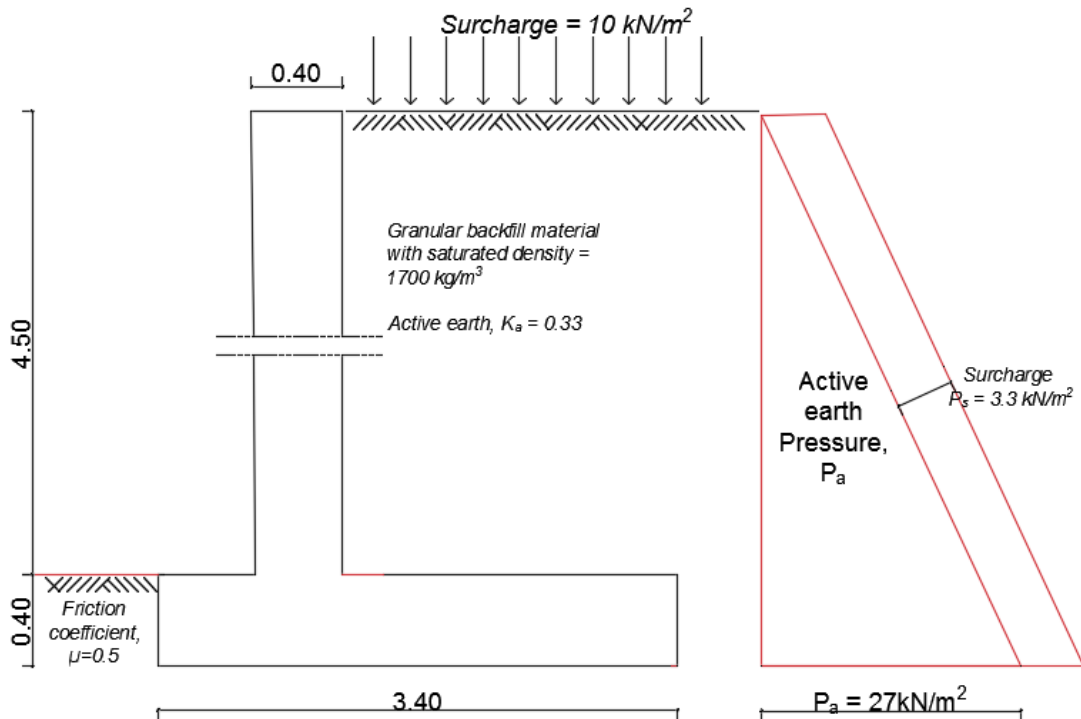


Figure 5.1 – Schematic view of case study retaining wall

The traditional design approach for retaining walls treats it like three separate cantilevers, that meet together at a joint i.e. the wall-base connection. Parts of the structure that are away from the wall-base connection are Bernoulli (or B-) regions. For these parts, the assumption of “linear strain distribution across the section” is valid, and the beam theory is suitable for design. However, the vicinity of the wall-base connection is a disturbed region (or D-region), and the beam theory is unsuitable for their design. The stress distribution is irregular, and would not be accurately predicted by the beam theory. In this chapter of the report, strut-and-tie methodology would be used to analyze force transfer in the D-region of the retaining wall shown in figure 5.1. The design loads acting on the structure has been analyzed, and the resulting bending moment acting on the three cantilevers (i.e. the wall, the heel-side of the base slab, and the toe-side of the base slab) computed. The load analysis and computation of bending moment is presented in Appendix 1. The design actions (loads) required for the strut and tie modeling are the boundary stresses caused by these bending moments. Figure 5.2 show the D-region of the retaining wall, with the bending moments acting on it boundaries.

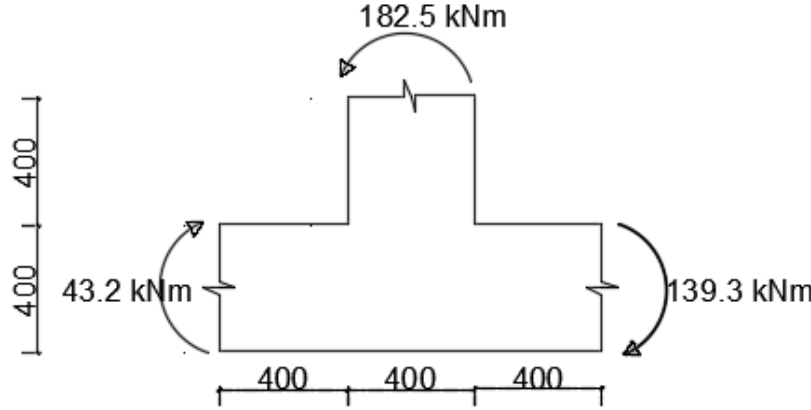


Figure 5.2 – Delineated D-region of retaining wall

The material properties that would be utilized for this design are:

$$f_{ck} = 30 \text{ N/mm}^2 \text{ thus } f_{cd}^3 = 20 \text{ N/mm}^2$$

$$f_{yk} = 500 \text{ N/mm}^2; \quad f_{yd} = 435 \text{ N/mm}^2$$

5.1 Strut and tie analysis of the joint

In this section, the delineated D-region of figure 5.2 would be analyzed using the strut-and-tie method. The flow of forces in the wall-base connection would be estimated to understand stress transfer in the connection, and to guide on a satisfactory way of detailing reinforcement for the connection. The sequence of steps involved in strut and tie design was illustrated in figure 2.4 and is followed in this section.

Boundary stresses for the D-region and force flow in section

The bending moments acting on the section causes bending stresses at the boundaries of the D-region. Assuming that the applied moment acts at the centerline of the section, the loading subjects part of the section to tensile stresses, and other parts to compressive stresses. With the section modulus $W = 1 \times 0.4^2 / 6 = 26.67 \cdot 10^{-3} \text{ m}^3$ (for 1m length of wall), the boundary stresses can be computed thus:

$$\sigma_{1,2} = \pm \frac{M}{W} = \frac{182.5}{26.67 \cdot 10^{-3}} = 6,844 \text{ kN/m}^2 \text{ (for the wall)}$$

$$\sigma_{1,2} = \pm \frac{M}{W} = \frac{139.3}{26.67 \cdot 10^{-3}} = 5,224 \text{ kN/m}^2 \text{ (for the heel slab)}$$

$$\sigma_{1,2} = \pm \frac{M}{W} = \frac{43.2}{26.67 \cdot 10^{-3}} = 1,620 \text{ kN/m}^2 \text{ (for the toe slab)}$$

These boundary stresses acting on the D-region are depicted in figure 5.3a. To be useful for strut and tie modeling, the resultant forces caused by these border stresses are computed from the area of the stress diagram. These resultant forces act through the centroid of the stress diagram as shown in figure 5.3b.

³ f_{cd} is 20 MPa when the characteristic strength is divided by the partial safety factor for concrete. In a strut and tie model, this value could be further reduced by a factor α_{cc} depending on whether the node is a CCC, CCT, CTT etc. Refer to section 2.4.3 of the report for more information on this matter.

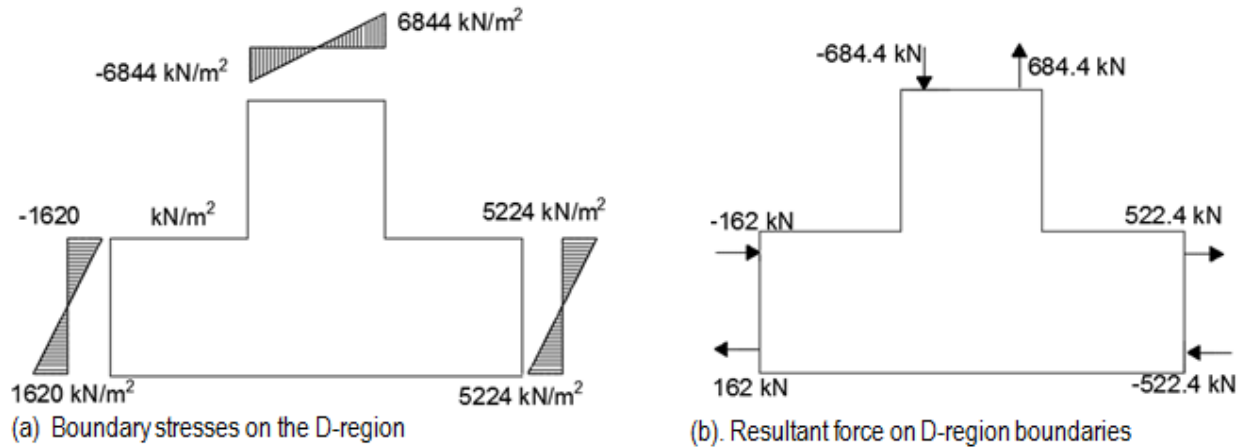


Figure 5.3 – Stresses and resultant forces acting on D-region

With the stresses and resultant forces acting on the boundary now determined, the next step is essentially placing a truss within the D-region to carry the forces through it. The model used should be compatible with the actual stress flow in the structure. The truss model consists of struts to carry compressive stresses, ties to carry tensile stresses and nodes where three or more struts and/or ties meet. The proposed strut and tie model for this section is illustrated in figure 5.4.

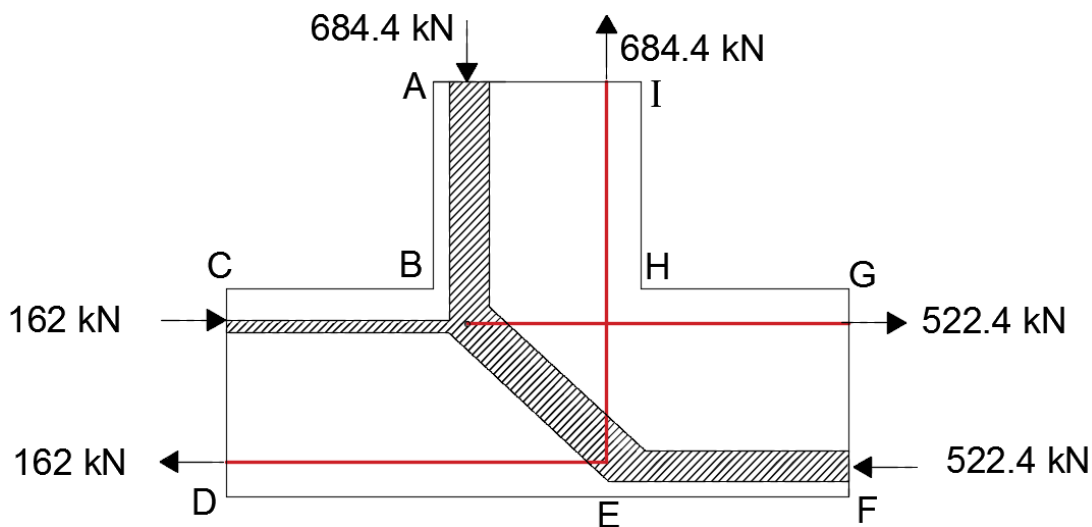


Figure 5.4 – Proposed strut and tie model

In figure 5.4, the strut models the compressive stress flow while the tie models the tensile stress flow in the section in response to applied loads. Nodes occur where three or more struts and/or ties meet. Ties are allowed to cross each other without a node, thus there is no node in point H. The nodes in figure 5.4 are located in points B and E. The node is essentially a volume of concrete in the region where struts and/or ties meet, and thus has defined geometric dimensions. The dimensions of the nodes, struts and ties would be determined based on the forces they are subjected to and their material strength. Treating the nodes as pinned joint, and applying the conditions for equilibrium i.e. $\sum F_x = 0$, $\sum F_y = 0$ and $\sum M = 0$, the internal force distribution can be obtained using the method of joint resolution (from structural analysis). The computed internal forces in the struts and tie of the D-region is presented in figure 5.5.

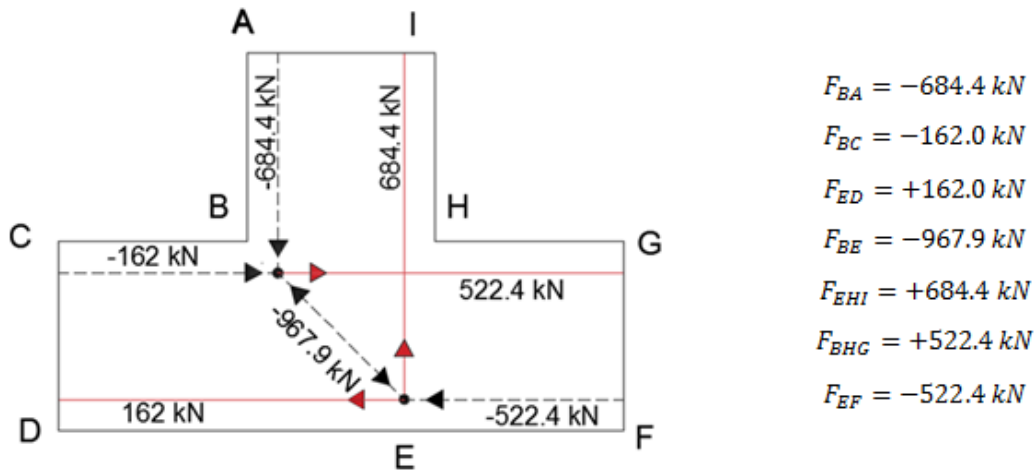


Figure 5.5 – Internal forces in strut and tie model

The internal forces in the struts and ties are illustrated in figure 5.5. Note that the angle between the ties and the inclined strut at nodes B and E is 45 degrees, thus well within the requirements of EC2 and the fib model code 2010. The inclined strut connecting nodes B and E transfers the largest internal forces, and it also plays the role of diverting compressive stresses from the wall into the heel of the base slab. Unlike the other struts (i.e. member BC, BA and EF) which can be treated as prismatic struts, the strut BE is a bottle-shaped strut, thus is likely to play a critical role in the performance of the joint. In the next section, geometrical dimensions of the struts, node and ties would be done.

Dimensioning of nodes, struts and ties

The concept of "hydrostatic node" would be used to dimension the nodes, struts and ties in this section. Hydrostatic node implies ensuring equal stress on all nodal face. The strut and tie model in figure 5.4 shows four struts and/or ties acting on nodes B and E each. To simplify the problem, the nodal forces would be resolved into two cases involving three forces each.

Node B

The four forces acting on node B is simplified to two cases with three forces each as illustrated in figure 5.6. The ties act from behind the node, and thus put the node in compression despite being a tensile member. The equilibrium conditions are met in the three cases.

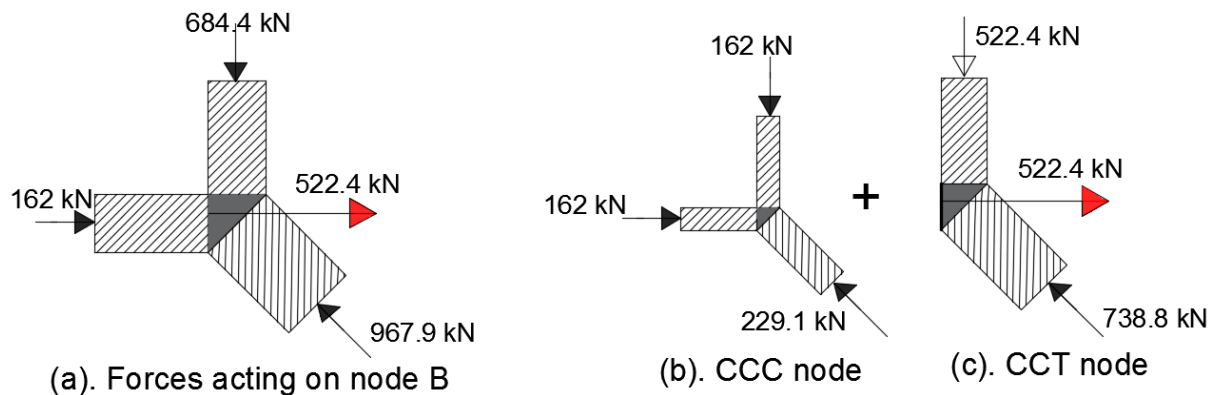


Figure 5.6 – Resolving Node B forces to two simpler models

We now have a CCC node (figure 5.6b) and a CCT node (figure 5.6c) replacing the original state of the node. The CCC and CCT nodes would be initially treated separately in this section, and later combined to determine the final dimensions of the node, struts and ties.

For the CCC Node (figure 5.6b)

Though this node is compressed on all faces, there is actually a tie (member BHG) that passes through it. This would be taken into consideration in determining the strength of the node. The maximum strength of the node from EC2 is determined using the expression:

$$\sigma_{Rdmax} = k_i \cdot [1 - f_{ck}/250] \cdot f_{cd}$$

Where k_i is 1.0 for a CCC node and 0.85 for a CCT node. Since a tie actually passes through this node, $k_i = 0.85$ would be used. Though this sub-node is CCC, the material strength would be treated like a CCT node. Thus, the nodal strength is:

$$\sigma_{Rdmax} = 0.85 \cdot [1 - 30/250] \cdot 20 = 14.96 \text{ N/mm}^2$$

Struts AB, CB and EB

Struts AB and CB are in uniaxial compression (thus prismatic), thus its strut strength is determined thus:

$$\sigma_{Rdmax} = \alpha_{cc} f_{ck} / \gamma_c = 0.85 \times \frac{30}{1.5} = 17 \text{ N/mm}^2$$

A value of 0.85 is used for α_{cc} in calculating the concrete compressive strength above. This value is used to provide additional safety in case of an unfavourable effect may result from the way the load is applied.

Strut BE is bottle-shaped and the strength is determined thus:

$$\sigma_{Rd,max} = 0.6 [1 - f_{ck}/250] f_{cd} = \sigma_{Rd,max} = 0.6 [1 - 30/250] 17 \approx 8.98 \text{ N/mm}^2 \text{ (*governs*)}$$

Since the smallest strength of any component in the nodal region is 8.98 N/mm^2 , this strength governs in the design. Next, the nodes would be dimensioned such that the maximum stress on any nodal face should not exceed 8.98 N/mm^2 . The capacity of the nodal face can be obtained using the expression:

$$F_{cu} = A_c \sigma_{Rd,max}$$

where F_{cu} is the compressive force acting on that nodal face, and A_c is the area of the nodal face. We assume a length of 1 m (*i.e.* 1000 mm). The width of the nodal face is thus obtained using:

$$w_i = F_{cu} / 1000 \cdot \sigma_{Rd,max}$$

Nodal face with strut AB:

$$w_{AB,1^4} = \frac{162 \cdot 10^3}{1000 \cdot 8.98} = 18.04 \text{ mm}$$

Nodal face with strut CB:

$$w_{CB} = \frac{162 \cdot 10^3}{1000 \cdot 8.98} = 18.04 \text{ mm}$$

Nodal face with strut EB:

⁴ Note that I used '1' in this notation $w_{AB,1}$ because there is additional width component from the CCT node in figure 5.6c. Combining both widths would give us the total strut width required for the member.

$$w_{EB,1} = \frac{229.1 \cdot 10^3}{1000 \cdot 8.98} = 25.51 \text{ mm}$$

For the CCT node (figure 5.6c)

The expression for maximum allowable material strength for CCT node is:

$$\sigma_{Rdmax} = k_i \cdot [1 - f_{ck}/250] \cdot f_{cd}$$

Where $k_2 = 0.85$ on account of the presence of tie in the node. This has already been taken into account (in the previous page) when determining the compressive strength of the node. Thus, the strength values here are similar to those used earlier, with the governing strength being 8.98 N/mm^2 . Consequently:

Nodal face with strut AB:

$$w_{AB,2} = \frac{522.4 \cdot 10^3}{1000 \cdot 8.98} = 58.20 \text{ mm}$$

Nodal face with strut BE:

$$w_{EB,2} = \frac{738.8 \cdot 10^3}{1000 \cdot 8.98} = 82.27 \text{ mm}$$

Nodal face with tie BHG

$$w_t = \frac{522.4 \cdot 10^3}{1000 \cdot 8.98} = 58.20 \text{ mm}$$

Note that $w_t = 58.20 \text{ mm}$ is the effective width of the concrete area that surrounds tie BHG. It does not contribute to tensile strength. It is only used here to define the tie geometry. The area of reinforcing steel required for the tie would be dimensioned later in this chapter.

Combined CCC and CCT: The final dimension for struts AB and EB is obtained by summing their contribution from the CCC and CCT node i.e. $w_{AB} = w_{AB,1} + w_{AB,2}$. This is repeated for w_{EB} . A summary of the forces and dimension for the components of node B is summarized in Table 5.1.

Table 5.1 – Summary of forces and geometry for Node B

Component	Member type	Axial force (kN)	Governing strength (N/mm ²)	Minimum width (mm)
B	Node		8.98	
A–B	Strut	684.4	8.98	76.22
C–B	Strut	162	8.98	18.04
E–B	Strut	967.9	8.98	107.8
B–H–G	Tie	522.4	8.98	58.20

To confirm that the node is indeed hydrostatic, and that the stresses are less than minimum σ_{Rdmax} , the expression below is used:

$$\frac{F_{AB}}{w_{AB}} = \frac{F_{CB}}{w_{CB}} = \frac{F_{EB}}{w_{EB}} = \frac{F_{BHG}}{w_t} \leq \sigma_{Rd,max}$$

$$\frac{684.4}{76.22} = \frac{162}{18.04} = \frac{967.9}{107.8} = \frac{522.4}{58.20} = 8.98 \text{ N/mm}^2$$

Thus the node is hydrostatic and not stressed beyond the design limit. Furthermore, with a width of 400 mm , there is enough space in the section to accommodate the struts, ties and nodes.

Node E

For simplicity, the four forces acting on node E is resolved to two cases with three forces each as illustrated in figure 5.7. The forces are in equilibrium at the node.

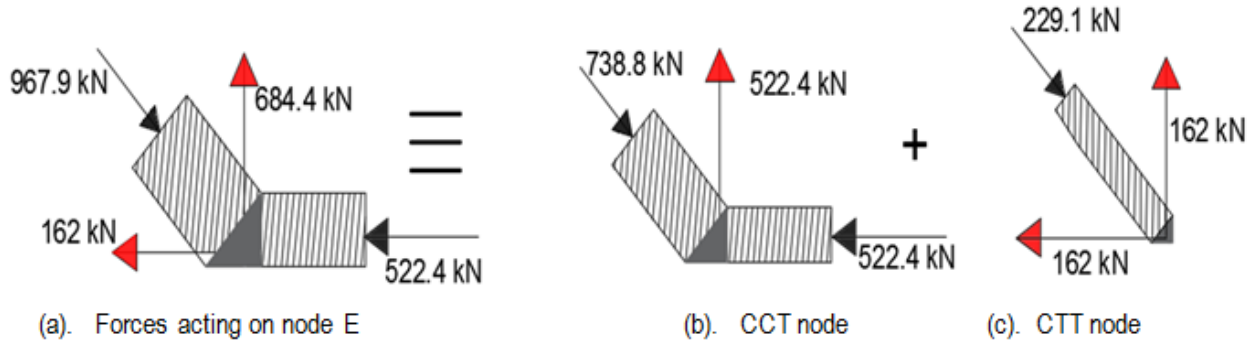


Figure 5.7 – Resolving Node E forces to two simpler models

The sub-nodes are now a CCT node and a CTT node. Like before, both would be initially treated separately, and the geometry later combined.

For CCT Node (figure 5.7b)

For the Node, the maximum allowable stress is obtained from the expression:

$$\sigma_{Rdmax} = k_i \cdot [1 - f_{ck}/250] \cdot f_{cd}$$

Though $k_i = 0.85$ for CCT node, this would be treated this like a CTT node because of the presence of two ties (as seen in figure 5.7a), thus $k_i = 0.75$. Therefore, nodal strength is:

$$\sigma_{Rdmax} = 0.75 \cdot [1 - 30/250] \cdot 17 = 11.22 \text{ N/mm}^2$$

For the struts, the bottle-shaped strut BE would give the lowest strength, determined via the expression:

$$\sigma_{Rd,max} = 0.6 \left[1 - \frac{30}{250} \right] \cdot 17 \approx 8.98 \text{ N/mm}^2 \text{ (governs)}$$

Thus, despite the CTT node having its strength further reduced, the bottle shaped strut is still governing. Consequently, the expressions that was used for node B is also applicable for this case. Thus the width of components in node E would be obtained using the expression:

$$w_i = \frac{F_{cu}}{1000 \cdot \sigma_{Rd,max}}$$

Nodal face with strut FE:

$$w_{FE} = \frac{522.4 \cdot 10^3}{1000 \cdot 8.98} = 58.20 \text{ mm}$$

Nodal face with strut BE:

$$w_{BE} = \frac{738.8 \cdot 10^3}{1000 \cdot 8.98} = 82.27 \text{ mm}$$

Nodal face with tie EHI:

$$w_{EHI,1} = \frac{522.4 \cdot 10^3}{1000 \cdot 8.98} = 58.20 \text{ mm}$$

For CTT Node (figure 5.7c)

Nodal face with tie DE:

$$w_{DE} = \frac{162 \cdot 10^3}{1000 \cdot 8.98} = 18.04 \text{ mm}$$

Nodal face with tie EHI:

$$w_{EHI,2} = \frac{162 \cdot 10^3}{1000 \cdot 8.98} = 18.04 \text{ mm}$$

Nodal face with strut BE:

$$w_{BE,2} = \frac{229.1 \cdot 10^3}{1000 \cdot 8.98} = 25.51 \text{ mm}$$

Combined CCC and CCT: The final dimension for struts BE and tie EHI is obtained by summing their contribution from the CCT and CTT node. This is summarized in table 5.2. As with node B, the nodes are hydrostatic, and the stresses on the nodal faces is below the design maximum allowable stress

Table 5.2 – Summary of forces and geometry for Node E

Component	Member type	Axial force (kN)	Effective strength (N/mm ²)	Minimum width (mm)
E	Node		8.98	
D–E	Tie	162	8.98	18.04
B–E	Strut	967.9	8.98	107.8
F–E	Strut	522.4	8.98	58.20
E–H–I	Tie	684.4	8.98	76.22

Bottle-shaped strut BE

From the dimension of nodes B and E in Table 1 and Table 2, it is clear that the bottle-shaped strut connecting node B and E transfers the largest internal force, and is thus critical to the performance of the joint. Apart from the axial compressive forces in the strut, there is also some transverse tensile stresses which could actually cause cracking longitudinally along the axis of the strut. These transverse cracks actually reduce the compressive strength of the strut. This was taken into account in the calculation of the concrete strength. However, the presence of transverse tensile stresses in the strut is still a concern, as it is the primary cause of diagonal tension cracking failure discussed in section 3.2 and section 3.4.4 of this report. The diagonal tension force would be estimated next using expressions from section 6.5.3 of EC2. Figure 5.8 illustrates the parameters used to compute the transverse tension force to be resisted.

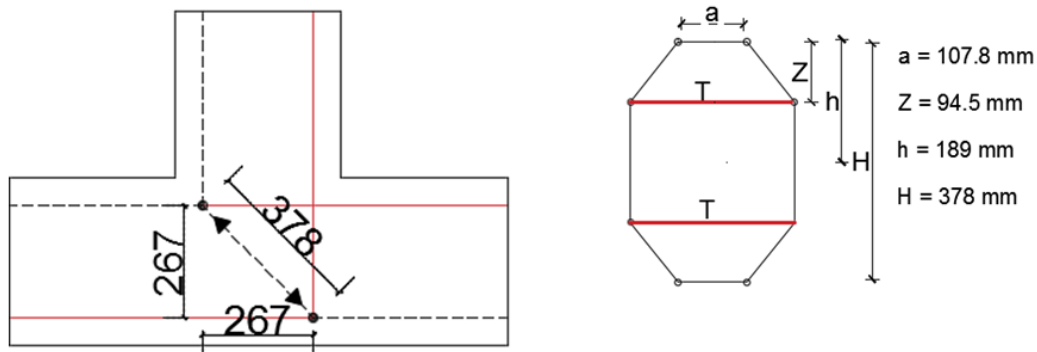


Figure 5.8 – Dimensions of the bottle-shaped strut BE

The joint region in this case is a fully disturbed with no B-region within it. For such a fully discontinuous region, clause 6.5.3(3) of EC2 gives the equation for computing transverse tension as:

$$T = \frac{1}{4} \cdot \left(1 - 0.7 \frac{a}{h}\right) \cdot F$$

$$T = \frac{1}{4} \cdot \left(1 - 0.7 \frac{107.8}{189}\right) \cdot 967.9 = \mathbf{145.4kN}$$

Thus, a tension force of 145.4kN is estimated from the transverse tensile stresses within the joint. Even if cracking is not prevented, the structural detail of the wall-base connection should be capable of preventing diagonal tension cracking failure from these tensile stresses. Typical strategies used for this purpose includes bending the main reinforcement into a loop within the joint, use of inclined stirrups to control the cracks, use of bent bar to cross the strut path etc. This topic was discussed extensively in section 3.4 of this report.

The dimension of all ties including the above transverse reinforcement is treated in next section.

5.2 Reinforcement design

In addition to ties include DE, EHI and BHG, additional ties exist due to transverse tension in the bottle-shaped strut 'BE'. However, the tie in strut BE is a secondary reinforcement, and may not be used in some structural details. In this section, the required area of steel for each of this tie would be estimated, and some aspects of detailing introduced.

Primary Reinforcement (Tie EHI)

$$\text{Axial Tensile Force, } F_{EHI} = 684.4 \text{ kN}$$

$$\text{Therefore } A_s = \frac{F_{EHI}}{f_{yd}} = \frac{684.4 \cdot 10^3}{435} = 1573 \text{ mm}^2/\text{m}$$

Provide 20 mm diameter bars at 175 mm spacing for tie EHI. $A_{s,prov.} = 1795 \text{ mm}^2/\text{m}$.

Primary Reinforcement (Tie DE)

$$\text{Axial Tensile Force, } F_{DE} = 162 \text{ kN}$$

$$\text{Therefore } A_s = \frac{F_{DE}}{f_{yd}} = \frac{162 \cdot 10^3}{435} = 373 \text{ mm}^2/\text{m}$$

An option is to provide 16 mm diameter bars at 200 mm spacing for tie DE. $A_{s,prov.} = 1005 \text{ mm}^2/\text{m}$. This seems cheaper in terms of usage of material. However, there is some benefit obtained if the rebar EHI bends, around node E (in figure 5.4) and becomes tie DE. The bend provides some confinement to the strut BE, and thus would improve strength of the node. In addition, it could save some fabrication (or workmanship cost) as the straight tie EHI would still have been bent to properly secure anchorage by bond. However, if EHI bends in to become Tie DE, the same fabrication cost (for bend) would still be incurred.

I propose the tie EHI (i.e. 20 mm diameter bars at 175 mm spacing) be bent around the node to form DE. It seems a waste of material, but it could save labour cost, while providing additional benefits to the joint.

Primary Reinforcement (Tie BHG)

$$\text{Axial Tensile Force, } F_{BHG} = 522.4 \text{ kN}$$

Therefore

$$A_s = \frac{F_{tu}}{f_{yd}} = \frac{522.4 \cdot 10^3}{435} = 1201 \text{ mm}^2/\text{m}$$

Provide 20 mm diameter bars at 250 mm spacing for tie BHG. $A_{s,prov.} = 1257 \text{ mm}^2/\text{m}$. A straight bar can be used here.

Transverse Ties (in for diagonal strut BE)

Since the transverse ties are for crack control, the yield stress for ULS (i.e. $f_{yd} = 435 \text{ MPa}$) would not be used to prevent occurrence of large cracks. In this case, the steel stress would be limited to $f_s = 200 \text{ MPa}$.

$$\text{Tensile Force (F}_{BE}) = 145.4 \text{ kN}$$

$$\text{Therefore } A_s = \frac{F_{BE}}{f_s} = \frac{145.4 \cdot 10^3}{200} = 727 \text{ mm}^2/\text{m}$$

Provide 10 mm diameter bars at 100 mm spacing for the tie smeared in a direction transverse to strut BE. $A_{s,prov.} = 785 \text{ mm}^2$. This area of steel should be provided where reinforcement is the strategy adopted in the detail to control diagonal cracking in the joint. Where looped reinforcement is used in the joint, there may be no need for this reinforcement.

Secondary reinforcement

16 mm diameter bars at 300 mm spacing should be used as distribution steel to support main reinforcement. This reinforcement should be placed on compression faces also to control crack.

5.3 Background to detailing

A schematic view of the retaining wall showing the main reinforcing bars is presented in figure 5.9 (without the reinforcement details at the joint). In the next chapter of this report, finite element software (ATENA) will be used to study the impact of the structural details used in the connection (i.e. the hatched circle in figure 5.9). For the wall reinforcement to be able to transfer its tensile load to the bottom slab, it needs to be properly anchored in the base slab. In what way does this anchorage affect the performance of the structure? What is the impact of bending the reinforcement towards the heel, or towards the toe, or not bending it at all (i.e. leaving it straight down)? These issues would be studied in the next chapter using FEM.

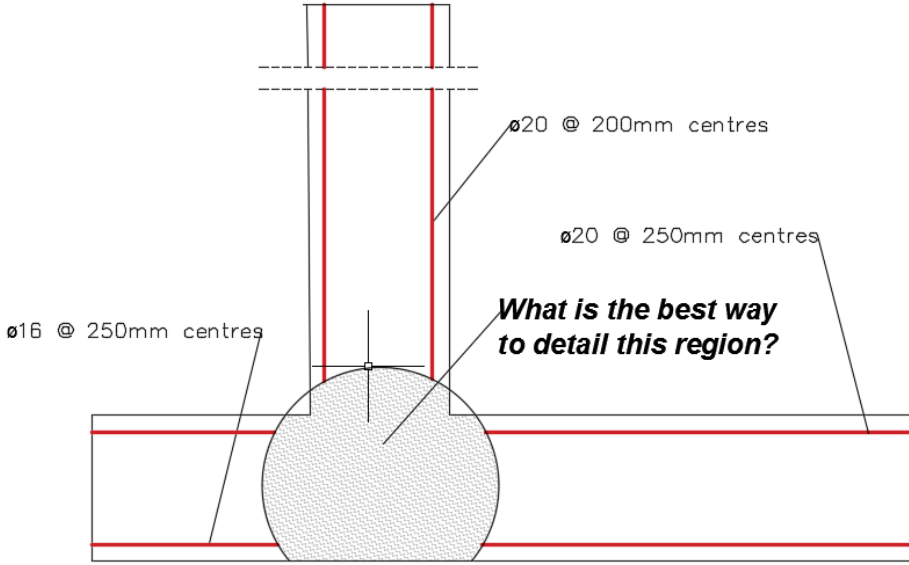


Figure 5.9 – Reinforcing bars in wall and base slab (excluding the connection).

Moment capacity of wall

The desired scenario occurs where the joint is stronger than the connected member i.e. the joint does not prevent the connected member from reaching their design capacity. In the next chapter, the flexural strength of the wall would be used as a reference strength to assess the efficiency of joint reinforcement details. Moment capacity for the wall would be computed next. Taking a 1m width of the wall with the following parameters:

Width, $b = 1000\text{mm}$; Wall thickness, $h = 400\text{mm}$; Concrete cover = 35mm;
 Effective depth = 335mm $f_{yd} = 435\text{ MPa}$ $f_{cd} = 20\text{ MPa}$ $A_{s,wall} = 1795\text{ mm}^2$

Assuming the bilinear stress strain relationship for concrete in compression:

For equilibrium, $\alpha \cdot f_{cd} \cdot b \cdot x_u = A_s \cdot f_{yd}$ thus $x_u = \frac{A_s \cdot f_{yd}}{\alpha \cdot b \cdot f_{cd}}$

Moment capacity $M_{Rd} = A_s \cdot f_{yd} (d - \beta \cdot x_u) = A_s \cdot f_{yd} \cdot d \cdot \left(1 - \frac{\beta \cdot \rho \cdot f_{yd}}{\alpha \cdot f_{cd}}\right)$

where $\rho = \frac{A_s}{b \cdot d} = 0.0054$; sectional area factor, $\alpha = 0.75$; and distance factor, $\beta = 0.39$

$$M_{Rd} = 1795 \times 435 \times 335 \times \left(1 - \frac{0.39 \times 0.0054 \times 435}{0.75 \times 20}\right) \times 10^{-6}$$

$$M_{Rd} = 245.7 \text{ kNm}$$

The above calculated moment capacity would serve as a reference to which the joint capacity would be compared in the next chapter.

Anchorage length for wall

To fully develop the above moment capacity, the wall reinforcement needs to be properly anchored in the base slab. In this case, anchorage would be facilitated by bond between the concrete and steel. From equation 8.4 of EC2, the required anchorage length can be computed using the expression:

$$l_{bd} \geq \alpha_1 \cdot \alpha_2 \cdot \alpha_3 \cdot \alpha_4 \cdot \alpha_5 \cdot l_{b,rqd} \geq l_{b,min}$$

The bond stress, $f_{bd} = 2.25 \cdot \eta_1 \cdot \eta_2 \cdot f_{ctd} = 3.0 \text{ MPa}$ (where $f_{ctd} = 1.333 \text{ MPa}$, and good bond is assumed, thus $\eta_1 = 1.0$, and with steel diameter being less than 32mm, thus $\eta_2 = 1.0$). Assuming constant bond stress, the basic required anchorage length ($l_{b,rqd}$) is next computed using the expression:

$$l_{b,rqd} = \frac{\emptyset \sigma_{sd}}{4 f_{bd}} = 725 \text{ mm}$$

with $\sigma_{sd} = f_{yd} = 435 \text{ MPa}$, diameter, $\emptyset = 20\text{mm}$, and a constant bond stress, f_{bd} of 3.0 MPa. The design anchorage length is computed next. Assumptions made include $\alpha_1 = 1.0$ (straight bar), $\alpha_2 = 0.7$ (thus we derive some benefit from having a cover of 65mm). $\alpha_3 = \alpha_4 = \alpha_5 = 1.0$ implying we take no benefit from confinement by transverse reinforcement, welded reinforcement or pressure. In reality, the lateral pressure acting on the wall could have provided some benefit in α_5 , but I have disregarded it in this computations. The design anchorage length is thus:

$$l_{bd} \geq 1 \times 0.7 \times 1 \times 1 \times 1 \times 725 = \mathbf{507.5 \text{ mm}}$$

The design anchorage length computed is more than the slab thickness, thus it would be appropriate to bend it. Does the direction it is bent to matter? This would be investigated in the next chapter in addition to other aspects of detailing the joint.

6. Finite Element Analysis of the D-region

In the last chapter, a preliminary analysis for the D-region of the case study retaining wall was studied using strut-and-tie methodology. Though the required area of reinforcement was calculated, detailing of the D-region was not undertaken. The position and general layout of reinforcing steel would play a vital role in the behaviour of the joint. Due to concrete's low strength in tension, steel is often relied on as the main tensile member in reinforced concrete (with the concrete strength usually ignored in design). Thus the steel layout plays a role in determining tensile stress and strain distribution within the joint, its failure mode, and even its ultimate capacity.

In this chapter, ATENA finite element software would be used to study different aspects and variants of reinforcement detailing for the D-region. Specific questions of interest include, “does the embedded length of the wall reinforcement (into the base slab) affect the joint efficiency?”, “does the direction of bend (for bent reinforcement) matter”, “how should the joint be detailed in order to meet the design requirements earlier discussed in section 3.1 of this report” etc. This chapter is set out as follows: the FEM layout used in the pre-processing is discussed in the next section, along with material parameters used. Section 6.2, presents a study on the impact of embedment depth (of wall reinforcement into base slab), effect of bending the wall reinforcement to the toe or to the heel, and joint improvement using diagonal bar (at re-entrant corner). For this study, several variants of the joint details would be analyzed and compared. It would provide a background knowledge that would be useful in later study of other reinforcement layouts typically used in practice. Section 6.3 is a detailed study of the two connection types earlier presented in figure 1.1. The remaining sections of the chapter studies the influence of bond model assumptions on the FEM results, (section 6.4), and improvements that can be made to the details to ensure that the structure achieves over 100% joint efficiency (section 6.5).

6.1 FEM Layout

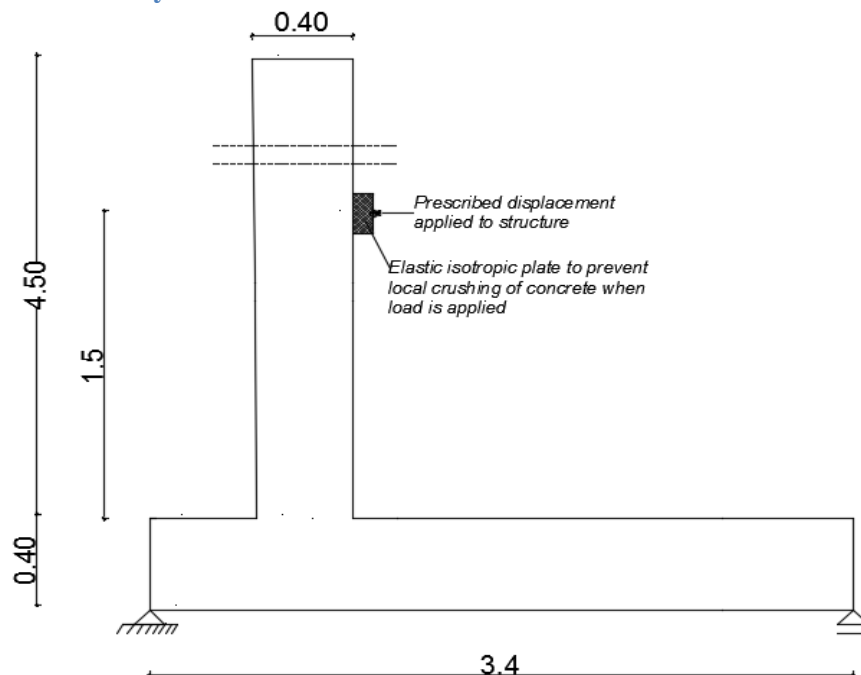


Figure 6.1 – Geometrical model used for FEM [m]

Figure 6.1 shows the geometrical model used to represent the retaining wall in FEM. The structure is idealized as being pin-supported at the toe, and supported by a roller at the heel. The structure was divided into four macro-elements to delineate the D-region from the rest of the structure. For meshing, quadrilateral element types are used for all the macro-elements. A finer mesh size is used for the macro-element representing the D-region of the structure, while a coarser mesh is used for the macro-elements that are outside the D-region. For the FEM analysis, the wall and base slab thickness of one metre (1 m) is assumed.

Material models used:

For concrete, the ATENA SBETA material model is used. The material parameters used for this work is thus:

$$f_{cd} = 20\text{MPa}; \quad f_{ctd} = 1.333\text{MPa} \quad E_c = 33,000\text{MPa} \quad \mu = 0.2$$

For tensile behaviour: Exponential softening model with fracture energy, $G_f = 72.5\text{N/m}$.

For compression: $\varepsilon_{c3} = 1.75\%$; $\varepsilon_{cu} = 3.50\%$.

With the model, there is a reduction of compressive strength when cracking occurs. In addition, several nonlinear aspects like cracking, tension softening, compression softening etc. are a feature of the material model. These and other features were discussed in section 4.3 of this report.

For steel: The bilinear elastic-perfectly plastic model is used. The material design strength, $f_{yd} = 435\text{MPa}$ and the modulus, $E_s = 200,000\text{MPa}$.

For the composite action of concrete and steel, perfect bond is assumed to exist. Also, the SBETA element allows for tension stiffening between steel and the cracked concrete.

Loading: The structure is idealized as being weightless with the loads on the structure comprising of a prescribed displacement and support reactions. The prescribed displacement was applied to a node placed at 1.5m height in the wall (above the base). In this position, it could be comparable to the triangular distribution of earth pressure in a typical retaining wall, with the resultant horizontal load acting at one-third of the wall height. The prescribed displacement was not applied directly to the wall to prevent local crushing at the point of action. Rather, a plane stress elastic plate (50mm thick and 100mm high) was placed on the wall, and the prescribed displacement was applied to a mid-node positioned 1.9m from the bottom of the structure. With this loading layout, no local crushing occurred at the point of load application.

Analysis aspect: An incremental-iterative procedure is used, in which the prescribed displacement is applied in small increments up till failure. For iteration, the regular Newton-Raphson method was used with the stiffness updated at every iteration. To obtain data for this study, monitoring points, cuts and moment lines were defined in the model. Data collected from monitoring point include the prescribed displacement, the reaction force at the point of load application, and the vertical and horizontal reactions at the support (to enable equilibrium check). The cuts provided stress and strain data at the cut section for study. Finally, the moment lines provided data on the bending moment that corresponds to the prescribed displacement. From section 5.3 of the report, an analytical moment capacity of 245.7kNm was estimated. In this chapter, it would be used as a reference moment capacity to evaluate the joint efficiency of the details studied.

6.2 Study on depth of embedment and direction of bend

In this section, the connection of the wall to the base slab would be studied. A key objective in the joint design is for the wall and the base slab to interact effectively together so that the structure achieves its full

capacity. That interaction between the wall and slab depends (to a great extent) on the reinforcement layout. To begin this study, a case where the wall reinforcement does not extend into the slab (thus no anchorage provided) would be studied first. Though this is not used in practice, it is a good starting point for this study. Afterwards, several variants of joint with reinforcements would be the focus.

6.2.1 Variant 1 – No embedment depth provided

In this variant, the wall reinforcement is terminated at the wall-slab interface, thus it does not extend into the base slab. The area of steel in the wall and base slab were calculated in the last chapter, and are shown in figure 5.9 of the report, with $A_{s,wall} = 1795 \text{ mm}^2$ for the wall, $A_{s,top\ of\ slab} = 1257 \text{ mm}^2$, and the steel provided at the bottom of the slab, $A_{s,bottom\ of\ slab} = 1005 \text{ mm}^2$. These reinforcement areas would be used for all the subsequent reinforcement layouts in this report. The D-region is illustrated in figure 6.2a.

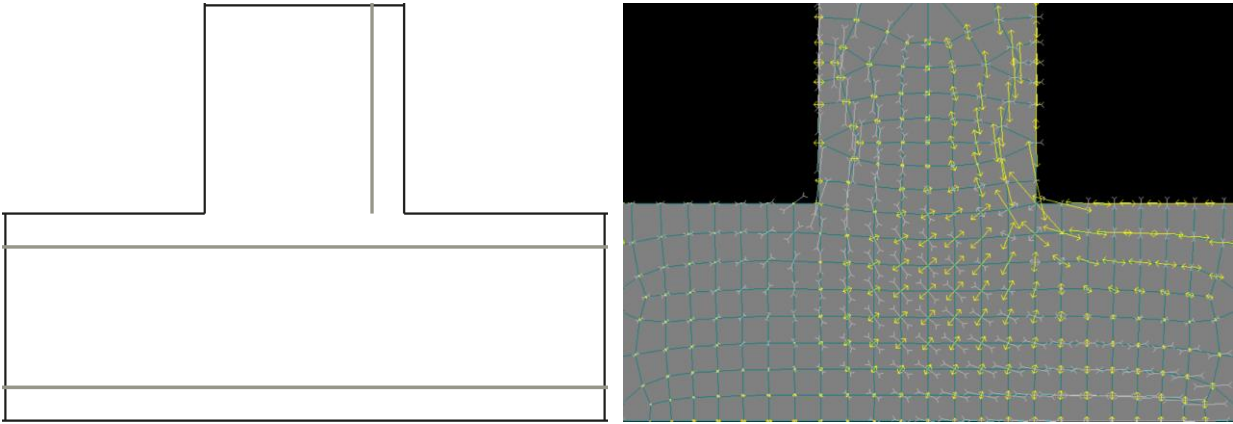


Figure 6.2 – (a). Schematic of variant 1, and (b). the stress tensor distribution before cracking

Equilibrium check: At all load steps, the horizontal reaction of the toe support was in equilibrium with the applied load (i.e. $\sum F_H = 0$), and the vertical reactions at the left and right supports were equal and opposite, thus $\sum F_V = 0$ at all load steps. With equilibrium confirmed, the behaviour of variant 1 would be discussed next.

Behaviour: Prior to the occurrence of the first crack, the load-displacement behaviour was linear. The structure behaved like an elastic isotropic material. The elastic stress distribution field in the structure is shown in figure 6.2b. The tensile stress distribution (i.e. yellow arrows in figure 6.2b) are vertical in the wall and horizontal in the top of the base slab (heel side). At the wall-slab connection however, the tensile stress field from the wall tries to deviate into the slab, and vice versa with the tensile stress deviation concentrated around the re-entrant corner. In a similar manner, the vertical compression stress field (i.e. the white arrows in figure 6.2b) from the wall deviated into the bottom part of the slab (heel side). This stress distribution is similar to that discussed in section 2.5.2 of this report, used for the strut and tie model. In the core of the joint, the deviated compression stress field occurs concurrently with a transverse tensile field (see the yellow arrows perpendicular to the white arrows in figure 6.2b). Understanding this stress state is vital to this study, as it depicts how the structure tries to distribute the load among its members, and how interaction between the wall and base slab is achieved. The stress distribution in this joint region is quite complex when compared to that of the adjacent B-region in the retaining wall. A key difference is illustrated in figure 6.3 for the load step at first cracking.

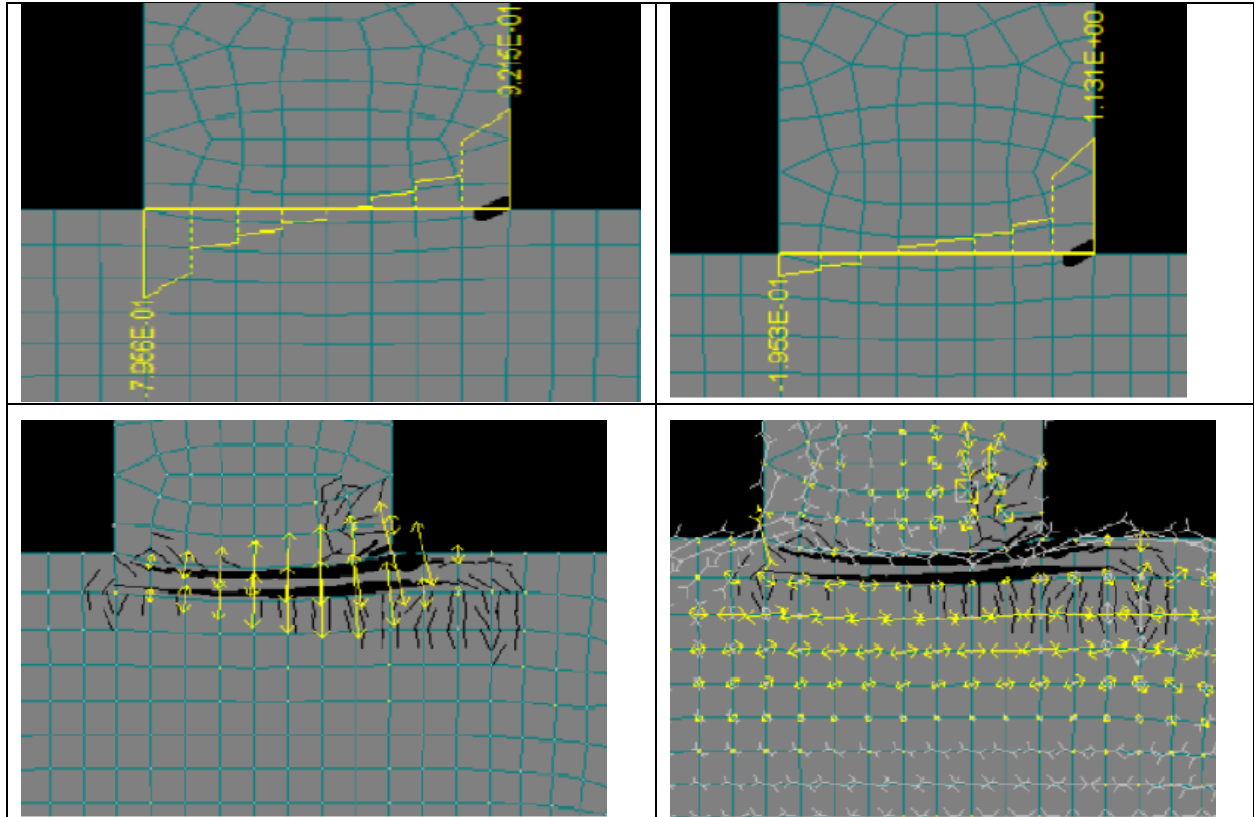


Figure 6.3 – (a). normal stress (σ_y) (b). maximum principal stress (σ_1) at wall-slab interface (c) Principal strain tensor, and (d). principal stress tensor

From figure 6.3a, the normal tensile stress $\sigma_y = 0.92 \text{ MPa}$ at the re-entrant corner is still lower than the effective tensile strength, yet it cracked. Figure 6.3b illustrates why; the principal stress at the re-entrant corner reached the effective tensile strength (i.e. 1.333 MPa), thus causing a crack to initiate at that corner, and tension-softening afterwards. With this illustration, it becomes clear that looking at normal stresses and strains (as done for B-regions) does not “paint the full picture” for D-regions. Thus, principal stresses and strains are very important parameters in this study. Note that this behaviour described above (for load increments up till first cracking) is similar for all the variants studied, thus would not be discussed in detail for any of the other variants.

For variant 1 without any anchorage length provided, some key observations are summarized next:

- After crack initiation, the crack just propagated inwards into the section in an almost straight line, with the cracks concentrated around the wall-slab interface. This is illustrated in figure 6.3c. While the reinforcement stiffened the wall part of the interface, the crack followed the weaker spot under the reinforcement. This resulted in the interface being almost fully cracked after the application of a rather small load. If some embedment depth were provided, it could have helped in controlling the cracks formed, and prevented a concentration of cracks at the wall-slab interface.
- While the tensile stress field was transferred from the wall to the slab in the linear elastic phase, there was no (or negligible) tension transfer after cracking (figure 6.3d). With further cracking, there was almost no tensile interaction between the wall and slab. This highlights the importance of the reinforcement in ensuring interaction between the wall and base slab. Reinforcement makes tension force transfer possible in the cracked structure, thus a reason why some anchorage length is required.

- Capacity of such a joint is very low, hence not used in practice.

Capacity and joint efficiency:

The ultimate capacity predicted from the FEM analysis is $37.7kNm$, while the cracking moment is $19.05kNm$. The analytical solutions would be computed next assuming 1-metre width of the wall. In computing the cracking moment, the steel is transformed to an equivalent concrete section using their moduli ratio. This is illustrated in figure 6.4.

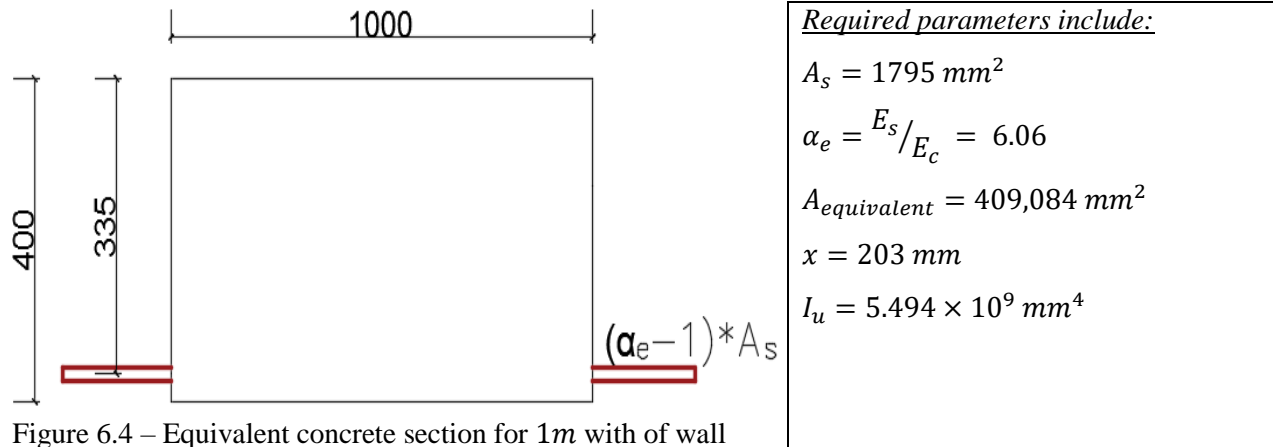


Figure 6.4 – Equivalent concrete section for 1m width of wall

Where x is the distance from the neutral axis to the outer compression fibre, and I_u is the uncracked second moment of area. The cracking moment is estimated next as:

$$M_{cr} = \frac{f_t \cdot I_u}{y} = \frac{1.333 \times 5.494 \times 10^9}{400 - 203} = 37.18kNm$$

Thus the cracking moment predicted by FEM ($19.05kNm$) is only 51.2% of the value computed using analytical expressions from beam theory ($37.18kNm$). Why this large variance? The answer is quite clear; the analytical result calculated above is based on Bernoulli linear strain assumption. However, this assumption is unsuitable for analyzing D-regions. Thus cracking initiated at a much lower bending moment because of stress concentration at the re-entrant corner. With this understood, it becomes clear why D-regions are treated differently from B-regions.

This is a very poor design and is thus never used. Studying this variant however shows the importance of anchorage in promoting interaction between the wall and the slab, providing tensile strength to the structure post-crack, transferring tensile load (or force) from the wall to the slab, and avoiding brittle failure. The next section studies the same section, but with the wall reinforcement now embedded in the base slab.

6.2.2 Study on variants with embedment depth provided

In this section, two reinforcement variants would be studied. Apart from the embedment depth provided for the wall reinforcement, the geometry is similar to variant 1. In variant 2, the main reinforcement in the wall extends 200mm deep into the bottom slab. For variant 3, the wall reinforcement extends 350mm into the bottom slab, and terminates where a nodal region should exist (following the strut and tie model proposed in figure 5.4). In both cases, perfect bond is assumed between concrete and steel.

6.2.2.1 Variant 2- Reinforcement embedded 200mm in slab

The geometry for this detail is presented in figure 6.5a. The reinforcement ends at the middle of the base slab, in a region where transverse tensile stresses occur concurrently with compressive stress field.

Behaviour: In the linear elastic stage prior to cracking, the stress distribution was similar to that in figure 6.2b with a cracking moment of $19.07kNm$. This was discussed in the last section. After cracking however, the stress distribution within the joint was determined by the layout of the reinforcement. The predominant principal stress tensor in the joint just prior to failure is shown in figure 6.5b.

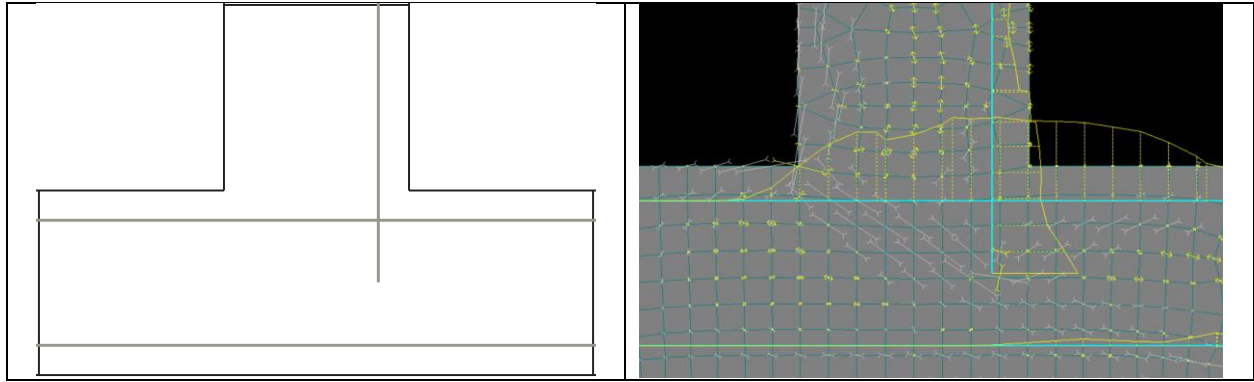


Figure 6.5 – (a). Schematic of variant 2, and (b). Predominant principal stress field post-crack

Unlike variant 1, the provision of some embedment depth for the wall reinforcement enabled a transfer of tensile force from the wall to the base slab, thus they continued to interact after cracking had occurred at the re-entrant corner. The layout of the reinforcement had significant impact on the stress and strain distribution within the joint. Some observations from the stress field for this variant are thus:

- The depth at which the wall reinforcement is terminated (or ended) has an impact on the orientation and angle of the inclined strut. This can be seen from figure 6.5b where the struts are oriented towards the reinforcement ends. Where the angle between the strut and tie is small, it could lead to a decrease in the strength of the inclined strut. This is one consequence of providing short embedment depth.
- From figure 6.5b, the compressive stress field can be observed to just flow past under the reinforcement. A node is not properly formed there, thus force transfer with this detail is inefficient. Also, the reinforcement does not provide any confinement to the concrete. This detail needs to be improved.
- Figure 6.5b also showed the stress distribution in the reinforcement. For the wall reinforcement, notice that the largest stress occurs at the tip. This stress concentration at the reinforcement tip occurred because perfect bond model was assumed in this FEM analysis. This subject would be considered further in section 6.4 where the influence of bond model is discussed. In this variant however, it has the negative impact of causing large cracks in the region of the reinforcement tip.

Concrete cracking (especially along the inclined strut) played a key role in the eventual failure of this detail. At low load, cracking initiated at the re-entrant corner due to stress concentrations caused by the opening moment. As the load increased, cracking initiated within the core of the joint when the transverse tensile stresses reached the concrete tensile strength. Additional cracks were also caused by concrete-steel interaction. For this detail, the cracks caused by transverse tension had the greatest impact on the structural performance. Figure 6.6a shows the joint with cracks. Notice from figure 6.6a that the principal strains

tensors are perpendicular to the inclined strut. The largest tensile strain occurred just under the reinforcement (see blue contour in figure 6.6b). At that point, the tensile strain (from transverse tension) were further aggravated by the tensile stress concentration at the end of the reinforcement. The end result of these large strains and cracks is a reduction in the strength and stiffness of the concrete within the joint.

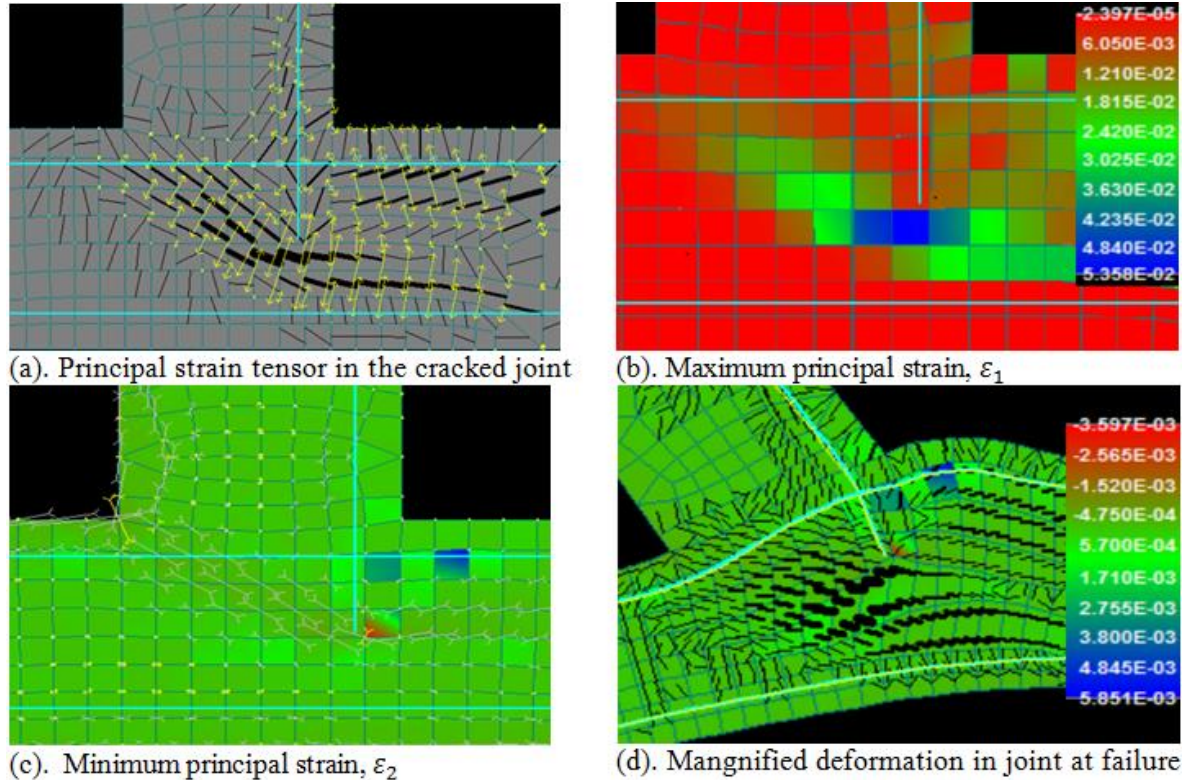


Figure 6.6 – Strain behaviour at failure for variant 2

Moment capacity and joint efficiency:

A peak moment of 127.3kNm was achieved with this reinforcement layout. The joint efficiency is thus only 51.8%. Prior to failure, the top reinforcement of the base slab yielded within the joint. The wall reinforcement however did not yield. Eventual failure of the structure occurred due to concrete crushing along the inclined strut after excessive diagonal tension cracking in the core of the joint (see red contour in figure 6.6c). Note that perfect bond is assumed thus slip is prevented in this model. The impact of this assumption on the joint capacity and failure mode is studied further in section 6.4 of this report.

Prior to failure, both the maximum principal strain, ϵ_1 in the concrete, and the minimum principal strain, ϵ_2 (i.e. largest magnitude of compressive strain) occurred in the vicinity of the reinforcement end tip. A few load steps after attaining its ultimate moment, the concrete strains at the location exceeded the ultimate compression strain, ϵ_{cu} of 3.5‰, thus the onset of crushing. But why did the concrete crush?

The presence of large cracks in the inclined strut (especially at the vicinity of the tip of the wall reinforcement) significantly reduced the concrete strength and stiffness. With the concrete stiffness significantly reduced, even a moderate stress level could lead to significant compressive strains as occurred in this case. One problem with this detail is that the embedment depth provided for the wall reinforcement was insufficient. Providing a longer embedment depth is likely to improve the detail as the reinforcement

(or tie) would have more interaction with the inclined strut thus ensuring a more efficient force transfer between concrete and steel. Though perfect bond was assumed in this analysis, it is not likely to be so in reality. In a real structure, some slip of the reinforcement relative to the concrete is likely to occur. The impact of this on the result is discussed in section 6.4.

6.2.2.2 Variant 3- Reinforcement embedded 350mm in slab

In this variant, the main reinforcement from the wall extended 350mm into the bottom slab. This way, it reached the theoretical nodal region of the strut and tie model earlier shown in figure 5.4. Figure 6.7 shows some post-processed data from the FEM analysis. Perfect bond between concrete and steel is also assumed in this analysis.

Behaviour: Up till the first crack, the section behaved like an elastic isotropic material with a linear relationship between force and displacement. Cracking occurred at $19.07kNm$, thus at a value lower than the analytical cracking moment. The reason was discussed in details in section 6.2.1. The similarity in pre-crack behaviour and cracking moment shows that the section behaves essentially the same regardless of the reinforcement layout up till cracking. After cracking, the reinforcement layout determines the stress and strain behaviour. For this variant, the predominant stress tensor after cracking is shown in figure 6.7a.

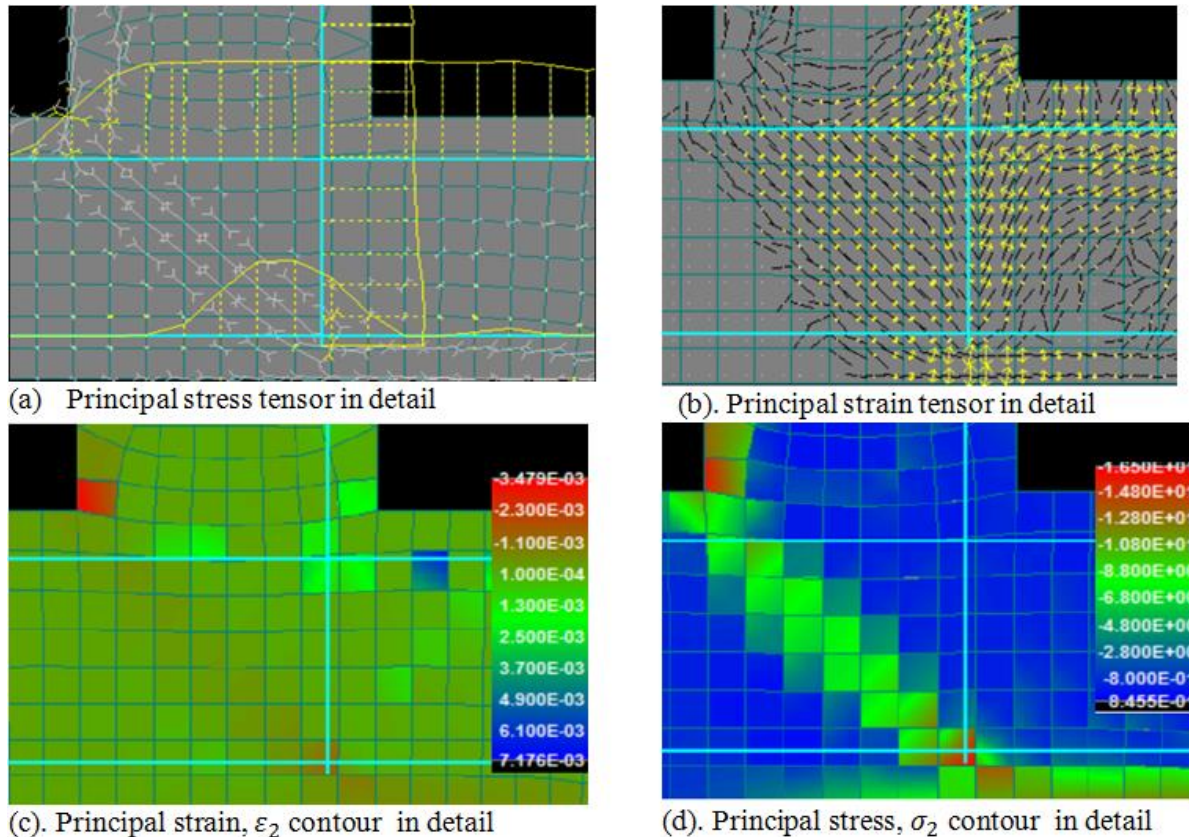


Figure 6.7 – Stress and strain distribution in joint for variant 3

Some key observations from figure 6.7 are discussed below:

- As in the earlier case (with variant 2), the embedment depth determined the orientation of the inclined strut. On comparing figure 6.7a with figure 6.5b, this fact becomes obvious. The inclined strut in this case is likely to be stronger on account of its greater angle of inclination with the ties.

- Unlike variant 2 where the inclined compressive strut just passed under the steel, variant 3 is more effective. Despite not enclosing the compressive strut (as a bent bar would achieve), the tie in this case intercepted the inclined strut (or compressive stress field), and interacted better with it. This is an improvement when compared with the earlier case.
- Notice the steel stress distribution in figure 6.7a, compared to that in figure 6.5b; the steel in this case has a better distribution along its embedded length. This results in much smaller cracks within the joint when compared to variant 2. However, it should be noted that the steel stress distribution in this variant is affected the assumption of perfect bond. With a bond-slip model, the stress at the reinforcement tip is likely to be negligible (almost zero). The impact of this is studied in section 6.4.
- The strain tensor shown in figure 6.7b gives a better performance than was seen in figure 6.6a. There are no large tensile strains along the inclined strut direction, and the crack widths are smaller.
- With reduced crack widths in this variant, the concrete within the joint core (especially the inclined strut) is likely to be stiffer. This would have a positive impact on the strut's compressive strains, as it would reduce on account of its higher stiffness.

Moment capacity and joint efficiency:

An ultimate moment of $215.8kNm$ was achieved using this structural detail. This represents over 87% joint efficiency. This is much higher than variant 2, thus there is noticeable benefit in having a longer embedment depth. This moment capacity however appears to be much higher than expected. To confirm this suspicion, this variant would be studied in a later section using a bond-slip model.

At failure there was a significant increase in the concrete compressive strain beyond the ultimate strain limit, ϵ_{cu} . With the inclined strut being stronger in this variant, the crushing did not take place within the core of the joint. Rather, crushing occurred at the compressive side of the wall slab interface (i.e. the part with red contour in figure 6.7c). Thus, this detail did not just increase the ultimate moment when compared to variant 2, it caused a change in failure location from the inclined strut, to the interface. That interface however is still part of the joint, so this is still a joint failure. Improvement is needed.

6.2.3 Study on direction of bend of reinforcement

Two variants would be studied here including one bent to the heel direction, and the second bent towards the toe. Bending of reinforcement is an effective way of providing anchorage where there is insufficient space to allow adequate anchorage length using a straight bar. However, does the direction of the bend have an impact on joint behaviour and its efficiency?

6.2.3.1 Variant 4 - Wall reinforcement bent towards the heel

In this variant, the main reinforcement from the wall is bent towards the heel side of the slab. The reinforcement extends $256mm$ (in a straight line) into the base slab, and is bent from that point to $1mm$ below the slab bottom reinforcement (thus at $336mm$ from the wall-slab interface). The radius of bend is $80mm$, with the reinforcement further extended horizontally after the bend. Note that the reinforcement does not reach our theoretical nodal point. Rather, it veers off the idealized tie direction before reaching the node (due to the bend). Variant 4 is illustrated in figure 6.8a.

Behaviour: The pre-crack behaviour was similar to the earlier variants studied (and illustrated in figure 6.2). With stress concentration at the re-entrant corner, cracking initiated at $19.1kNm$ (like the previous variant discussed). After cracking, the stresses and strains were influenced by the reinforcement layout. Figure 6.8b would be used to discuss the strain state in the joint just prior to the peak load.

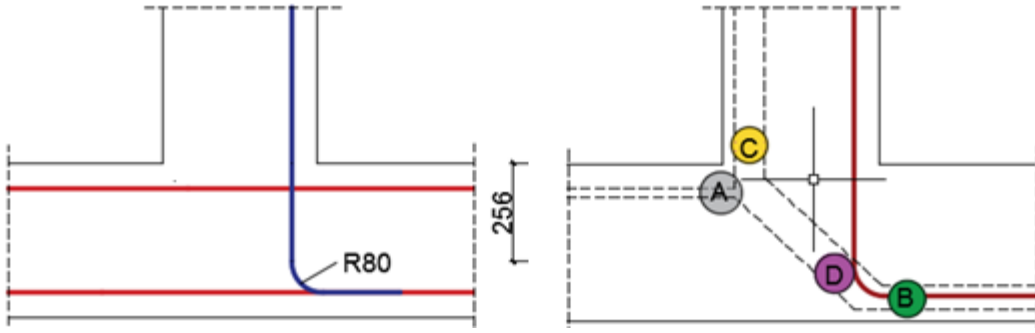


Figure 6.8 – (a) Illustration of variant 4, and (b). schematic to illustrate strains in the detail

Prior to (and at) failure, regions A and B of figure 6.8b had the minimum normal strains, ϵ_{xx} i.e. largest magnitude of compressive strain. Similarly, region C had the largest magnitude of compressive normal strain, ϵ_{yy} . At failure however, the principal compressive strains in regions A,B and C were at least four times lower than the ultimate strain limit, ϵ_{cu} . Rather, crushing of the inclined strut occurred around the point where the bend of the reinforcement started (i.e. region D in figure 6.8b, also shown depicted by the red contour in figure 6.9a). Thus failure is within the joint, and at a moment of 184.9kNm (only 75% efficiency). What could be responsible for this premature failure? This would be explained using illustration in figure 6.9.

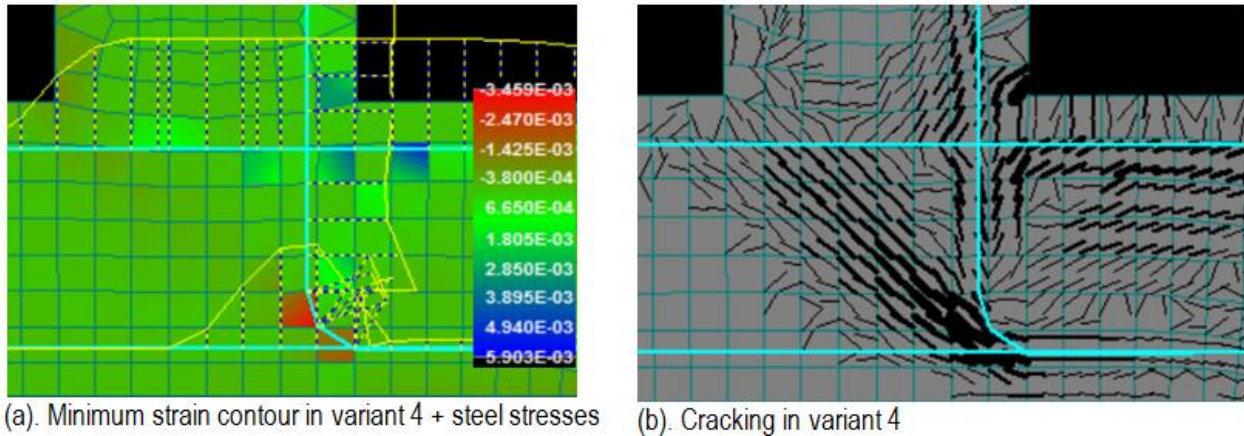


Figure 6.9 – Illustration of concrete strains, steel stresses and cracking in variant 4

From figure 6.9a, the reason is quite obvious: diagonal tension cracking failure. With the structure subjected to opening moments, transverse tension occurred within the joint which caused cracking of the inclined strut (when the concrete tensile strength is reached). These cracks must have weakened the inclined strut and caused it to crush at a moderate stress level. Also, in figure 6.9a, notice the stress concentration at the bent part of the reinforcing bar. In this model, the stress concentration at that region aggravated the cracks that had been caused by transverse tension. However, the steel concentration at that bent part is likely to have occurred because perfect bond is assumed, thus slip prevented. The impact of the bond model on the result is considered further in section 6.4.

Other important observations from this variant are summarized thus:

- Large cracks were observed in the inclined strut within the joint. With the orientation of the bent part of the reinforcement away from the inclined strut, it did not offer much in helping to control transverse cracking in the inclined strut.

- Looking at figure 6.9a, notice the elevated stress at the bent part of the reinforcement, and almost no stress after the bend. Its like an imaginary bearing plate around the bent part. This would not be the case if a bond-slip model were used. This is likely to have had an impact on the result.
- For such a detail bent towards the heel, the (straight) depth of embedment before the bend matters. If the steel were taken much deeper into the slab (probably up to the theoretical node) before bending, it would have resulted in an even higher ultimate moment, and a better steel stress distribution.

Moment capacity and joint efficiency:

The ultimate moment achieved by this detail is $184.9kNm$, representing a joint efficiency of 75%. On failure mode, this variant had large cracks from transverse tension (caused by the opening moments). These cracks caused reduced concrete stiffness, which made the inclined strut susceptible to large strains, and eventual crushing. With the reinforcement oriented away from the inclined strut, it did not assist in controlling the cracks in the inclined strut. In the next section, a bent reinforcement that crosses the path of the inclined strut would be studied and compared to this.

6.2.3.2 Variant 5 - Wall reinforcement bent towards the toe

The geometry for this detail is shown in figure 6.10a. The main reinforcement from the wall extends $256mm$ (in a straight line) into the base slab, and is bent towards the toe with a radius of $80mm$. Thus, the bend of the bar ends at $1mm$ below the slab bottom reinforcement, and is further extended horizontally after the bend.

Behaviour: The pre-crack behaviour is similar to all the other variants with a cracking moment of $19.08kNm$. Tensile stress concentration at the re-entrant corner caused cracking at a bending moment much lower than the analytical cracking moment determined based on Bernoulli linear strain assumption. With further loading, the top reinforcement in the base slab yielded first within the joint, followed later by yielding of the reinforcement in the wall. After this, the wall carried more load till eventual failure occurred.

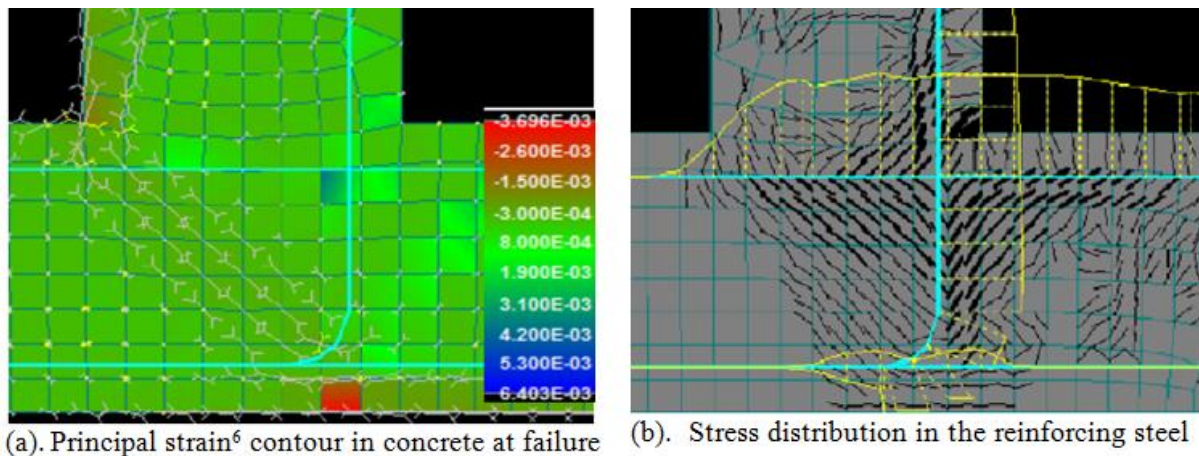


Figure 6.10 – ATENA post-processing illustrations for variant 5

The stress field field behaved closely like the idealization in the strut and tie model (see figure 5.4). Some observations made pertaining the stresses within the joint in this variant are enumerated thus:

- The compressive stress fields from the slab and the inclined strut, met with the bent reinforcement at a clearly defined nodal region. This can be seen from the illustration in figure 6.10a. Thus, there was

adequate interaction between the struts and ties at the node. This way, force transfer at the nodal region is effective.

- The reinforcing steel (or tie) also had a more favourable stress distribution (figure 6.10b) than variant 4. There was no stress concentration at the bend, and no yielding of the reinforcement at that point.
- With the bent reinforcement crossing the path of the inclined strut, it helped in controlling transverse cracking within the strut. Consequently, this variant had a lower crack width than all the variants already discussed thus far. This implies that the inclined strut with this variant would be stronger and stiffer than the previous ones. No wonder it did not crush despite being attaining a higher peak moment than the previous 4 variants.

Moment capacity and joint efficiency:

This variant attained an ultimate moment of $217.3kNm$ representing 88.4% efficiency. Despite conforming closely to the idealized strut and tie model, this joint detail still failed to reach the design strength of the wall. Compressive strains (in excess of ϵ_{cu}) occurred in the concrete that was outside the bent reinforcement region (red contour in figure 6.10a). This failure mode is more like spalling of the concrete outside the bent part of the bar. At the time this failure occurred, the maximum compressive strain at all other location (other than failure location) was less than 1.4‰ (much lower than ϵ_{cu})!!! Thus, there was still capacity left in the structure, when this localized failure occurred. Where this failure mode can be prevented, there is a chance that over 100% joint efficiency can be achieved. However, this variant exhibited a lot of positive in its behaviour. It could probably be improved upon. This would be the goal of the next variant.

6.2.4 Variant 6 – Improved detail with diagonal bar at re-entrant corner

In this variant, a diagonal bar is placed at 45° around the re-entrant corner to stiffen the joint region in hope that it would enable at least 100% efficiency, and also prevent failure from occurring within the joint. In line with the recommendation of Nilsson (1973), the area of steel used for the diagonal bars is about 50% of the area of steel provided for the wall.

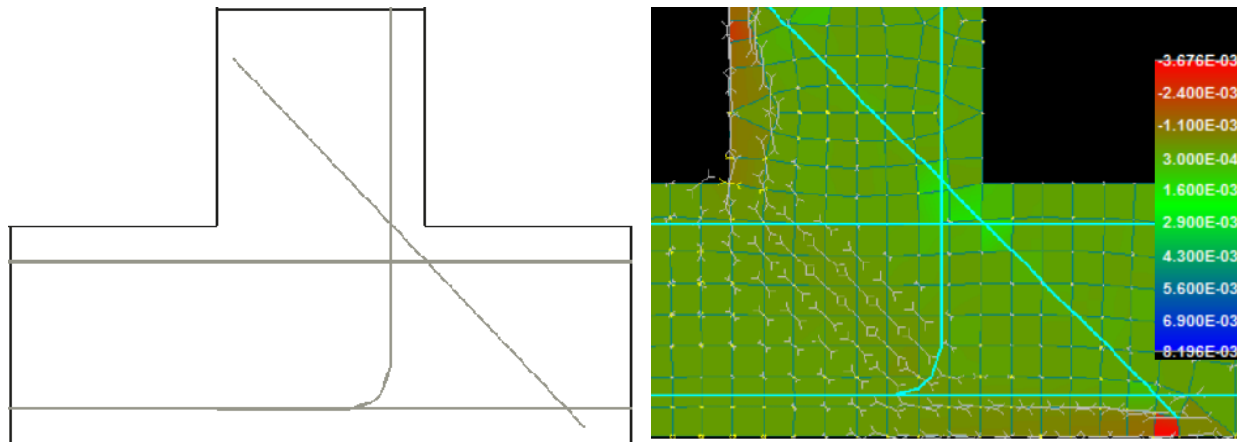


Figure 6.11 – (a). Illustration of variant 6, and (b). Minimum principal strain contour, ϵ_2 at failure

With this variant, an ultimate moment of $249.9kNm$ was achieved, which meets the design requirement. This ultimate moment attains a joint efficiency of 101.7% when compared to the design strength of the wall (i.e. $245.7kNm$)⁵. Also, unlike all the variants studied earlier, failure did not occur within the joint or at the

⁵ Despite the addition of inclined bar at re-entrant corner, the reference moment remains $245.7kNm$. At the section where failure occurred, the inclined bar did not add to its strength. This failure location can be seen in figure 6.11b (the red contour).

wall base connection. Rather, the largest magnitude of compressive strains at failure (hence crushing when ϵ_{cu} is reached) occurred along the member length adjacent to the joint (see the red contours in figure 6.11b). The joint is not governing in this case, and does not prevent the connected members from reaching their capacity. The works of Nilsson (1973), Campana, Ruiz and Muttoni (2013, Nabil, Hamdy and Abobeah (2014) etc. further give credence to the fact that joint efficiency can be improved by placing a diagonal bar at the re-entrant corner subjected to tensile stress concentration. However, in what way did the diagonal bar help to achieve this in variant 6?

Prior to the initiation of the first crack, the section behaved like an elastic isotropic material similar to all the other variants earlier studied. The presence of the diagonal bar did not alter the stress distribution at that load level. Thus, there was still tensile stress concentration at the re-entrant corner. Cracking occurred when the maximum principal stress, σ_1 reached the concrete tensile strength, with the cracking moment being $20.0kNm$. This value is marginally larger than the other variants because the addition of the diagonal bar slightly increased the second moment of area of the section around the re-entrant corner. Thus, the addition of diagonal bar had negligible influence prior to cracking. Its influence increased in significance after cracking has been initiated at the re-entrant corner. After cracking, the steel was activated and the impact of the diagonal bar grew with as the load increased. Some key observations on its impact are discussed thus:

- Better representation of the stress field at the re-entrant corner: From the principal stress distribution that was shown in figure 6.2b, it can be seen that the tensile stress field around the re-entrant corner is neither vertical nor horizontal, but is on the average at approximately 45° . This orientation of the tensile stress field occurred as tension from the wall tried to divert into the slab. With the diagonal bar placed at approximately 45° , it provides strength and stiffness that enabled the structure to cope better with the stress field at that location. For this reason, the diagonal bar was the most stressed (after cracking), and had the largest strain up till a bending moment of $140kNm$. In the absence of such a diagonal bar, the vertical reinforcement from the wall, and horizontal reinforcement are more stressed resulting in more strains within the joint.
- Better crack control: This variant had the lowest crack widths both at the re-entrant corner and the inner core where transverse tension occurs. While FEM predicts a maximum crack width of 1.1mm for the re-entrant corner of variant 5 (without the diagonal bar) at a bending moment of $200kNm$, the addition of a diagonal bar caused the maximum crack width to reduce to 0.58mm at a similar bending moment. Slightly smaller crack widths were also obtained within the core subjected to transverse tension. While this is largely attributable to the bent part of the reinforcement crossing the path of the inclined strut, the addition of a diagonal bar improved it a bit further.
- Reduced stress concentration within the joint: In the absence of the diagonal bar, the reinforcing steel had its maximum stresses (and consequently strains) within the joint. This is illustrated as zone A in figure 6.12a for variant 5. When the diagonal bar is added, the steel stresses within the joint are reduced, and the region where steel stresses and strains are critical moved out towards zone B (in figure 6.12b). Though the diagonal bar yielded (first), it did not yield within the joint. Thus, no plastic hinge was formed within the joint. This way, the joint had higher stiffness than the adjacent connected members.



(a) Zone of tensile concentration in variant 5
 (b). Zone of tensile concentration in variant 6
 Figure 6.12 - Zone of tensile stress concentration and yielding in variants 5 and 6

- **Increased joint rigidity:** After extensive crack propagation at the re-entrant corner, and formation of a plastic hinge within the joint (for variant 5 without a diagonal bar), the interaction between the wall and the slab (heel side) is reduced. With the formation of a plastic hinge within the joint, it would be easier for the wall and slab to rotate away from each other. However, with the addition of a diagonal bar, interaction is maintained between the wall and heel side of the slab. The crack widths formed in that location are relatively smaller, and the concrete within the cracks contributes to joint stiffness via the tension stiffening effect. The result is thus a stiffer joint with better interaction between the wall and the slab. This would be further discussed in the next section where the moment-curvature behaviour of the various variants are discussed.

In concluding this section, it is obvious that for this retaining wall joint, the reinforcement bent towards the toward the toe (i.e. crossing the path of the inclined strut) is more effective than that reinforcement bent towards the heel. The strength of the joint may however be reduced by the cracking behaviour at the re-entrant corner. Adding a diagonal bar at the re-entrant corner would improve the efficiency of such structural detail.

6.2.5 Summary on preliminary study

Without exception, all the variants behaved in a similar manner prior to cracking, with cracking occurring at approximately $19.1kNm$. This value is just about 51% of the analytical cracking moment ($37.18kNm$) computed using the beam theory. This variance occurred because of tensile stress concentration in the re-entrant corner. The beam theory which is based on Bernoulli's linear strain assumption is not valid around the re-entrant corner as the stress and strain field is disturbed (i.e. a D-region). This subject was discussed extensively in chapter 2 of this report. Thus, considering only normal stresses (σ_x and σ_y) for the region did not give a full indication of the actual stress state within the section. Rather, the principal stresses and strains proved to be more reliable in understanding its behaviour.

The reinforcement layout did not have much influence prior to crack initiation. After cracking however, the reinforcement details played a vital role in the behaviour and performance of the joint. Some performance indicator for the variants studied are compared in Table 6.1.

Table 6.1 – A summary of FEM outcomes for variants 2 to 6

Variant	M_{ult} (kNm)	Efficiency M_{ult}/M_{Rd}	Max. conc. stress (MPa)	Crack width @ 170kNm		Comments
				At re-entrant corner	Max from transverse tension	
Variant 2: anchored 200mm into base slab	127.3	51.8%	13.06	Failed	Failed	The embedment depth of steel bar is insufficient thus there is poor interaction between reinforcing steel and inclined strut. Large cracks occurred in the core of the joint due to transverse tensile stresses. These cracks weakened the inclined strut, resulting in the strut crushing. Failure is within the joint. Structural detail is inefficient
Variant 3: anchored 350mm into base slab	215.8	87%	18.19	1.41mm	0.52mm	The reinforcement reached the nodal zone. It intercepted the strut path (without enclosing it). The angle between the inclined strut and the tie is larger. This would make the strut stronger. With the strut stronger, failure occurred at the wall-slab interface. Better performance, but improvement still required.
Variant 4: Bent to heel	184.9	75%	16.66	1.92mm	1.56mm	Large cracks propagated within the core of the joint due to the action of transverse tensile stresses (from the opening moment). With the reinforcement bent away from the inclined strut, it did not help to control cracks. The inclined strut was weakened by cracks, causing it to have large strains at moderate stress level. The strut eventually crushed.
Variant 5: Bent to toe	217.3	88.4%	18.35	1.55mm	0.49mm	The stress field approximates closely to the assumed strut and tie model. The bent part of the reinforcement helped to control cracks. Thus the inclined strut is stronger and did not crush. It still failed prematurely with a wide crack forming around re-entrant corner and extending downwards into the slab.
Variant 6: Diagonal bar at re-entrant corner	249.9	101.7%	20.05	0.77mm	0.36mm	The addition of diagonal bar stiffened the overall joint. Unlike other variants, yielding of steel did not occur within the joint Also, failure occurred outside the joint after exceeding the design moment of the structure. This variant meets the design objective.

The importance of a reasonable embedment depth was studied. For variant 2 with an embedment depth of 200mm, the compressive stress field just flowed past under the reinforcement, without having much interaction with it. Force transfer between the concrete strut and the reinforcement tie was inefficient, and the joint capacity was small. Also, large cracks formed within the joint which made the joint susceptible to large strains, even at moderate stress level. When a longer embedment depth (i.e. 350mm) was used, there was noticeable improvement in the behaviour of the joint. The reinforcement intercepted the inclined strut, and force transfer between concrete and steel improved. Also, it was shown that the embedment depth of the wall reinforcement has impact on the orientation of the inclined struts formed by the concrete. The

larger the angle between the strut and the tie, the stronger the strut is likely to be. For this reason, design code usually prescribed limits for the angle. In detailing, the embedment depth should be deep enough to ensure that the angle between the ties and struts is within the limits specified in codes.

The impact of the direction of the bend is also studied in this section. A design in which the reinforcing bar is bent to enclose the inclined strut is a better detail, than the one that bends away from the strut. When it crosses the path of the inclined strut (as in variant 5 and 6), it helps to control cracks from transverse tension. This makes the strut stiffer and less susceptible to crushing. In addition, the bent part of the reinforcement also provides some confinement to the inclined strut, and thus increases its compressive strength. In this work, variant 4 with reinforcement bent away from the inclined strut had a diagonal tension cracking failure mode. The orientation of the reinforcement did not offer much in controlling cracking of the inclined strut. In contrast, diagonal tension cracking failure was prevented by variant 5. This proves that the direction to which the reinforcement is bent matters.

The addition of a diagonal bar at the re-entrant corner resulted in a stronger joint that meets the design objective. In figure 6.13, the relationship between moment and curvature⁶ for the different variants is compared. Variant 6 with the diagonal bar at the re-entrant corner is much stiffer and stronger than any of the other variants. Failure occurred along the connected member (outside the joint) as is desired. Thus, the joint did not limit the structure from achieving its full capacity. Furthermore, it had the lowest crack width at the re-entrant corner as seen in Table 6.1

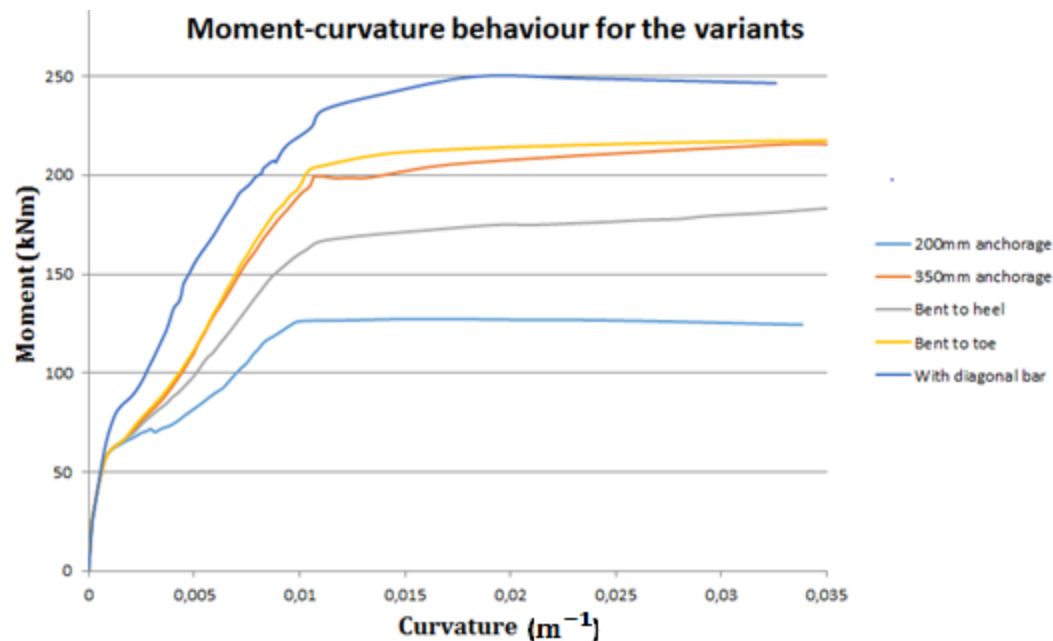


Figure 6.13 – Moment-curvature comparison for the various variants

⁶ In plotting the moment-curvature diagram for figure 6.13, a cross-section taken along the eventual failure section. Example, for variant 4 (bent to heel), a cross section is taken along the base slab passing the point where eventual crushing occurred. For that, the concrete strain at that location and the steel strain (in the top reinforcement) provide data used to estimate curvature. Similarly, for other variants, the concrete strain at point of eventual failure is used along with the steel stress in that cross section.

From figure 6.13, notice that the detail bent towards the heel has lower joint stiffness than that bent towards the toe. Also, the importance of sufficient embedment depth can also be inferred from the plot.

In modeling the variants presented in this section, perfect bond is assumed. With cracking playing a significant role in the behaviour and capacity of the joints, there is likely to be some slip between the steel and the surrounding concrete. Thus, the assumption of perfect bond is likely to have had an impact on the capacities predicted. This impact would be discussed in section 6.4 where bond models would be used in FEM analysis of these variants.

With the knowledge obtained from this section, the reinforcement layouts earlier shown in figure 1.1 of this report would be studied in-depth in the next section of this report.

6.3 Focus on thesis variants

This section reports on a study carried out on the two structural details that are shown below in figure 6.14. These details are quite common in practice, thus a proper understanding of their behaviour and performance could prove useful to structural safety. The same geometrical dimensions used in the previous section would be adopted for this case. The difference however can be seen in the reinforcement layout at the joint region, and the addition of the compression reinforcement in the wall. In this section, perfect bond is assumed to exist between the reinforcement and the surrounding concrete. In section 6.4, the impact of this assumption on the results obtained from the FEM analysis is studied.

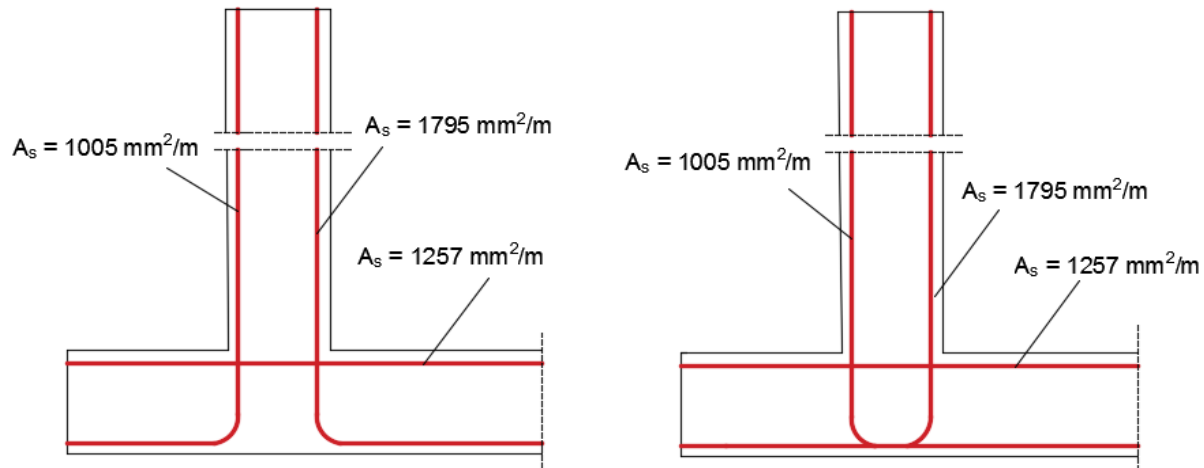


Figure 6.14 – Typical structural details of the retaining wall to be studied. They would be subsequently referred to as (a). Reinforcement Layout 1, and (b). Reinforcement Layout 2 respectively.

In the linear elastic stage, the behaviour of both structural details was similar with cracking occurring prematurely at approximately 19.4kNm (i.e. approximately 52% of the analytical cracking moment of 37.18kNm) on account of stress concentration at the re-entrant corner. The reason for this variance was discussed in section 6.2.1, thus would not be repeated here. The goal of this section is to understand how a joint with these structural details behaves by examining its stresses and strains, failure mode, and joint efficiency. The knowledge gained from the last section would prove useful here.

6.3.1 Reinforcement Layout 1

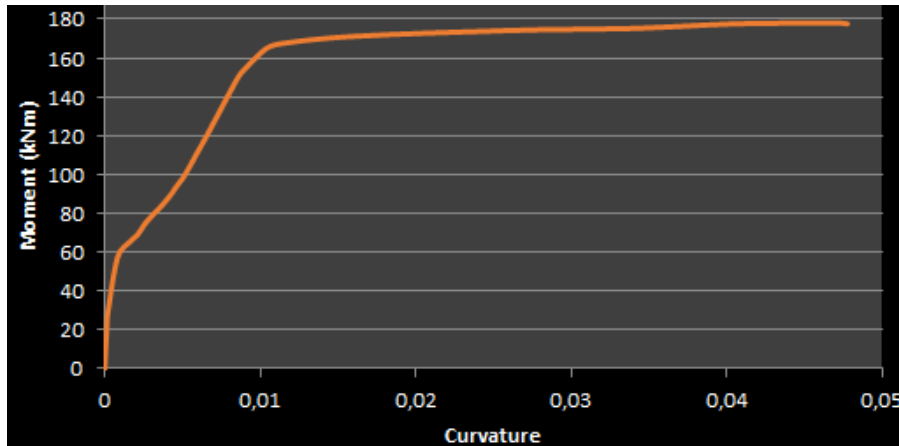


Figure 6.15 –Moment curvature diagram for Reinforcement Layout 1

The structural detail is illustrated in figure 6.14a, and the moment curvature relationship is illustrated in figure 6.15. The curvature used for figure 6.15 is taken from a vertical cross-section taken across the base slab (within the joint). This layout attained a peak moment of 178 kNm, thus approximately 72% joint efficiency (reference moment is 245.7 kNm). In this report, the stresses, strains and cracking behaviour are studied at four points along the moment-curvature plot (i.e. 19, 100, 160 and 178 kNm) to understand how the structure with this detail behaved from crack initiation to failure.

AT THE FIRST CRACK (19 kNm)

Prior to the first crack, the structure behaves like an elastic-isotropic material with a linear load-displacement behaviour. The first crack was initiated in the re-entrant corner at a moment of 19.42 kN. The stress tensor at this load level is shown in figure 6.16a.

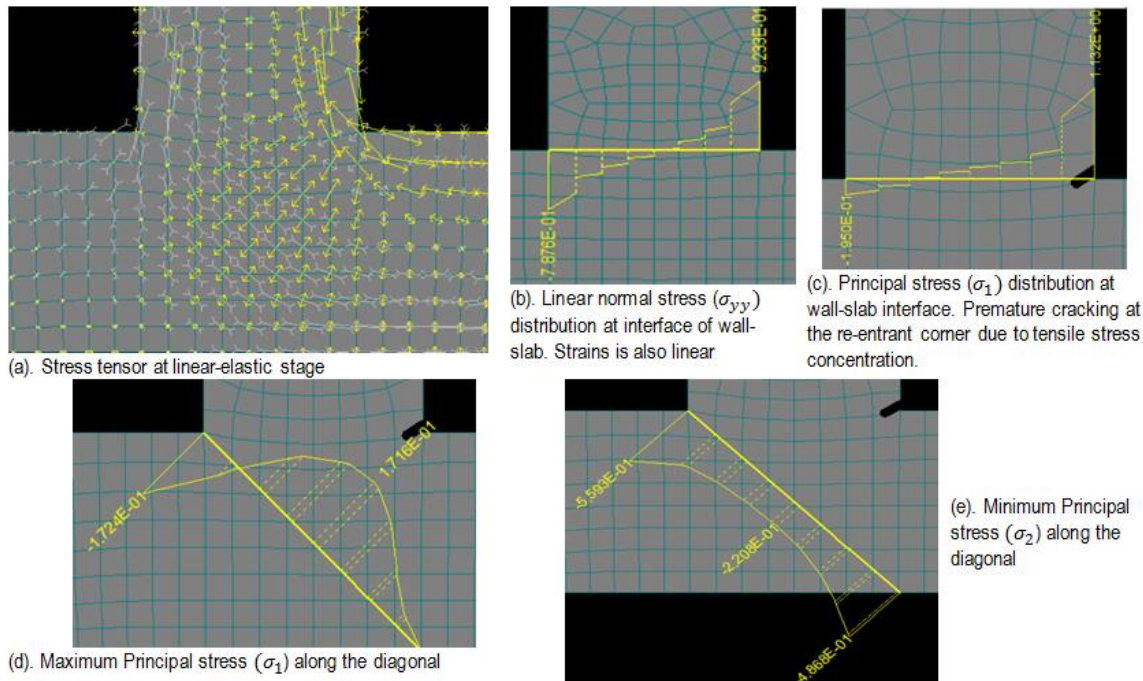


Figure 6.16 – Stress distribution in the structure at occurrence of the first crack

At wall-slab interface

The distribution of the normal stress σ_{yy} along the wall-slab interface is shown in figure 6.16b. As expected, the stress profile across the wall is linear with tension on one side and compression on the other. The maximum normal tensile stress σ_{yy} at this load level is 0.92 MPa. As this is lower than the effective tensile strength of concrete (i.e. 1.33 MPa), why did it crack? This can be answered by considering the maximum principal stress σ_1 , which exceeded the concrete tensile strength, hence the crack. The value of principal stress σ_1 in figure 6.16c is 1.13 MPa (i.e. lower than $f_t^{ef} = 1.33 \text{ MPa}$). This is because the concrete had cracked and softened afterwards, hence the reason the value is lower than the effective tensile strength. Thus, for this re-entrant corner, looking at normal stresses alone does not give the full picture. Using principal stresses is more reliable in predicting the behaviour of a D-region (like this one).

Within the joint

Within the joint, the stress state is disturbed. In figure 6.16a, the compressive stress field occurs concurrently with transverse tension. This has impact on the behaviour of the strut. Figure 6.16d and e show the maximum principal stress σ_1 and minimum principal stress σ_2 along the diagonal. Figure 6.17 illustrates this stress state. Figure 6.17b shows the stress state in a small segment of the middle of the inclined strut in figure 6.17a. At this load step, the maximum principal tensile stress in the inclined strut ($\sigma_1 = 0.17 \text{ MPa}$) and the minimum principal stress ($\sigma_2 = -0.22 \text{ MPa}$) as shown in figure 6.16d and e are still quite small in magnitude. With increasing load however, the stresses grow in magnitude and play a bigger role in the behaviour of the joint.

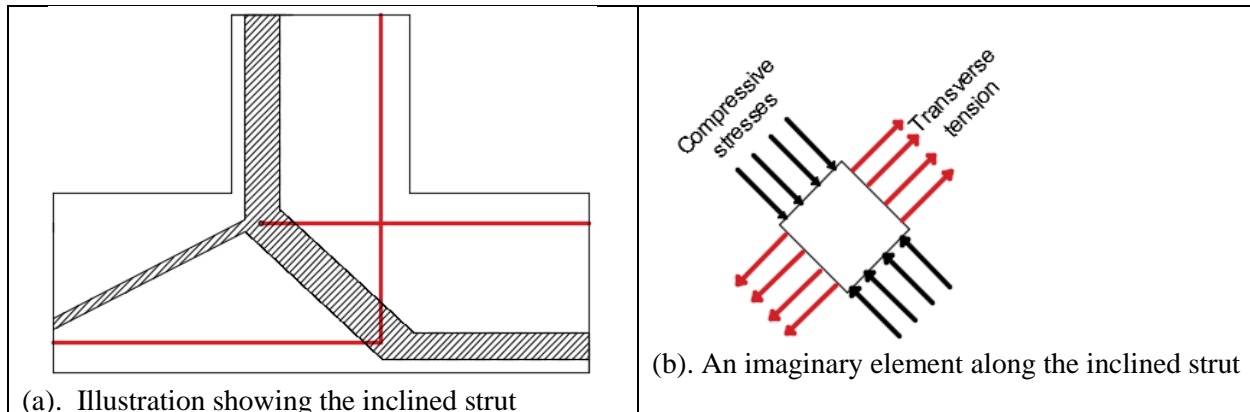


Figure 6.17 – The inclined strut and its stress state

The stress state (in figure 6.16a) within the joint at this pre-crack stage is important as it reflects how the structure inherently distributes the load applied to it. Key for this detail is the biaxial stress state in the inclined strut which is illustrated in figure 6.17b.

AT A BENDING MOMENT OF 100 kNm

Figures 6.18b and c shows the strain distribution across the wall (section A-A in figure 6.18a) and base-slab (section B-B) respectively at a bending moment of 100 kNm. Both section A-A and B-B were taken just 10 cm away from the D-region. As can be seen, their strains are linear thus complying with Bernoulli's linear strain assumption. The D-region however behaved differently.

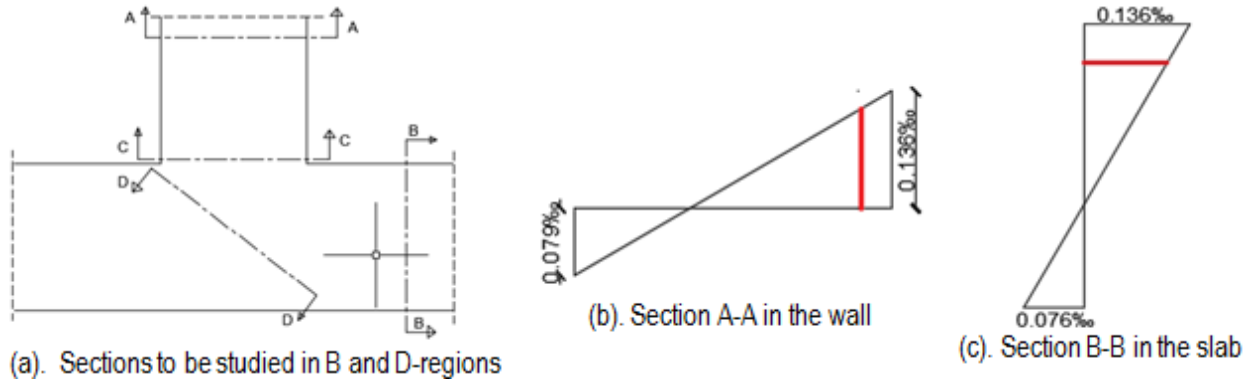


Figure 6.18 – Strain profile in B-region of wall and base slab (just 10cm away from the defined D-region)

Figure 6.19 shows the normal stress and strain distribution along the wall-slab interface within the D-region. From figure 6.19a, it is obvious that Bernoulli's linear strain assumption is not valid in this region. With the concrete compressive strains still lower than $\varepsilon_c = 1.75\text{‰}$, the concrete compression stress block is still below its peak compressive stress. When compared to the linear elastic case in figure 6.16b, the neutral axis had reduced at this higher load level. The reason is quite obvious from figure 6.19b. Some of the inner fibres initially in compression (during the linear elastic stage) are now in tension. The concrete in the outer fibres (around the re-entrant corner) had cracked and softened, thus causing the tensile stresses to move further inwards into the sections, hence reducing the neutral axis depth at this load level.

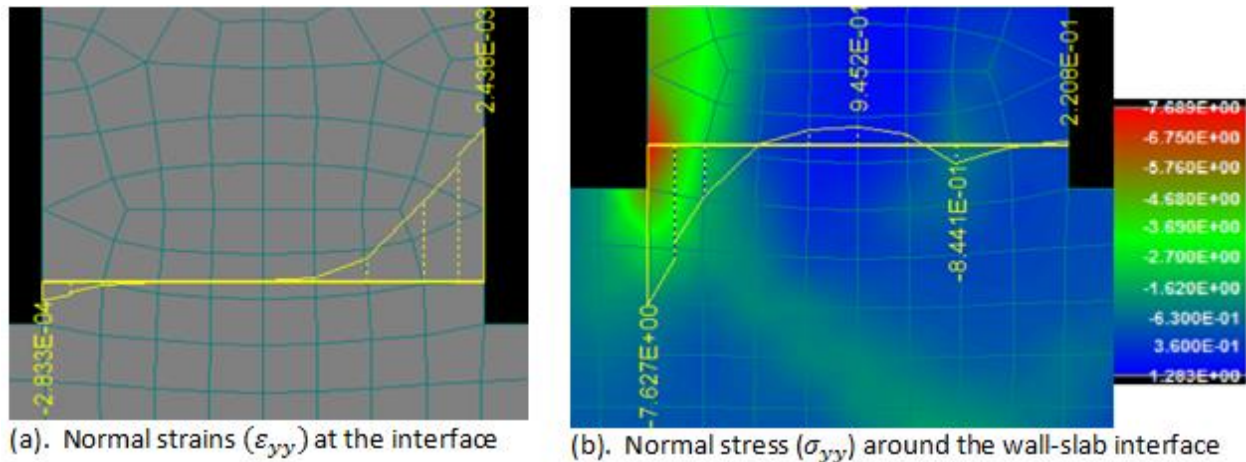


Figure 6.19 – Strains and stresses round the wall-slab interface (section C-C) at a load of 100 kNm

For the inclined strut, the stress and strain profile are shown in figure 6.20a and b respectively. At this load level, there were already cracks in the strut due to transverse tension within the strut. The largest cracks formed around the bent part of the reinforcement. The green contour in figure 6.20a shows a clearly defined compressive stress field, that looks like the inclined strut from the assumed strut-and-tie model. Notice however that there is very little interaction between the bent bar and the inclined strut. This will play a crucial role in the eventual performance of the joint.

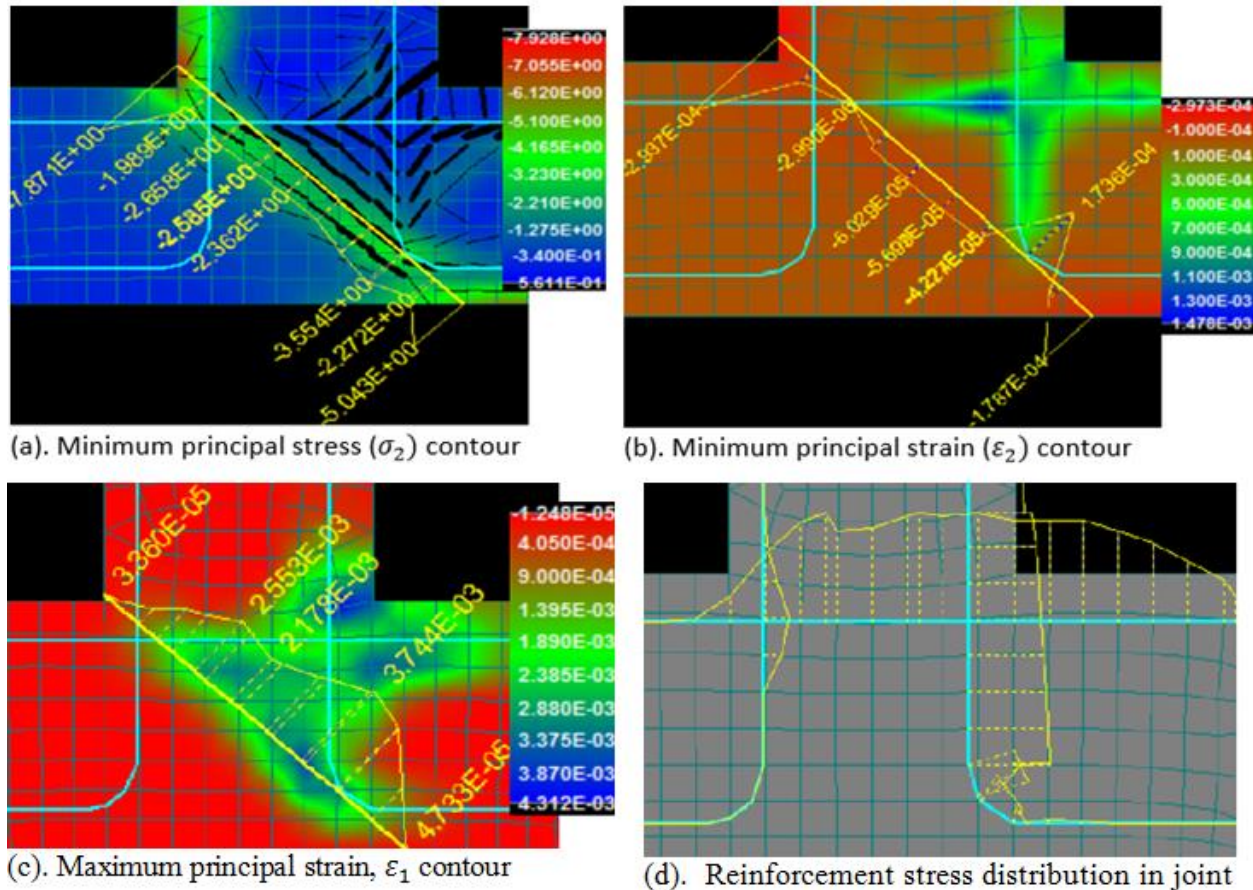


Figure 6.20 – Stress and strain contours with in the joint at 100 kNm

From figure 6.20a, the compressive stress in the middle of the inclined strut is quite smaller than at the ends. Similarly, the strains at this load level (figure 6.20b) are concentrated at the ends, and much lower at the middle of the inclined strut. The crack widths are still comparatively small, and their impact on the concrete stiffness is not so significant as yet. Around the bent part of the bar, the minimum principal strain, ϵ_2 seems to be tensile. The reason is clear from figure 6.20c where the maximum principal strain, ϵ_1 profile shows a concentration of tensile strains in the concrete around the bent part of the bar. This is due to a concentration of steel stresses at that location (figure 6.20d). This is the main reason why the largest cracks within the strut occurred at that point.

From figure 6.20c, the region (i.e. green and blue contour) between the re-entrant corner and the inclined strut is the location where most deformations were occurring in this detail, particularly cracking and tensile strains. At this load level, the maximum crack width predicted by FEM was 0.58 mm in the inclined strut, and 1.02 mm at the re-entrant corner. As the load increased beyond this, the transverse cracks in the inclined strut grows at a faster rate than that at re-entrant corner crack.

AT A BENDING MOMENT OF 160 kNm

While the wall reinforcement did not yield (for this reinforcement layout), the top reinforcement of the base slab yielded within the joint. This section examines the specific parts of the structure to understand how it behaved after the steel had yielded. The distribution of steel stresses at 160 kNm would be discussed first. It is illustrated in figure 6.21.

From figure 6.21a, the top reinforcement (in the base-slab) has its largest tensile stresses within the joint region. The steel stress reached 435 MPa at a point within the joint hence yielding. Note that the steel stresses outside the D-region are much lower compared to the joint region. This concentration of steel stress resulted in large strains within the joint. With stiffness being a major requirement for joints, these large strains are not good when occurring in the joint. For the wall, notice how the reinforcing steel had its largest stresses and strains within the joint at the location where it was bent from. This stress concentration is likely due to the assumption of perfect bond (which must have prevented slip in that region between the reinforcing bars and the surrounding concrete). In section 6.4, this detail would be studied further using a model that allows slip.

In figure 6.21b, notice the large cracks that occur along the inclined strut direction. These cracks were initiated by transverse tensile stresses caused by the opening moments acting on the corner joint. These crack grew as the load steps increased, and progressively weakened the concrete strut. In this model, note that the concentrated steel stress around the bent bar further aggravated these cracks in the detail. This is the reason for the large crack that occur just outside the bent part of the reinforcing bar in figure 6.21b.

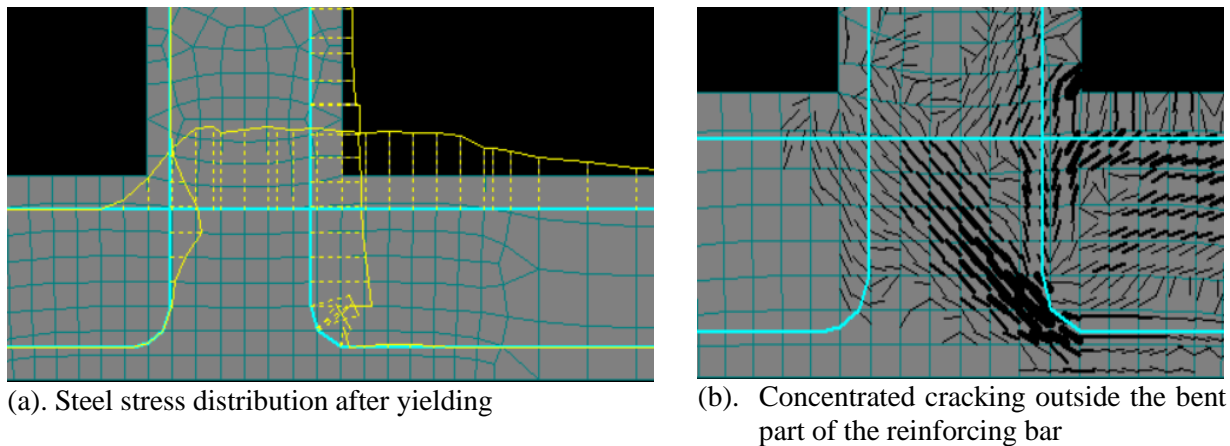


Figure 6.21 – Steel stress distribution in the section

At this load, the strains in the B-region of the wall and base slab still complied with Bernoulli linear strain assumption (see figure 6.22 below). Since this is not the critical part of the joint, it would not be discussed any further.

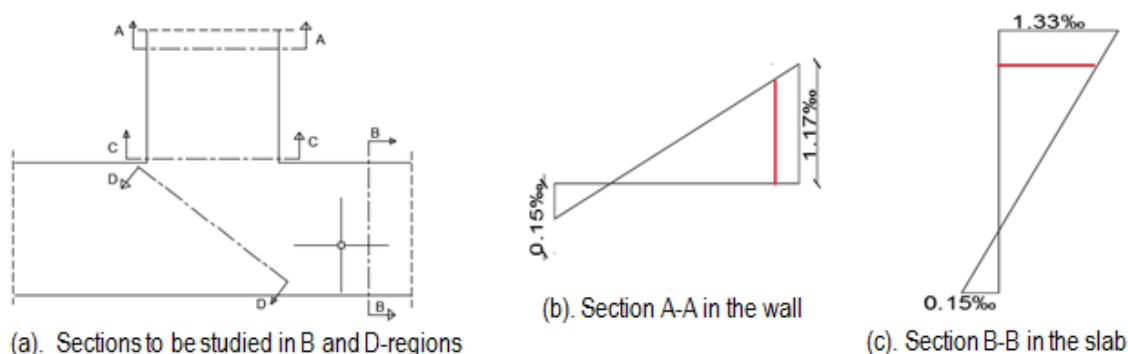


Figure 6.22 – Strain distribution within the B-region

For the D-region, the behaviour is quite different. It would explained using the minimum principal stress, σ_2 and strain, ϵ_2 contour plots in figure 6.23 below.

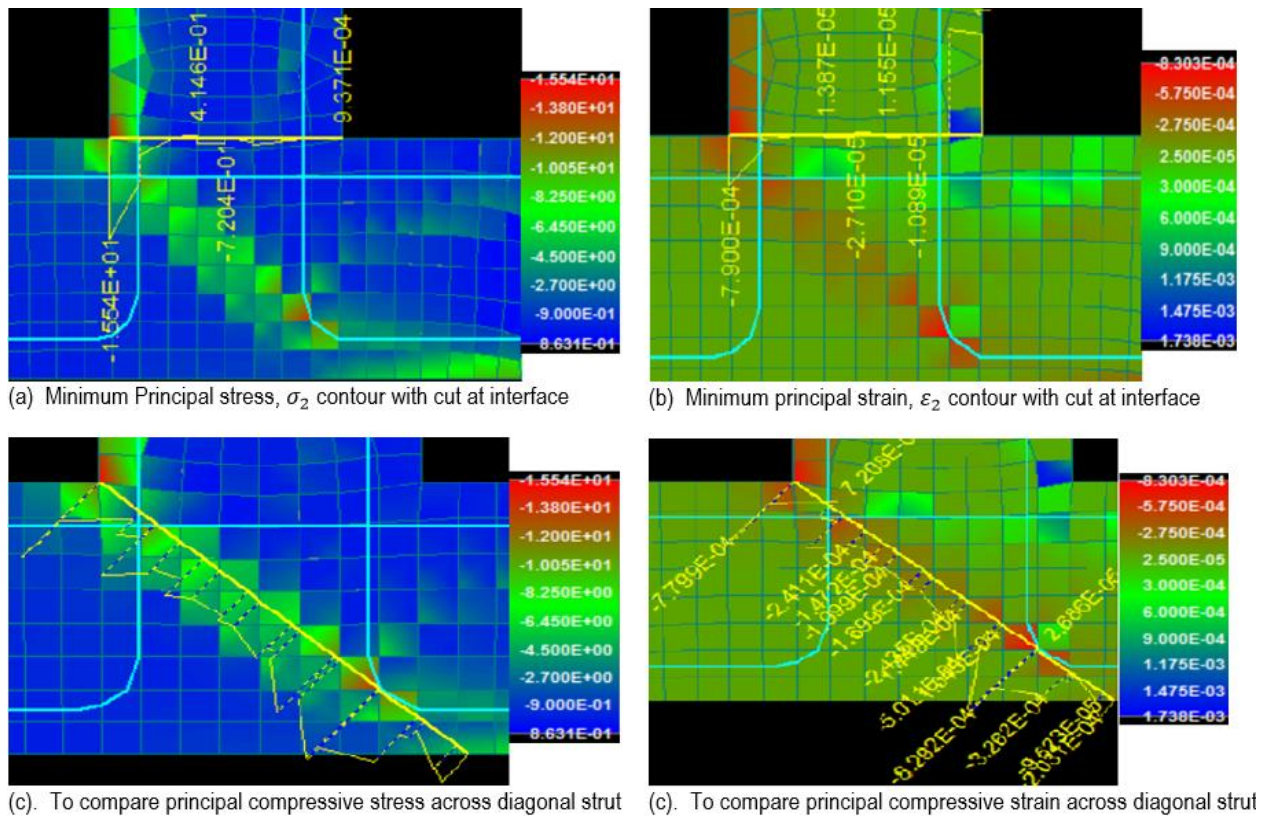


Figure 6.23 – Minimum principal stress and strain contour (with cuts) at 160kNm

Along the wall-slab interface, the critical point is the compressive stress and strain concentration at the end (see red contour in figure 6.23a). The largest magnitude of compression stress occurred at that point. The minimum principal strain at this point was 0.79‰. Since it was less than $\epsilon_{c3} = 1.75\text{‰}$, the concrete stress block is still linear.

For the inclined strut, compressive stress and strain concentration is also noticeable at a localized point just outside the bent bar. From figure 6.23c, note the large principal compressive stress around the bent reinforcement (14.07MPa). The table below presents the principal stress and strain data from an integration point at the interface and at the inclined strut (around the bend).

Location	Principal stress, σ_2 (MPa)	Principal strain, ϵ_2
Wall-slab interface	15.54	0.79‰
Inclined strut (around the bend)	14.07	0.83‰

From the above table, though the wall-slab interface was subjected to higher compressive stress, it was less strained when compared with the inclined strut (around the bent part of the reinforcement). The presence of large cracks (up to 1.3mm) in the inclined strut made it weaker in compression than the wall-slab interface. The concrete in the inclined strut was also less stiff, hence more susceptible to higher strains even though it was less stressed. The cracking in the inclined struts are mainly from transverse tension. It is further aggravated by tensile stress concentration due to the direction the reinforcement was bent as was shown in figure 6.21a. If the reinforcement were bent towards the toe (thus crossing the inclined strut), it

would have helped to control the crack width, and it would have provided some confinement to the inclined strut. But being bent away from the inclined strut, it could not provide these benefits to the structure.

Beyond this load (where the base slab top reinforcement yielded), the compressive strains within the inclined strut increased at a faster rate than the wall-base connection up till failure.

AT BENDING MOMENT OF 178.1 kNm (PEAK MOMENT)

This moment corresponds to the ultimate moment achieved by this detail. The B-region still complied with Bernoulli linear strain assumptions. The interesting aspect however was in the inclined strut of the D-region. Only this will be discussed in detail here. Figure 6.24 shows the minimum principal stress and strain contour at this load level.

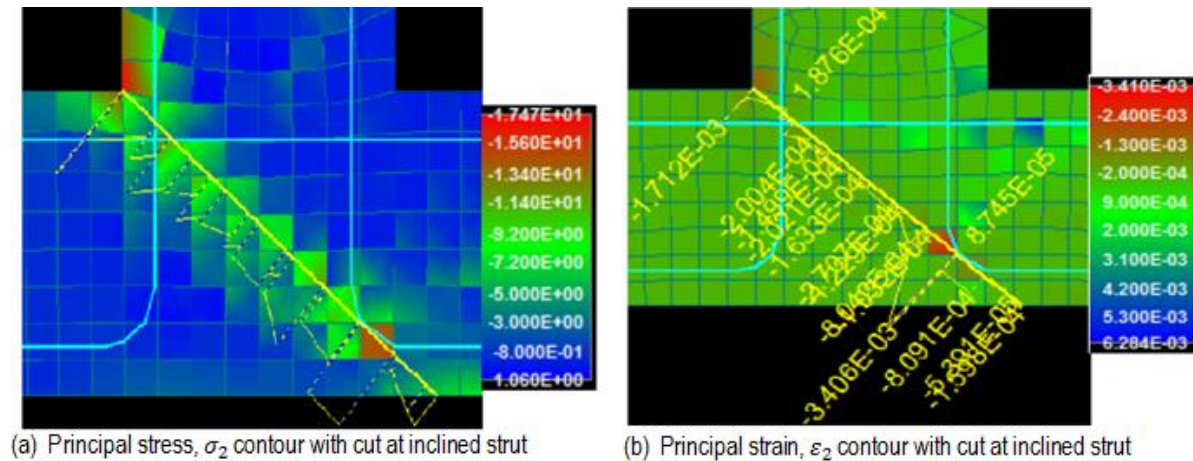


Figure 6.24 – Contour plots for minimum principal stress and strain at peak moment

To discuss figure 6.24, key data is presented in the table below for the integration point where minimum strains occurred in both the wall and the base slab (see the red contour in figure 6.24a and b).

Location	Principal stress, σ_2	Principal strain, ϵ_2
Wall-slab interface	17.47 MPa	1.73‰
Inclined strut (around the bend)	8.27 MPa	3.41‰

Looking at the table above reveals a lot about how the structure behaved at peak moment. While the more heavily stressed wall-base slab interface had a strain of only 1.73‰, the inclined strut(around the bent bar) which had softened to a stress of only 8.27 MPa had reached 3.41‰ (almost $\epsilon_{cu} = 3.5\text{‰}$). The structure actually failed immediately after this load-step thus quite brittle performance after the peak moment. As explained earlier, cracking within the inclined strut caused this premature and brittle failure of the structure. This cracking was initiated by transverse tension within the inclined strut, and further aggravated by the concentrated steel stress around the bent part of the wall reinforcement (inside the joint). At this load step, the maximum steel stress achieved by the wall reinforcement outside the joint was about 310 MPa (much less than yield stress), while it had a concentrated steel stress of 432 MPa at the bent part within the joint. The orientation of the bend was a key reason for the tensile stress concentration. This would become more obvious when the next detail (Reinforcement Layout 2) is discussed in the next section of this report.

Figure 6.25 compares the stress-strain behaviour of a volume of concrete in the wall slab interface to that of the concrete in the inclined strut (around the bent part of the reinforcement). These two point correspond to the red contour in figure 6.24b.

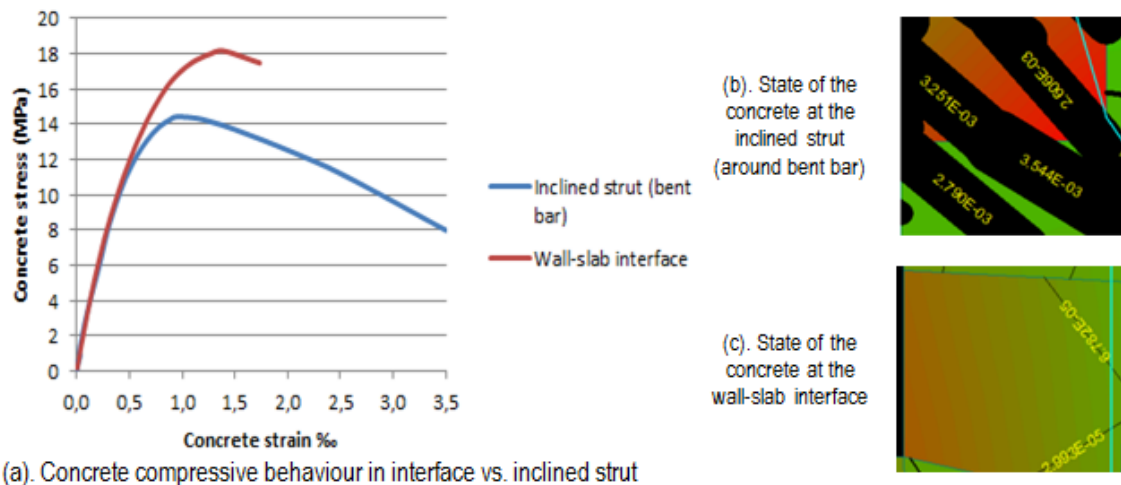


Figure 6.25 – Comparison of concrete compression behaviour up to 178.1kNm (peak moment)

From the behaviour of the stress-strain curves in figure 6.25a, it is very obvious that a volume of concrete around the bent part of the reinforcement was less stiff and thus more susceptible to compressive strain and eventual crushing. The reason is obvious: Cracks!!! Figures 6.25b and c compare cracks at both locations at this load level. This comparatively large crack around the bent bar caused significant softening of the concrete in that region. Eventual failure occurred there when the concrete crushed. In comparison, the element around the wall-slab interface performed better because the cracks were much smaller.

With the inclined strut already at strain of 3.41‰ (almost ϵ_{cu}), the very next load applied caused it to crush, thus resulting in brittle failure at a moment lower than the capacity of the wall. But what is the mechanism that caused this failure? This would be studied in the next section.

HOW DID FAILURE OCCUR?

In chapter 5 on strut and tie modelling, the boundary stresses on the D-region (caused by the moments acting on the wall) were resolved into resultant force acting on the D-region. This is presented in figure 6.26a.

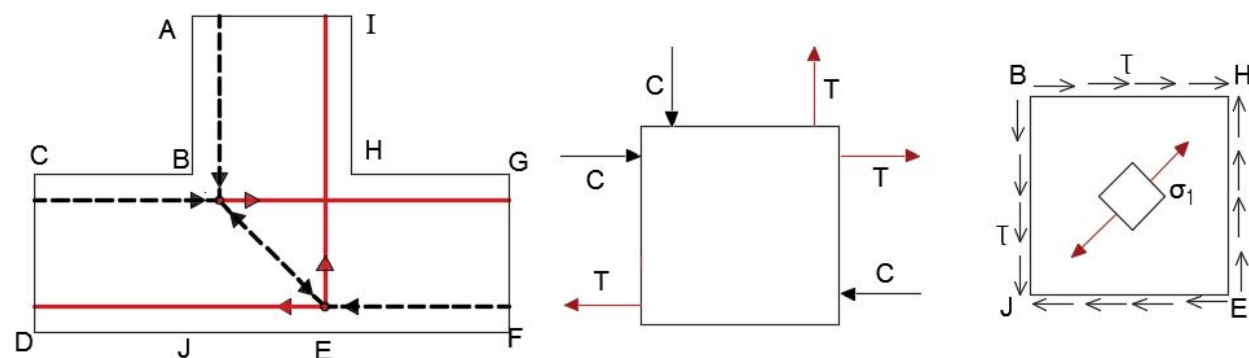


Figure 6.26 – (a). Strut and tie model for joint, (b). Free body illustration of the joint with resultant force acting, and (c). the resultant forces exert shearing stresses on the corner joint.

The strut and tie model in figure 6.26a shows the internal forces acting on the retaining wall D-region with the red arrows denoting tension and the black (and dashed) arrows depicting compression. Looking at the corner alone (figure 6.26b), the resultant forces from the applied bending moments actually subject the corner joint to shear stresses as shown in figure 6.26c. This loading illustrates the stress state within the joint, with a tensile stress field acting along HJ direction (i.e. parallel to the principal stress, σ_1), and a compressive stress field perpendicular to it (i.e. along AC direction). A good design should be able to cope with this stress field, and transfer load efficiently between steel and concrete, without premature failure of either.

In our detail however, the reinforcement from the wall (or tie) did not reach the nodal region in the slab (point C in figure 6.26c). By bending the reinforcement before it reached the node E (in figure 6.26a), it veered off the direction of the idealized tie from strut and tie. This is a key deficiency in the design of this detail. Thus, compressive stresses in the inclined strut (along AC in figure 6.26c) are not well balanced by a tension tie from the wall (i.e. BC). This deficiency in the detail resulted in a joint with lower resistance to shear. A good structural detail would place the reinforcement to such depth that it reaches the node, and allows for efficient load transfer between the concrete and steel. The shear stiffness of this joint is critical to its performance. Figure 6.27a presents the shear stress, τ_{xy} contour within the corner joint.

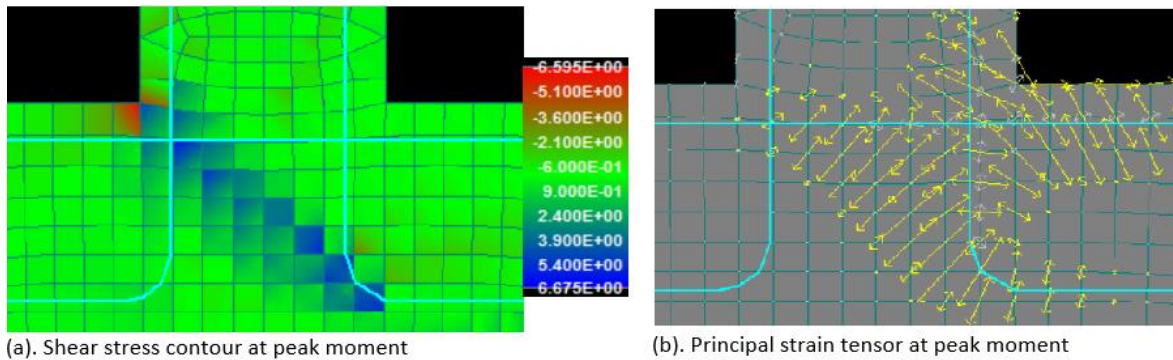


Figure 6.27 – Shear stress, τ_{xy} and principal strain tensor within the joint region of the structure

From the shear stress contour in figure 6.27a, notice the presence of tensile stresses (from shear) along the orientation of the inclined strut. Accompanying such stresses would be strains. Figure 6.27b shows the principal strain tensor within the joint. From the tensor orientation, the strains appear to be tearing open the structure along the inclined strut. To illustrate further, figure 6.28 shows a magnified deformed shape of the joint just prior to failure load.

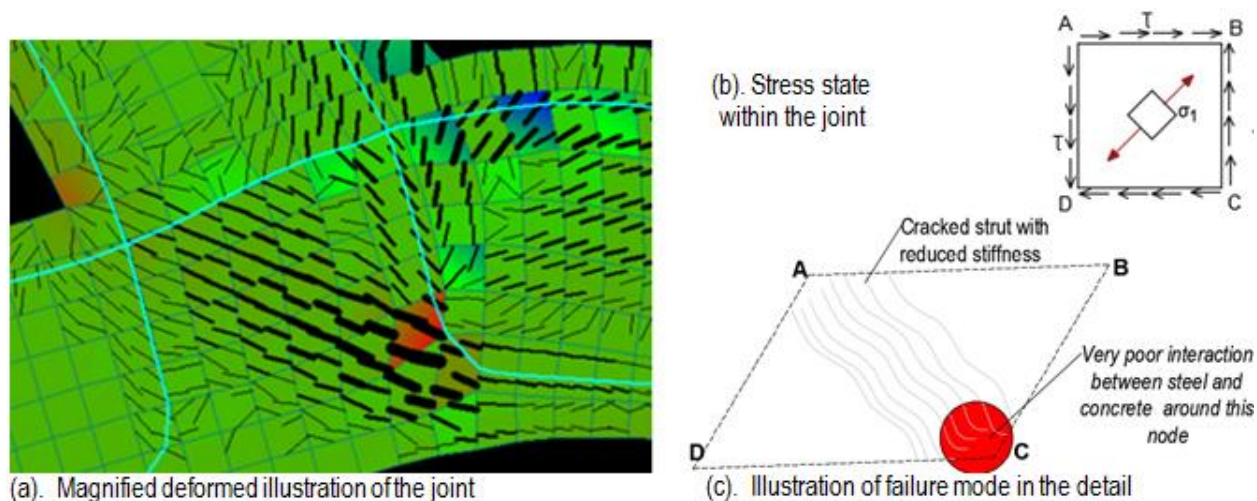


Figure 6.28 – Illustration of how failure occurred

From figure 6.28a, notice the shape of element at the start of the bend (with red contour). This is the deformed shape for a body subjected to the shear stress state shown in figure 6.28b. The element tries to elongate along HJ direction and compress about BE direction. The elongation along HJ caused the cracking in the strut, while the compression along BE caused the cracked strut to crush. A joint with adequate shear rigidity would have capacity to resist these shear stress without premature failure. However, this detail was not able to. The reason is illustrated in figure 6.28c: the interaction between the tie and the inclined strut around the nodal region (i.e. point E) was not adequate. With the tie not reaching the theoretical nodal region, force transfer was not effective between the inclined struts and the tie. Consequently, shear failure occurred in the joint, with the inclined strut crushing after large diagonal tension cracking had occurred. This explain how the joint failed.

JOINT EFFICIENCY AND SUMMARY ON ITS PERFORMANCE

With a peak moment of 178.1kNm, the detail had a joint efficiency of 72%. This is not satisfactory as it means that the joint would fail before the members it connects. In his experimental work (discussed in Chapter 3 of this report), Nilsson (1973) achieved a 60% efficiency for a similar joint that had its reinforcement bent to the heel. The FEM result in this study however predicts a joint efficiency that is 12% higher than his experimental results. Why did this variance occur in the results?

One likely reason concerns the assumption of perfect bond between concrete and steel in the material model used. In reality, there would always be some slip between the concrete and the steel. With large cracking occurring around the reinforcement in this layout, slip is likely to have a value that is not negligible. This assumption of perfect bond might have caused the additional capacity predicted by the FEM software. This assumption is further investigated in section 6.4.

Another likely reason for this variance concerns the fracture energy, G_f . For this analysis, a fracture energy of $72.5N/m$ was defined in the software. However, with concrete being a heterogeneous material, there is a likely to be variability in this parameter. To check sensitivity of the FEM result to this material parameter, the moment and joint efficiency at four different fracture energies are shown below:

Fracture Energy	$72.5N/m$	$50N/m$	$25N/m$	$10N/m$
Peak moment	178.1	171.7	164.8	153
Joint Efficiency	72.5%	70%	67%	62.3%

From the table above, it is quite obvious that the result is sensitive to the fracture energy, G_f . With a lower fracture energy, the joint efficiency approaches the 60% obtained by Nilsson (1973) experiments. In practice, this material parameter depends on several factors including size of aggregate used, water-cement ratio, age of concrete etc. With all these factors having an influence, fracture energy is also a likely reason for the variance.

Though this structural detail is quite popular in practice, it is nevertheless a deficient detail. It is likely to fail prematurely from the effects of diagonal tension cracking along the inclined strut. A better detail can be designed that takes the effect of transverse tension into account. One of such is studied in next section.

6.3.2 Reinforcement Layout 2

With the previous reinforcement layout failing prematurely, an improvement is made to the detail in reinforcement layout 2 earlier shown in figure 6.14b. This structural detail gives an improved performance by attaining a peak moment of $215.4kNm$ before failure, thus representing 88% joint efficiency. In this section, the detail is studied to understand the reasons why it gave an improved performance, and to find out why it failed without achieving 100% joint efficiency.

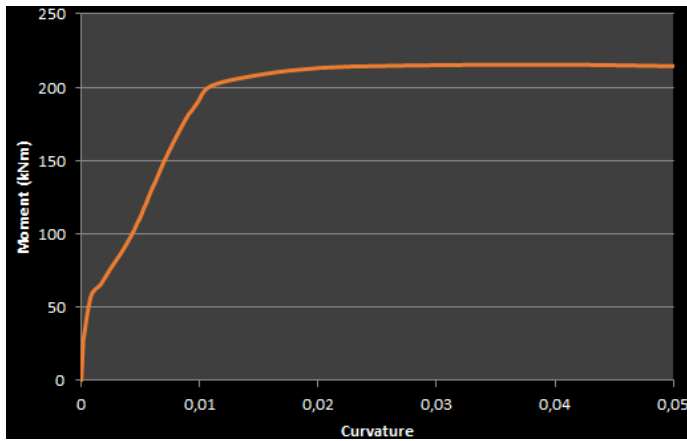
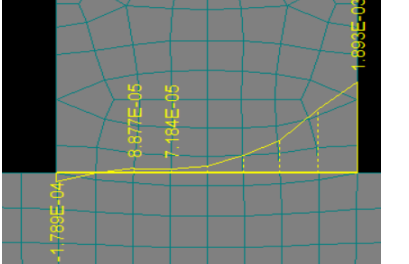
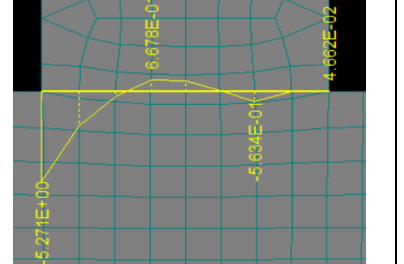
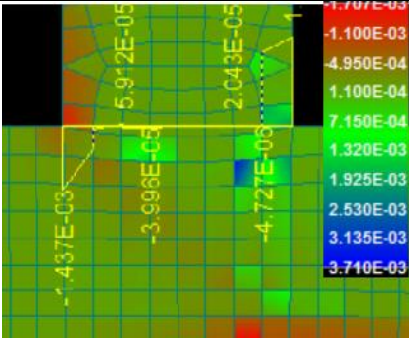
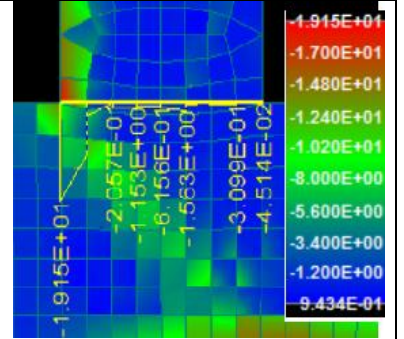
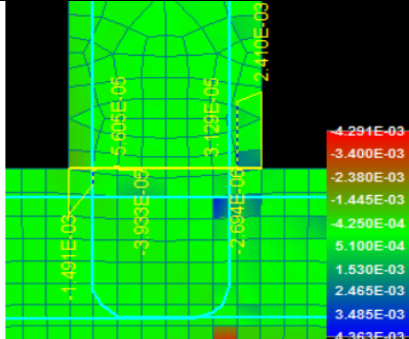
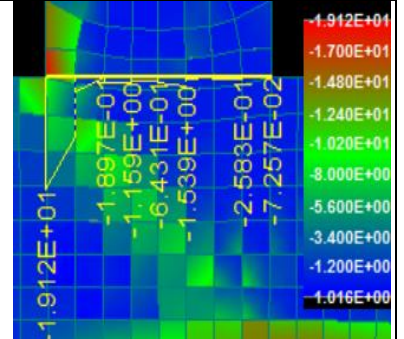


Figure 6.29 – Moment-curvature plot for reinforcement layout 2

For the previous detail, the parts of the structure that were vital to its performance were the inclined strut (within the joint) and the wall-slab interface. A cut taken across both sections is studied in this section to understand how the stresses and strains evolved with loading. These are presented in a Table 6.1 (for a section at the wall base interface) and Table 6.2 (for a cut along the inclined strut).

Table 6.1 – Stress-strain behaviour along wall-slab interface at different moments

<p style="text-align: center;">$M = 19.33kNm$</p> <p><u>Load at which cracking was initiated.</u> The distribution of strains, ϵ_{yy} and stress, σ_{yy} are linear across the section. Tensile stress, σ_{yy} was only $0.92MPa$ yet it cracked. Cracking occurred prematurely at the re-entrant corner due to tensile stress concentration. Crack initiated at this load step because the maximum principal stress, σ_1 reached material tensile strength.</p>	<p>(a). Normal strain, ϵ_{yy} (averaged)</p>	<p>(b). Normal stress, σ_{yy}</p>
---	--	---

<p>$M = 101 \text{ kNm}$</p> <p>After crack initiation, the material behaviour is increasingly non-linear as the cracks grew. Outer fibres (near the re-entrant corner) softened in tension and inner fibres carried more tension. Thus, cracks propagated inwards. Concrete stress is still below the peak compressive stress since strain is less than $\varepsilon_{c3} = 1.75\%$.</p>	 <p>(c). Normal strain, ε_{yy} (averaged)</p>	 <p>(d). Normal stress, σ_{yy} (averaged)</p>
<p>$M = 215.2 \text{ kNm}$</p> <p>At this load, the structure has reached 1.71‰ compressive strain. It was however only 1.44‰ at this wall-base interface. The concrete stress was 19.15 MPa at this interface. So the wall-slab interface had the highest compressive stress, but not the highest strain in the structure.</p>	 <p>(e) Minimum principal strain, ε_2</p>	 <p>(f) Minimum principal stress σ_2</p>
<p>$M = 212 \text{ kNm}$</p> <p>Concrete compressive strains exceeded 3.5‰ in the structure. However, the minimum principal strain at this interface was only 1.49‰. This wall-slab interface did not govern the capacity of the structure. Compression failure did not occur here in the interface, and the steel did not yield in the wall at failure.</p>	 <p>(g) Minimum principal strain, ε_2</p>	 <p>(h) Minimum principal stress σ_2</p>

The evolution of stress-strain behaviour at the wall-base interface is discussed in Table 6.1 above. Before cracking, the section behaved in a linear elastic manner with stress concentration at re-entrant corner. At first crack, the normal tensile stress, σ_{yy} was only 0.92 MPa . Cracking occurred because the principal stress reached the material tensile strength. From this, it is obvious that this section is disturbed, and the stress calculated based on Bernoulli linear strain assumption is not reliable here. The behaviour at higher loads is also shown in Table 6.1. When the structure failed, the minimum strain in this wall-slab interface was less than 1.50‰. Despite being subjected to the largest magnitude of compressive stress (19.15 MPa), this wall-slab interface was not the weak point for the structure.

Table 6.2 – Stress-strain behaviour along inclined strut at different moments

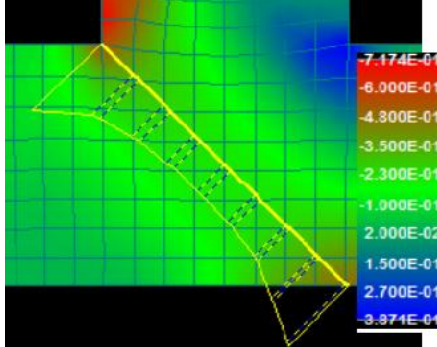
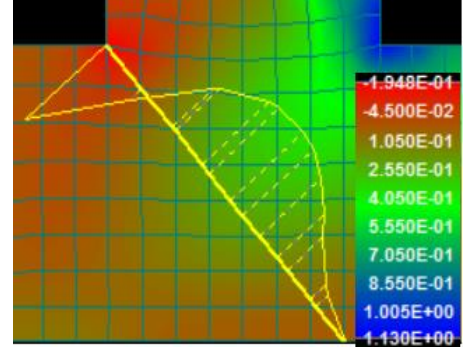
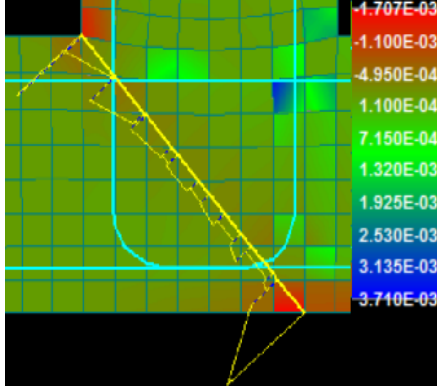
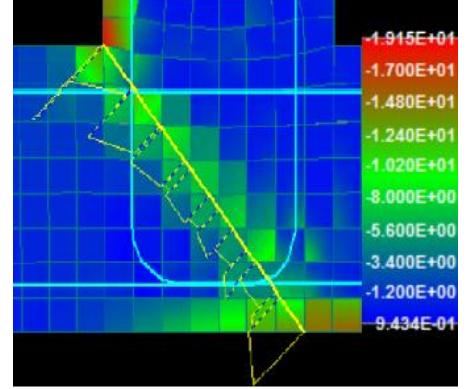
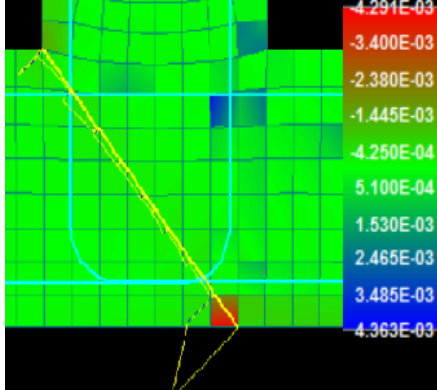
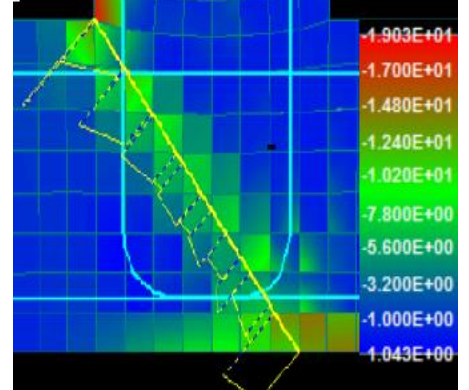
<p>$M = 19.33 \text{ kNm}$</p> <p>The inclined strut is subjected to compressive principal stress, σ_2 (figure a) and transverse tension, σ_1 (figure b). The compressive stress in the strut is elevated at the ends, and quite uniform in the middle part. On the other hand, transverse tension is largest in the middle of the inclined strut.</p>	 <p>(a) Minimum principal stress, σ_2</p>	 <p>(b) Maximum principal stress, σ_1</p>
<p>$M = 215.2 \text{ kNm}$</p> <p>The structure reached 1.71‰ strain at this load. Unlike Reinforcement Layout 1, the ultimate strain was not within the inclined strut. Rather, it was at the outer fibres near the corner joint-heel slab interface. The principal compressive stress, σ_2 along the inclined strut was still quite uniform except at the ends where they were elevated.</p>	 <p>(c). Minimum principal strain, ϵ_2</p>	 <p>(d). Minimum principal stress, σ_2</p>
<p>$M = 212 \text{ kNm}$</p> <p>Here, the concrete strains exceeded 3.5‰. Compression softening occurred in the outer fibres at failure location, while inner fibres close to the softened concrete had higher stress. Failure did not occur within the inclined strut. Rather, crushing of concrete occurred at the outer fibres near the corner joint-heel slab interface. This detail prevented diagonal tension cracking failure.</p>	 <p>(e). Minimum principal strain, ϵ_2</p>	 <p>(f). Minimum principal stress, σ_2</p>

Table 6.2 illustrates how the stresses and the strains evolved with load with this detail. With the bent part of the reinforcement crossing the inclined strut, this structural detail performed better than Reinforcement Layout 1 earlier studied. While transverse tension still caused cracking within the inclined strut, the reinforcement that crossed the strut was effective in controlling the crack width, thus they were much smaller when compared with the case in Reinforcement Layout 1. This made the inclined strut stronger, stiffer and less susceptible to compressive strain.

In Reinforcement Layout 1, cracks in the inclined strut were aggravated by stress concentration at the bent part of the steel. How does this detail deal with that issue of stress concentration at the bent part of the reinforcement? This is illustrated in figure 6.30 for the load step just prior to failure.

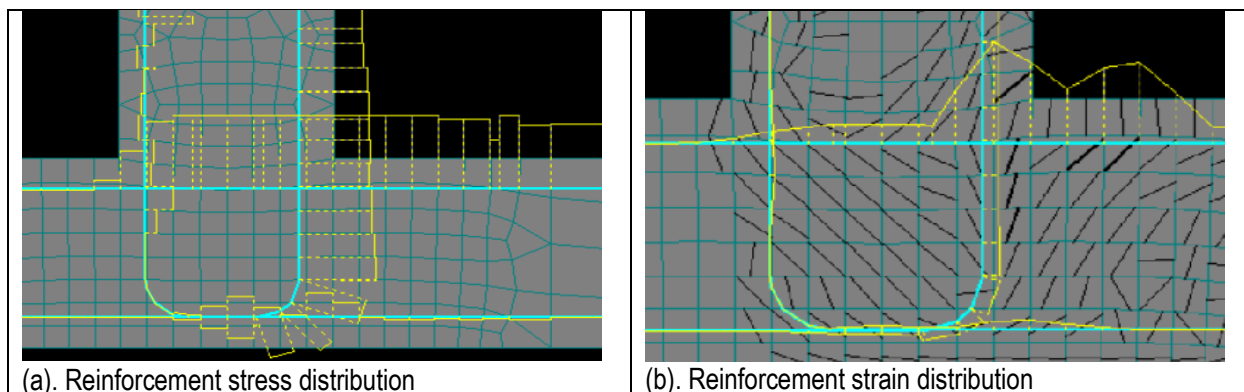


Figure 6.30 – Reinforcement stress and strain distribution in Reinforcement Layout 2

From figure 6.30a, notice that the steel stress (of the retaining wall) starts reducing around the bent part of the reinforcement. This improvement in steel stress behaviour can be attributed to the effect of bearing of the inclined strut on the bent part of the reinforcement. This is unlike Reinforcement Layout 1 which relied entirely on bond stress for force transfer between concrete and the reinforcing steel. Additional force transfer by bearing occurs in this case. Thus, no cracks occurred in the inclined strut from steel stress concentration. This, combined with the fact that the cracks (from transverse tension) were small made the inclined strut stronger.

Also from figure 6.30b, notice that the steel (at the top of the slab) had large plastic strains around the re-entrant corner. Steel strains of up to 16.6‰ were recorded at that point at failure. In comparison, the largest steel strains around the bent part of the steel (within the core of the joint) was just 1.82‰. This concentration of steel strains around the re-entrant corner had an impact on how the structure behaved at failure. This would be discussed next.

HOW FAILURE OCCURRED?

Failure occurred by crushing of concrete after excessive yielding had taken place in the top horizontal reinforcing steel (up to 16.6‰ strain in steel) around the re-entrant corner. The location that crushed is illustrated by the red contour in figure 6.31a. To understand the mode of failure, a magnified illustration of the deformed joint is shown in figure 6.31b. From the illustration, the applied opening moments appears to be tearing open the structure vertically along the joint – slab (heel side) interface outside the core bounded by the reinforcement. Notice large cracks open along that region in figure 6.31b.

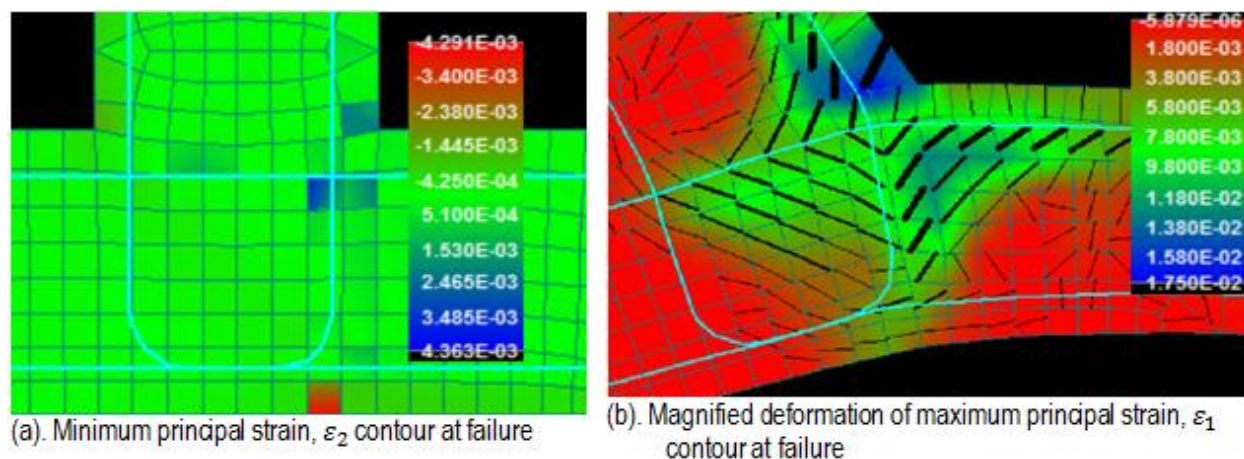


Figure 6.31 – Location of eventual failure and deformed displacement diagram

To gain deeper insight into what is happening at that point, the principal strain tensor with the joint is presented in figure 6.32a. It shows a concentration of tensile strains around just outside the region defined by the reinforcement within the joint. With the strains playing a key role in that region, figure 6.32b compares the normal strains, ε_{xx} at a cross-section around the joint – slab (heel side) interface with that of a B-region just 50cm away. While the B-region had rather small strains and a strain distribution that complied with Bernoulli linear strain assumption (figure 6.32d), same cannot be said of the D-region at the joint – slab (heel side) interface. There is a compressive strain concentration there which exceeded concrete ultimate strain, ε_{cu} . Why did failure not occur within the core of the joint as was the case with Reinforcement Layout 1? The only difference between both details is the orientation of the bent part of the reinforcement. This is obviously the reason for the difference in performance. But how?

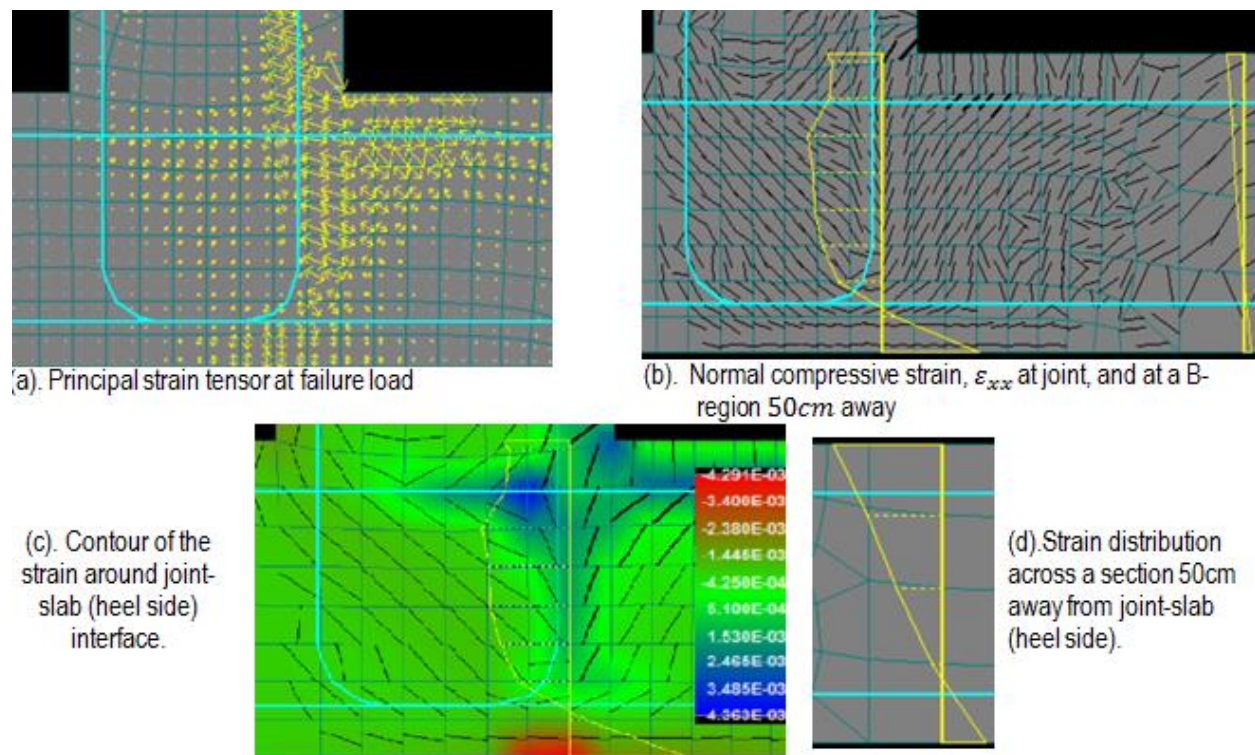


Figure 6.32 – Strains around failure location for Reinforcement Layout 2

Bending the wall reinforcement to cross the path of the inclined strut provided several benefits to the structure. Some of these benefits include:

- It controlled crack width within the inclined strut, thus making it stiffer and stronger
- Bearing stresses from the inclined strut (acting on the bent part of the reinforcement) provided additional force transfer capacity, thus preventing the stress concentration (in reinforcing steel) that occurred in Reinforcement Layout 1.
- The bent part of the steel provided confinement to the inclined strut, thus increasing its effective compressive strength.

These benefits made the inclined strut stiffer, and thus less susceptible to crushing. Thus this detail successfully prevents diagonal tension cracking failure. Nevertheless, joint failure still occurred, though around the joint-heel slab interface. The failure is schematized in figure 6.33 below. The detail improved the stiffness of the joint's core, but not the overall joint stiffness. Further improvement needs to be made.

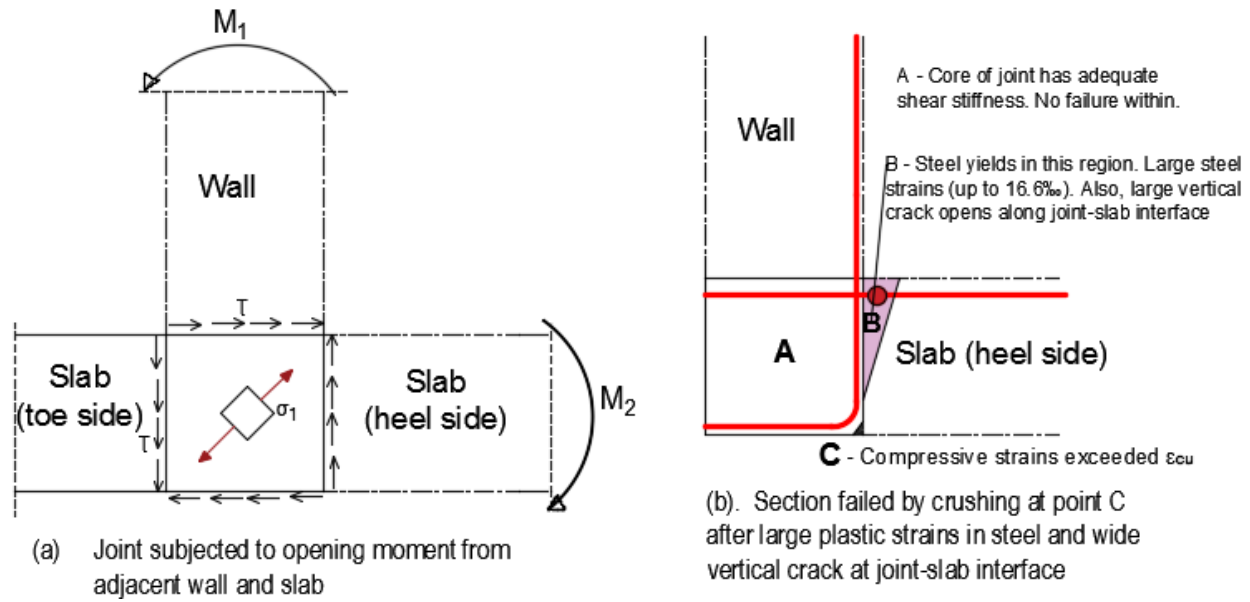


Figure 6.33 – Illustration of failure mode of Reinforcement Layout 2

JOINT EFFICIENCY AND SUMMARY ON ITS PERFORMANCE

With a failure moment of 215.4 kNm , the joint efficiency of this detail is 88%. While it did not achieve the goal of 100% joint efficiency, it is nevertheless an improvement when compared to Reinforcement Layout 1. Nilsson (1973) performed experiments on a several samples with a similar detail, and obtained results between 82% and 101%. He attributed the scatter in the result to difference in anchorage length among the samples he tested. The tensile reinforcement ratio also had an impact on his results with higher joint efficiency obtained for samples with the lower tensile reinforcement ratio. The 88% predicted by FEM in this study falls within the range of his experimental results. Nevertheless, it still does not meet the design objective of minimum 100% joint efficiency. Further improvement is required.

With diagonal tensile cracking failure already prevented by this detail, a more efficient structural detail can be obtained if cracking in re-entrant corner can be controlled. Such a detail should:

- Effectively control transverse tension cracking within the inclined strut.
- Effectively control re-entrant corner cracking, limiting width of cracks formed.
- Ensure overall joint stiffness (and not just stiffness of the inner core that was achieved with Reinforcement Layout 2).
- Prevent excessive strains within the joint (both steel and concrete strains). Though yielding of steel should occur before failure, it should however occur outside the joint i.e. along the adjacent connected member

All the above requirements are met when a diagonal bar is added at the re-entrant corner. This would be briefly discussed in section 6.5 of this report.

6.4 Impact of bond model on FEM results

In the previous section, some of the FEM result seemed quite optimistic when compared with experimental results earlier discussed in Chapter 3 of this report. In the FEM models analyzed, perfect bond was assumed to exist between the reinforcing steel and the concrete. However, with cracking playing a vital role in the joint behaviour, some slip is likely to have occurred between the embedded steel and the surrounding

concrete. In this section of the report, the impact of the bond model (assumed in the analysis) on the FEM result is studied.

6.4.1 Comparison of perfect bond assumption with bond-slip model

In this section, a structure is analyzed to study the impact of the bond model used (in the FEM software) on the result obtained from the FEM analysis. The geometrical model used is illustrated in figure 6.34. The structure is a wall-base corner which is used to model a symmetrical half of a U-shaped structure (the line of symmetry is in the right edge of the base slab). The interface between the wall and the slab is modelled by a no-tension interface element. The bar being studied (i.e. the red bar in figure 6.34) would be varied in this study (i.e. 100mm, 200mm and 330mm embedment depths). Only this reinforcement (consisting of two 12mm bars embedded into the base slab) would be modelled with a bond-slip relation. Perfect bond would be assumed for the other reinforcing bars used in the structure. The other reinforcements are strong enough to prevent premature failure of the wall or slab.

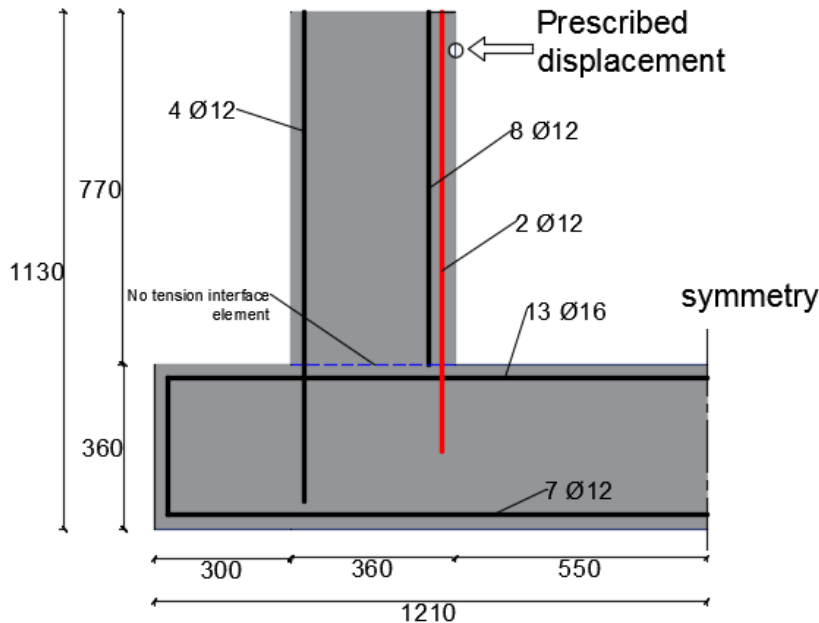


Figure 6.34 - Geometrical model to study impact of bond model (Kabele, Červenka and Červenka)

Material:

Concrete: Modelled using ATENA SBETA element. The wall is made of C40 concrete class, while the base slab of C30 concrete. The material data for the base slab are summarized thus:

$$E_c = 30000 \text{ MPa}; \quad f_c = 25.5 \text{ MPa}; \quad f_t = 2.32 \text{ MPa}; \quad \text{and} \quad G_f = 58 \text{ N/m}$$

Reinforcement: Bilinear elastic-perfectly plastic model used with $E_s = 210 \text{ GPa}$ and $f_y = 700 \text{ MPa}$

Bond: For each embedment length provided for the bar being observed, the behaviour for five bond assumptions is studied. These include perfect bond assumption and four CEB-FIP bond-slip models (i.e. for good bond-confined concrete, good bond - unconfined concrete, poor bond - confined concrete, and poor bond - unconfined concrete). More information on these models are presented in Appendix 2. It is assumed that ribbed reinforcement is used in this analysis.

Loading and analysis:

Loading: The load cases applied to the structure in this analysis consist of a prescribed horizontal displacement and the support reactions. The prescribed displacements are applied in incremental step around the top of the wall as shown in figure 6.34. For the support reactions, the structure is restrained from horizontal displacement along the line of symmetry, and the node at the end (or toe) of the base slab is pinned.

Solution method & data collection: The regular Newton-Raphson solution method is used in this analysis, with stiffness updated at each iteration. In order to study the load-displacement behaviour, monitoring points are defined at the point of load application. Horizontal displacement and reaction forces are collected from that monitoring point.

Results

The horizontal force applied to the wall induces a moment at the wall-base connection. This moment is resisted by two forces i.e. compression in the wall-base contact, and tension in the embedded steel. On applying load to the structure, the joint opens as seen in figure 6.35. It opens because a no-tension interface is used. The tension in the two 12mm bars are transferred to the base slab by bond stress alone.

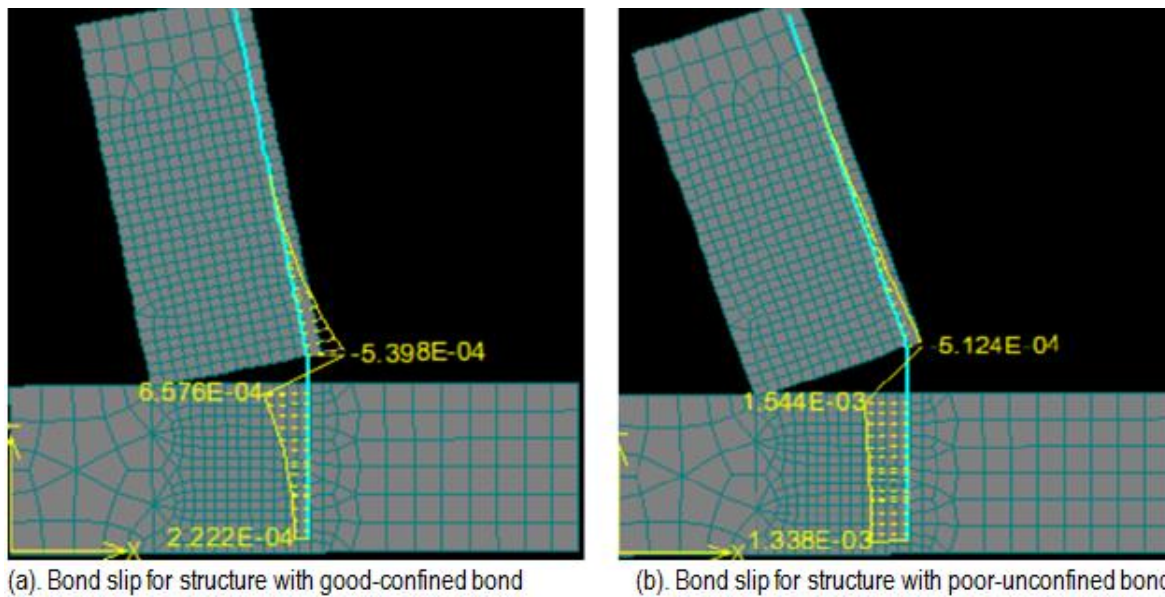


Figure 6.35 – Reinforcement slip [m] distribution along embedded bar at 4mm prescribed displacement

The behaviour and capacity of the structure is strongly influenced by the bond model used. In general, the force on the structure increased with increasing prescribed displacement up to a peak. Afterwards, the capacity decreases as the prescribed displacement is further increased. Table 6.3 shows the maximum horizontal force attained by the structure for the different bond models studied. The behaviour is illustrated graphically in figure 6.36.

Table 6.3 – Maximum force attained by the structure for different bond assumptions

Bond model used	Peak force (kN) attained for the provided anchorage length		
	100mm	200mm	330mm
Perfect Bond	94.95	94.95	94.95
Good bond – Confined concrete	46.59	94.34	94.94
Good bond – Unconfined concrete	31.85	60.59	94.94
Poor bond – Confined concrete	26.92	51.15	80.03
Poor bond – Unconfined concrete	16.92	34.37	57.04

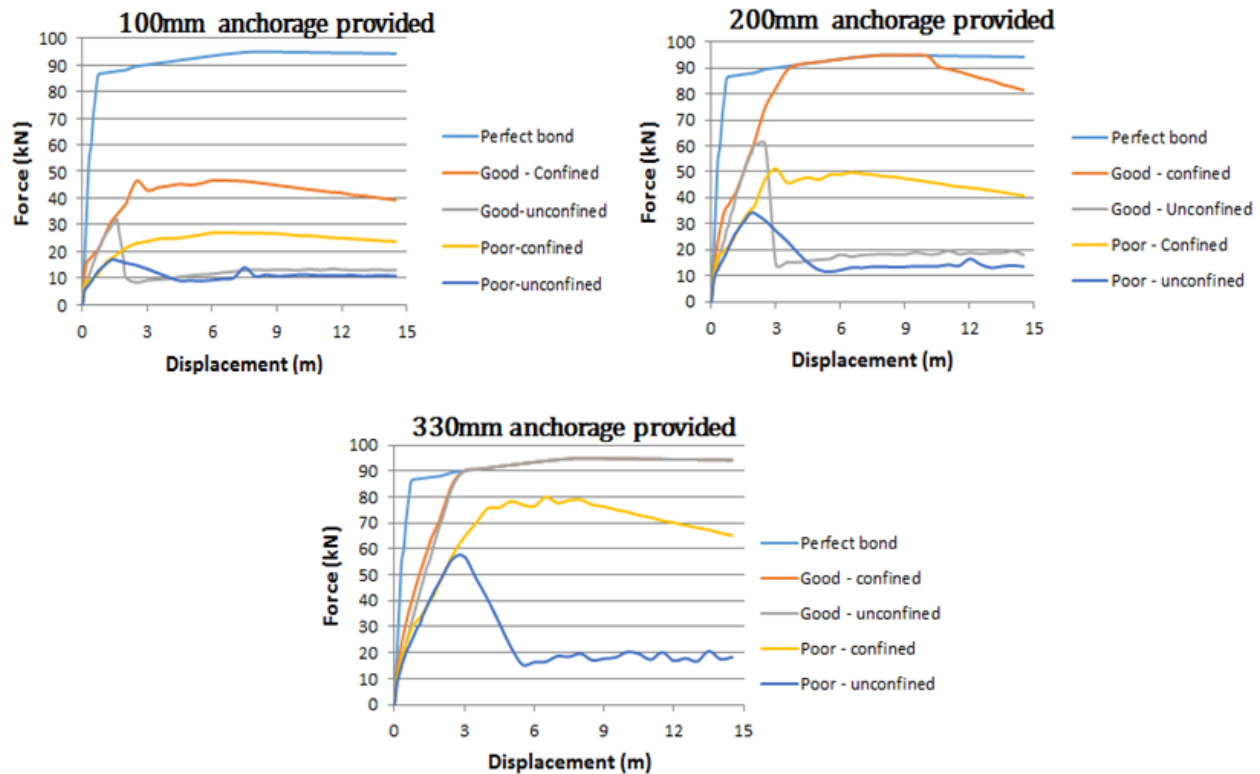


Figure 6.36 – Force-displacement diagram for the models at different embedment depths

On examining Table 6.3, it can be seen that the assumption of perfect bond has impact on the result obtained from the FEM analysis. Regardless of the embedment depth provided, it predicts same capacity for the structure. Thus, with a perfect bond assumption, the anchorage length provided did not matter.

When compared with the other models in Table 6.3, it is obvious that perfect bond assumption overestimates the capacity of the structure. For instance, where the bond quality is poor, and the concrete is unconfined, the FEM software predicts 17.92kN capacity for the structure if only 100mm anchorage length is provided. In contrast, a much higher capacity of 94.95kN is predicted where perfect bond is assumed. Even when the bond quality is good, and the concrete is confined, the structure attains less than 50% of that predicted if perfect bond is assumed (for 100mm anchorage length).

Furthermore, it can be seen that the bond quality, degree of confinement and anchorage length matters when a bond-slip model is used. The cases with poor bond quality achieved lower capacity than the cases with good bond quality. Higher capacity is also attained when the concrete is confined. Confining the concrete

also ensured a better post-peak performance as seen in figure 6.36. On the anchorage length, it can be seen that capacity attained by the structure approached that of perfect bond assumption, as the anchorage length increased.

In concluding this section, it has been demonstrated that the bond model used in the FEM analysis could have an impact on the result predicted by the FEM software. In some of the results presented above, perfect-bond assumption predicted results that were comparatively higher than those obtained when a bond-slip model is used. In the same manner, perfect bond assumption made in the retaining wall studied in sections 6.2 and 6.3 could be responsible for the disparity between some of the FEM result, and the experimental results earlier presented in Chapter 3. This would be investigated in the next sections of this report.

6.4.2 Variants 2 – 6 with bond-slip model

For the variants discussed in section 6.2 of this report, perfect bond was assumed to occur between the concrete and the steel. However, from the bond study in the last section, it is obvious that the perfect-bond assumption could have resulted in an over-estimation of capacity of some of those joints. This section briefly discusses the results of variants 2 to 6 (of section 6.2) when a bond-slip model is defined in the FEM analysis. In this analysis, only the main tension reinforcement from the wall is modelled with a bond-slip model. Perfect bond is assumed for the other reinforcements in the structure. For the bond-slip model, only the CEB-FIP models for good bond - confined concrete and poor bond – unconfined concrete bond-slip are used. More information on their parameters is provided in Appendix 2. The maximum bending moment attained by variants 2 to 6 using bond models are summarized in Table 6.4.

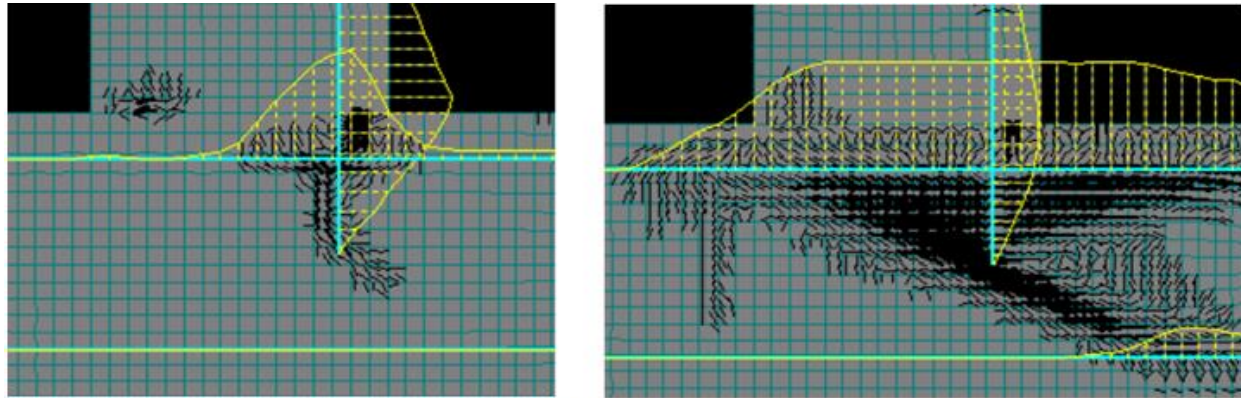
Table 6.4 – Peak moment and joint efficiencies of variants 2 – 6 (bond-slip models considered)

Variant	Peak moment (kNm) achieved and Joint efficiency (%)		
	<i>Perfect bond assumption</i>	<i>Good Bond – confined concrete</i>	<i>Poor bond – unconfined concrete</i>
Variant 2 (200mm anchorage)	127.3 kNm (51.8%)	98.5 kNm (40.0%)	54.8 kNm (23.7%)
Variant 3 (350mm anchorage)	215.8 (87.8%)	151.8 (61.8%)	83.2 kNm (33.9%)
Variant 4 (bent to heel)	184.9 (75.3%)	151.8 (61.8%)	149.6 kNm (60.9%)
Variant 5 (bent to toe)	217.3 (88.4%)	194.7 (79.2%)	188.4 kNm (77.0%)
Variant 6 (bent to toe + diagonal bar)	249.9 (101.7%)	246.5 (100.3%)	245.5 kNm (99.9%)

From the results in Table 6.4 above, it is obvious that the perfect bond assumption over-estimates the capacity in some of the instances. Some aspects of the structural behaviour would be discussed here in the light of comments earlier made in section 6.2 (where perfect bond was assumed). The discussion would focus on the ways in which the variants (with bond-slip model) differs in behaviour from scenario with perfect bond. Further discussion of the bond-slip models used is presented in Appendix 2.

Variant 2: Wall reinforcement embedded 200mm into base slab

When perfect-bond was assumed (see section 6.2.2.1), this concrete (along the inclined strut) crushed after large transverse tension cracks had occurred along the inclined strut, and in the vicinity of the reinforcement end (or tip). In figure 6.5b, a large stress concentration occurred at the reinforcement end. However, with large cracks propagating around the reinforcement, slip between the steel and the surrounding is inevitable. Figure 6.37 shows the stress distribution along the steel (at peak moment) when bond-slip model is used.



(a). Steel stress for poor bond-unconfined concrete (b). Steel stress for good bond- confined concrete
Figure 6.37 – Steel stress distribution and crack at peak moment for variant 2

On comparing figure 6.37 with figure 6.5a, it can be seen that perfect-bond assumption leads to much higher steel stress at the reinforcement tip. In contrast, when bond models is used, slip is not prevented, thus no concentrated steel stress occur at the reinforcement tip. This difference in behaviour has impact on the capacity and failure mode and capacity attained. From Table 6.4, it can be seen that the capacity and joint efficiency depend on the bond model used.

When the bond quality is poor and the concrete is unconfined, bond failure is likely to occur if the anchorage length provided is inadequate (as is the case in this variant). The structure attained 23.7% joint efficiency. This is much lower than the 51.8% joint efficiency predicted when perfect bond is assumed. In this case, bond failure occurs by splitting of the unconfined concrete. When the bond quality is good and the concrete is confined, it attains a higher capacity (40% joint efficiency). With the concrete confined, there is no bond failure due to splitting of concrete. Rather, the structure carried further load till crushing of the concrete occurred along the inclined strut.

In summarizing the performance, this detail provides a joint efficiency between 23.7% - 40% depending on the bond quality and degree of confinement. Where the concrete is not confined, bond failure (by splitting of concrete) occurs. Where the concrete is confined and the bond quality is good, bond failure is prevented. However, the structure's still fails prematurely after wide cracks formed along the inclined strut. These cracks weaken the inclined strut, and causes it to crush at a relatively low applied load. Thus, it can be seen that the joint efficiency attained by this details is sensitive to the bond and confinement conditions. A realistic joint efficiency ranges 23.7% - 40% depending on the bond and confinement conditions.

Variant 3: Wall reinforcement embedded 350mm into base slab

When a bond-slip model is used for this detail, it has a similar impact on the FEM results as was explained in the previous case (for 200mm embedment length). The steel stress distribution along the embedded bar

is shown in figure 6.38. Unlike the case with perfect-bond (see figure 6.7a), there is no elevated stress at the reinforcement tip. For the model with poor bond quality and unconfined concrete, bond failure occurred as in the case of the 200mm embedment length. However, the longer anchorage length provided a more surface area for force transfer by bond. Thus, the detail achieved a joint efficiency of 33.9% . This is still much lower than the 87.8% joint efficiency predicted by the FEM software if perfect bond is assumed. When the bond condition is good, and the concrete is confined, the detail attained a higher joint efficiency of 61.8%. Eventual failure occurred when the concrete (along the inclined strut) crushed after much cracking had propagated along the inclined strut.

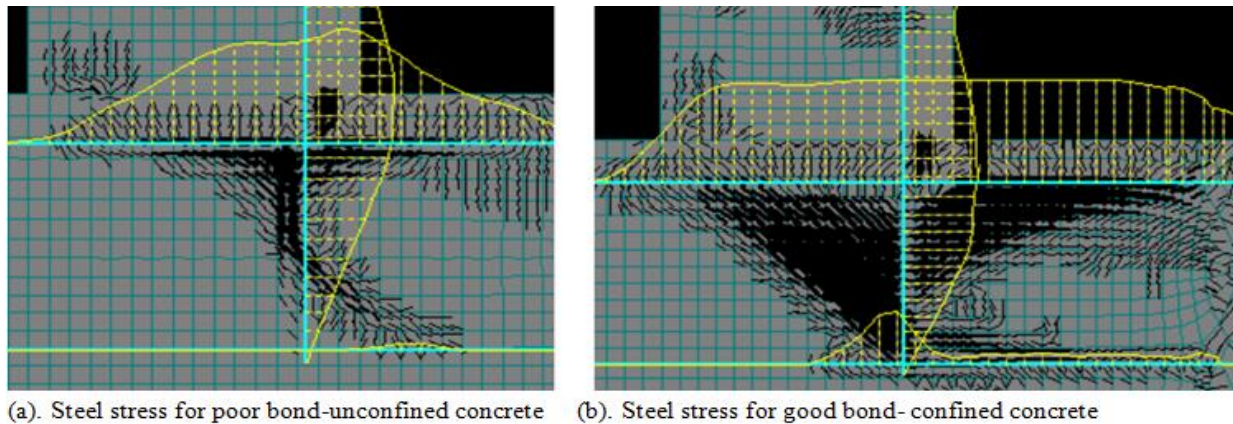


Figure 6.38 – Steel stress distribution and crack at peak moment for variant 3

Variant 4: Wall reinforcement bent towards the heel

In the discussion of this variant in section 6.2.3.1 (which assumed perfect bond), the structure failed by crushing of the concrete around the bent part of the reinforcing bar after wide cracks had occurred in that vicinity. With the perfect bond assumption, the wall reinforcement had a stress concentration around the bent bar as was shown in figure 6.9a. When a bond-slip relation is defined for the wall reinforcement, there is no such stress concentration around the bent part of the reinforcement. The stress distribution along the reinforcement is shown in figures 6.39 a and b. There is no stress concentration at the bend for the good bond – confined concrete case, and the poor bond – unconfined concrete case. This is one of the impact of using a bond-slip model.

From the analysis, the structure attains a joint efficiency between 60.9% (for poor bond – unconfined concrete) to 61.8% (where the bond is good and the concrete confined). These are lower than the 75.3% predicted when perfect-bond is assumed. Unlike variant 2 and 3, bond failure does not occur in this detail. This is due to the fact that the anchorage length provided was adequate.

Regardless of the bond-slip model, the structure still failed prematurely with the joint's performance preventing the adjacent connected members from reaching their full capacity. The opening moment acting on the structure caused transverse tension within the joint (as was illustrated in figure 6.28). The cracks caused by these transverse tension weakened the inclined strut, and led to its crushing prematurely. With the reinforcement oriented away from the inclined strut, it did not help to control crack width in the inclined strut. This is one of the main disadvantage of the detail. This has been discussed extensively in section 6.3.1. The principal strain contour at failure, and the principal strain tensor are shown in figures 6.39c and d respectively. The inclined strut crushed in the region of the bent bar (see the red contour in figure 6.39c). Thus, the behaviour is similar to what was discussed in section 6.2.3 (where perfect bond was assumed).

The capacity predicted is however very different. This result (using bond models) approximates more closely with experimental results earlier discussed in Chapter 3 of this report.

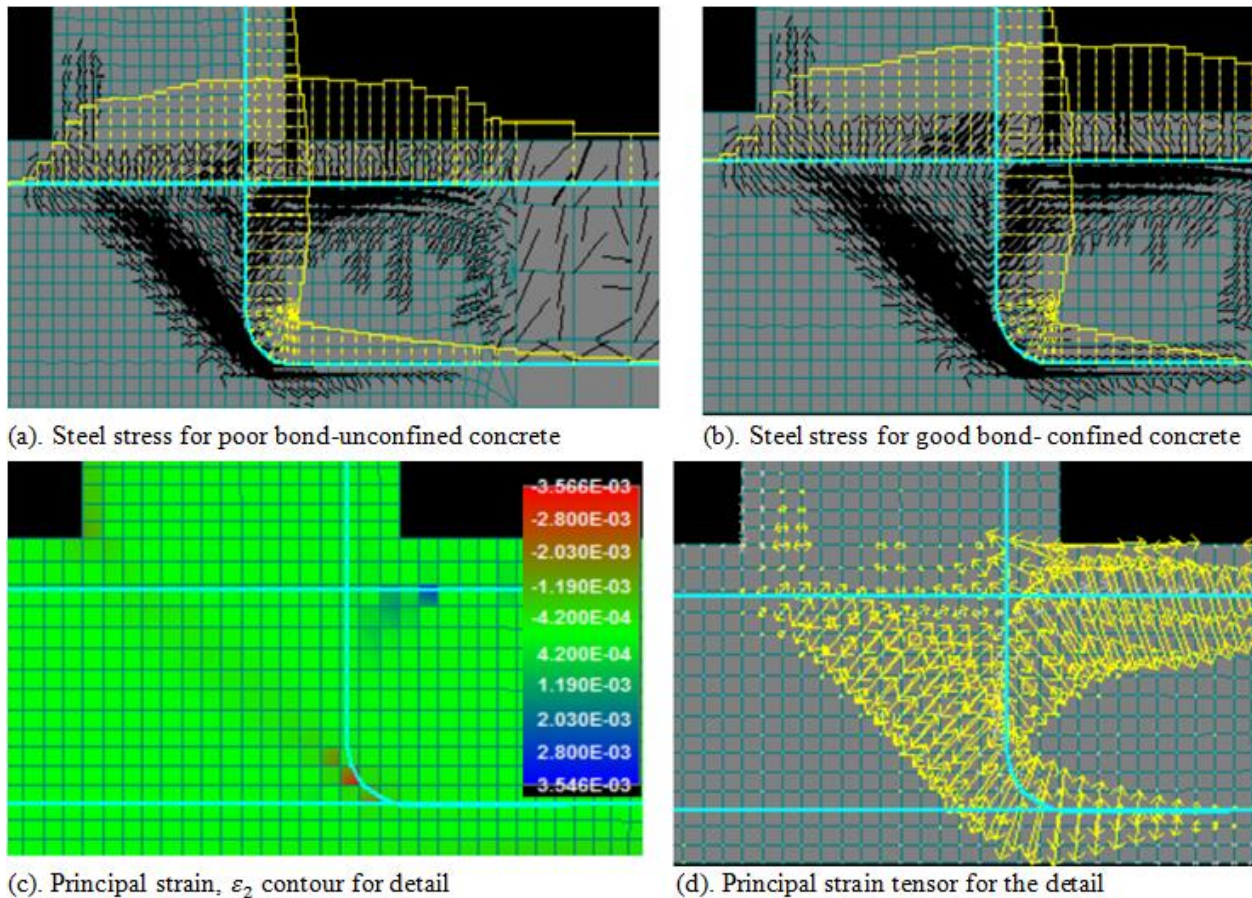
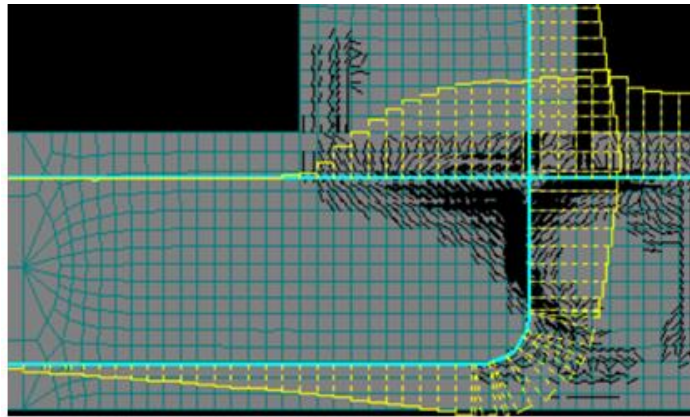


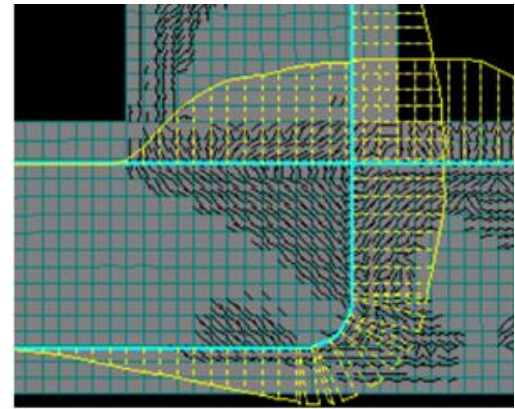
Figure 6.39 – Post-processed data for variant 4

Variant 5: Wall reinforcement bent towards the toe

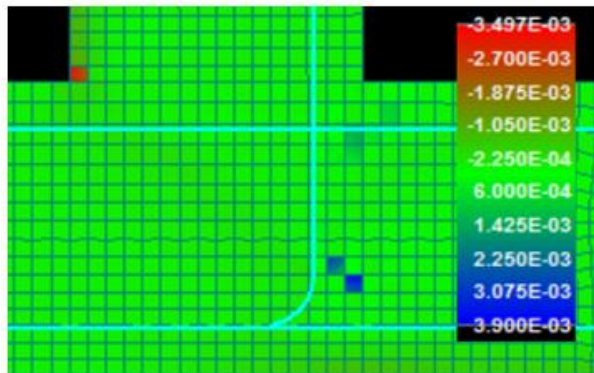
When a bond-slip is used for the main reinforcement of variant 5, a joint efficiency between 77% - 79% is predicted from the FEM analysis. This is lower than the 88.4% joint efficiency predicted when perfect bond is used. The steel stress distribution and crack pattern in the corner joint is shown in figures 6.40a and b. This detail prevented both bond failure and diagonal tension cracking failure. The reason is quite obvious when the crack pattern for variant 4 (i.e. figures 6.39a and b) is compared with that for variant 5 (figures 6.40a and b). There is less cracking (along the direction of the inclined strut) in variant 5. This made the inclined strut in this detail is stronger and stiffer in this variant. Eventual failure is by crushing of the concrete along the wall-base interface after the top steel in the base slab had yielded. The location is indicated by the red contour in figure 6.40c.



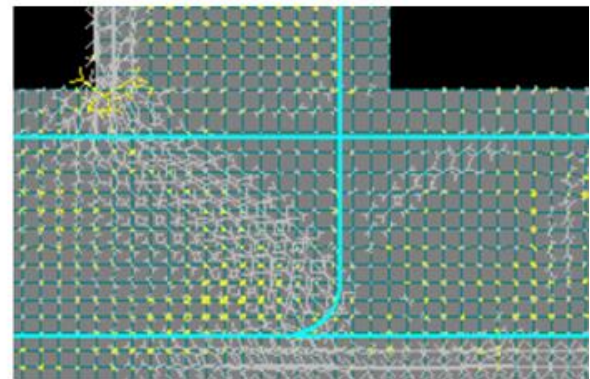
(a). Steel stress for poor bond-unconfined concrete



(b). Steel stress for good bond- confined concrete



(c). Principal strain, ε_2 contour for detail



(d). Principal stress tensor for the detail

Figure 6.40 – Post-processed data for variant 5

Variant 6: Wall reinforcement bent towards the toe + diagonal bar at re-entrant corner

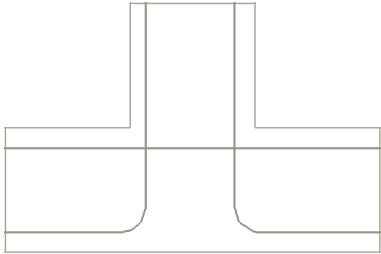
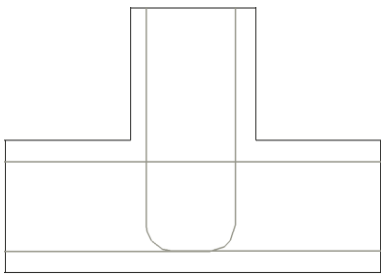
The use of bond-slip model did not have significant impact on the capacity of this variant. Regardless of the bond model assumed, the failure does not occur within the joint. The adjacent connected member were able to achieve their full capacity, as the joint strength did not limit them. Failure occurred along the adjacent connected member (see the red contour in figure 6.11). Thus, this detail meets the requirements that were discussed in section 3.1.

More information on the bond-slip model used, and discussion on some of these variants is presented in Appendix 2. The rest of the report would focus on the two thesis reinforcement layout earlier shown in figure 1.1 (and again in figure 6.14).

6.4.3 Thesis variants (or layouts) with bond-slip model

In this section, the two reinforcement layouts earlier discussed in section 6.3 (with perfect-bond assumed) is re-analyzed using bond-slip model. The peak bending moment and the joint efficiency attained are summarized in Table 6.5 below.

Table 6.5 – Peak moment and joint efficiencies of thesis variants (bond-slip models considered)

Variant	Peak moment (kNm) achieved and Joint efficiency (%)		
	<i>Perfect bond assumption</i>	<i>Good Bond – confined concrete</i>	<i>Poor bond – unconfined concrete</i>
 <i>Reinforcement Layout 1</i>	178.0 kNm (72.4%)	152.8 kNm (62.2%)	151.7 kNm (61.7%)
 <i>Reinforcement Layout 2</i>	215.4 (87.7%)	203.1 (82.7%)	198.0 kNm (80.6%)

When modelled using a bond-slip model, a joint efficiency of approximately 62% joint efficiency is predicted for Reinforcement Layout 1. This values is much closer to the experimental result (i.e. 60% joint efficiency) reported by Nilsson. Thus, modelling this detail with perfect bond (which predicted 72.4% joint efficiency in section 6.3) gave results that was too optimistic!!!

For Reinforcement Layout 2, a joint efficiency between 80.6% - 82.7% (i.e. approximately 82%) was obtained when a bond slip model is used. This result is smaller than the 87.7% obtained when perfect-bond was assumed to occur between the wall's reinforcing steel and the concrete. With Nilsson's (1973) experiments predicting 82% - 101%, this result is close to the range of value from his experiments.

Both of these details were discussed extensively is section 6.3. A few additional information would be discussed here.

Reinforcement Layout 1

Figure 6.41 illustrate some of the results from the FEM analysis for this detail modelled using a bond-slip relation for the wall's main reinforcing steel. On comparing figures 6.41a and b, it can be see the model with poor bond – unconfined concrete (i.e. figure 6.41a) requires a longer anchorage length than the detail modelled as having good bond – confined concrete (i.e. figure 6.41b). Also, note that there is no concentrated stress at the bent part of the reinforcing bar, as was the case when perfect bond was assumed

(see figure 6.21a). This is one way in which the defined bond-slip relation affects the structural behaviour of the detail.

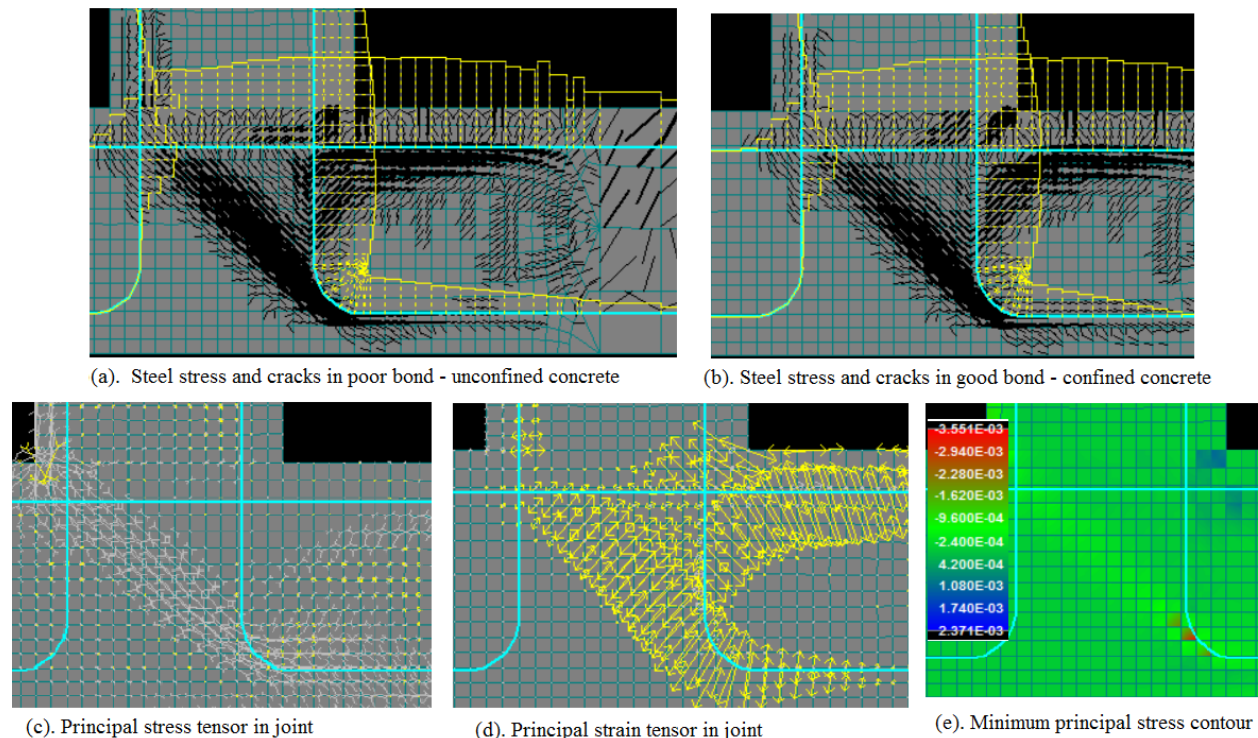


Figure 6.41 – Post-processed information from Reinforcement Layout 1 FEM analysis

From figure 6.41c, the compressive stress field (or inclined strut) can be seen flowing past around the bent part of the reinforcing bar. With the reinforcement bent away from the inclined strut, it did not help to confine it, nor did it help to control transverse cracking along the inclined strut. This is a key deficiency in this detail. Eventual failure was by crushing of the inclined strut after extensive cracking had weakened it. This has been discussed extensively in section 6.3.1.

Thus, when bond-slip model is used, the failure mode does not change. However, the joint efficiency is lower than the value predicted when perfect-bond is assumed. The joint efficiency (i.e. 62%) predicted this model is quite close to the experimental value obtained in the work of Nilsson (1973).

Reinforcement Layout 2

Figure 6.42 illustrate some of the results from the FEM analysis for Reinforcement Layout 2 modelled using a bond-slip relation. As expected, the model with good bond – confined concrete required less anchorage length than the model with poor bond and unconfined concrete. This can be seen on comparing figures 6.42a and b. In comparison with Reinforcement Layout 1, there is less cracking within the core of the joint (even though Reinforcement Layout 2 carried a higher load). With the reinforcement crossing the path of the inclined strut, it helped to control cracking within the core of the joint. Consequently, diagonal tension cracking failure did not occur in this detail.

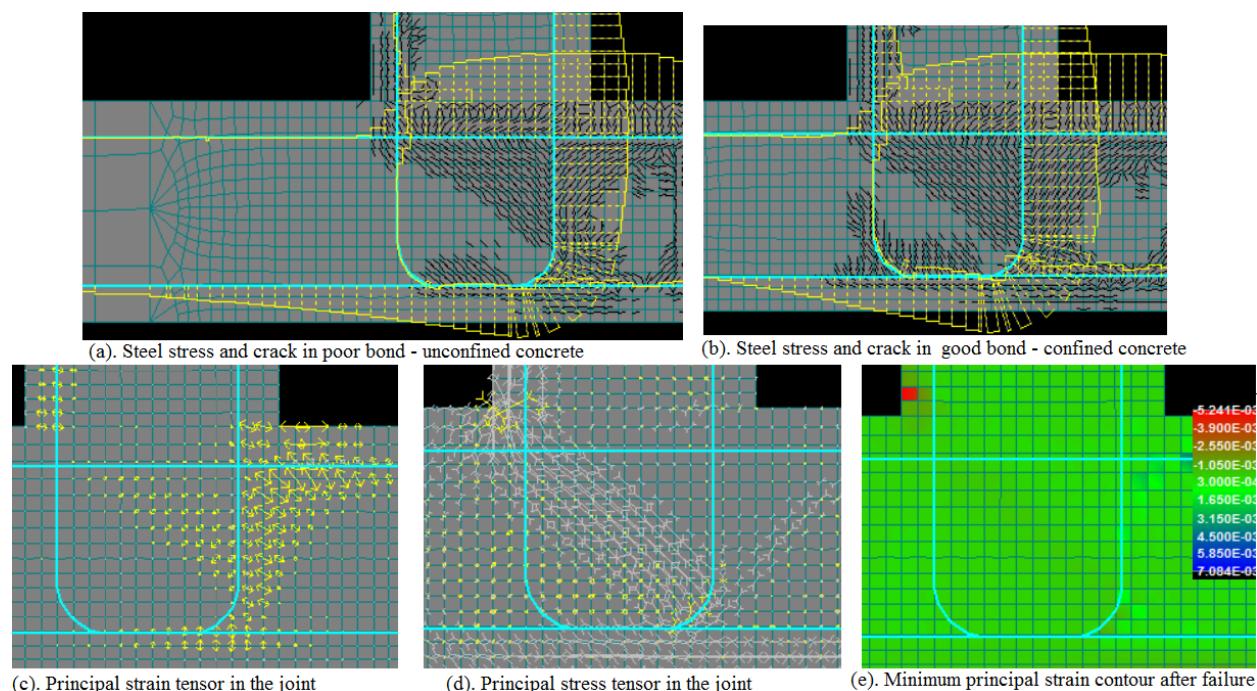


Figure 6.42 – Post-processed information from Reinforcement Layout 2 FEM analysis

The largest principal strains tensor (as shown in figure 6.42c) occur outside the core of the joint i.e. the vertical section from the re-entrant corner downwards into the base slab. This strains (which is tensile) would cause the crack pattern as was shown in figure 3.15 of this report. Careful examination of figure 6.42a and b reveals a continuous crack extending vertically downwards from the re-entrant corner region into the base slab. This confirms that the same cracking behaviour seen in figure 3.15 occurs in this detail.

Figure 6.42d shows a concentration of compression stress field in the nodal region (around the wall slab interface). For failure, crushing of concrete occurred in the wall (around the wall-slab interface) after the top reinforcement of the base slab had yielded around within the joint (near the re-entrant corner).

Conclusion of section

In concluding this section of the report, it is obvious that the assumption of perfect bond in the FEM analysis reported in section 6.3 over-estimated the joint efficiencies of the detail. When bond-slip behaviour is taken into account in the modelling, Reinforcement Layout 1 achieved an average joint efficiency of 62%, while Reinforcement Layout 2 attained an average joint efficiency of 82%. Both of these results conform closely to the values of joint efficiency reported by Nilsson (1973) for similar details.

With both of these detail not achieving 100% joint efficiency, further improvement is required. The goal (or objective) of the joint design is for a joint that is at least as strong as that of the adjacent connected members. The performance of such a joint should not prevent the adjacent connected member from reaching their ultimate capacity. In the next section, two details that met this objective are presented.

6.5 Satisfactory details

6.5.1 Reinforcement Layout 2 + diagonal bar at re-entrant corner

In the last section, Reinforcement Layout 2 prevented diagonal tension cracking failure (hence better than Reinforcement Layout 1), but still failed without reaching the structure's ultimate capacity. In this section, the detail is improved by adding a diagonal bar placed at an angle of 45° at the re-entrant corner. This caused the detail to achieved a peak moment of 253.3 kNm , which represents a joint efficiency of approximately 103%. Also, failure did not occur in the joint, or within the immediate vicinity of the joint region. Rather it occurred along the connected member as indicated by the red contour shown in figure 6.43a. This joint detail did not prevent the structure from achieving its full strength. This is the desirable behaviour from a properly designed joint.

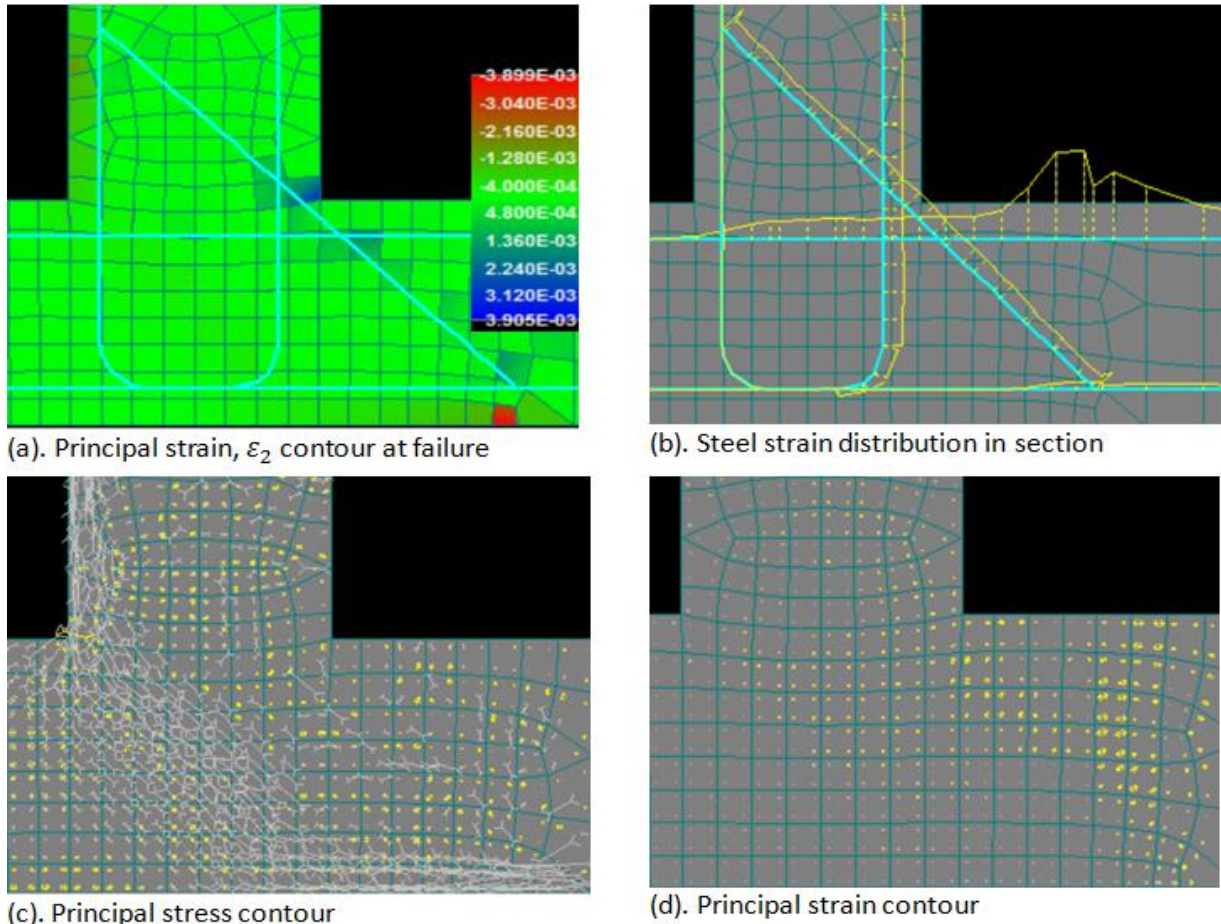


Figure 6.43 - Reinforcement layout 2 improved with diagonal bar. Failure outside the joint (red contour)

The addition of diagonal bar strengthened the entire joint region. Consequently, the strains within the joint were smaller than those along the adjacent connected member. Notice the large steel strains that occurred outside the joint (in figure 6.43b) after yielding. The steel strain in that location was about 9%. In comparison however, there was no yielding of steel within the joint. Concrete strains were also relatively small within the joint. The yellow arrows in the principal strain contour (figure 6.43d) shows that the largest strains occurred away from the joint region. These improvements are direct benefit derived from adding the diagonal bar Reinforcement Layout 2. Some key contributions the bar made are enumerated below:

- With its orientation (45° angle), it carried the radial stress at re-entrant corner more effectively (after cracking) than either a vertical or horizontal reinforcement could do. It was the most stressed (and strained) bar initially as it is the main bar that coped with the stress concentration at the corner.
- With the bent part of the bar crossing the inclined strut, the detail was effective in controlling diagonal tension cracking and limiting the width of cracks formed. It was also very effective in controlling the crack width at the re-entrant corner.
- The diagonal bar prevented separation of the wall from the slab (heel side). Utilizing the non-linear effects of bond and tension stiffening, the diagonal bar ensured continued interaction of the connected component at the joint up till failure
- With efficient load transfer between the tie (i.e. main reinforcement from wall) and the strut (i.e. the inclined compressive stress field), the corner joint had a relatively high shear rigidity to cope with the shear stresses it was subjected to by the external opening moments. The comparatively high rigidity is obvious from the moment curvature plot in figure 6.44. It was able to sustain a higher bending moment with lower curvatures.
- With the steel not yielding within the joint (thus no plastic hinge forming there), the bottom side of the joint was not subjected to the elevated compressive stresses that had caused failure in the case of Reinforcement Layout 2.

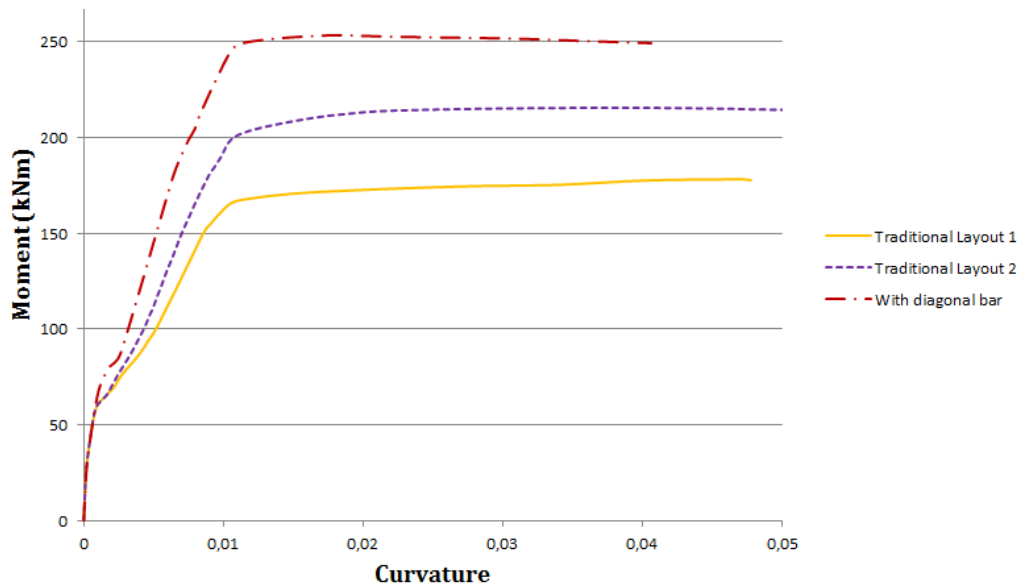


Figure 6.44– Moment-curvature plot comparison of thesis variants

From figure 6.44, the moment curvature behaviour is similar (for all three layouts) prior to cracking. The stress distribution at this stage was similar, as they all complied with the theory of elasticity. The stress tensor was shown in figure 6.2b. After cracking however, the structure now acted as a composite structure. From figure 6.44, it can be seen that the addition of diagonal bar improved the stiffness of the cracked structure. This increase in overall joint stiffness is a key benefit that the previous two layouts did not have. While Reinforcement Layout 2 improved the stiffness within the core of the joint thus preventing diagonal tension failure, it did not stiffen the entire joint region. The addition of the diagonal bar achieved this, and resulted in more parts of the structure carrying the load, rather than a local concentration of stresses within the joint.

6.5.2 Looped detail + diagonal bar at re-entrant corner

Bending the reinforcement into a loop is often an efficient way of detailing against diagonal tension failure. When subjected to opening moment, the loop tries to tighten, and thereby subject the enclosed concrete to compression. This way, the effect of transverse tensile stresses is reduced and the width of cracks within the enclosed concrete is small. In this detail, a diagonal bar is placed 45° around the re-entrant corner to control re-entrant corner crack, as well as to strengthen the joint. This detail is illustrated in figure 6.45a.

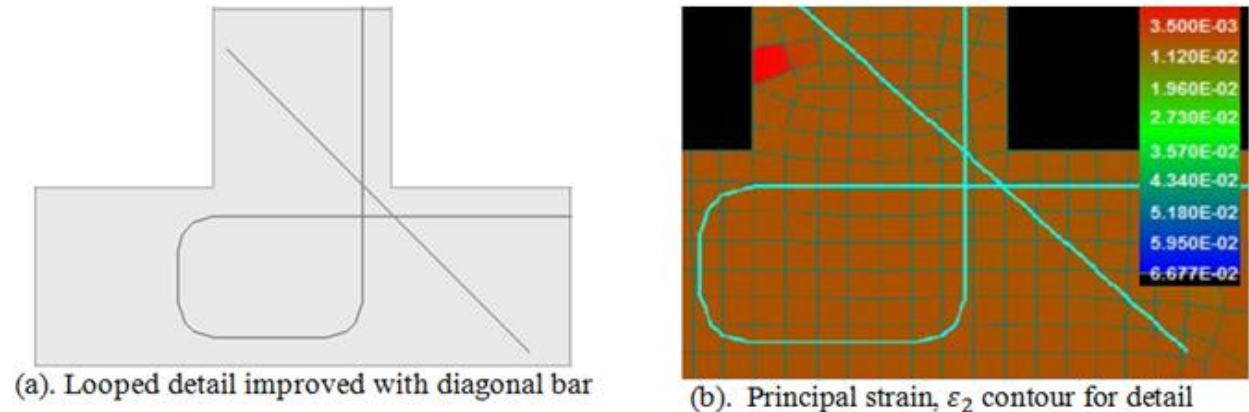


Figure 6.45 – Looped reinforcement detail + diagonal bar at re-entrant corner

From result of the FEM analysis, this detail effectively prevented diagonal tension cracking failure. Using a good bond – confined concrete bond-slip model for the looped reinforcement, the detail attained a peak bending moment of 253kNm (representing 102% joint efficiency). Eventual failure occurred in the wall (away from the joint as seen in figure 6.45b) after the wall reinforcement had yielded. Experimental works reported by Nilsson (1973), Nabil, Hamdy and Abobeah (2014) and Campana, Ruiz and Muttoni (2013) further support the fact that a looped reinforcement layout with diagonal bar placed at the re-entrant corner provides joint efficiencies that are at least 100%. Thus, this is another suitable reinforcement layout than can be adopted in detailing retaining walls.

6.6 Summary to this section of study

In summary, some key results obtained from the FEM analysis is summarized in Table 6.6 below.

Table 6.6 – Summary of some key results from the FEM analysis

Variant	Peak moment (kNm) achieved and Joint efficiency (%)		
	<i>Perfect bond assumption</i>	<i>Good Bond – confined concrete</i>	<i>Poor bond – unconfined concrete</i>
Reinforcement Layout 1	178.0 kNm (72.4%)	152.8 kNm (62.2%)	151.7 kNm (61.7%)
Reinforcement Layout 2	215.4 (87.7%)	203.1 (82.7%)	198.0 kNm (80.6%)
Reinforcement Layout 2 + diagonal bar at re-entrant corner	253.3 kNm (103.1%)	253.1 kNm (103%)	252.6 kNm (102.8%)
Looped reinforcement + diagonal bar at re-entrant corner	260.4 kNm (106%)	253.0 kNm (103%)	249.1 kNm (101.4%)

In Table 6.6, two structural details achieved over 100% joint efficiency. These detail have some similar behaviour which made them more effective than Reinforcement Layouts 1 and 2. These behaviour should be considered and provided for in a good detailing design. Some of these include:

1. The detail should deal effectively with transverse tension within the joint. Cracks formed from transverse tension should be properly controlled so as not to excessively weaken the inclined strut. This is one of the reasons Reinforcement Layout 1 failed prematurely. Bending the reinforcement to cross the crack path (as is done for Reinforcement Layout 2) proved effective in this study. Using looped reinforcement was also effective in this study as the loop introduced compressive stresses to the joint which limited the width of cracks. Diagonal tension cracking failure should be avoided by good detail design.
2. The detail should cope well with cracking at re-entrant corner. The propagation of re-entrant corner cracks around the joint region was one of the reasons why Reinforcement Layout 2 failed without reaching full capacity. Though cracking cannot be avoided at the re-entrant corner, provision should however be made in the structural detailing to control it. In this study, a diagonal bar placed 45° at that corner was effective for this purpose.
3. The detail should prevent large strains within the joint. Yielding of steel within the joint should be avoided. Also, excessive compressive strain of concrete should be avoided. All the details in this study that had large strains within the joint did not achieve 100% joint efficiency.
4. The joint should have adequate shear stiffness. The opening moments acting on the corner joint actually subjected it to shear stresses. The design engineer should ensure that the detail can provide adequate shear resistance for the overall joint.
5. For a structure subjected to opening moment, provision of a diagonal bar at the re-entrant corner is quite essential. Its impact in this study was significant especially in the area of stiffening the overall joint (thus preventing large strains within the joint) and controlling re-entrant cracks. FIB (2010a) recommends the use of inclined bars for all types of re-entrant corners such as those on dapped ends, openings, corbels etc.

7 Conclusions and recommendations

The performance of the retaining walls shown in figure 1.1 has been the object of this study. With their reinforcing bars detailed differently, the joint behaviour has been studied in this thesis to provide answer to the following questions:

- How efficient are the joints made with these reinforcement layouts?
- In what way does the reinforcement detail affect stress and strain behaviour within the joint?
- What is the mode of failure of these joints?, and
- What improvement can be made to the detail if the joint efficiency is less than 100%?

The combination of lateral loads (acting on the wall) and gravity load (acting on the slab) subjects the joint to an opening moment. This opening moment acting on the retaining wall causes a tensile stress concentration at the re-entrant corner. It also causes transverse tensile stress to act concurrently with compressive stresses within the core of the joint. This was illustrated in Section 6.2.1 (see page 87) and section 6.3.1 (see page 109 – 110). These stress state and the cracks caused by them play a vital role in determining the behaviour and eventual capacity of the joint.

7.1 Conclusions

Reinforcement layout 1

In this layout, the main reinforcement from the wall is bent towards the heel as was shown in 6.14a. The corner joint with this reinforcement layout attained 62% joint efficiency in this thesis work (when bond-slip model is used). This result is quite close to that reported by Nilsson (1973) whose experimental work on a similar detail attained 60% joint efficiency (see section 3.4.1.3 on page 43). At failure, the inclined strut crushed after excessive diagonal tension cracking had occurred along the strut. Some deficiencies noted from its behaviour include:

- The nodal region is not properly formed in this detail. This made force transfer between the wall's main reinforcement (or tie) and the inclined strut to be ineffective.
- Poor control of the diagonal tension crack
- Tensile strains concentration in the concrete (along the inclined joint). It acted like the shear stresses (caused by the opening moment) was tearing open the joint along the inclined strut (see figure 6.27b)
- Low shear stiffness of joint

To understand the key weakness of this detail, reference would be made to the strut and tie model earlier shown in figure 5.4. There, the tie from the wall reached the nodal region at point E. In Reinforcement Layout 1 however, this is not the case. With the reinforcing bar bent away from the inclined strut before reaching the node, the tie is not properly anchored in the nodal region in this reinforcement detail. In figure 6.41c, the compressive stress field (or strut) can be seen flowing past the bent part of the embedded reinforcing bar. Thus, the tie (EHI in figure 5.4) has very little interaction with the inclined strut, BE. Consequently, force transfer between the strut and the tie is not very effective at the node, E. This is one of the key reasons for the low shear stiffness of the core of this detail. The problem with this structure is in the way the joint is detailed around node E. Improvement is required in this region if the structure is to attain a higher joint efficiency.

Also, large cracks were observed to have formed along the inclined strut in this detail. These cracks initiated and propagated in the inclined strut due to the effect of transverse tension in the joint (caused by the opening moments). With the main reinforcement bent away from the inclined strut, it did not help to control width. This is another key failure of Reinforcement Layout 1. These wide cracks caused a reduction of the strength and stiffness of the inclined strut, thus making it susceptible to large compressive strains, even at moderate stress levels. At failure, the inclined strut was not the most stressed part of the structure (in compression), nevertheless, it had the largest compressive strains (see the contour plot in figures 6.28a and 6.41c). This happened due to significant reduction of the concrete stiffness on account of transverse tension cracking in the strut. This issue is discussed with more details in section 6.3.1 (see page 108 – 111).

Reinforcement layout 2

In this detail, the main reinforcement from the wall is bent towards the toe so that it crosses the path of the inclined strut (see figure 6.14b). This detail attained an average joint efficiency of 82% (i.e. 20% higher joint efficiency when compared to Reinforcement Layout 1). This joint efficiency predicted by FEM for this detail is within the range of value (82% - 101%) determined experimentally by Nilsson (1973). Some key observations from this detail include:

- A clearly defined nodal region was formed in this layout as can be observed in figure 6.10a. The struts and the ties converged at a clearly defined region, from where they were transferred or redirected. At the node, compressive forces from the struts were in equilibrium with tensile forces in the reinforcement. Thus, force transfer between the struts and tie is effective in this case.
- The bent part of the steel provided some confinement for the concrete, hence it increased the compressive strength of the inclined strut.
- Lower crack width within the core of the joint. The bent part of the reinforcement that crossed the inclined strut helped to control crack width. This made the inclined strut of this detail stiffer and stronger than that of Reinforcement Layout 1.
- Unlike Reinforcement Layout 1 (see figure 6.27b), the tensile strains were small within the core of the joint. The largest tensile strains in the concrete occurred outside the joint's core along the joint - slab (heel side) interface (as seen in figure 6.42c and 6.32a).
- With the inclined strut (concrete) bearing against the bent part of the steel, additional force transfer capacity from bearing is utilized in this detail. This is quite different from the case of Reinforcement Layout 1 which relied entirely on bond for force transfer.

In this reinforcement layout, there is adequate interaction between the reinforcement (tie EHI) and the inclined strut (BE), thus a node is properly formed at point E (as seen in figure 5.4). This way, the force transfer is more effective between the strut and tie at the nodal region. Also, it ensured that the joint possessed a higher shear stiffness than that of Reinforcement Layout 1. The Compressive strains within the core of the joint were much smaller, and failure did not occur there. Thus this detail effectively prevented diagonal tension cracking failure. However, it did not reach 100% joint efficiency.

Failure was caused by a wide cracking from the re-entrant corner which propagated vertically downwards into the slab. The crack width was large because the steel located at the top of base-slab (which had yielded) had large strains (up to 16.6‰) around the point. The concrete experienced its largest tensile strains in this region causing a reduction in the depth of neutral axis as the crack propagated vertically downwards into

the base slab. Concrete crushing occurred in the outer fibres at failure. This issue is discussed in section 6.3.2 (see page 115 to 117). In his experiment, Nilsson's (1973) noticed a similar failure mode for this type of detail, and his photograph illustration can be seen in figure 3.15 of this report.

Improving Reinforcement Layout 2

Reinforcement layout 1 had failed due to diagonal tension cracking along the inclined strut. This failure mechanism restricted the structure to 62% joint efficiency in this study. In contrast, Reinforcement layout 2 prevented diagonal tension cracking failure, and attained a higher efficiency of 82%. It was limited by crushing of the joint -slab interface after the top reinforcement in the slab had yielded and sustained large strains. In his work on samples similar to Reinforcement layout 2, Nilsson (1973) obtained joint efficiencies between 82% - 101%. This indicates that the Reinforcement layout 2 is able to take even more load. The feasibility of this was also studied.

When the cross sectional area of reinforcing steel (which yielded) at the top of base-slab was increased in the FEM analysis, the structure was able to attain an even higher joint efficiency. In this work, 82% joint efficiency was attained when 20mm bars at 250mm spacing (i.e. 4 - Ø20) was used as reinforcement at the top of the slab (with failure at slab-heel interface as was illustrated in figure 6.33). When that reinforcement is increased to 20mm bar at 200mm spacing (i.e. 5 - Ø20), the structure attained 89.5% joint efficiency when bond slip model was used (and 95.2% joint efficiency for perfect bond). Also, crushing of concrete no longer occurred at the joint – slab (heel side) interface. Rather, crushing of concrete occurred at the wall – slab interface. This higher capacity obtained results fits well with the experimental result.

Despite the increase in joint efficiency, the structure did not meet 100% joint efficiency. A solution studied in this work (and proposed in literature) involves the use of diagonal bars at the re-entrant corner. When a diagonal bar was placed at 45° angle around the re-entrant corner (as seen in section 6.5.1), it helped to strengthen the overall joint region. FEM analysis of this improved detail achieved a joint efficiency of 103%. Some noticeable contribution of the diagonal bar include:

- It helped to control crack propagation at the re-entrant corner. This resulted in smaller crack widths.
- It increased the strength and stiffness of the entire joint region. The concrete strains (both tensile and compressive) within the joint of this were much smaller than the other variants studied.
- Yielding of steel did not occur within the joint, thus no plastic hinge formed in the joint.

With the diagonal bar controlling re-entrant corner cracking, and the bent part of the wall reinforcement controlling cracks from transverse tension within the joint, eventual failure did not occur within the joint. Rather, it occurred outside the joint region in one of the adjacent connected members (see figure 6.43a). Thus, this improved joint did not prevent the adjacent connected member from achieving their full capacity.

Impact of bond model

The results obtained from the FEM analysis is sensitive to the bond model used. When perfect bond was assumed to occur between the steel and the surrounding concrete, ATENA FEM software predicted quite optimistic results. For Reinforcement Layout 1, a joint efficiency of 72% was predicted when perfect bond is assumed (see section 6.3.1). In comparison, an average of 62% joint efficiency was obtained when bond-slip model is used (see section 6.4.3). The joint efficiency obtained with a bond-slip model approximates more closely to the experimental results (i.e. 60%) reported by Nilsson (1973). For reinforcement layout 2, a joint efficiency of 88% was attained when perfect bond is assumed (see section 6.3.2). This is 6% higher than the 82% efficiency attained when bond-slip model is used in the FEM analysis (see section 6.4.3).

For the models with perfect-bond, relative slip between the reinforcing bar and the surrounding concrete is prevented. This had the impact of causing higher steel stresses along the embedded bar (when compared to models where bond-slip relations is defined). This is a probable reason for the higher joint efficiency attained by the structure when perfect bond is assumed.

7.2 Recommendations

Some aspect of this work recommended for further study include:

- Cracking (from both transverse tension and at re-entrant corner) has been shown to play a vital role in the behaviour and ultimate capacity of the details studied. Adding steel fibres to concrete is known to provide benefit in terms of crack control and improved post-crack behaviour. What would be the impact of adding steel fibres locally (at the joint region) in these details. Further study can be conducted in this subject area.
- Further study into detailing aspect of other joint types e.g. ledge joint, dapped end, corbels etc. would provide further knowledge on detailing aspect of reinforced concrete structures.

References

- Abdul-Wahab, H.M.S and Al-Roubai, A.A.M. (1998). Strength and behaviour of steel fibre reinforced concrete corners under opening bending moment. Magazine of Concrete Research, 1998, 50, No. 4. Available online: <http://www.icevirtuallibrary.com/doi/pdf/10.1680/mac.1998.50.4.305>. [Accessed 23 February 2016].
- Bahn, B.Y. and Hsu, T.T.C. (1998) Stress–strain behavior of concrete under cyclic loading. ACI Material Journal. Title No. 95-M18: PP 178–193. [Online] Available at: ftp://ftp.ecn.purdue.edu/spujol/CE676%20References%20Behavior%20of%20Reinforced%20Concrete%20Elements/Book%208/8_4.pdf [Accessed: 8 April 2016].
- Beer, F.P., Johnston, E.R., DeWolf, J.T., and Mazurek, D.F. (2011). Statics and Mechanics of Materials. McGraw-Hill, New York
- Bhatt, P., MacGinley, T.J. and Choo, B.S (2014). Reinforced concrete design to eurocodes - Design theory and examples. 4th edition. CRC Press. Boca Raton, Florida.
- Calavera, J. (2012). Manual for Detailing Reinforced Concrete Structures to EC2. Spon press, London.
- Campana, S., Ruiz, M.F. and Muttoni, A. (2013). Behaviour of nodal regions of reinforced concrete frames subjected to opening moments and proposals for their reinforcement. Engineering Structures 51 pp 200–210. Online: <http://www.sciencedirect.com/science/article/pii/S014102961300059X> [Accessed 1 December 2015].
- CEB (1993). CEB-FIP Model Code 1990 – Design Code. Comité Euro-International du Béton, Thomas Telford, London.
- CEB (1996). RC Frames Under Earthquake Loading: State of the Art Report. Thomas Telford, London.
- Červenka, V., Jendele, L. and Červenka, J.(2016). ATENA Program Documentation, Part 1: Theory. [Online] Available at: http://www.cervenka.cz/assets/files/atena-pdf/ATENA_Theory.pdf [Accessed: 8 January 2016].
- Cook, R.D., Malkus, D.S., Plesha, M.D. and Witt, R.J. (2002). Concepts and applications of finite element analysis, 4th Edition. John Wiley & Sons Inc. New York.
- Cunningham, L.S (2000). Automatic Design of Concrete Structures Using a Strut & Tie Approach. Ph.D Thesis. University of Glasgow. [Online] Available at: <https://theses.gla.ac.uk/1726/1/2000cunninghamphd.pdf> [Accessed: 4 February 2016].
- Fib (2008). Fib bulletin No. 45, Practitioners’ guide to finite element modeling of reinforced concrete structures. Lausanne, Switzerland.
- Fib (2009). Structural Concrete: Textbook on behaviour, design and performance. Second edition, Volume 1.
- Fib (2010a). Structural Concrete: Textbook on behaviour, design and performance. Second edition, Volume 4.
- Fib (2010b). Structural Concrete: Textbook on behaviour, design and performance. Second edition, Volume 2.
- Hendy, C.R. and Smith, D.A. (2007). Designers’ Guide to EN1992-2: Eurocode 2: Design of concrete structures part 2, concrete bridges. Thomas Telfords, London.

- Hsu, T.T.C. and Mo, Y.L. (2010). Unified Theory of Concrete Structures. *John Wiley and Sons*, West Sussex, UK
- Kabele, P., Červenka, V. and Červenka, J. (2010). ATENA Program Documentation, Part 3-1: Example Manual for ATENA Engineering. [Online] Available at: http://www.cervenka.cz/assets/files/atenapdf/ATENA-Engineering_Example_Manual.pdf. [Accessed: 1 July 2016].
- Kaliluthin, A.K., Kothandaraman, S. and Suhail-Ahamed, T.S. (2014). A Review on Behavior of Reinforced Concrete Beam-Column Joint. *International Journal of Innovative Research in Science, Engineering and Technology*, Vol. 3, Issue 4. [Online] Available at: http://www.ijirset.com/upload/2014/april/59_A%20Review.pdf [Accessed: 26 February 2016].
- Kassem, w. (2014). Strength Prediction of Corbels Using Strut-and-Tie Model Analysis. *International Journal of Concrete Structures and Materials*. Vol.9, No.2, pp.255–266. [Online] Available at: <http://link.springer.com/article/10.1007%2Fs40069-015-0102-y> [Accessed: 10 December 2015].
- Lowes, L.N. (1999). Chapter 3: Reinforcing steel material model. [Online] Available at: [http://faculty.washington.edu/lowes/dissertation/dissertation/dissertation.book\(chapter3.pdf](http://faculty.washington.edu/lowes/dissertation/dissertation/dissertation.book(chapter3.pdf). [Accessed: 8 April 2016].
- MacGregor, J.G. and Wight, J.K. (2005). Reinforced Concrete Mechanics and Design. 4th edition. Prentice Hall, Upper Saddle River, New Jersey.
- Mosley, B., Bungey, J. and Hulse, R. (2012). Reinforced Concrete Design to Eurocode 2. Palgrave Macmillan, Hampshire, United Kingdom.
- Muttoni, A., Schwartz, J. and Thurlimann, B. (1997). Design of Concrete Structures with Stress Fields. Birkhauuser verlag, Basel, Switzerland.
- Nabil, M., Hamdy, O. and Abobeah, A. (2014). Affecting aspects on the behaviour of frame joints. *HBRC Journal* [Online]. Available <http://www.sciencedirect.com/science/article/pii/S1687404814000996>. [Accessed: 21 February 2016].
- Nilson, A.H., Darwin, D. and Dolan, C.W. (2004). Design of Concrete Structures. 14th edition. McGraw-Hill, New York.
- Nilsson, I.H.E. (1973). Reinforced concrete corners and joints subjected to bending moment : design of corners and joints in frame structures. Document D7:1973, National Swedish Institute for Building Research, Stockholm.
- Park, R. & Paulay, T. (1975). Reinforced Concrete Structures, 1st edition, John Wiley & Sons, New York.
- Schlaich, J., Schafer, K. and Jennewein, M. (1987). Towards a consistent design for structural concrete. *PCI Journal*. V. 32(1987), No. 3, pp. 75-150.
- Schlaich, J. and Schafer, K. (1991). Design and detailing of structural concrete using strut-and-tie models. *The Structural Engineer*, Vol 69, No. 6. [Online] Available at: <https://www.istructe.org/journal/volumes/volume-69-%28published-in-1991%29/issues/issue-6/articles/design-and-detailing-of-structural-concrete-using>. [Accessed: 13 January 2016].
- Shah, A., Haq, E. and Khan, S. (2011). Analysis and Design of Disturbed Regions in Concrete Structures. *Procedia Engineering Journal – Elsevier*. Volume 14, PP 3317–3324. [Online] Available at: <http://www.sciencedirect.com/science/article/pii/S1877705811014962> [Accessed: 24 November 2015].

- Tjhin, T.N. and Kuchma, D.A. (2002). Computer-Based Tools for Design by Strut-and-Tie Method: Advances and Challenges. ACI Structural Journal, Title no. 99-S60. [Online] Available at: http://www.gdace.uem.br/Rafael/Mestrado_4065/Programas/Cast_Paper.pdf [Accessed: 24 November 2015].
- Torrenti, J.-M., Pijaudier-Cabot, G. and Reynouard, J.-M. (2010). Mechanical behaviour of concrete. John Wiley and Sons, London
- Vrouwenvelder, A.C.W.M. (2003), The plastic behaviour and the calculation of beams and frames subjected to bending", Lecture book for Plastic Analysis of Structures (CIE4150). Delft University of Technology, The Netherlands

Appendix 1: Background to study case

Problem is taken from Mosley, Bungey and Hulse (2012) - Example 10.6

To study the role of detailing in a structure, a case study structure would be required. The case used for this work is a cantilever retaining wall supporting a 4.5m high backfill of granular material with a saturated density of 1700 kg/m^3 and a surcharge of 10 kN/m^2 . The geometrical details of the wall are shown in figure A1 below:

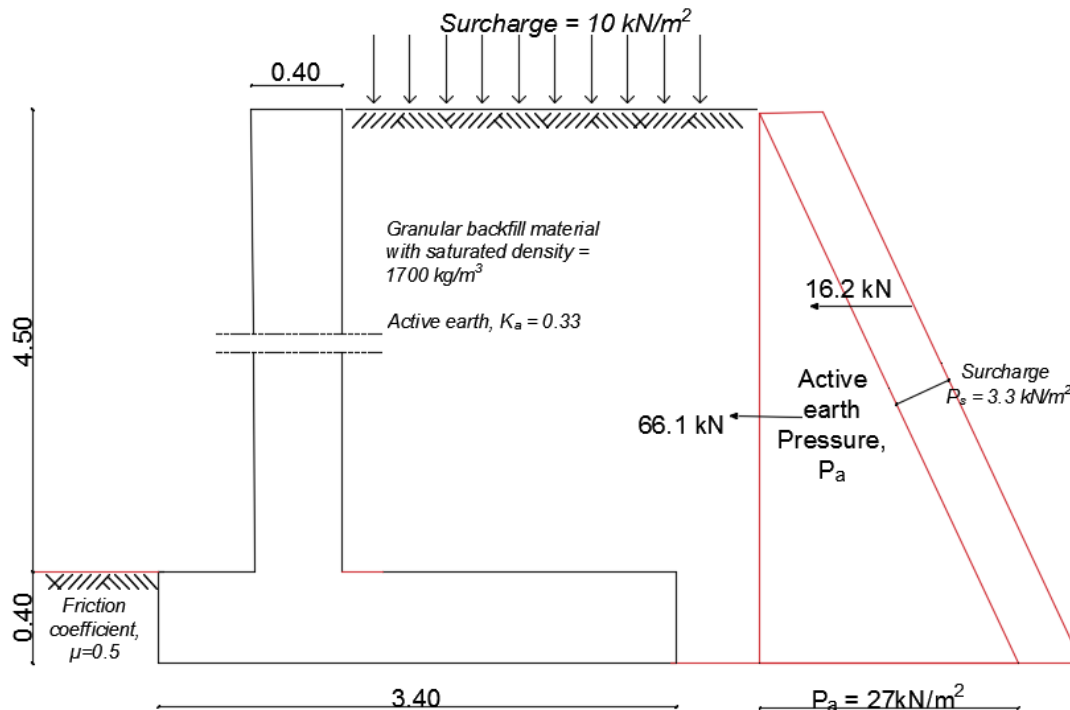


Figure A1– Study case study retaining wall

In this section, I would undertake a preliminary sizing of the wall, and check for stability against overturning and sliding. The loads and resulting moments acting on the structure would also be computed. Stresses from these moments would constitute the boundary stresses for the strut and tie model (in Chapter 5 of the main report). Useful parameters are summarized thus:

Concrete: C30/37

Steel: $f_{yk} = 500 \text{ N/mm}^2$

Coefficient of friction (μ) = 0.50

Active earth pressure $k_a = 0.33$

Preliminary sizing

Mosley, Bungey and Hulse (2012) suggest that wall thickness could be 80mm per metre depth of backfill. Also, the thickness of the base slab should be in the same order as that of the stem.

Therefore, for 4.5m high wall, the thickness should be $\approx 80 \times 4.5 = 360 \text{ mm}$. Use a wall 400mm thick, and base slab 400mm thick. Therefore total height of structure = $4.5 + 0.4 = 4.9 \text{ m}$. The geometrical dimensions are clearly illustrated in figure A1.

Forces (loads) acting on the structure

The main forces acting on the wall would come from gravity loads (or dead weight), lateral loads from active earth pressure of the backfill, lateral load from the surcharge, and reaction from the soil.

Lateral loads from earth pressure and surcharge

$$P_a = k_a \rho g h = 0.3 \cdot 1700 \cdot 10^{-3} \cdot 9.81 \cdot 4.9 \approx 27 \text{ kN/m}^2 \text{ (from active earth)}$$

$$P_s = k_a \cdot q = 0.33 \cdot 10 = 3.3 \text{ kN/m}^2 \text{ (from surcharge)}$$

The earth pressure has a triangular distribution, while the surcharge pressure is constant over the height of the wall. Both of these loads are illustrated in figure A1. For a wall of one metre width, the resultant horizontal loads from these pressure is:

$$\text{For active earth: } 0.5 \times 27 \times 4.9 \approx 66.1 \text{ kN} \text{ (acting at a third from the bottom of the wall)}$$

$$\text{For surcharge: } 3.3 \times 1 \times 4.9 = 16.2 \text{ kN} \text{ (acting at centre of the wall)}$$

Both the lateral load from active earth pressure surcharge on structure are illustrated in figure A1 above.

Vertical Loads: Include permanent load from the structure and backfill, and variable load from surcharge

Permanent

$$\text{Wall } 0.4 \times 4.5 \times 25 = 45 \text{ kN}$$

$$\text{Base } 3.4 \times 25 \times 0.4 = 34 \text{ kN}$$

$$\text{Permanent backfill } 2.2 \times 4.5 \times 1700 \cdot 10^{-3} \times 9.81 \approx 165.1 \text{ kN}$$

$$\text{Variable (surcharge) } 2.2 \times 10 = 22 \text{ kN}$$

Note that all the above vertical forces are per metre width of the wall.

Stability checks

Overturning: To check resistance against overturning, the moment would be taken around the toe of the base slab, and the overturning moment compared with the restoring moment. From table A1 in EC7, the following partial factors would be used: $\gamma_f = 1.1$ for unfavourable overturning moment, $\gamma_f = 0.9$ for favourable overturning moment, and $\gamma_f = 1.5$ for unfavourable variable load. The unfavourable overturning moments are caused by the lateral loads, while the weight of the structure act to restore it.

$$\text{Overturning moment: } (1.1 \times 66.1 \times 4.9/3) + (1.5 \times 16.2 \times 4.9/2) = 178.3 \text{ kNm}$$

$$\text{Restoring moment: } 0.9 \cdot (45 \times 1 + 34 \times 1.7 + 165.1 \times 2.3) = 434 \text{ kNm}$$

Restoring moment > Overturning moment, therefore the structure is stable against overturning.

Sliding check: Assuming no heel or toe beam is used, our check criterion is:

$$\mu(1.0 \cdot G_k + 1.0 \cdot V_k) \geq \gamma_f \cdot H_k$$

Where the vertical loads are favourable against sliding, and the lateral loads unfavourable. From Table A3 of EC7, $\gamma_f = 1.35$ for unfavourable loading from permanent earth pressure, and $\gamma_f = 1.5$ for unfavourable variable load. And $\gamma_f = 1.0$ for all favourable load)

$$\text{Sliding force: } 1.35 \cdot 66.1 + 1.5 \cdot 16.2 = 113.5 \text{ kN}$$

Resistance to sliding: $0.5 \cdot (165.1 + 45 + 34) = 122 \text{ kN}$

Since sliding resistance exceeds the design sliding force, adequate safety against sliding failure. No need for heel or toe beam (which would have provided us with passive resistance).

Bearing pressure

The lateral forces try to overturn the structures, while self-weight, permanent backfill and surcharge try to restore it. This action causes differential pressures on the foundation from the heel to the toe. These would be determined here. For partial safety factor for computing bearing pressures, EC7 recommends $\gamma_f = 1.0$ for favourable permanent loads, $\gamma_f = 0$ for the surcharge (thus its positive benefit disregarded), $\gamma_f = 1.35$ for unfavourable permanent actions, and $\gamma_f = 1.5$ for unfavourable variable action. The expression for bearing pressure at toe and heel is thus:

$$\sigma_{1,2} = \frac{N}{A} \pm \frac{M \cdot y}{I}$$

Where M is bending moment about the centerline of the base slab, and N is vertical load on it. For 1m length of wall, the area, $A = D$; $y = D/2$; and $I = D^3/12$. Thus our expression becomes:

$$\sigma_{1,2} = \frac{N}{D} \pm \frac{6M}{D^2}$$

$$M = 1.35 \cdot (66.1 \times 4.9/3) + 1.5 \cdot \left(16.2 \times \frac{4.9}{2}\right) + 1.35 \cdot (45 \times 0.7) - 1 \cdot (165.1 \times 0.6) \\ \approx 148.8 \text{ kNm}$$

$$N = 1.35 \cdot (45 + 34) + 1.0 \times 165.1 = 271.7 \text{ kN}$$

$$\text{Bearing pressures: } \sigma_{1,2} = \frac{271.7}{3.4} \pm \frac{6 \times 148.8}{3.4^2} = 157.1 \text{ kN/m}^2 \text{ (at toe) and } 2.7 \text{ kN/m}^2 \text{ (at heel).}$$

This is illustrated below in figure A2.

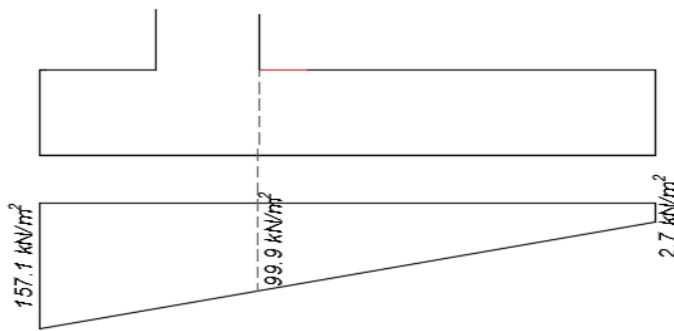


Figure A2 – Illustration showing soil bearing pressure on structure

Calculation of bending moments for design

For design, the retaining wall is often treated like three cantilevers (the wall, toe-side part of the slab, and heel-side part of the slab) all fixed to the wall base-connection. In this section, I would compute the bending moment acting on each of these cantilevers. Design of reinforcement would be done using the strut-and-tie

methodology, and is reported in chapter 5 of the main report. The design moments computed here would be used as boundary loads on the D-region in the strut and tie design.

Wall design moment

For a wall height of 4.5m, maximum force at wall-base connection is:

$$H_{\text{wall}} = \gamma_f \cdot \frac{1}{2} K_a \rho g h^2 + \gamma_f \cdot P_s \cdot h$$

$$H_{\text{wall}} = 1.35 \times \frac{1}{2} \times 0.33 \times 1700 \cdot 10^{-3} \times 9.81 \times 4.5^2 + 1.5 \times 3.3 \times 4.5$$

$$H_{\text{wall}} = 75.2 + 22.3 = 97.5 \text{ kN}$$

Lateral force from active earth component is 75.2kN, and is acting on the wall at one-third the height from the base. Also, lateral force of 22.3kN from surcharge acts at the middle of the wall. The maximum bending moment on the wall is thus:

$$M_{\text{Ed,wall}} = 75.2 \times \left(0.2 + \frac{4.5}{3}\right) + 22.3 \times \left(0.2 + \frac{4.5}{2}\right) = \mathbf{182.5 \text{ kNm}}$$

Bending moment in base slab (heel side)

The moments in the heel side of the base slab are caused by the self-weight of the slab, the weight of the backfill, and the bearing stresses from the soil on the base slab. γ_f is 1.35 for self-weight, 1.0 for the backfill. Taking bending moment acting around the centreline of the stem from the above mentioned loads, the design moment is computed thus⁷:

$$M_{\text{Ed}} = 1.35 \times 34 \times \left(\frac{3.4}{2} - 1\right) + 1.0 \times 165.1 \left(0.2 + \frac{2.2}{2}\right) - 2.7 \times 2.2 \times 1.3 - (99.9 - 2.7) \times \frac{1}{2} \times 2.2 \\ \times \left(0.2 + \frac{2.2}{3}\right) = 139.3 \text{ kNm}$$

$$\mathbf{M_{Ed,heel side} = 139.3 \text{ kNm}}$$

Base slab reinforcement (toe side)

The moment acting on the toe side would be computed from equilibrium i.e. the sum of moments acting about the toe should be zero.

$$\mathbf{M_{Ed,toe side} = 43.2 \text{ kNm}}$$

⁷ The third term of the equation is the rectangular part of the soil bearing stresses, while the fourth expression of the equation capture the triangular part of the soil bearing stresses.

Appendix 2: Bond

1. Background information

The key requirement in defining a reinforcement bond model is the bond-slip relationship. In such a model, the bond stress, τ_b is made to depend on the value of the displacement slip between the reinforcing bar and the surrounding concrete. For this work, the bond-slip model used is according to CEB-FIP model code 1990. This is one of the three bond-slip options available in ATENA FEM software. With this model, the bond-slip relation is defined based on concrete compressive strength, reinforcement type (ribbed or smooth), bar diameter, quality of concrete casting (as it affects bond quality) and the confinement conditions. The expressions used to define the bond slip models can be seen in Section 3.1 of CEB-FIP model code 1990. A summary of these expressions (which is implemented in ATENA FEM software) is illustrated in figure A3 below.

(a). Parameters used in CEB-FIP model code 1990 to define bond stress-slip relationship

	Column 2	Column 3	Column 4	Column 5
	Unconfined concrete*		Confined concrete†	
	Good bond conditions	All other bond conditions	Good bond conditions	All other bond conditions
s_1	0.6 mm	0.6 mm	1.0 mm	1.0 mm
s_2	0.6 mm	0.6 mm	3.0 mm	3.0 mm
s_3	1.0 mm	2.5 mm	Clear rib spacing	Clear rib spacing
α	0.4	0.4	0.4	0.4
τ_{\max}	$2.0\sqrt{f_{ck}}$	$1.0\sqrt{f_{ck}}$	$2.5\sqrt{f_{ck}}$	$1.25\sqrt{f_{ck}}$
τ_f	$0.15\tau_{\max}$	$0.15\tau_{\max}$	$0.40\tau_{\max}$	$0.40\tau_{\max}$

*Failure by splitting of the concrete.

†Failure by shearing of the concrete between the ribs.

(b). An illustration of the analytical bond-slip relationship (for monotonic load)



Figure A3 – Parameters used to define bond-slip relation in ATENA (CEB, 1993)

2. Bond stress-slip relationship for this thesis work

From figure A3, bond-slip relation can be defined for four scenario i.e. good bond conditions – unconfined concrete, good bond condition – confined concrete, poor bond conditions – unconfined concrete and poor bond condition – confined concrete. From the model, when the concrete is unconfined, bond failure is by splitting of the concrete. For confined concrete, bond failure is by shearing of concrete between the ribs. For this work, ribbed bar is used. The bond-slip relation implemented in ATENA for the four scenarios is shown in Table A1.

Table A1 – Bond slip relations in ATENA for this work

Good bond – Confined concrete	Slip (mm)	0.00	0.25	0.50	1.00	3.00	15.00	1000
	Bond, τ_b (MPa)	3.000	3.939	5.685	7.500	7.500	3.000	3.000
Good bond – unconfined concrete	Slip (mm)	0.00	0.15	0.30	0.60	1.00	1000	
	Bond, τ_b (MPa)	0.900	3.444	4.548	6.000	0.900	0.900	
Poor bond – Confined concrete	Slip (mm)	0.00	0.25	0.50	1.00	3.00	15.00	1000
	Bond, τ_b (MPa)	1.500	1.971	2.844	3.750	3.750	1.500	1.500
Poor bond – unconfined concrete	Slip (mm)	0.00	0.15	0.30	0.60	2.50	1000	
	Bond, τ_b (MPa)	0.900	1.722	2.274	3.000	0.450	0.450	

In section 8.4.2 of Eurocode 2, the design value of ultimate bond stress is expressed as:

$$f_{bd} = 2.25 \cdot \eta_1 \cdot \eta_2 \cdot f_{ctd}$$

Where $\eta_1 = 1.0$ for good bond conditions and $\eta_1 = 0.7$ for other cases. $\eta_2 = 1.0$ in this work since the bar diameter is less than 32mm. With $f_{ctd} = 1.333 \text{ MPa}$ in this work, the ultimate bond stress from EC2 expressions are:

$$f_{bd} = 3.0 \text{ MPa} \quad (\text{for good bond}) \quad \text{and} \quad f_{bd} = 2.1 \text{ MPa} \quad (\text{for poor bond})$$

On comparing this analytical bond stress to the data for Good bond – Confined concrete scenario in Table A1, the 3.0MPa computed above (from EC2 expression) is actually the minimum bond stress in that model. The mean bond-stress that would occur with the model is actually higher than 3.0MPa. The actual value depend on the amount of slip that occur. Similarly, for poor bond, the mean bond stress would also depend on the slip that occur. Such consideration could have some impact when analytical results is compared to FEM result as would be seen in the next section of this Appendix 2.

3. Further discussion comparing bond models with perfect bond and analytical solution

Table A2 shows the results from the earlier analysis earlier discussed in section 6.4.2 for variants 2 - 5. In this section of Appendix 2, some aspects of their bond behaviour is discussed. The study shows some ways in which the perfect bond assumption influences the structural behaviour.

Table A2 – Some results from variants 2 and 3

Variant	Peak moment (kNm) achieved and Joint efficiency (%)		
	Perfect bond assumption	Good Bond – confined concrete	Poor bond – unconfined concrete
Variant 2 (200mm anchorage)	127.3 kNm (51.8%)	98.5 kNm (40.0%)	54.8 kNm (23.7%)
Variant 3 (350mm anchorage)	215.8 (87.8%)	151.8 (61.8%)	83.2 kNm (33.9%)
Variant 4 (bent to heel)	184.9 (75.3%)	151.8 (61.8%)	149.6 kNm (60.9%)
Variant 5 (bent to toe)	217.3 (88.4%)	194.7 (79.2%)	188.4 kNm (77.0%)

The main reinforcement in the retaining wall consist of five 20mm diameter bars (i.e. 5 Ø20 bars). Some properties of this reinforcement is are presented thus:

Area of embedded steel, $A_s = 1795 \text{ mm}^2$; Perimeter of embedded, $p = 314.16 \text{ mm}$

3.1 Variant 2 (embedded 200mm into base slab)

Assuming poor bond – unconfined concrete

With the analytical ultimate bond stress, f_{bd} of 2.1 MPa, the force, F that would be transferred by bond for this bar embedded 200mm into the base slab is computed thus:

$$F = f_{bd} \cdot p \cdot L = 2.1 \times 314.16 \times 200 \cdot 10^{-3} = \mathbf{131.9 \text{ kN}} \quad (\text{Analytical bond capacity})$$

Next, this would be compared with the actual force transferred by the reinforcement.

Maximum steel stress, $f_{s,max}$ (in wall reinforcement) = 90.79 MPa (From FEM)

$$\text{Force in reinforcement} = f_{s,max} \cdot A_s = 90.79 \times 1795 \cdot 10^{-3} = \mathbf{163.0 \text{ kN}}$$

From the above calculation, a force of 131.9kN is estimated as the maximum force that can be transferred by bond based on analytical computation. However, based on the maximum steel stress predicted by FEM for the reinforcement, a higher force of 163kN was transferred. Why is this disparity?

The answer can be traced to the bond-slip model used. For the analytical solution, a constant bond stress is used. In the FEM computation, a slip-dependent bond stress is used. This is the reason for the disparity. The bond stress and slip displacement profile along steel (for this detail) are shown in figure A4 below. On visually examining figure A4a, some of the bond stresses along the reinforcement are higher than 2.1MPa. Thus with the bond stress not constant (as assumed in the analytical solution), there is some disparity between the force computed analytically and that observed from FEM. Figure A4b show the bond profile along the embedded steel when the structure carried its peak load. The slip continued afterwards as seen in figure A4c.

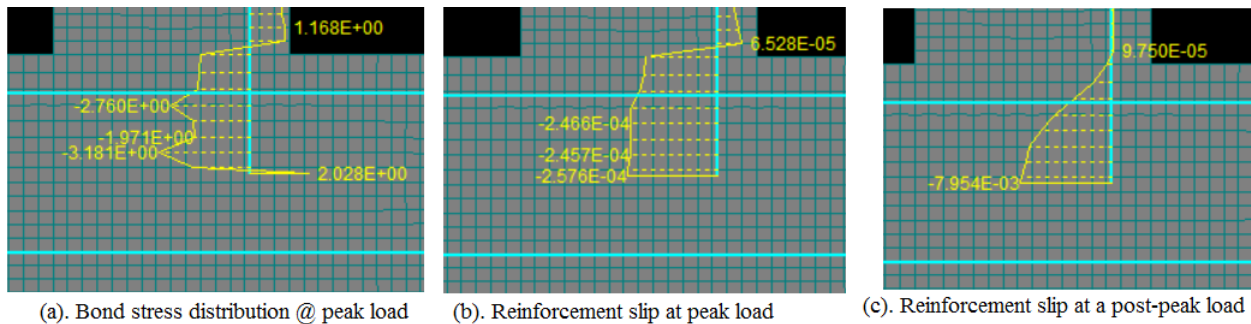


Figure A4 – Bond stress and slip distribution from FEM analysis (poor bond – unconfined concrete)

For this detail, bond failure occurred, thus causing the structure to fail prematurely. At peak load, minimum concrete strain, ϵ_2 was 0.4‰ and the steel stress was only 81.66MPa. Nevertheless, the structure could not carry a higher load. With the concrete being unconfined, bond failure is by splitting of the concrete.

Assuming good bond – confined concrete

When good bond – confined concrete is assumed, the structure is expected to carry a higher load than the poor bond – unconfined concrete scenario. With the ultimate bond stress, f_{bd} of 3.0 MPa, the force that can be transferred by bond for this bar embedded 200mm is computed thus:

$$F = f_{bd} \cdot p \cdot L = 3.0 \times 314.16 \times 200 \cdot 10^{-3} = \mathbf{188.5 \text{ kN}} \quad (\text{Analytical bond capacity})$$

From the FEM analysis, the maximum steel stress, $f_{s,max}$ attained by the wall reinforcement is 114.2MPa.

$$\text{Force in reinforcement} = f_{s,max} \cdot A_s = 114.2 \times 1795 \cdot 10^{-3} = \mathbf{205.0 \text{ kN}}$$

As in the previous case, the force transferred by bond (205 kN) is higher than the capacity computed analytically. The bond stress in the FEM is not constant (like the 3.0 MPa assumed in analytical solution). Rather the value is higher, and it depends on the amount of slip. This can be inferred from figure A5 below.

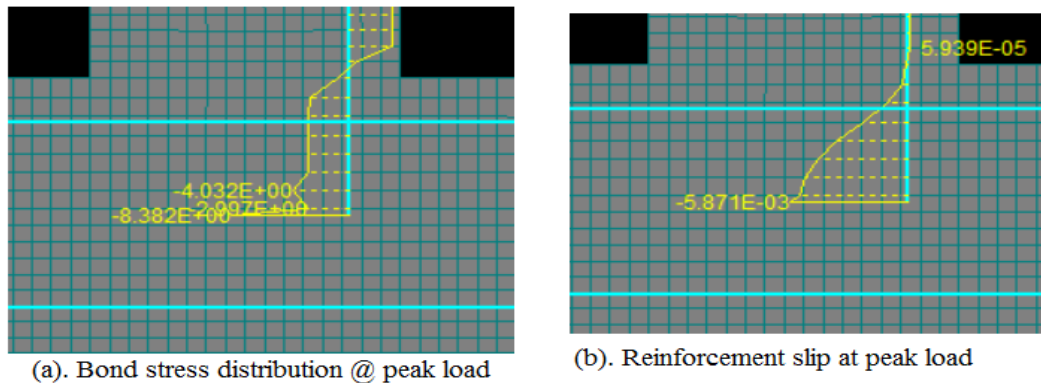


Figure A5 – Bond stress and slip distribution from FEM analysis (good bond – confined concrete)

In this case, the detail failed by crushing of the inclined strut after extensive diagonal tension cracking. With good bond properties, the structure was able to provide a higher load carrying capacity than the poor bond – unconfined concrete.

3.2 Variant 3 (embedded 350mm into base slab)

The horizontal force – displacement plot for 3 bond scenarios is shown in figure A6 below.

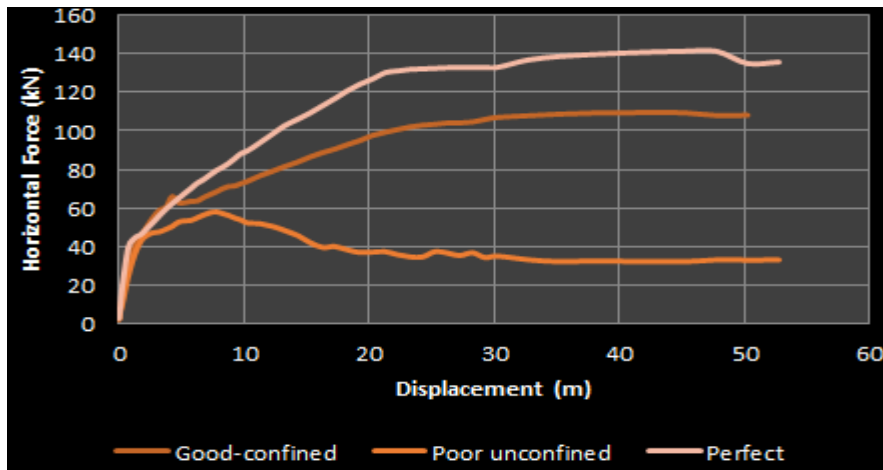


Figure A6 – Force – displacement diagram for bar embedded 350mm deep

From figure A6, the detail modelled with poor bond – unconfined concrete reached a peak load at a relatively small displacement and decreased afterwards. Bond failure occurred for this scenario. The other two models (i.e. perfect bond model, and good bond condition – confined concrete model) continued to take more load increments until diagonal tension cracking failure occurred. Thus, bond failure did not occur for both of these details. Further discussion on these details are presented below.

Assuming poor bond – unconfined concrete

$$F = f_{bd} \cdot p \cdot L = 2.1 \times 314.16 \times 350 \cdot 10^{-3} = \mathbf{230.9 \text{ kN}} \quad (\text{Analytical bond capacity})$$

$$\text{Maximum steel stress, } f_{s,max} \text{ (in wall reinforcement)} = 149.6 \text{ MPa}$$

$$\text{Force in reinforcement} = f_{s,max} \cdot A_s = 149.6 \times 1795 \cdot 10^{-3} = \mathbf{268.5 \text{ kN}}$$

In this case, the maximum force in the steel (268.5kN) exceeded the analytical bond capacity. The reason for this variance is clear: the average of the bond stress in the FEM analysis (from figure A7a below) is higher than the 2.1 MPa used in the analytical solution

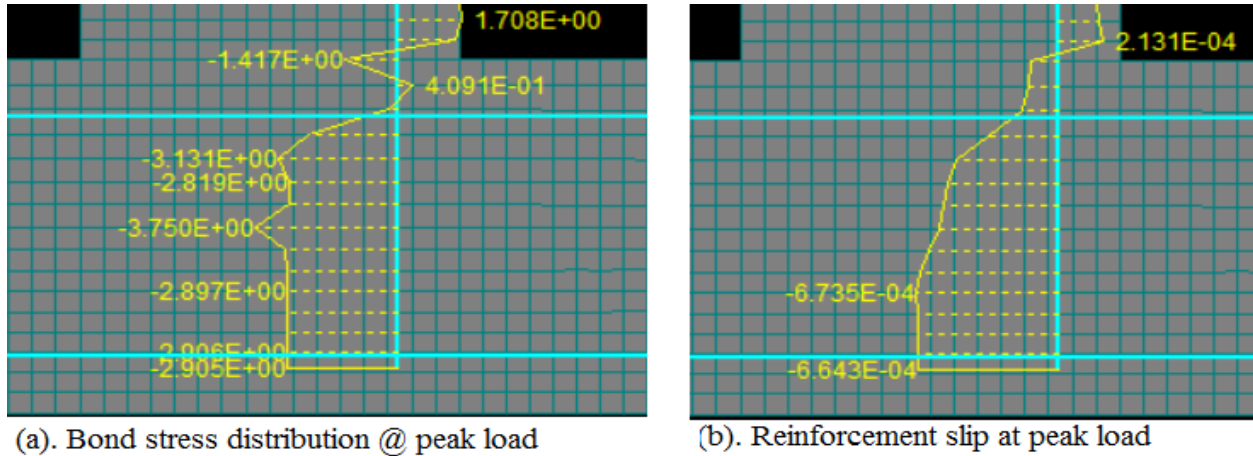


Figure A7 - Bond stress and slip distribution from FEM analysis (poor bond – unconfined concrete)

With the bond – slip relation having an impact on steel stress (and consequently axial force in the reinforcing steel), it is very likely to have impact on the structural capacity attained by the structure. In this detail, bond failure occurred. Thus the force carried by the structure reached a maximum, and started reducing afterwards. At this point, concrete compressive strains were much below the ultimate strain, and the steel stress well below yield. Thus, bond failure is the key reason why this detail attained only 33.9% as was shown in Table A2.

Assuming good bond – confined concrete

$$F = f_{bd} \cdot p \cdot L = 3.0 \times 314.16 \times 350 \cdot 10^{-3} = \mathbf{329.9 \text{ kN}} \quad (\text{Analytical bond capacity})$$

$$\text{Maximum steel stress, } f_{s,max} \text{ (in wall reinforcement)} = 283.4 \text{ MPa}$$

$$\text{Force in reinforcement} = f_{s,max} \cdot A_s = 283.4 \times 1795 \cdot 10^{-3} = \mathbf{508.7 \text{ kN}}$$

The distribution of bond stress and displacement slip along the reinforcement is shown in figure A8 below. Bond stresses that are higher than the assumed value (3.0 MPa) were achieved by this detail.

Compared with the analytical solution, this disparity in bond stress (due to the bond-slip model used in the FEM software) is the reason for the disparity. The average bond stress along the embedded steel (from the FEM illustrations above) depend on the bond condition and the confinement condition of the concrete.

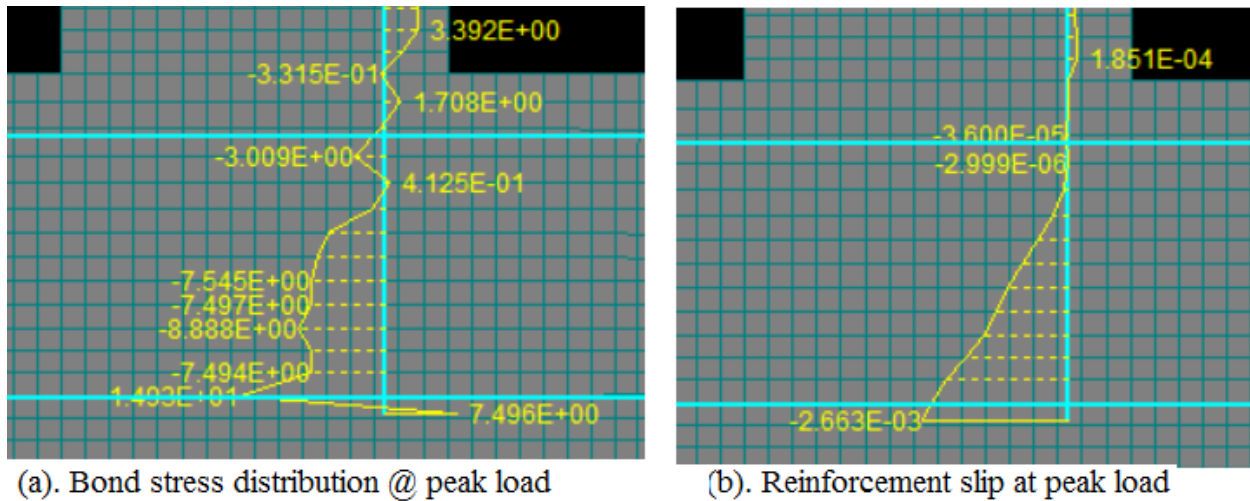


Figure A8 - Bond stress and slip distribution from FEM analysis (good bond – confined concrete)

3.3 Bent bars provided with sufficient anchorage length

Looking at Table A2, there is a large disparity between the peak moment achieved by the poor bond – unconfined concrete and the good bond – confined concrete model. In contrast, such large disparity in predicted peak moment does not occur for variants 4 and 5. In those variant, the reinforcement are bent and further extended to provide adequate anchorage length. This way, the steel was able to develop it strength without being limited by bond conditions. For this reason, bond failure did not occur in variant 4 and 5.

However, on comparing the capacity predicted by these bond – slip models, with the peak moment computed using perfect bond, there is a disparity. The assumption of perfect-bond seems to over-estimate the capacity.

Conclusion

From the above study, the impact of the bond slip model on the steel stress (and consequently the structural capacity is quite clear). It also had impact on the failure with bond failure occurring where the anchorage length is inadequate. Where the bond quality is good, and the concrete is confined, bond failure is unlikely.

When perfect bond is assumed, there is no slip between the steel bars and the surrounding concrete. In this work, the details modelled with perfect bond are observed to predict a relatively higher capacity than those with bond-slip models. With slip prevented in the model, this is likely to result in higher stresses in the reinforcing steel (and consequently higher steel force). This occurrence of higher stresses (due to the model) is a probable reason why it predicted higher capacity in the above cases.